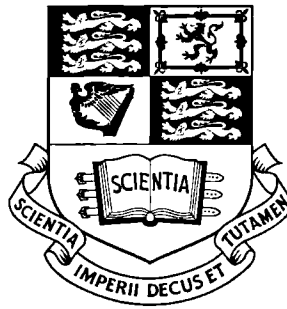# A New Approach to Structural Stainless Steel Design

A thesis submitted to the University of London

for the degree of Doctor of Philosophy

By

Leroy Gardner

Department of Civil and Environmental Engineering

Imperial College of Science, Technology and Medicine

London, SW7 2BU

August 2002

ABSTRACT

Current structural stainless steel design codes are based largely on assumed analogies with carbon steel behaviour. This is advantageous for designers in terms of ease of transition from carbon steel to stainless steel design, but detrimental in terms of making efficient use of the particular behavioural properties exhibited by stainless steel. The primary aim of this study was therefore to develop a more rational and efficient design method for stainless steel structures, whilst, where possible, maintaining consistency with the carbon steel design approach.

As part of the current study, laboratory tests were performed on cold-formed austenitic stainless steel hollow sections. A total of 33 stub column tests, 22 pin-ended column tests, 9 simply-supported beam tests and numerous material coupon tests were performed. These test results were used in conjunction with existing test results to develop and calibrate a new structural design method for stainless steel. A numerical modelling programme was conducted in parallel with the testing programme. Sophisticated FE models were developed and, following accurate replication of test results, a consistent approach to the modelling of stainless steel structures was defined.

The new design approach recognises that placing cross-sections into discrete behavioural classes is inappropriate for stainless steel, since there is no sharply defined yield point. Instead, with a more appropriate material model, member strengths are assessed using a local buckling strength derived from the deformation capacity of the cross-section. It may therefore be viewed as a continuous method of cross-section classification and member design. Comparison between test results and predicted results according the current European design guidance (given in Eurocode 3: Part 1.4) and according to the proposed design method was made. The comparison revealed that the proposed design method offers an average increase in member capacity of 21% and a reduction in scatter of the prediction.

ACKNOWLEDGEMENTS

CONTENTS

CHAPTER 1 – INTRODUCTION

CHAPTER 2 – LITERATURE REVIEW

CHAPTER 3 – EXPERIMENTAL STUDY

CHAPTER 4 – NUMERICAL MODELLING

CHAPTER 5 – ANALYSIS OF RESULTS AND DEVELOPMENT OF DESIGN METHOD

CHAPTER 6 – DESIGN METHOD

NOTATION

a_g	Generalised shape factor
a_p	Geometric shape factor
A	Gross cross-sectional area
A_{eff}	Effective cross-sectional area
B	Breadth
c	Half-width of tensile weld residual stress block
CHS	Circular hollow section
D	Depth
D_0	Outer diameter
e	eccentricity of loading
E_0	Young's modulus (or initial tangent modulus)
$E_{0.2}$	Tangent modulus (stiffness) at 0.2% proof stress
FE	Finite element
F_u	Ultimate load
$F_{u,Test}$	Test ultimate load
$F_{u,ENV}$	Ultimate load predicted by ENV 1993-1-4 (1996)
$F_{u,Prop}$	Ultimate load predicted by proposed design method
i	Radius of gyration

k	Buckling coefficient
L	Length
L_E	Effective length
LVDT	Linearly-varying displacement transducer
M_u	Ultimate bending moment
$M_{u,Test}$	Test ultimate bending moment
$M_{u,ENV}$	Ultimate bending moment predicted by ENV 1993-1-4 (1996)
$M_{u,Prop}$	Ultimate bending moment predicted by proposed design method
n	Ramberg-Osgood exponent between zero strain and $\varepsilon_{t0.2}$
$n'_{0.2,u}$	Compound Ramberg-Osgood exponent based on $\sigma_{0.2}$ and σ_u
$n'_{0.2,1.0}$	Compound Ramberg-Osgood exponent based on $\sigma_{0.2}$ and $\sigma_{1.0}$
R	Radius
RHS	Rectangular hollow section
r_i	Internal corner radius
SHS	Square hollow section
t	Thickness
w	Plate width
W_{eff}	Effective section modulus
W_{el}	Elastic section modulus
W_{pl}	Plastic section modulus
α	Imperfection factor
β	Element slenderness
β_{web}	Web slenderness
β_{flange}	Flange slenderness

β_M	Equivalent uniform moment factor
δ_u	Displacement at ultimate load
ε_0	Elastic strain at the material 0.2% proof stress $= \sigma_{0.2}/E_0$
ε_{LB}	Local buckling strain
$\varepsilon_{t0.2}$	Total strain at 0.2% proof stress
ε_{tu}	Total strain at ultimate stress
ε_{pu}	Plastic strain at ultimate stress
λ	Slenderness ratio $= L_E / i$
$\bar{\lambda}$	Non-dimensional slenderness
$\bar{\lambda}_0$	Limiting slenderness
ν	Poisson's ratio
$\sigma_{0.2}$	0.2% proof stress
$\sigma_{0.2,c}$	0.2% proof stress of corner material
$\sigma_{1.0}$	1.0% proof stress
σ_{LB}	Local buckling stress
σ_r	Residual stress
σ_{rc}	Compressive residual stress
σ_{rt}	Tensile residual stress
σ_u	Ultimate stress
$\sigma_{u,c}$	Ultimate stress of corner material
σ_y	Yield stress
χ	Cross-section aspect ratio
χ	Buckling reduction factor
χ_y and χ_z	Buckling reduction factors about the y (major) and z (minor) axes, respectively

χ_{min} The lesser of χ_y and χ_z

ψ Ratio of end stresses in a compression element

ω_0 Imperfection amplitude

LIST OF FIGURES

LIST OF TABLES

CHAPTER 1

INTRODUCTION

1.1 BACKGROUND

Since its inception during the early part of the twentieth century, designers, engineers and architects alike, have used stainless steel in both practical and imaginative ways, with further use certain to arise as we enter a global transition towards sustainable development and reduction in environmental impacts. Adoption of stainless steel for primary structural components is, however, currently rather limited, with wider application being inhibited by a lack of structural design guidance that makes optimal use of its particular material behaviour.

1.2 HISTORY AND MATERIAL PROPERTIES

The commercial birth of stainless steel is generally attributed to an English metallurgist, Harry Brearley, in 1913. Brearley referred to the material as 'rustless steel' and it was a cutlery manager, Ernest Stuart, who popularised the term 'stainless'. The first austenitic (chromium-nickel) stainless steels were patented by Maurer and Strauss of Krupps in 1912-1913. Stainless steel is now used as a general expression to describe corrosion resistant iron alloys that contain a minimum of 11% chromium. A thorough account of the initiation and growth of stainless steel production is given by Truman (1985).

In addition to the clear aesthetic appeal of stainless steel there are other increasingly strong arguments for adopting the material in structures. The corrosion resistance of stainless steel makes it one of the most durable families of construction materials; a material with no need for protective coatings against corrosion has clear advantages in terms of economy, weight savings, reduction in environmental impact and lower maintenance costs. The fire resistance of stainless steel has been shown to be superior to that of carbon steel, reducing or even eliminating the need for protective fire coatings to be applied to structural members. The combination of the residual value of the alloy content of stainless steel and the economic advantages gained from re-melting scrap in the dominant electric arc process has resulted in a high level of recycling of material.

The initial cost of structural stainless steel products is approximately four times that of the equivalent carbon steel product. However, using a whole-life costing approach to material selection and considering the additional benefits in terms of durability, fire resistance and recyclability, stainless steel becomes a far more attractive option. This is discussed in more detail by Gardner & Nethercot (2002).

1.3 MATERIAL GRADES AND PRODUCT FORMS

There is a wide variety of stainless steel grades that fall into four main groups; austenitic, ferritic, matensitic and duplex. The most common grades for structural and architectural applications are the austenitic and duplex grades, with the duplex stainless steels offering higher strength and wear resistance than the austenitics, but at greater expense. It should be noted that there are a number of different stainless steel designation systems. The system adopted in the remainder of this thesis will be that given in the European material standard, BS EN 10088-1 (1995), with Table A.1 showing equivalent designations. For each standard stainless steel grade, BS EN 10088-1 (1995) defines a steel name and a steel number. It is the steel number that will be referred to throughout the thesis. Stainless steel product forms include: plate, sheet, tube, bar, cold-formed structural sections and hot-rolled structural sections, with the most commonly used products for structural applications being cold-formed (square, rectangular and circular) hollow sections.

The current study is focused upon austenitic stainless steel though the findings are, in principle, applicable to any material that exhibits rounded stress-strain behaviour. Similarly, this study

deals primarily with cold-formed hollow section products, though extension of the findings to other forms of structural cross-section has no conceptual barriers.

1.4 USES IN CONSTRUCTION

The use of stainless steel in construction is growing rapidly, yet its exploitation as a primary structural material remains rather limited, with the dominant applications being of a specialist or prestigious nature. Figures 1.1 and 1.2 show examples of landmark structures that have made use of stainless steel. Figure 1.1 shows the cladding on the Chrysler Building in New York, which, completed in 1929, is one of the earliest examples. Figure 1.2 shows The Gateway Arch (completed in 1965) in St. Louis, Missouri, which is the second largest structural application of stainless steel in the world.

Figure 1.1: *Chrysler Building, New York*
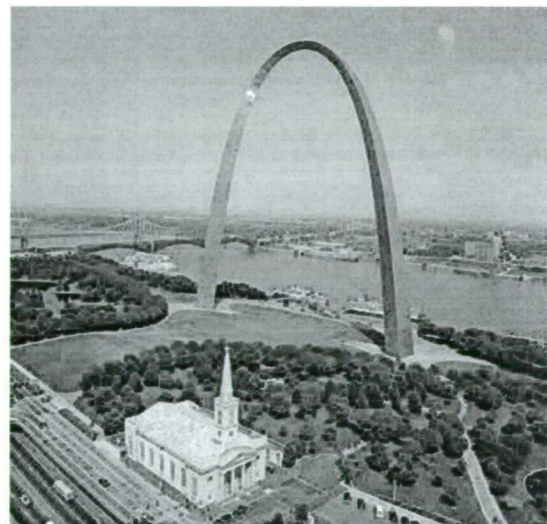
Figure 1.2: *The Gateway Arch, St. Louis*

Numerous other examples of architectural applications of stainless steel have been given by Baddoo et al. (1997). Extensive specialist use of stainless steel is made by the offshore and nuclear power industries to meet stringent safety and performance requirements whilst minimising the need for maintenance.

1.5 OUTLINE OF THESIS

This Chapter provides a broad introduction to the origins of stainless steel, the variety of available products and material grades, the uses of stainless steel in the construction industry and an overview of the remainder of the thesis.

Chapter 2 contains a review of the literature that is relevant to this research project. The review is intended to give an overview of important topics, with the majority of the literature being introduced and discussed at the relevant stage in the thesis.

An extensive laboratory testing programme was conducted as part of the study, including material coupon tests, stub column tests and member tests. Tests were carried out on square, rectangular and circular hollow sections (SHS, RHS and CHS respectively). Full details are reported in Chapter 3.

Chapter 4 describes a numerical modelling programme that was run in parallel with the laboratory testing programme. Following successful replication of experimental behaviour, parametric studies were conducted to investigate the effect of variation in key individual parameters and to generate further results in areas unexplored experimentally.

Development of a more rational and more efficient method for the structural design of stainless steel is described in Chapter 5. The design method includes a continuous rather than a discretised method of cross-section classification and member design, and is based upon a more accurate material model.

In Chapter 6 the new design method is presented in a clear format, and validated against all available test results. Comparison is also made with the current European design rules given in ENV 1993-1-4 (1996). Worked examples are included to demonstrate the design method. A summary of the important findings from the project, conclusions and suggestions for further work are provided in Chapter 7.

CHAPTER 2

LITERATURE REVIEW

2.1 INTRODUCTION

This chapter is divided into broad subject areas, and presents a brief review of previous work that is pertinent to this thesis. From the re-appraisal of existing design guidance, to the compilation and re-evaluation of previous test results, and ultimately through to the development of a more efficient approach to the design of stainless steel structures, widespread investigation has been conducted.

2.2 INTERNATIONAL RESEARCH PROGRAMMES

The increase in use of stainless steel in construction, and hence the need for an improved understanding of its structural response, has been recognised by research institutions around the world. A number of major research programmes into the structural use of stainless steel have been carried out over the past 50 years, and with increased vigour during the past 15 years. Results from these research programmes have enabled the development and publication of design guidance.

Early investigations into stainless steel structures were conducted in North America during the 1950s and 1960s. Hammer & Petersen (1955) and Dubuc et al. (1956) both noted the

difficulties that are associated with predicting the structural response of a material that has no sharply defined yield point, and that behaves anisotropically. Further work was carried out by Johnson & Winter (1966) with the aim of assembling basic information for a design specification.

Aoki (2000) explained the ongoing process of overcoming the restrictions of using stainless steel as a structural material in Japan's building code.

An abundance of suitable raw materials in South Africa is at least partly responsible for the commencement of research into structural applications of stainless steel at Rand Afrikaans University in Johannesburg during the early 1980s. The work, outlined by Van den Berg (2000), was used extensively by the American Society of Civil Engineers in their stainless steel cold-formed design specification published in 1991 (ASCE, 1991).

In Australia, Rasmussen (2000a) described how a market survey to investigate the feasibility of promoting cold-formed stainless steel tubes in structural applications in the late 1980s led to the commencement of a research programme at the University of Sydney. The aim of this programme was to develop load tables for stainless steel tubular columns and beams.

On the European scene, a significant joint industry project, managed by the UK Steel Construction Institute, was conducted between 1988 and 1991. Details of the project are included in the Euro Inox 'Design Manual for Stainless Steel Structures' (Euro Inox, 1994). More recently, research institutions from the UK, Finland, France, Germany, Italy and Sweden formed a partnership for an ECSC project entitled 'Development of the use of stainless steel in construction'. The three-year project commenced in 1996, and a summary of the project findings was reported by Baddoo & Gardner (2000).

In the UK, Mann (1993) recognised that the lack of stainless steel technical data in some areas was restricting full exploitation of the material's properties. It was explained that due to the high initial material cost, the structural use of stainless steel must be as efficient as possible.

Kouhi et al. (2000) described how close co-operation between the Finnish stainless steel industry and VTT Building Technology led to the common conclusion that national guidelines on the structural use of stainless steel should be prepared, since no such guidelines existed at that time.

2.3 STRUCTURAL STAINLESS STEEL DESIGN GUIDANCE

Since the early laboratory testing during the 1950s and 1960s, design rules for stainless steel structures have been put forward. Historically stainless steel design rules have been based on assumed analogies with carbon steel behaviour, with modifications made where necessary to fit in with test results.

The earliest dedicated stainless steel structural design code was published by the American Iron and Steel Institute in 1968, and was entitled 'Specification for the Design of Cold-formed Stainless Steel Structural Members'. The design rules were based primarily on the work carried out by Johnson & Winter (1966). With an improved understanding of the structural behaviour of stainless steel and an increased availability of test results (Wang & Errara, 1971), a revised version of the Code was published in 1974 (AISI, 1974). Further research enabled the development of the ASCE Structural Stainless Steel Design Standard (ASCE, 1991), which effectively superseded the AISI standard in North America. Background and commentary to the ASCE Structural Stainless Steel Design Standard were reported by Lin et al. (1992).

In 1991, following the joint industry project, managed by the UK Steel Construction Institute, the Euro Inox 'Design Manual for Structural Stainless Steel' was completed; but not published until 1994 (Euro Inox, 1994). Derived from entirely the same material, the 'Concise Guide to the Structural Design of Stainless Steel', based on BS 5950-1 (1990) Structural use of steelwork in buildings, was published by the UK Steel Construction Institute (Burgan, 1992). The current European design standard for stainless steel structures, ENV 1993-1-4 (1996) was introduced in 1996. ENV 1993-1-4 (1996) forms Part 1.4 of Eurocode 3: Design of steel structures, and contains supplementary rules for stainless steels. Its present status is that of a European prestandard, with conversion to a full European standard currently underway. ENV 1993-1-4 (1996) is the document that will be referred to, and used for comparison with the proposed design approach, throughout the thesis.

In 1995, the Japanese stainless steel structural design standard was issued (SSBJA, 1995). Based largely on the Canadian design standard for carbon steel, the South African structural stainless steel code was published in 1997 (SABS, 1997). Most recently, in 2001, the Australian and New Zealand design code for cold-formed stainless steel structures (Aust/NZS, 2001) was published. Development of the Code was described by Rasmussen (2000b).

2.4 LABORATORY TESTING

Central to the development of efficient codified design rules is the availability of high quality laboratory test data. With the limited use of stainless steel in structures, it is unsurprising that the volume of test results for stainless steel structures is currently relatively low, with some areas virtually unexplored. This section contains a brief review of laboratory tests conducted on stainless steel structural members.

The early laboratory tests carried out in North America by Hammer & Petersen (1955) and Dubuc et al. (1956) investigated the flexural buckling of hollow section columns. The hollow sections were formed by welding pairs of channel sections or top-hat sections. A large number of tests were conducted, but they were not reported in sufficient detail to incorporate into the validation of the proposed design method.

Johnson & Winter (1966) presented details of tests carried out on cold-formed stainless steel flexural and compression members. The flexural members were top-hat shaped, and tested in four-point bending to investigate the behaviour of thin stiffened compression flanges. Two types of cross-section were tested in compression, back-to-back channel sections (forming an I-section), and tip-to-tip lipped channel sections (forming a rectangular hollow section). In both cases, joining of the sections was by means of epoxy adhesive, in order to eliminate distortions and residual stresses that would be induced as a result of welding. An effective width formulation was successfully used to predict strength and deflections of the beams, whilst the tangent modulus formula gave satisfactory prediction of column behaviour. Wang et al. (1975) conducted further tests on similar specimens to those investigated by Johnson & Winter (1966). The 1968 AISI guidance was found to be conservative in predicting both beam and column strength.

The current study is focused upon structural austenitic stainless steel hollow sections. Table 2.1 gives a summary of all tests conducted on hollow sections that have been reported in sufficient detail. These tests were conducted as part of the current study (described in Chapter 3), and as part of other studies, reported by Ala-Outinen & Oksanen (1997), Chryssanthopoulos & Kiymaz (1998), Liu & Young (2002), Mirambell & Real (2000), Rasmussen & Hancock (1993a, 1993b), Talja & Salmi (1995), Young & Hartono (2002) and Young & Liu (2002); all described in detail in Chapter 5.

Table 2.1: *Tests conducted on stainless steel hollow sections*

Structural configuration	No. of SHS tested	No. of RHS tested	No. of CHS tested
Stub columns	20	18	10
Flexural buckling - pinned	16	20	10
Flexural buckling - fixed	8	16	12
In-plane bending	11	12	8
Lateral torsional buckling	-	0	-
Axial load plus bending	4	8	8

Although this study is focused upon hollow sections, it is envisaged that the proposed design method may be extended to cover all cross-section types. Laboratory tests on stainless steel open-sections that may be used for the validation of such an extension have been conducted by Dier (1991), Rhodes et al. (2000), Talja (1997, 1999), Mirambell & Real (2000), Yamada & Kato (1988) and Bredenkamp & Van den Berg (1995).

2.5 MATERIAL MODELLING

The cross-section classification and member design for stainless steel structures according to ENV 1993-1-4 (1996) uses a simple bi-linear (elastic, perfectly-plastic) material stress-strain model. For structural design purposes this model provides a satisfactory representation of carbon steel stress-strain behaviour. However, for stainless steel, which exhibits rounded stress-strain behaviour with a high degree of strain hardening, the representation is less accurate. For improved efficiency, a more precise material model has to be incorporated into a stainless steel structural design method.

A widely used model for the description of non-linear material stress-strain behaviour was originally proposed by Ramberg & Osgood (1943). The basic expression was modified by Hill (1944) to produce its most commonly adopted form given in Equation 2.1, where $\sigma_{0.2}$ is the material 0.2% proof stress, E_0 is the material Young's modulus, and n is a strain hardening exponent.

$$\varepsilon = \frac{\sigma}{E_0} + 0.002\left(\frac{\sigma}{\sigma_{0.2}}\right)^n \qquad (2.1)$$

Although to a lesser extent than stainless steel, aluminium also exhibits rounded stress-strain behaviour. Equation 2.1 appears in an informative annex of the European aluminium structural design code, ENV 1999-1-1 (1999).

When applied to stainless steel, Equation 2.1 can provide an excellent description of stress-strain behaviour below the material 0.2% proof stress. However, at higher strains it was observed (Gardner & Nethercot, 2001a) that the model tends to overestimate the material strength. This problem is discussed in detail in Section 4.2, where a compound (two-stage) Ramberg-Osgood model that enables accurate description up to far higher strains is discussed. The initiative to use a two-stage Ramberg-Osgood model was conceived by Mirambell & Real (2000).

2.6 CROSS-SECTION BEHAVIOUR AND THE INFLUENCE OF STRAIN HARDENING

To investigate the behaviour of aluminium cross-sections, Faella et al. (2000) conducted a total of 80 stub column tests. The tests were performed on specimens with a wide range of width-to-thickness ratios. Analysis of the experimental results enabled the calibration of empirical expressions, leading to improved cross-section classification that takes account of the restraining action of the flanges on the webs, and vice versa. The general expressions adopted for linking cross-section slenderness and cross-section deformation capacity are employed in the current study.

The concept of a generalised shape factor that takes account of material strain hardening properties, in addition to the geometric properties of a cross-section, was explained by Mazzolani (1995), and applied to aluminium structural components in bending. The current study applies this concept to stainless steel structural components in bending.

Stainless steels exhibit a significantly higher level of strain hardening than carbon steels. Whether the straining be during the formation of the flat sheet, during fabrication of the cross-sections, or during structural service, the effect of strain hardening cannot be overlooked.

Hasan & Hancock (1988) conducted a series of bending tests on cold-formed carbon steel RHS. The results of the tests showed that observed bending resistance exceeded the predicted plastic moment resistance by 23%. This was despite the ultimate tensile stress of the sections (based on coupon tests), only being 17% higher than the yield stress.

Kemp et al. (2002) carried out 32 tests on closely restrained carbon steel beams to investigate the additional moment resistance that resulted from strain hardening. A significant increase in moment resistance beyond the fully plastic moment resistance of the beams was observed in all cases. A theoretical basis for the prediction of moment resistance providing an additional 8% of strength above the conventional plastic resistance was presented.

The effect of strain-hardening and residual stresses on the strength of stainless steel lipped channel sections was investigated by Coetzee et al. (1990). Stress-strain curves were compared for virgin sheet material (using longitudinal compression results), weighted average properties, determined by cutting the section into strips, and finally stub column tests. It was concluded that the virgin sheet mechanical properties give the lowest stress-strain curves, and the weighted average properties give the highest stress-strain curves. Both of these stress-strain curves are free from residual stress, so the difference can be assumed to be due to the effect of cold-working during forming. The stress-strain curves for the stub column tests were between these two extremes, and represent the actual behaviour of the column including enhanced strength corners, and residual stresses.

2.7 RESIDUAL STRESSES

Residual stresses can be defined as the stresses that exist within a member when no external loading is applied. The importance of residual stresses on the behaviour of structural members has been known for some time. A thorough description of the formation and effects of residual stresses in steel sections was presented by Lay & Ward (1969).

Residual stresses fall into two distinct groups. Those that are induced through differential cooling of the material, typically after either a hot-rolling process or after welding, and those that are induced due to inelastic material deformations, such as cold-rolling. Both types of residual stresses exist in cold-formed stainless steel hollow sections.

Differences between the thermal properties of stainless steel and carbon steel suggest that the magnitude of weld-induced residual stresses in stainless steel would be more severe. Investigations into residual stresses have been carried out by Bredenkamp et al. (1992) and Lagerqvist & Olsson (2001). A discussion of their findings is given in Section 4.3.3.

During the 1970s, Ingvarsson (1975, 1977, 1979) investigated the occurrence of deformational residual stresses in cold-formed steel sections. The induction of circumferential deformational residual stresses during cold-forming is well understood, but Ingvarsson explained the formation of longitudinal residual stresses, which have a much greater effect on member behaviour. Residual stress distributions for cold-formed channel sections and hollow sections were presented.

Residual stresses in cold-formed steel members were also investigated by Weng & Pekoz (1988). An electrical discharge machining (EDM) technique was used to section the members, rather than the traditional saw-cutting techniques that can induce additional deformations and heat into thin-walled sections. It was found that residual stress distributions in cold-formed sections were quite different from those in hot-rolled sections. The column curve used in the AISI specification for the design of cold-formed steel structural members (AISI, 1974), which was derived from hot-rolled sections, was therefore considered questionable.

Residual stress measurements made on cold-formed stainless steel cross-sections are scarce. The only known investigation of deformationally induced residual stresses was conducted by Rasmussen & Hancock (1993a). This work is considered in more detail in Section 4.3.2.

2.8 ELEVATED TEMPERATURE BEHAVIOUR

The design of structures at elevated temperatures has received increasing attention over the past few years. Despite this, no European fire design guidance currently exists for stainless steel structures, though recent investigations have acknowledged that stainless steel has superior fire resistance to carbon steel.

Ala-Outinen (1999) reported on tests performed on stainless steel compression members exposed to fire. The purpose of the study was to determine whether austenitic stainless steel

sections could be used in load-bearing structures without the need for fire protection, based on an exposure limit of 30 minutes. It concluded that load levels (elevated temperature resistance divided by room temperature resistance) of up to 0.4 could be sustained after 30 minutes of exposure.

Based on the results of experimental and numerical studies, Baddoo & Gardner (2000) proposed expressions for the design of stainless steel members in fire. An interesting part of the study discussed the idea of elevated temperature cross-section re-classification (based upon reduced, elevated temperature material properties), though no firm recommendations could be made due to lack of appropriate test data.

2.9 NUMERICAL MODELLING

Numerical modelling of structural stainless steel members under a variety of loading configurations has been successfully performed by a number of researchers. However, often models have been relatively simplistic, and agreement between test and finite element results has been achieved by selecting a suitable level of imperfection. The aim of the numerical investigations conducted in this study is to develop a consistent approach to the modelling of structural stainless steel members by careful analysis of the individual key input parameters. A general review of other numerical modelling studies of stainless steel structural members is given below. More detailed consideration is included in Chapter 4.

Talja & Salmi (1995) employed the finite element package ABAQUS to model stainless steel square and rectangular hollow sections under a variety of loading conditions. It was observed that bending strength was severely underestimated if elastic-plastic material properties were adopted with no account for strain hardening.

Rasmussen & Rondal (1997b) described the FE modelling of stainless steel pin-ended columns. Average material stress-strain curves, derived from stub column tests, were incorporated throughout the cross-sections, with no account made for the strength enhancements that exist in the corner regions. This has two clear drawbacks. The first, noted by the authors, is that by averaging the extreme fibre strength enhancements throughout the cross-section, the models would tend to predict conservative overall buckling loads, and the second is that the local buckling behaviour of the plates within the cross-sections is altered.

Sedlacek & Stangenberg (1999) reported numerical simulations of tests on stainless steel welded I-section beams in four-point bending and welded I-section columns subjected to minor axis flexural buckling. Modelling was conducted using the finite element software, MARC 7.2. Parametric studies were carried out to investigate the effect of variation in flange and web slenderness. Replication of test behaviour was achieved with an adequate degree of accuracy.

Mirambell & Real (2000) described an experimental and numerical investigation into the flexural behaviour of stainless steel beams, with particular attention on the calculation of deflections. The FE models employed beam elements (local buckling effects were therefore ignored), and measured material stress-strain data. Deflections were generally underestimated.

2.10 DISCUSSION

The purpose of this chapter has been to provide an overview of the subjects that are investigated within this thesis, allowing further literature to be introduced and examined in more detail within the appropriate chapter.

In general, research into stainless steel structures has been relatively limited, though by assuming analogies with carbon steel and aluminium behaviour, sufficient progress has been made to permit the development of a number of structural design codes. Departure from some of these assumed analogies to enable the development of a more rational and more efficient approach to the structural design of stainless steel is a key component of this thesis.

CHAPTER 3

EXPERIMENTAL STUDY

3.1 INTRODUCTION

A laboratory testing programme was carried out to investigate the behaviour of stainless steel cross-sections and members. Tests were conducted on square, rectangular and circular hollow sections (SHS, RHS and CHS respectively). All tests were performed in the Civil and Environmental Engineering Department Structures Laboratory at Imperial College. This chapter reports on the different aspects of the experimental study; the purpose of the tests, the testing apparatus and methods employed, and the test results.

Tensile and compressive coupon tests were carried out on flat material cut from the faces of finished SHS and RHS to determine the material stress-strain behaviour. Coupons cut from the corner regions of the cross-sections were also tested to investigate the effect of strain hardening.

Stub column tests were conducted on SHS, RHS and CHS to enable the development of a relationship between cross-section slenderness and deformation capacity, and to determine ultimate load carrying capacities.

Member tests on SHS and RHS beams and columns were conducted to investigate structural behaviour and determine ultimate load carrying capacities.

Initial geometric imperfections and residual stresses were measured to aid the explanation of structural performance and to use as a basis in numerical models.

The laboratory test results were also used as a means to validate numerical models. Full details of the numerical modelling programme can be found in Chapter 4.

3.2 DETAILS OF MATERIAL SUPPLY

Section sizes were chosen to fill gaps in existing tests data and to ensure that a range of practical cross-section slendernesses were covered by the testing programme. The SHS and RHS were supplied in 6m lengths by Perchcourt Ltd (UK stainless steel stockists), though the sections originated from numerous tube producers. The CHS were sourced from a previously conducted testing programme at Imperial College.

All specimens were Grade 1.4301 stainless steel, supplied in the 'as-rolled' condition. Due to its combination of relative economy, strength and adequate corrosion resistance, this is frequently used for structural applications.

3.2.1 Chemical composition

The chemical compositions of the SHS and RHS test specimens, as provided by the mill certificates, are presented in Table 3.1. No chemical composition details were available for the CHS.

3.2.2 Coil material properties

The material properties of the coil from which the SHS and RHS test specimens were formed, as provided by the mill certificates, are presented in Table 3.2. Where results from more than one sample were supplied, average values have been determined. No coil material properties were available for the CHS. Definitions for the symbols used in Table 3.2 are as follows: $\sigma_{0.2}$ and $\sigma_{1.0}$ are material proof strengths at 0.2% and 1.0 % offset strain respectively, σ_u is ultimate tensile material strength, A_5 is a measure of ductility and HB30 and HRB are measures of hardness (Brinell and Rockwell, respectively).

Table 3.1: *Chemical composition (% by weight) of SHS and RHS test specimens*

Section size	Supplier	C	Si	Mn	P	S	Cr	Ni	Mo	Ti	N	Others
SHS 80×80×4	Stala Tube	0.050	0.46	1.50	0.027	0.002	18.3	8.6	-	-	0.050	-
SHS 100×100×2	Padana Tubi	0.044	0.46	1.29	0.028	0.003	18.1	8.2	-	-	-	-
SHS 100×100×3	Marcegaglia	0.050	0.41	1.56	0.026	0.009	18.1	8.6	-	-	-	-
SHS 100×100×4	Stala Tube	0.040	0.48	1.54	0.026	0.001	18.3	8.5	-	-	0.045	-
SHS 100×100×6	Stala Tube	0.035	0.46	1.50	0.024	0.001	18.2	8.6	-	-	0.054	-
SHS 100×100×8	Stala Tube	0.021	0.35	1.67	0.024	0.001	18.0	8.1	-	-	0.068	0.461
SHS 150×150×4	Stala Tube	0.032	0.42	1.5	0.027	0.001	18.1	8.7	-	-	0.065	-
RHS 60×40×4	Stala Tube	0.040	0.45	1.49	0.026	0.003	18.3	8.7	-	-	0.041	-
RHS 120×80×3	La Meusienne	0.039	0.29	0.85	0.026	0.001	18.1	8.5	0.32	-	0.041	-
RHS 120×80×6	Stala Tube	0.050	0.47	1.57	0.030	0.001	18.0	8.5	-	-	0.052	-
RHS 150×100×4	Stala Tube	0.032	0.43	1.51	0.028	0.001	18.4	8.6	-	-	0.074	-
RHS 100×50×2	Stala Tube	0.033	0.45	1.47	0.025	0.001	18.2	8.6	-	-	0.066	-
RHS 100×50×3	La Meusienne	0.038	0.34	0.88	0.024	-	18.3	8.5	0.26	-	0.046	-
RHS 100×50×4	Marcegaglia	0.050	0.33	1.01	0.024	0.013	18.4	8.5	-	-	-	-
RHS 100×50×6	Stala Tube	0.019	0.35	1.63	0.029	0.001	18.2	8.2	-	-	0.069	0.393

Table 3.2: *Coil material properties for SHS and RHS test specimens*

| Section size | Supplier | $\sigma_{0.2}$ (N/mm²) | $\sigma_{1.0}$ (N/mm²) | σ_u (N/mm²) | A_5 (%) | Hardness | |
						HB30	HRB
SHS 80×80×4	Stala Tube	291	343	628	54	174	-
SHS 100×100×2	Padana Tubi	275	317	623	53	-	82
SHS 100×100×3	Marcegaglia	286	-	634	58	-	-
SHS 100×100×4	Stala Tube	299	343	620	55	176	-
SHS 100×100×6	Stala Tube	279	321	605	55	172	-
SHS 100×100×8	Stala Tube	295	338	620	58	-	-
SHS 150×150×4	Stala Tube	304	349	613	54	169	-
RHS 60×40×4	Stala Tube	279	322	615	57	168	-
RHS 120×80×3	La Meusienne	485	510	685	43	-	89
RHS 120×80×6	Stala Tube	289	331	616	55	177	-
RHS 150×100×4	Stala Tube	289	342	600	53	176	-
RHS 100×50×2	Stala Tube	319	369	634	55	167	-
RHS 100×50×3	La Meusienne	485	510	685	43	-	89
RHS 100×50×4	Marcegaglia	258	-	596	55	-	-
RHS 100×50×6	Stala Tube	318	359	612	54	165	-

3.3 MATERIAL TESTS

Tests were conducted to determine the basic stress-strain behaviour of material cut from the flat faces and corner regions of finished SHS and RHS. Tensile and compressive coupon tests were performed because it has been observed (Johnson & Winter, 1966) that stainless steels show non-symmetrical stress-strain behaviour, particularly in cold-worked material. Tensile tests were also conducted on corner coupons to investigate the extra degree of strength that is achieved in these strongly cold-worked regions.

3.3.1 Tensile coupons

Tensile coupon tests were conducted in accordance with ASTM A370-87a (ASTM, 1987).

3.3.1.1 Preparation of coupons

Parallel coupons were machined from the four faces of the cross-sections using a tipped slot-drill. Some machining difficulties were encountered due to the through-thickness (bending) residual stresses that were locked into the cross-sections during the manufacturing process route. The residual stresses caused the coupons to curve outwards as machining progressed. The problem was minimised by providing greater restraint and support to the sections. The coupons were not straightened by inelastic bending deformations prior to testing, to ensure that the material was tested in the same state as it was within the cross-section. Figure 3.1 shows the effect of the bending residual stresses on a set of typical tensile coupons. The nominal dimensions of the tensile coupons were 320×30 mm where possible, or 320×20 mm for the smaller cross-sections. Holes were drilled and reamed 20 mm from each end of the coupons for pins to be inserted to prevent slippage of the coupons in the jaws of the testing machine.
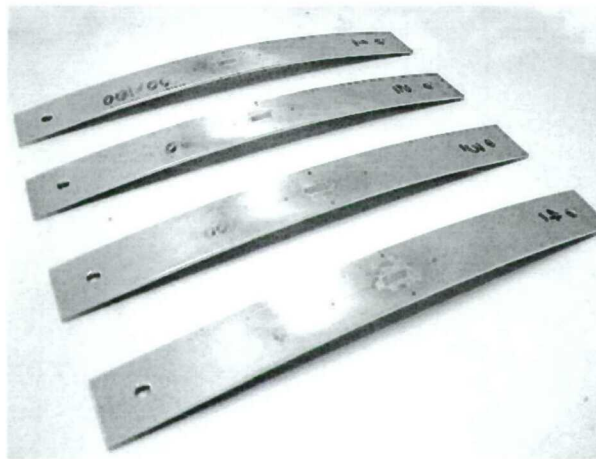
Figure 3.1: *Effect of bending residual stresses on tensile coupons*

3.3.1.2 Instrumentation and data acquisition

Linear electrical post-yield strain gauges, capable of reaching 20% strain, were affixed to the midpoint of each side of the tensile coupons. Strain indicator lines were also marked at 10mm intervals. Pressure, strain, displacement and input voltage were all recorded using the data

acquisition equipment DATASCAN and logged using the DALITE computer package. All data were recorded at 4 second intervals.

3.3.1.3 Testing

The tensile tests were performed using an Amsler 350kN hydraulic testing machine. Strain rates were within the limits prescribed by ASTM A370-87a (ASTM, 1987), with fracture occurring, on average, after about 45 minutes.

3.3.2 Compressive coupons

The compressive coupon tests needed to be performed in a bracing jig to prevent minor axis buckling of the test piece. The jig had to be sufficiently tight to prevent buckling, but also loose enough to allow unrestrained expansion due to Poisson's effect.

3.3.2.1 Preparation of coupons

The coupons were machined from the four faces of the cross-sections using the same procedure as for the tensile coupons. The nominal dimensions of the coupons were 72×16 mm. Early tests highlighted the importance of having the ends of the compressive coupons parallel to one another to a tight tolerance, in order that the coupon would be compressed uniformly. To this end, each coupon was milled with a second skim-pass.

3.3.2.2 Bracing jig and instrumentation

The bracing jig was designed after considering previous jigs (Rockey & Jenkins, 1957; Rasmussen & Hancock, 1990) and making appropriate improvements. A general view of the jig is shown in Figure 3.2.

The height of the bracing jig was 70 mm. The test pieces protrude 2mm above the jig to allow the compressive load to be applied safely to approximately 2% strain, without applying load to the jig itself. The test pieces also protrude 1 mm either side of the central part of the bracing jig to enable strain gauges to be attached to the edges of the coupons.
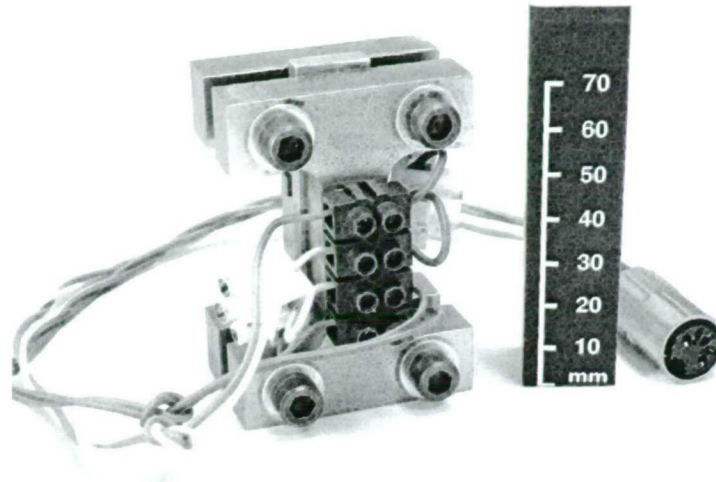
Figure 3.2: *General view of compressive coupon bracing jig*

Two linear electrical resistance strain gauges were attached at mid-height to each compressive coupon, with one on each edge. The dimensions of the compressive coupon test pieces, and the positions of the strain gauges are shown in Figure 3.3.
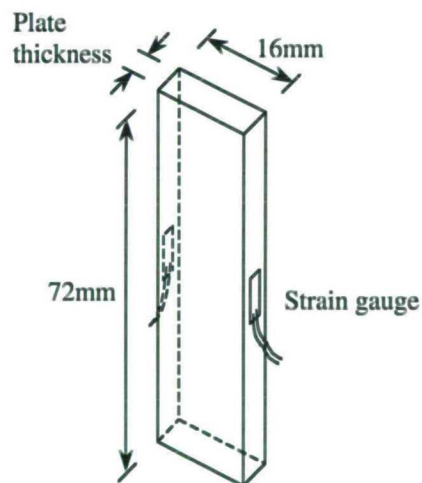
Figure 3.3: *Compressive coupon test piece*

3.3.2.3 Friction

Tests on coupons in compression have been conducted in previous studies. Talja & Salmi (1995) layered the contact surfaces of their bracing jig with Teflon to reduce friction between the jig and the test piece. With the same aim, Rasmussen & Hancock (1990) smeared the

contact surfaces of their bracing jig with a thin layer of lubricating paste prior to assembly. Lubricating paste was also employed in the current study.

The level of friction was assessed by placing spacers between the bracing jig and lower platen of the testing machine (leaving the test piece with nothing positive to react against), and measuring the load required to push the test piece through the bracing jig. The load required was very small, and it was concluded that friction had a negligible effect on the behaviour of the compressive coupons.

3.3.2.4 Testing and data acquisition

The test arrangement is shown in Figure 3.4. Load was applied though a 10T Amsler hydraulic loading rig. The load was measured using a 10T load cell. Data acquisition was as for the tensile tests, with readings taken at 2 second intervals.
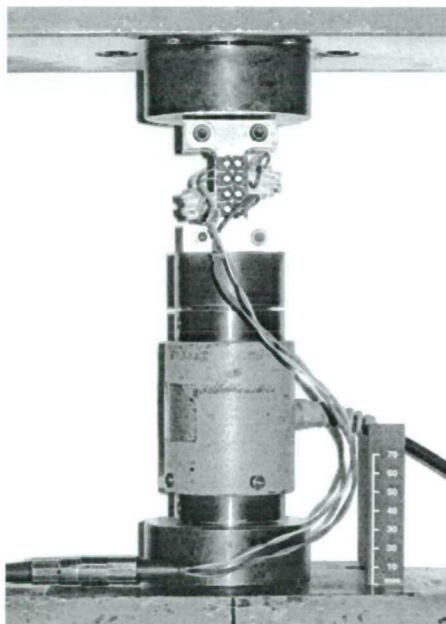
Figure 3.4: *Compressive coupon test arrangement*

Alignment loads were applied to the coupons up to a maximum of approximately 10% of the predicted 0.2% proof strength of the material. The edge strains were compared. Small adjustments to the position of the coupons were made until the disparity between the two edge strains was less than 5%. This ensured that the load was applied approximately concentrically.

Loading rates were chosen such that 2% compressive strain was achieved after approximately 30 minutes, at which point the test was terminated.

3.3.3 Corner coupons

3.3.3.1 Preparation of coupons

The corner coupons were machined from the SHS and RHS in the same manner as the flat coupons. As with the flat coupons, bending residual stresses caused the coupons to curve outwards upon removal from the cross-section. The nominal length of the coupons was 320 mm.

3.3.3.2 Loading configuration and instrumentation

The non-symmetrical shape of corner specimens means that bending stresses would be introduced into the coupons upon straightforward application of tensile stress. Additionally, flattening of the ends of the coupons to enable them to be gripped would deform the shape of the coupon upon testing, and alter its material properties.

This led to the idea of testing the corner coupons in pairs. The ends of the coupons were gripped symmetrically around steel bars, which had the same radius as the internal corner radii of the test pieces, as shown in Figure 3.5. Each pair was removed from the same corner of the cross-section with the aim of achieving similar material properties. In general, ultimate failure of the coupon pairs was simultaneous.
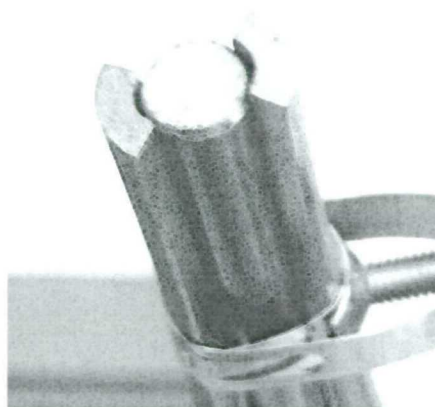
Figure 3.5: *Tensile testing configuration for corner coupons*

Linear electrical post-yield strain gauges were affixed to the midpoint of each side of the tensile coupons. No difficulty was encountered in attaching strain gauges to the inner and outer radii of the test pieces. Strain indicator lines were marked at 10mm intervals.

3.3.3.3 Testing and data acquisition

The loading rates were similar to those employed in the flat material tensile tests, with fracture of the coupons occurring after approximately 45 minutes of testing. Data acquisition was also as for the flat tensile coupon tests.

3.3.4 Labelling convention

Tensile and compressive coupon tests were conducted on material cut from the flat faces of the finished SHS and RHS. A labelling convention was devised for the faces of the cross-section, whereby the welded face was labelled 'Face 1', the face opposite the welded one was labelled 'Face 4', and the two faces adjacent to the welded face were labelled 'Face 2' and 'Face 3'. The labelled convention is illustrated in Figure 3.6.

Face 4

Face 3

Face 2

Face 1 (welded)
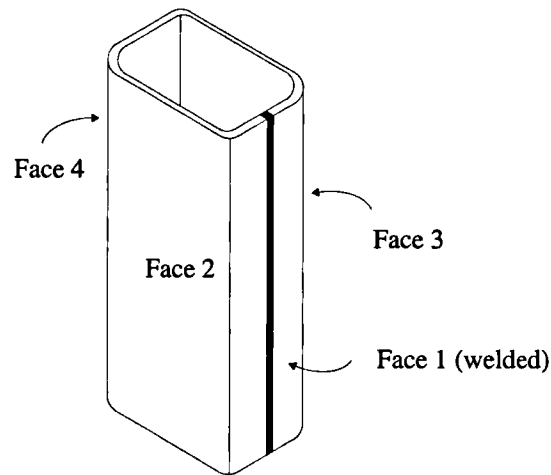
Figure 3.6: *Labelling convention for faces of cross-sections*

3.3.5 Results

Weighted average material properties from the coupon tests are presented in Tables 3.3 and 3.4. The weighted average values were determined by considering the nominal area of material that

Table 3.3: *Weighted average measured material properties for SHS coupons*

Coupons	E_o (N/mm²)	$\sigma_{0.2}$ (N/mm²)	$\sigma_{1.0}$ (N/mm²)	σ_u (N/mm²)	ε_{pu} (%)	Modified R-O coefficients		
						n	$n'_{0.2,u}$	$n'_{0.2,1.0}$
SHS 80×80×4- TF	186600	457	525	706	0.43	5.0	3.2	3.5
SHS 80×80×4- TC	215000	594	723	820	0.30	4.5	6.0	4.5
SHS 80×80×4- CF	203200	416	544	-	-	3.5	-	3.1
SHS 80×80×4- A- TF	-	-	-	-	-	-	-	-
SHS 80×80×4- A- TC	-	-	-	-	-	-	-	-
SHS 80×80×4- A- CF	206300	261	316	-	-	11.5	-	1.5
SHS 100×100×2- TF	201300	382	424	675	0.56	6.6	2.3	2.8
SHS 100×100×2- TC	197400	587	745	820	0.18	3.5	6.0	5.0
SHS 100×100×2- CF	207100	370	446	-	-	4.7	-	2.4
SHS 100×100×3- TF	195800	388	433	691	0.57	5.6	2.4	3.2
SHS 100×100×3- TC	-	-	-	-	-	-	-	-
SHS 100×100×3- CF	208800	379	468	-	-	3.8	-	2.6

Table 3.3 (continued): *Weighted average measured material properties for SHS coupons*

Coupons	E_0 (N/mm²)	$\sigma_{0.2}$ (N/mm²)	$\sigma_{1.0}$ (N/mm²)	σ_u (N/mm²)	ε_{pu} (%)	Modified R-O coefficients		
						n	$n'_{0.2,u}$	$n'_{0.2,1.0}$
SHS 100×100×4- TF	191300	465	519	713	0.45	5.7	2.9	3.7
SHS 100×100×4- TC	-	-	-	-	-	-	-	-
SHS 100×100×4- CF	203400	437	563	-	-	3.9	-	2.9
SHS 100×100×6- TF	198400	501	571	715	0.39	5.2	3.7	3.9
SHS 100×100×6- TC	-	-	-	-	-	-	-	-
SHS 100×100×6- CF	197900	473	590	-	-	4.4	-	2.6
SHS 100×100×8- TF	202400	328	378	653	0.52	6.4	2.2	2.6
SHS 100×100×8- TC	-	-	-	-	-	-	-	-
SHS 100×100×8- CF	205200	330	392	-	-	6.4	-	2.1
SHS 150×150×4- TF	206000	314	358	659	0.54	6.8	2.2	2.2
SHS 150×150×4- TC	194000	563	649	844	0.20	5.2	2.9	3.5
SHS 150×150×4- CF	195400	294	366	-	-	4.5	-	2.3

Note: All symbols defined in Section 4.2.4

Key: TF – Tension Flat
        TC – Tension Corner
        CF – Compression Flat

Table 3.4: *Weighted average measured material properties for RHS coupons*

Coupons	E_0 (N/mm^2)	$\sigma_{0.2}$ (N/mm^2)	$\sigma_{1.0}$ (N/mm^2)	σ_u (N/mm^2)	ε_{pu} (%)	Modified R-O coefficients		
						n	$n'_{0.2,u}$	$n'_{0.2,1.0}$
RHS 60×40×4- TF	192800	489	591	705	0.40	3.9	5.1	4.6
RHS 60×40×4- TC	-	-	-	-	-	-	-	-
RHS 60×40×4- CF	193100	469	617	-	-	3.6	-	3.0
RHS 120×80×3- TF	209300	419	488	739	0.54	4.1	2.9	3.6
RHS 120×80×3- TC	-	-	-	-	-	-	-	-
RHS 120×80×3- CF	197300	429	536	-	-	4.2	-	2.9
RHS 120×80×6- TF	194500	509	572	714	0.40	5.3	3.5	3.6
RHS 120×80×6- TC	-	-	-	-	-	-	-	-
RHS 120×80×6- CF	192300	466	591	-	-	4.4	-	2.8
RHS 150×100×4- TF	205800	297	345	663	0.62	8.0	2.3	2.4
RHS 150×100×4- TC	191700	572	690	809	0.20	4.6	4.8	4.0
RHS 150×100×4- CF	200300	319	386	-	-	4.7	-	2.0

Table 3.4 (continued): *Weighted average measured material properties for RHS coupons*

Coupons	E_0 (N/mm²)	$\sigma_{0.2}$ (N/mm²)	$\sigma_{1.0}$ (N/mm²)	σ_u (N/mm²)	ε_{pu} (%)	Modified R-O coefficients		
						n	$n'_{0.2,u}$	$n'_{0.2,1.0}$
RHS 100×50×2- TF	208000	403	443	707	0.57	6.9	2.2	2.6
RHS 100×50×2- TC	-	-	-	-	-	-	-	-
RHS 100×50×2- CF	205900	370	442	-	-	5.2	-	2.4
RHS 100×50×3- TF	203600	479	563	716	0.48	4.2	4.1	4.2
RHS 100×50×3- TC	-	-	-	-	-	-	-	-
RHS 100×50×3- CF	200900	455	572	-	-	4.1	-	3.0
RHS 100×50×4- TF	208000	471	530	702	0.45	5.2	3.2	3.5
RHS 100×50×4- TC	-	-	-	-	-	-	-	-
RHS 100×50×4- CF	203900	439	562	-	-	3.8	-	3.3
RHS 100×50×6- TF	187200	605	686	754	0.36	5.7	6.0	4.5
RHS 100×50×6- TC	197700	631	773	802	0.18	3.5	10.0	6.0
RHS 100×50×6- CF	206300	494	649	-	-	4.0	-	3.2

Note: All symbols defined in Section 4.2.4

Key: TF – Tension Flat
TC – Tension Corner
CF – Compression Flat

each coupon represented within the cross-section. The modified Ramberg-Osgood coefficients are defined in Section 4.2.4.

The average tensile 0.2% proof strength, $\sigma_{0.2}$ from all tests conducted in the current study (given in Tables 3.3 and 3.4) is approximately 430 N/mm^2, with the average ultimate strength, σ_u at approximately 700 N/mm^2. BS EN 10088 Stainless Steels – Part 2 (1995) Technical delivery conditions for sheet/plate and strip for general purposes gives minimum specified values of 0.2% proof strength and ultimate tensile strength for various grades. Values are dependent upon whether the material was hot-rolled or cold-rolled, and since this is often not known, it is usual to take the lower values. For Grade 1.4301 these are $\sigma_{0.2}$ = 230 N/mm^2 and σ_u between 520 and 720 N/mm^2.

The comparison reveals that the measured 0.2% proof strengths are approximately double those given in the material standard. This is, however, not a deficiency in the material standard since this is intended for flat sheet, though it does demonstrate the pronounced response of stainless steel to strain hardening, and highlights the need for a material standard for cold-formed products that takes this into account. The average measured ultimate tensile strength is within the range specified by the material standard. This would be expected since the ultimate tensile behaviour is less sensitive to strain hardening.

3.4 SHS AND RHS STUB COLUMN TESTS

A total of 17 SHS and 16 RHS stub columns were tested in pure axial compression. Of the 16 RHS, 8 had an aspect ratio of 0.67, and 8 had an aspect ratio of 0.5.

3.4.1 Testing Procedure

3.4.1.1 Preparation of stub column specimens

The stub column specimens were cut roughly to length using a rotary hacksaw. Their ends were milled flat and square to a tolerance of ±0.02 mm to achieve accurate seating in the testing machine. Prior to testing, strain visualisation grids were marked onto the faces of the specimens, and measurements of geometry, including initial imperfections were taken. Figure 3.7 shows a specimen prior to testing.
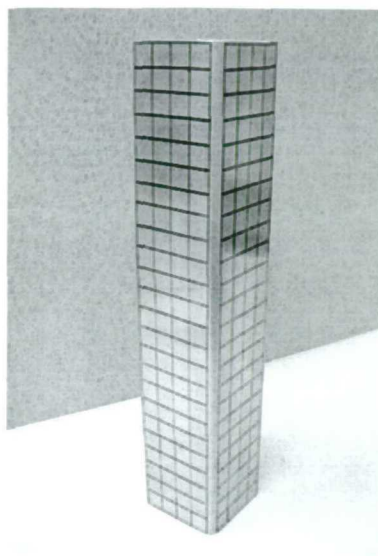
Figure 3.7: *Undeformed stub column specimen prior to testing*

The nominal lengths of the stub columns were chosen such that they were sufficiently short not to fail by overall buckling, yet still long enough to contain a representative residual stress pattern. Guidelines provided by the Structural Stability Research Council (Galambos, 1998) state that for cold-formed shapes, the length of the stub column should not be less than three times the largest dimension of the cross-section and no more than 20 times the least radius of gyration.

Two specimens, SHS 80×80×4-ASC1 and SHS 80×80×4-ASC2, were annealed in a furnace at approximately 1000°C for 15 minutes to investigate the difference in behaviour between annealed and cold-worked material.

3.4.1.2 Test set-up

The tests were carried out in a 300T Amsler hydraulic testing machine. The set-up was load-controlled through an Amsler control cabinet. The dimensions of the testing machine limited the maximum length of specimen to approximately 550 mm. The end platens of the testing machine were fixed flat and parallel. A general view of the SHS and RHS test set-up is shown in Figure 3.8.

3.4.1.3 Alignment

Alignment of the specimens was necessary to ensure that the compressive load was introduced concentrically. This was carried out by applying a small alignment load to the specimens, approximately 10% of the predicted failure load, $F_{u,\,pred}$, and observing the variation in corner strains. The specimens were adjusted until the variation between strains at any corner from the average strain was less than 5%. Linearity of the stress-strain plot was used to confirm that the alignment load was below the proportional limit.

3.4.1.4 Loading rates

Loading rates were set such that ultimate load would be reached after 30-45 minutes, and the test would be completed following an appropriate amount of unloading after 60-80 minutes.
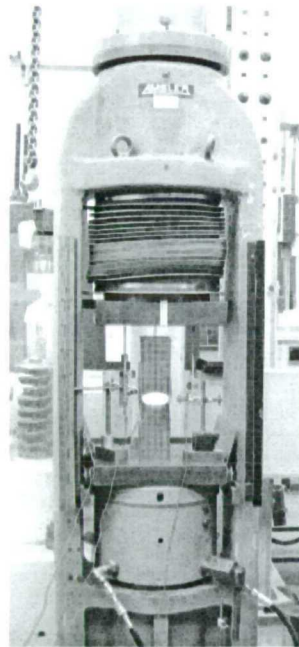
Figure 3.8: *General view of SHS and RHS test set-up*

3.4.2 Instrumentation

3.4.2.1 Displacement transducers

Three linear displacement transducers were used to determine the end shortening of the stub columns, between the end platens of the testing machine. Figure 3.9 shows a schematic view of their layout.
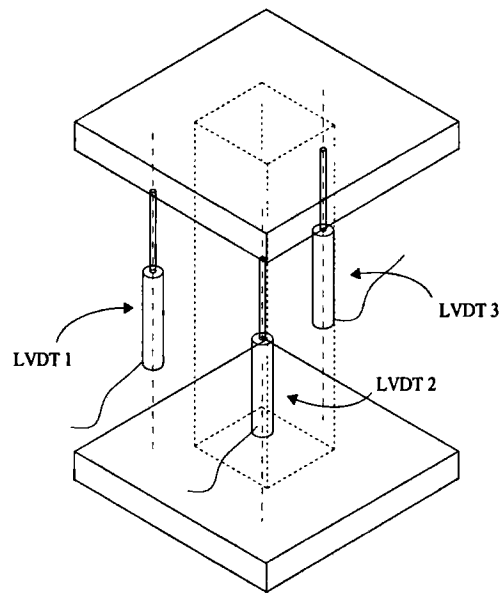
Figure 3.9: *Location of displacement transducers*

3.4.2.2 Strain gauges

Talja & Salmi (1995) attached four strain gauges to their stub column specimens at the mid-height, and in the locations shown in Figure 3.10.
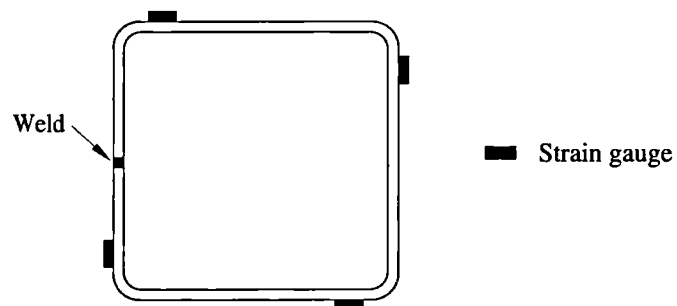
Figure 3.10: *Talja & Salmi (1995) layout of strain gauges for SHS and RHS specimens*

In the current study, four linear electrical resistance strain gauges were also affixed to each specimen at mid-height, but in the orientation shown in Figure 3.11. The strain gauges were positioned at a distance of four times the material thickness from the corners and were initially used for alignment purposes.
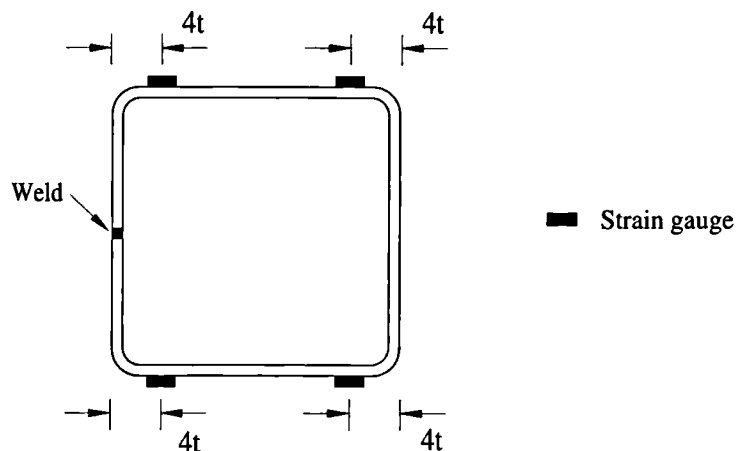
Figure 3.11: *Location of strain gauges on SHS and RHS specimens*

It is clear that the translational symmetry of the chosen orientation makes for more straightforward adjustments during alignment.

3.4.2.3 Data acquisition

Load, strain, displacement, and input voltage were all recorded using the data acquisition equipment DATASCAN and logged using the DALITE computer package. All data were recorded at 2 second intervals.

3.4.3 Measured Dimensions

The average measured dimensions for the SHS and RHS stub column specimens are presented in Tables 3.5 to 3.7. It is worth noting that all measured internal corner radii are less than two times the material thickness, which is the minimum recommended bend radius for austenitic stainless advised by Baddoo & Burgan (2001).

3.4.4 Initial Geometric Imperfection Measurements

Measurements of local initial geometric imperfections on cold-formed sections have been previously carried out to varying degrees of sophistication. For stub columns, measurement of initial imperfections is often omitted. Schafer & Peköz (1998) conducted a detailed assessment

Table 3.5: *Measured dimensions for SHS stub columns*

Specimen identification	Depth, D (mm)	Breadth, B (mm)	Thickness, t (mm)	Length, L (mm)	Internal corner radius, r_i (mm)	Area, A (mm^2)
80×80×4- SC1	79.8	79.9	3.68	400.2	4.6	1080
80×80×4- SC2	80.1	80.1	3.82	399.9	4.4	1124
80×80×4- SC3	80.1	79.9	3.83	399.4	4.4	1125
80×80×4- ASC1	79.5	79.7	3.77	400.4	4.1	1105
80×80×4- ASC2	79.7	79.6	3.68	399.8	4.4	1080
100×100×2- SC1	100.2	100.0	1.91	400.5	1.3	743
100×100×2- SC2	99.9	100.0	1.91	400.2	1.3	739
100×100×3- SC1	100.1	100.3	2.87	400.0	1.5	1101
100×100×3- SC2	100.1	100.1	2.84	399.8	1.5	1089
100×100×4- SC1	99.8	99.9	3.84	399.8	4.5	1431
100×100×4- SC2	99.7	99.8	3.83	400.4	4.5	1426
100×100×6- SC1	100.1	100.1	5.94	399.8	5.8	2147
100×100×6- SC2	100.2	100.1	5.92	399.6	5.8	2153
100×100×8- SC1	100.3	100.7	7.97	399.1	8.0	2785
100×100×8- SC2	100.1	100.7	7.97	400.0	8.0	2781
150×150×4- SC1	150.4	149.9	3.79	449.9	5.8	2167
150×150×4- SC2	150.2	150.0	3.74	450.7	6.0	2139

Table 3.6: *Measured dimensions for RHS stub columns with aspect ratio of 0.67*

Specimen identification	Depth, D (mm)	Breadth, B (mm)	Thickness, t (mm)	Length, L (mm)	Internal corner radius, r_i (mm)	Area, A (mm^2)
60×40x4- SC1	60.0	40.0	3.83	180.3	2.9	675
60×40x4- SC2	60.0	40.0	3.82	179.6	2.9	675
120×80x3- SC1	120.1	80.2	2.93	359.9	4.6	1109
120×80x3- SC2	120.0	80.2	2.91	360.0	4.6	1100
120×80x6- SC1	119.9	80.4	5.85	360.1	7.0	2107
120×80x6- SC2	120.0	80.3	5.85	360.1	7.0	2108
150×100x4- SC1	149.9	99.9	3.82	450.4	5.6	1799
150×100x4- SC2	149.9	99.9	3.83	450.0	5.6	1805

Table 3.7: *Measured dimensions for RHS sub columns with aspect ratio of 0.5*

Specimen identification	Depth, D (mm)	Breadth, B (mm)	Thickness, t (mm)	Length, L (mm)	Internal corner radius, r_i (mm)	Area, A (mm^2)
100×50×2- SC1	99.8	49.8	1.85	300.6	2.3	529
100×50×2- SC2	99.8	50.0	1.84	299.8	2.3	529
100×50×3- SC1	100.1	50.1	2.89	299.9	3.1	811
100×50×3- SC2	100.1	50.0	2.89	300.0	3.1	811
100×50×4- SC1	99.7	49.9	3.73	300.4	3.6	1026
100×50×4- SC2	99.8	49.8	3.68	300.6	3.6	1014
100×50×6- SC1	100.1	50.1	5.95	300.0	5.6	1558
100×50×6- SC2	100.0	50.1	5.96	300.1	5.5	1559

of initial geometric imperfections on cold-formed channel sections. In their experimental set-up, the specimens were mounted on the table of a milling machine, and a displacement transducer, fitted in the head of the milling machine, was employed to trace the local geometric imperfections. A similar arrangement was adopted in this study.

3.4.4.1 Measurement apparatus

A general view of the set-up of the measurement apparatus is shown in Figure 3.12. A mechanical dial gauge indicator was fitted into the head of the milling machine, and the stub column specimens were clamped to the bed. An automatic feed was used to pass the specimen under the dial gauge indicator, along its length. Readings were taken at regular intervals. Imperfections measurements were made on all four faces of the cross-sections. In general, measurements were only taken along the centreline of each of face, though in some cases more readings were taken to give an imperfection profile for the complete surface of each face.

Head of milling machine

Dial gauge indicator   Specimen

Bed of milling machine
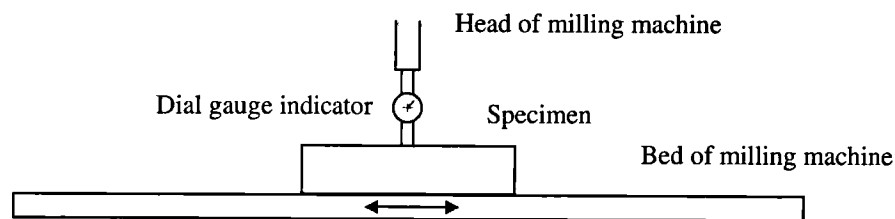
Figure 3.12 *Initial imperfection measurement set-up*

3.4.4.2 Observations

The initial imperfections measurements highlighted that the ends of the prepared specimens were flared outwards. This is believed to be due to the through-thickness residual stresses, generated during the cold-rolling process, and released upon cutting of the section. The outward flaring response indicates tensile residual stresses on the outer surface of the sections, and compressive residual stresses on the inner surface.

3.4.4.3 Summary of initial geometric imperfections

Tables 3.8 and 3.9 present a summary of initial geometric imperfection magnitudes that were measured along the centrelines of the faces of the SHS and RHS stub column specimens. The maximum magnitude of imperfection for each of the faces of the cross-section, and the mean

maximum magnitude of imperfection are reported. The datum for the imperfection measurements is a straight line connecting the ends of each stub column face.

Table 3.8: *Maximum magnitudes of initial geometric imperfections for SHS stub columns*

Specimen identification	Maximum imperfection magnitude (mm)				
	Face 1	Face 2	Face 3	Face 4	Mean
SHS 80×80×4- SC1	-	-	-	-	-
SHS 80×80×4- SC2	-	-	-	-	-
SHS 80×80×4- SC3	0.26	0.24	0.24	0.31	0.26
SHS 80×80×4- ASC1	0.41	0.27	0.25	0.45	0.34
SHS 80×80×4- ASC2	0.03	0.26	0.06	0.06	0.10
SHS 100×100×2- SC1	0.45	0.19	0.19	0.30	0.28
SHS 100×100×2- SC2	0.30	0.20	0.19	0.26	0.24
SHS 100×100×3- SC1	0.38	0.27	0.29	0.36	0.33
SHS 100×100×3- SC2	0.42	0.28	0.29	0.37	0.34
SHS 100×100×4- SC1	0.38	0.20	0.24	0.47	0.32
SHS 100×100×4- SC2	0.40	0.21	0.27	0.38	0.31
SHS 100×100×6- SC1	0.34	0.25	0.24	0.35	0.29
SHS 100×100×6- SC2	0.37	0.22	0.26	0.35	0.30
SHS 100×100×8- SC1	0.26	0.35	0.18	0.35	0.28
SHS 100×100×8- SC2	0.20	0.11	0.06	0.15	0.13
SHS 150×150×4- SC1	0.63	0.29	0.31	0.60	0.46
SHS 150×150×4- SC2	0.62	0.27	0.14	0.52	0.38

3.4.5 Stub Column Results

3.4.5.1 General behaviour

Compression tests on stub columns reveal the average compressive response of the cross-sections. Ultimate failure is due to local buckling of the cross-section. For cross-sections

comprising slender elements local buckling may occur in the elastic range. For more stocky cross-sections, local buckling may occur following significant inelastic deformation.

Table 3.9: *Maximum magnitudes of initial geometric imperfections for RHS stub columns*

Specimen identification	Maximum imperfection magnitude (mm)				
	Face 1	Face 2	Face 3	Face 4	Mean
RHS 60×40×4- SC1	0.08	0.24	0.23	0.08	0.16
RHS 60×40×4- SC2	0.09	0.22	0.24	0.07	0.15
RHS 120×80×3- SC1	0.07	0.67	0.72	0.11	0.39
RHS 120×80×3- SC2	0.10	0.70	0.76	0.09	0.41
RHS 120×80×6- SC1	0.21	0.40	0.50	0.16	0.32
RHS 120×80×6- SC2	0.21	0.44	0.54	0.19	0.34
RHS 150×100×4- SC1	0.29	0.38	0.36	0.25	0.32
RHS 150×100×4- SC2	0.29	0.34	0.40	0.21	0.31
RHS 100×50×2- SC1	0.07	0.28	0.46	0.03	0.21
RHS 100×50×2- SC2	0.06	0.39	0.28	0.08	0.20
RHS 100×50×3- SC1	0.09	0.66	0.66	0.09	0.37
RHS 100×50×3- SC2	0.09	0.81	0.73	0.08	0.43
RHS 100×50×4- SC1	0.07	0.27	0.25	0.02	0.15
RHS 100×50×4- SC2	0.03	0.33	0.32	0.05	0.18
RHS 100×50×6- SC1	0.05	0.27	0.33	0.09	0.18
RHS 100×50×6- SC2	0.02	0.27	0.33	0.06	0.17

3.4.5.2 True end shortening

The Centre for Advanced Structural Engineering, University of Sydney (1990) observed that there was a discrepancy between stub column end shortening obtained from strain gauge measurements and from displacement transducer measurements. This discrepancy was thought to exist because the displacement transducer measurements also include the deformation of the end platens. The same phenomenon was observed in the current test programme.

The deformation of each end platen, δ_{Platen} was elastic, and thus proportional to the applied stress, σ. This can be expressed as in Equation 3.1, where k is a constant. This leads to the definition of true end shortening, e_{True} as a function of the displacement transducer end shortening, e_{LVDT} and the end platen deformation, δ_{Platen}, given in Equation 3.2.

$$\delta_{Platen} \quad = \quad k \, \sigma \tag{3.1}$$

$$e_{True} \quad = \quad e_{LVDT} - 2 \, \delta_{Platen} \tag{3.2}$$

The constant k can be derived following Equations 3.3 to 3.6, where the true strain is taken as that measured by the strain gauges.

$$\delta_{Platen} \quad = \quad \frac{1}{2}(e_{LVDT} - e_{True}) \tag{3.3}$$

$$= \quad \frac{L}{2}(\varepsilon_{LVDT} - \varepsilon_{True}) \tag{3.4}$$

$$= \quad \frac{L}{2}\sigma\left(\frac{1}{E_{0,LVDT}} - \frac{1}{E_{0,True}}\right) \tag{3.5}$$

$$\therefore \quad k \quad = \quad \frac{L}{2}\left(\frac{1}{E_{0,LVDT}} - \frac{1}{E_{0,True}}\right) \tag{3.6}$$

where L is the length of the stub column specimen, and $E_{0,\,LVDT}$ and $E_{0,\,True}$ are the initial tangent moduli as determined from the displacement transducer and strain gauge measurements respectively.

Hence the true deformations of the stub columns have been determined, and all future usage of stub column end shortening relates to the true values. Average load-end shortening curves cannot be directly produced from the strain gauge measurements since local buckling distorts the readings.

3.4.5.3 Load-end shortening curves

Load-end shortening curves from the stub column tests are shown in Figures 3.13 to 3.28.

Figure 3.15: *SHS 100x100x2 stub column load-end shortening curves*
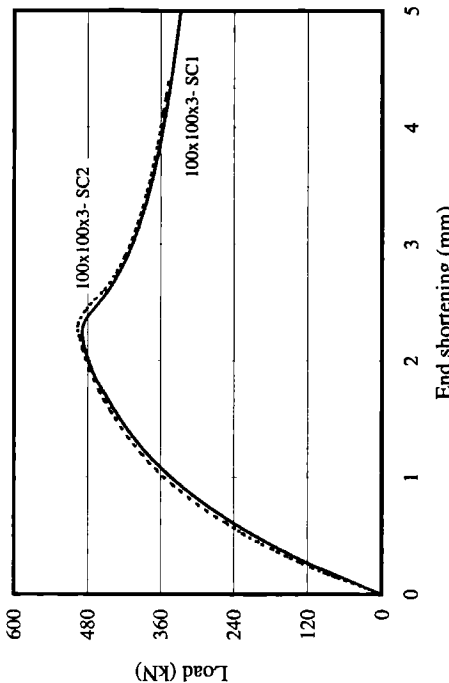
Figure 3.16: *SHS 100x100x3 stub column load-end shortening curves*

Figure 3.13: *SHS 80x80x4 stub column load-end shortening curves*

Figure 3.14: *Annealed SHS 80x80x4 stub column load-end shortening curves*

Figure 3.19: *SHS 100x100x8 stub column load-end shortening curves*

Figure 3.20: *SHS 150x150x4 stub column load-end shortening curves*

Figure 3.17: *SHS 100x100x4 stub column load-end shortening curves*

Figure 3.18: *SHS 100x100x6 stub column load-end shortening curves*
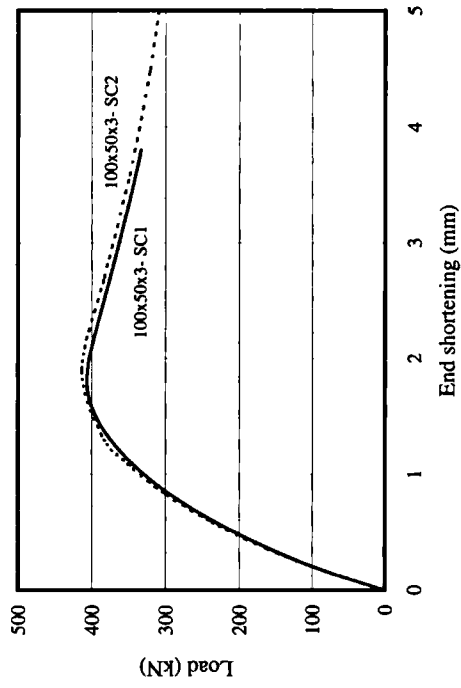
Figure 3.23: *RHS 100×50×3 stub column load-end shortening curves*
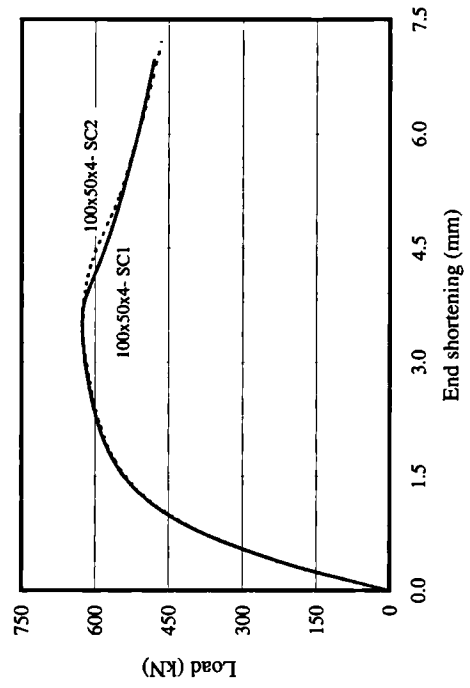
Figure 3.24: *RHS 100×50×4 stub column load-end shortening curves*
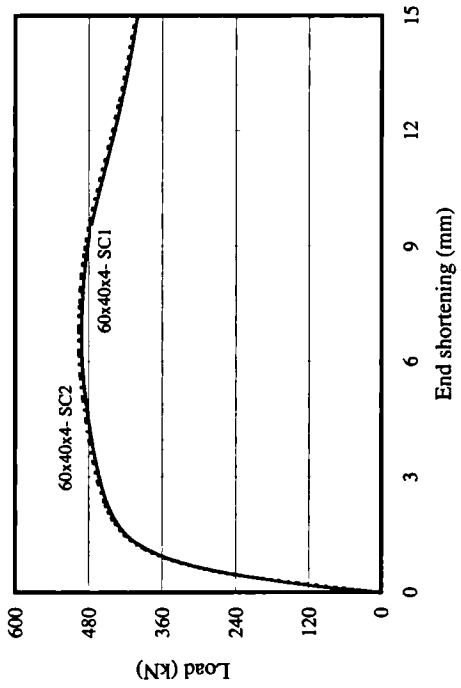
Figure 3.21: *RHS 60×40×4 stub column load-end shortening curves*

Figure 3.22: *RHS 100×50×2 stub column load-end shortening curves*

Figure 3.25: *RHS 100x50x6 stub column load-end shortening curves*
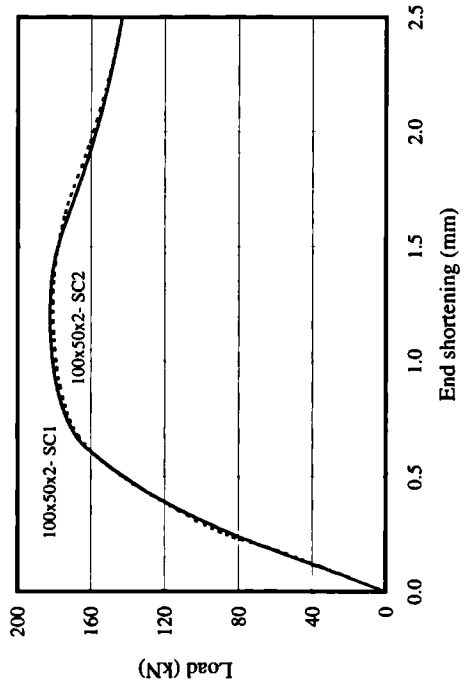
Figure 3.26: *RHS 120x80x3 stub column load-end shortening curves*
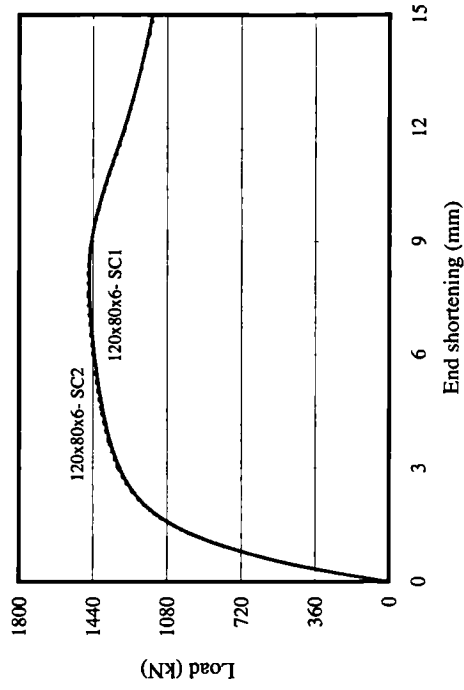
Figure 3.27: *RHS 120x80x6 stub column load-end shortening curves*
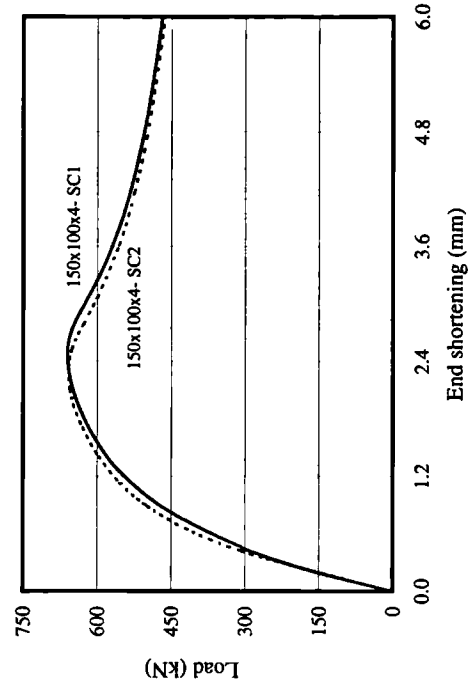
Figure 3.28: *RHS 150x100x4 stub column load-end shortening curves*

3.4.5.4 Behaviour of annealed specimens

Figure 3.29 shows the load-end shortening curves for five SHS 80×80×4 stub columns of similar nominal cross-section and length. Two of the stub columns (labelled 'Annealed'), SHS 80×80×4-ASC1 and SHS 80×80×4-ASC2, were annealed whereas the remaining three (labelled 'Cold-worked'), SHS 80×80×4-SC1, SHS 80×80×4-SC2 and SHS 80×80×4-SC3, remained in their cold-worked state.
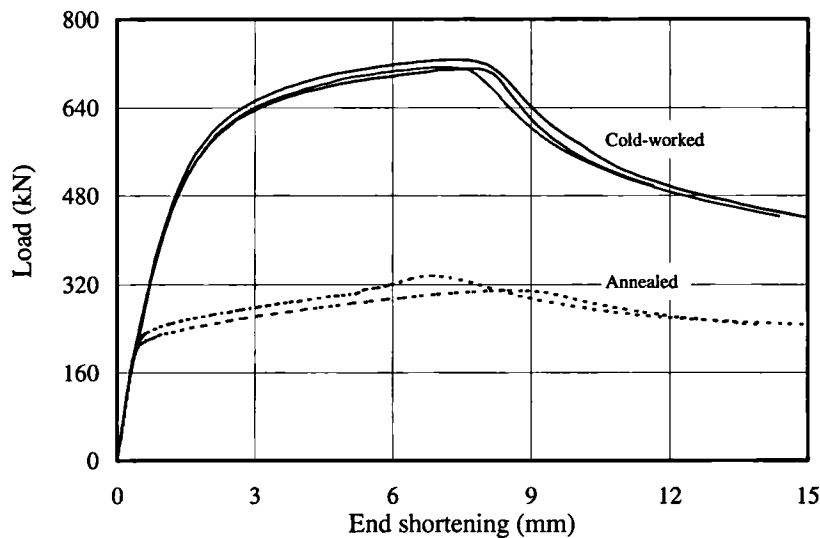
Figure 3.29: *Comparison between annealed and cold-worked stub columns*

Figure 3.29 shows the load-end shortening curves for the cold-worked specimens are far more rounded than the annealed ones. The ultimate load carrying capacities of the cold-worked stub columns are approximately two times those of the annealed specimens.

3.4.5.5 Deformed stub column specimens

All stub columns exhibited a similar failure mode whereby the four faces of the cross-sections buckled locally, alternately inwards and outwards. Photographs of typical failure modes (SHS 100×100×2 and RHS 100×50×6) are shown in Figures 3.30 and 3.31, respectively.

3.4.5.6 Summary of results

A summary of the results from the stub column tests is presented in Tables 3.10 and 3.11. For each test, the ultimate load and the end shortening at ultimate load have been tabulated.
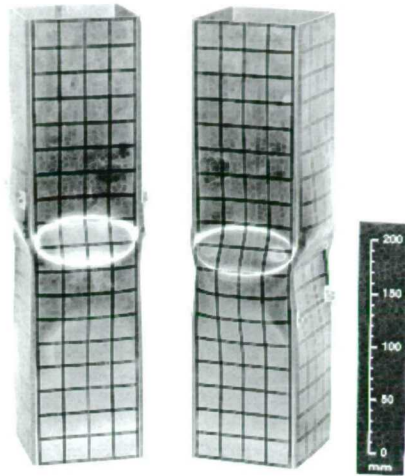
Figure 3.30: *Deformed 100×100×2 stub columns*
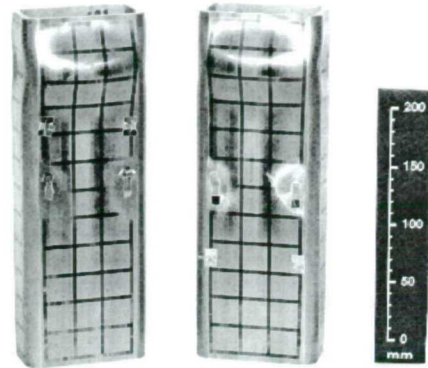
Figure 3.31: *Deformed 100×50×6 stub columns*

Table 3.10: *Summary of results from SHS stub column tests*

Specimen identification	Ultimate load, F_u (kN)	End shortening at F_u (mm)
SHS 80×80×4- SC1	727	7.4
SHS 80×80×4- SC2	714	7.2
SHS 80×80×4- SC3	711	7.7
SHS 80×80×4- ASC1	309	8.6
SHS 80×80×4- ASC2	335	7.1
SHS 100×100×2- SC1	197	1.1
SHS 100×100×2- SC2	187	0.9
SHS 100×100×3- SC1	489	2.2
SHS 100×100×3- SC2	496	2.3
SHS 100×100×4- SC1	779	4.0
SHS 100×100×4- SC2	774	4.0
SHS 100×100×6- SC1	1513	13.4
SHS 100×100×6- SC2	1507	13.5
SHS 100×100×8- SC1	1630	29.0
SHS 100×100×8- SC2	1797	38.2
SHS 150×150×4- SC1	726	1.7
SHS 150×150×4- SC2	713	1.6

Table 3.11: *Summary of results from RHS stub column tests*

Specimen identification	Ultimate load, F_u (kN)	End shortening at F_u (mm)
RHS 60×40×4- SC1	492	6.7
RHS 60×40×4- SC2	497	6.7
RHS 120×80×3- SC1	452	1.6
RHS 120×80×3- SC2	447	1.6
RHS 120×80×6- SC1	1459	7.8
RHS 120×80×6- SC2	1465	7.9
RHS 150×100×4- SC1	660	2.5
RHS 150×100×4- SC2	659	2.3
RHS 100×50×2- SC1	182	1.2
RHS 100×50×2- SC2	181	1.3
RHS 100×50×3- SC1	407	1.8
RHS 100×50×3- SC2	415	1.8
RHS 100×50×4- SC1	626	3.5
RHS 100×50×4- SC2	627	3.7
RHS 100×50×6- SC1	1217	9.3
RHS 100×50×6- SC2	1217	9.8

3.5 CHS STUB COLUMN TESTS

Four CHS stub columns were tested in pure axial compression. Two had a nominal cross-section of 103×1.5 mm and two 153×1.5 mm.

3.5.1 Testing Procedure

3.5.1.1 Preparation of stub column specimens

The stub columns were cut roughly to length using a rotary hacksaw. The specimens were then turned on a lathe to achieve flat and parallel ends to a tolerance of ±0.02 mm. This ensured

accurate seating of the stub columns against the parallel end platens of the testing machine. Prior to testing, measurements of geometry and initial imperfections were taken, and strain visualisation grids were marked onto the surfaces of the two CHS 103×1.5.

3.5.1.2 Test set-up, alignment and loading rates

The two CHS 103×1.5 were tested in the same 300 T Amsler hydraulic testing machine as the SHS and RHS stub columns. The two CHS 153×1.5 were too large for this machine, so were tested in a 35 T Amsler hydraulic testing machine. General views of the test set-ups are shown in Figures 3.31 (a) and 3.32 (b).
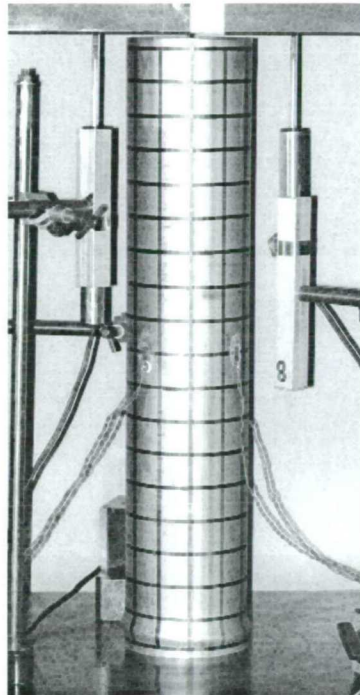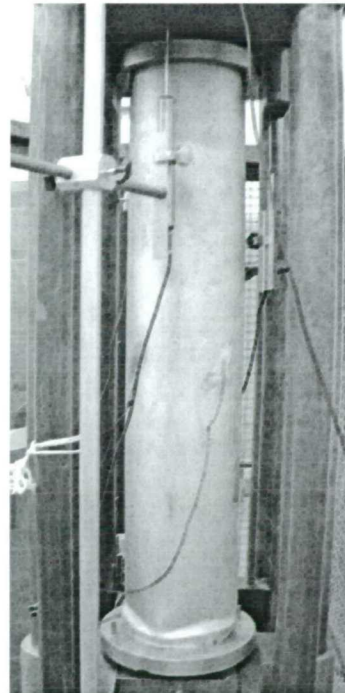
(a) CHS 103×1.5   (b) CHS 153×1.5

Figure 3.32: *General views of CHS test set-ups*

Alignment of the CHS specimens was conducted in a similar way to the SHS and RHS. Similar loading rates were also adopted.

3.5.2 Instrumentation

3.5.2.1 Displacement transducers and data acquisition

Three linear displacement transducers were used to measure the average end shortening of the stub columns between the platens of the testing machines. The orientation of the displacement transducers and the method of data acquisition were as for the SHS and RHS stub column tests.

3.5.2.2 Strain gauges

Four linear electrical strain gauges were attached to each specimen at mid-height, and mutually perpendicular, as shown in Figure 3.33. As with the SHS and RHS stub columns, the strain gauges were used initially for alignment.
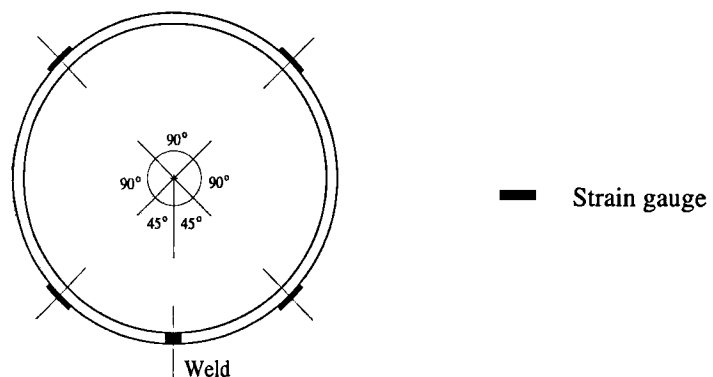
Figure 3.33: *Location of strain gauges for CHS specimens*

3.5.3 Measured Dimensions

The average measured dimensions for the CHS stub column specimens are presented in Table 3.12.

3.5.4 Initial Geometric Imperfections

For the two CHS 103×1.5, detailed initial geometric imperfection measurements were taken. Due to constraints on resources, a less rigorous assessment of imperfections was carried out for the two CHS 153×1.5.

Table 3.12: *Measured dimensions for CHS stub columns*

Specimen identification	Outer diameter, D_o (mm)	Thickness, t (mm)	Length, L (mm)	Area, A (mm²)
103×1.5- SC1	103.2	1.50	506.8	480
103×1.5- SC2	103.1	1.50	507.2	477
153×1.5- SC1	153.1	1.43	757.7	683
153×1.5- SC2	153.4	1.45	757.6	690

A general view of the measurement apparatus employed for the CHS 103×1.5 specimens is shown in Figure 3.34. The stub columns were fastened vertically to the flat bed of a precision rotary table, and centred. A dial gauge indicator mounted on a vertical sliding support arrangement was used to measure the imperfections on a grid of points on the surface of the specimens. For the CHS 153×1.5, imperfection measurements were taken at a total of 15 discrete points.
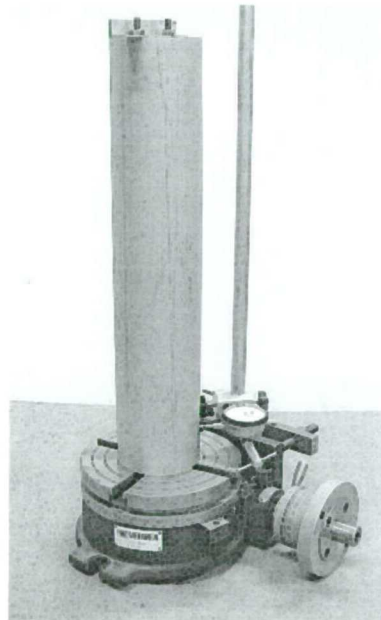
Figure 3.34: *Apparatus employed for CHS imperfection measurement*

Maximum initial geometric imperfections amplitudes (defined as maximum deviation from a perfect cylinder of diameter equal to the average measured diameter from the CHS specimens) of 0.22 mm for CHS 103×1.5 and 0.27 mm for CHS 153×1.5 were observed.

3.5.5 Stub Column Behaviour

3.5.5.1 Load-end shortening curves

Load-end shortening curves from the CHS stub column tests are shown in Figures 3.35 and 3.36.
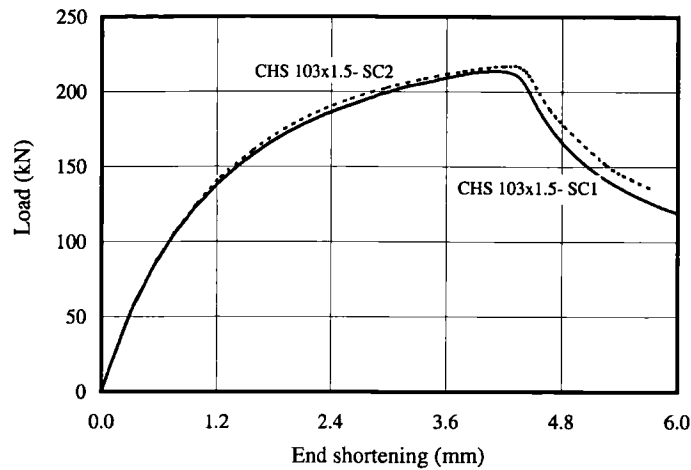
Figure 3.35: *CHS 103x1.5 stub column load-end shortening curves*
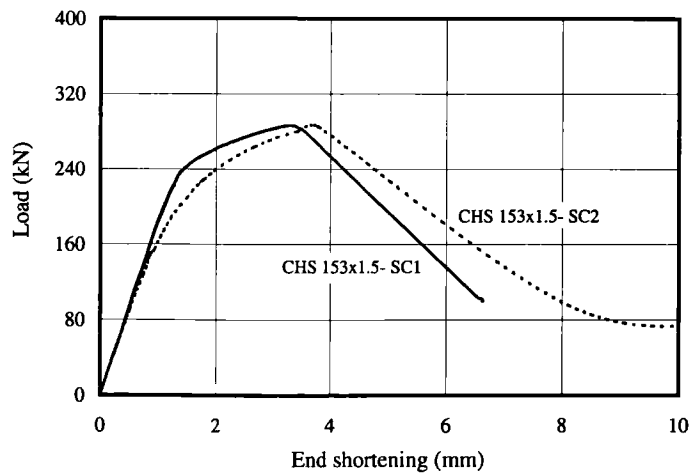
Figure 3.36: *CHS 153x1.5 stub column load-end shortening curves*

Unloading of the two CHS 153x1.5 stub columns was extremely rapid. The shape of the unloading path is therefore dominated by the characteristics of the testing machine, until the stable post-buckling path is established.

3.5.5.2 Deformed specimens

Photographs of the deformed pairs of CHS 103×1.5 and 153×1.5 stub columns are shown in Figures 3.37 to 3.38 respectively.

Figure 3.37: *Deformed CHS 103×1.5 stub columns*   **Figure 3.38:** *Deformed CHS 153×1.5 stub columns*

3.5.5.3 Summary of results

A summary of the results from the CHS stub column tests is given in Table 3.13.

Table 3.13: *Results from CHS stub column tests*

Specimen identification	Ultimate load, F_u (kN)	End shortening at F_u (mm)
103×1.5- SC1	214	4.1
103×1.5- SC2	217	4.2
153×1.5- SC1	287	3.3
153×1.5- SC2	286	3.9

3.6 SHS AND RHS PIN-ENDED COLUMN TESTS

22 tests were carried out on SHS and RHS columns with pin-end conditions. Nominal column lengths ranged between one and two metres. Members were orientated such that flexural buckling failures were observed about the major and minor axes. The aims of the tests were to generate member capacity data and to investigate the interaction between local and global phenomena.

3.6.1 Testing Procedure

3.6.1.1 General arrangement

The general arrangement of the test rig is shown in Figure 3.39. The rig had a capacity of 3000 kN, and was anchored to the strong floor of the laboratory using high tensile bolts. The columns were loaded centrally through knife-edges by means of a 300 T hydraulic loading jack. The set-up was load-controlled through an Amsler control cabinet. Large-bore rigid hydraulic piping was used to achieve maximum responsiveness during loading and unloading. Smaller bore flexible piping was found to induce a time lag effect due to the friction of the oil in the pipe assembly.

3.6.1.2 End conditions

The end preparation for the pin-ended column specimens was as for the stub columns. The top and bottom ends of the specimens bore against ground end plates that were fixed to hardened steel knife-edges, as shown in Figure 3.40.

Figure 3.41 shows a system of sliding clamps that was designed to fit onto the end plates to allow a series of different cross-section sizes to be tested.

3.6.1.3 Safety considerations

Since the components of the knife-edge assemblages at the top and base of the columns were free to move, and failure of the pin-ended columns could be relatively sudden, particular consideration had to be given to safety.
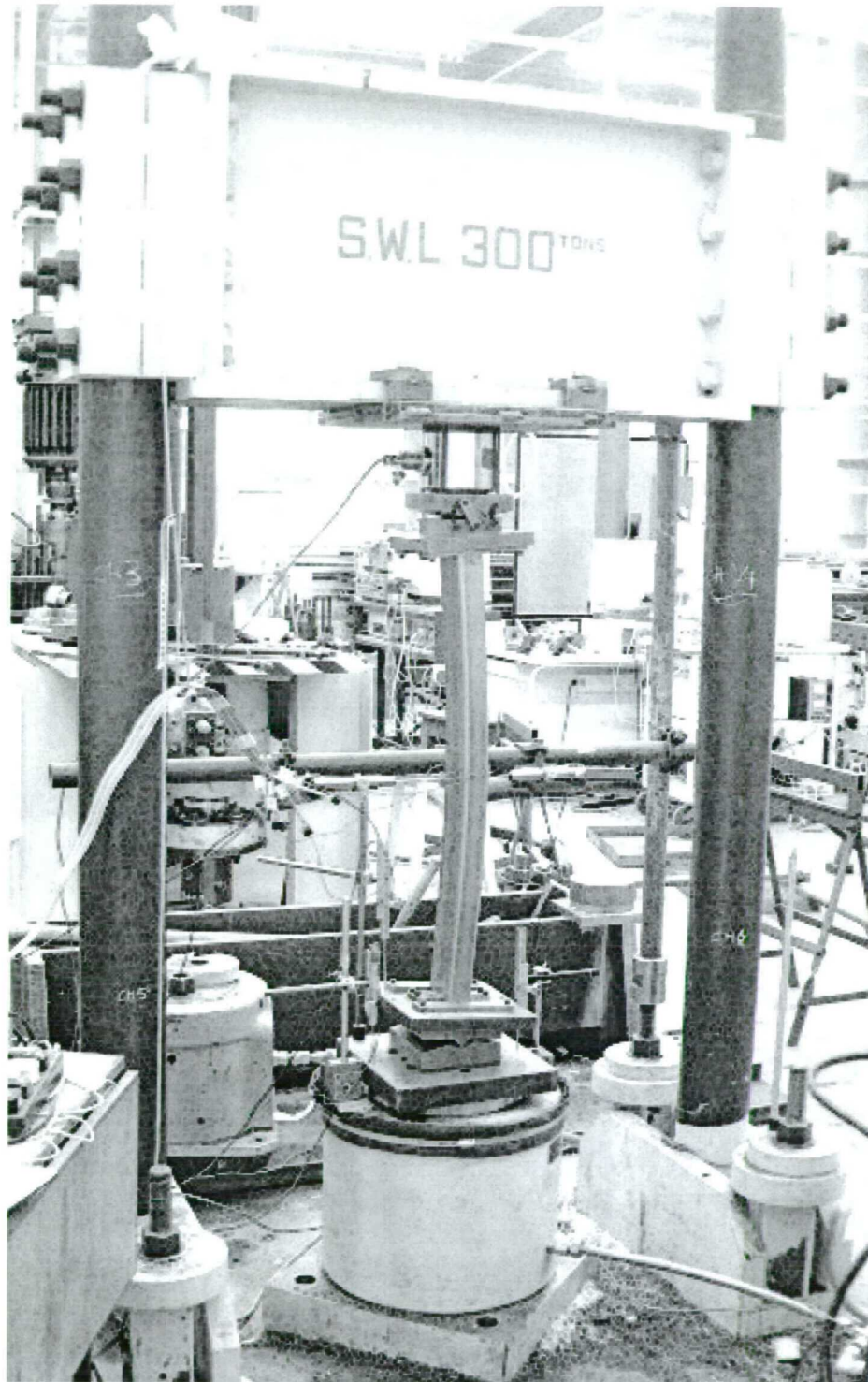
Figure 3.39: *General view of test set-up for pin-ended columns*
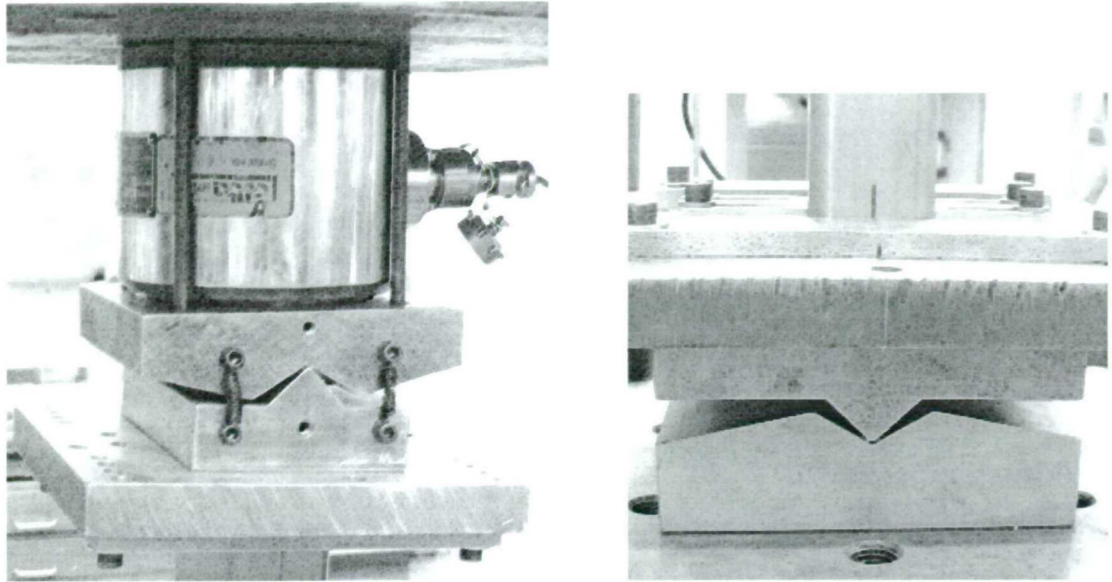
(a) Top detail   (b) Base detail

Figure 3.40: *End conditions for pin-ended columns*
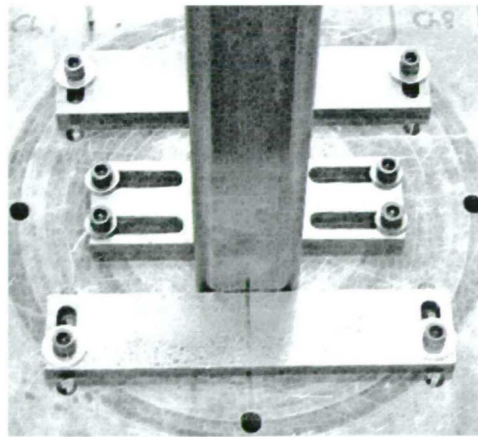
Figure 3.41: *System of sliding clamps to incorporate different cross-section sizes*

For the top knife-edge, a solid bar was fixed between the two components when test was not being performed to secure its position. A series of springs, which prevented overall translational movements, but still allowed free rotation of the knife-edge, were employed during testing. These features can be seen in Figure 3.42.
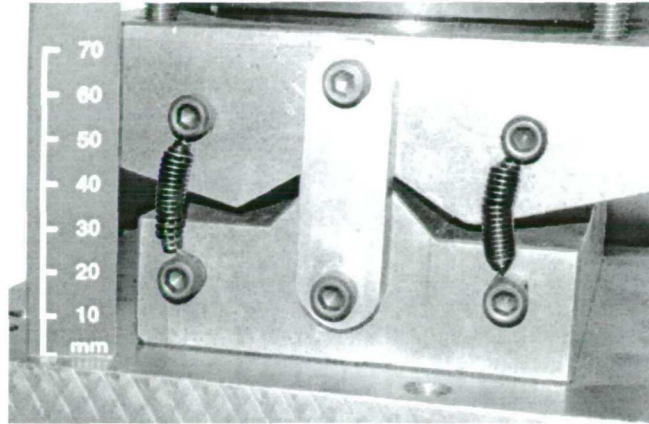
Figure 3.42: *Safety features on top knife-edge*

Additionally, a frame was constructed around the test set-up, and a tie was loosely attached to the test specimens. The tests were stopped before excessive lateral deflection was observed.

3.6.2 Instrumentation

3.6.2.1 Displacement transducers

Displacement transducers were used to measure the lateral deflection, end shortening and end rotation of the columns. The location of the displacement transducers is shown in Figure 3.43.

3.6.2.2 Strain gauges

Four linear electrical resistance strain gauges were affixed to each specimen at mid-height, and at a distance of four times the material thickness from the corners, as for the stub columns. The strain gauges were initially used for alignment purposes. During testing, the strains gauges were used to measure the extreme fibre strains on the convex and concave faces of the columns.

3.6.3 Initial out-of-straightness

Initial out-of-straightness of the pin-ended columns was evaluated about both principal axes. Rasmussen & Hancock (1990) and Talja & Salmi (1995) evaluated global column
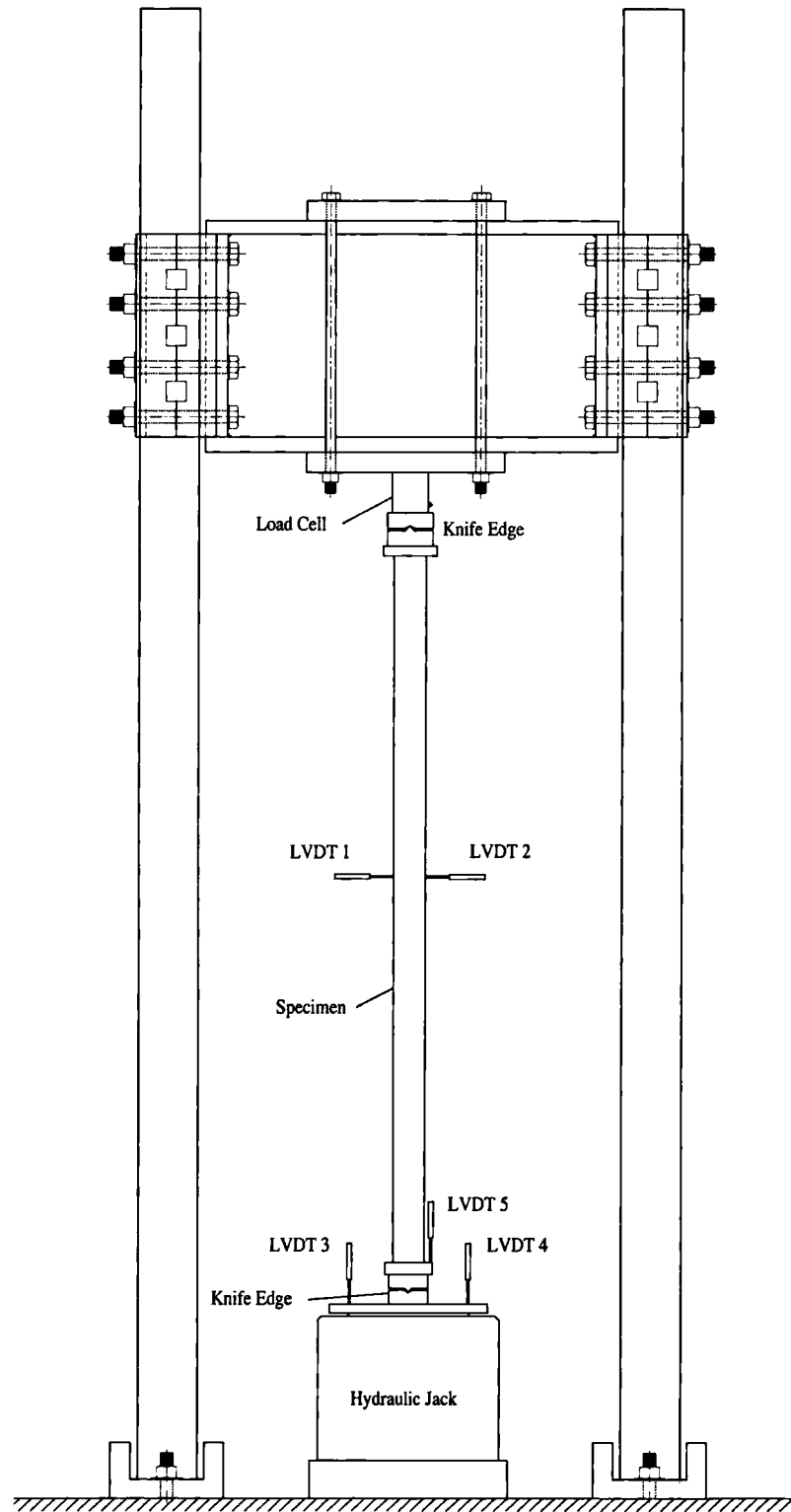
Figure 3.43: *Instrumentation for pin-ended columns*

imperfections by stretching a piano string between the ends of the columns, and measuring the distance to the column faces. In this study, a straight edge was used in place of a piano string, and the imperfections measured using feeler gauges. The shape of the imperfections were assumed to be single half-sine waves, and their magnitudes are presented in Tables 3.14 and 3.15.

Imperfections v_0 relate to those in the principal buckling direction and imperfections v_1 relate to those at right angles to the principal buckling direction.

3.6.4 Measured Dimensions

The average measured dimensions for the pin-ended column specimens are presented in Tables 3.14 and 3.15.

3.6.5 Column Buckling Results

3.6.5.1 Load-lateral deflection curves

Load-lateral deflection curves from the pin-ended column tests are shown in Figures 3.44 to 3.64.
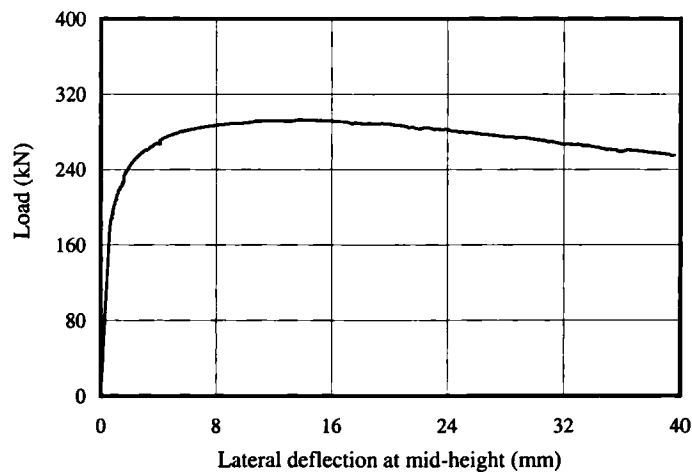
Figure 3.44: 2m SHS 80x80x4 pin-ended column load-lateral deflection curve

Table 3.14: *Measured dimensions and imperfections for pin-ended SHS columns*

Column identification	Length, L (mm)	Depth, D (mm)	Breadth, B (mm)	Thickness, t (mm)	Internal corner radius, r_i (mm)	Area, A (mm^2)	Imperfection, v_0 (mm)	Imperfection, v_1 (mm)
SHS 80×80×4-LC-2m	2000.7	79.5	79.8	3.74	4.5	1093	0.4	0.1
SHS 80×80×4-LC-1.9m	1899.8	79.7	79.6	3.78	4.5	1106	0.4	0.4
SHS 100×100×2-LC-2m	2000.3	99.8	99.9	1.86	1.3	723	0.1	0.1
SHS 100×100×3-LC-2m	2000.4	100.1	100.2	2.83	1.5	1089	0.1	1.0
SHS 100×100×4-LC-2m	2000.4	99.8	100.0	3.77	4.5	1410	0.6	0.2
SHS 100×100×6-LC-2m	1999.9	100.1	100.5	5.92	5.8	2145	0.3	0.3
SHS 100×100×8-LC-2m	1999.6	100.1	100.7	7.96	8.0	2778	0.3	0.4
SHS 150×150×4-LC-2m	1999.8	150.4	150.0	3.77	5.8	2159	0.0	0.2

Notes: v_0 is imperfection in buckling direction

v_1 is imperfection at 90° to buckling direction

Table 3.15: Measured dimensions and imperfections for pin-ended RHS columns

Column identification	Buckling axis	Length, L (mm)	Depth, D (mm)	Breadth, B (mm)	Thickness, t (mm)	Int. corner rad., r_i (mm)	Area, A (mm²)	Imperfection, v_0 (mm)	Imperfection, v_1 (mm)
RHS 60×40×4-LCJ-2m	major	2000.1	60.0	40.0	3.83	2.9	675	1.0	0.0
RHS 100×50×2-LCJ-2m	major	2000.2	99.8	49.8	1.83	2.3	523	0.6	0.0
RHS 100×50×3-LC-2m	minor	2000.2	100.1	50.1	2.87	3.1	807	1.1	0.3
RHS 100×50×4-LC-2m	minor	2000.2	99.7	49.9	3.70	3.6	1018	0.8	0.1
RHS 100×50×6-LC-2m	minor	2000.2	100.0	50.0	5.96	5.5	1559	0.0	0.8
RHS 120×80×3-LC-2m	minor	1999.0	120.0	80.2	2.91	4.6	1101	1.1	0.5
RHS 120×80×6-LC-2m	minor	2000.4	120.0	80.4	5.87	7.0	2115	0.5	0.4
RHS 150×100×4-LC-2m	minor	1999.5	149.8	99.9	3.79	5.6	1787	0.1	0.2
RHS 60×40×4-LC-1m	minor	1000.2	59.9	39.9	3.82	2.9	673	0.2	0.1
RHS 100×50×2-LC-1m	minor	1000.2	99.8	50.0	1.82	2.3	522	0.1	0.0
RHS 100×50×3-LC-1m	minor	1000.1	100.1	50.0	2.86	3.1	804	1.0	0.1
RHS 100×50×4-LC-1m	minor	999.6	99.7	50.3	3.73	3.6	1028	0.6	0.1
RHS 100×50×6-LC-1m	minor	999.8	100.0	50.1	5.94	5.6	1555	0.1	0.3
RHS 120×80×3-LC-1m	minor	1000.6	120.0	80.2	2.86	4.6	1083	1.0	0.0

Notes: v_0 is imperfection in buckling direction

v_1 is imperfection at 90° to buckling direction
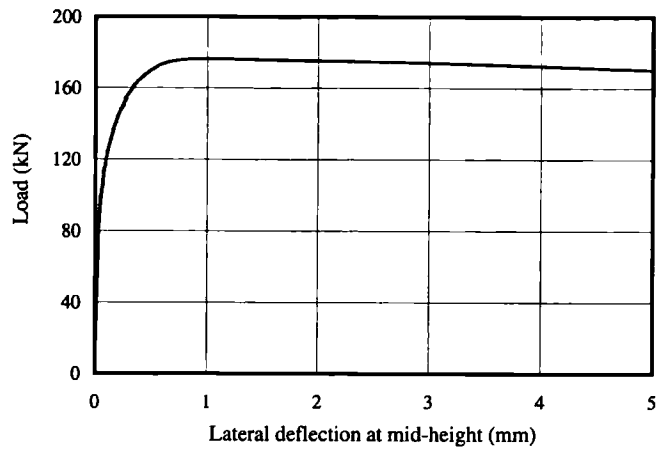
Figure 3.45: *2m SHS 100×100×2 pin-ended column load-lateral deflection curve*
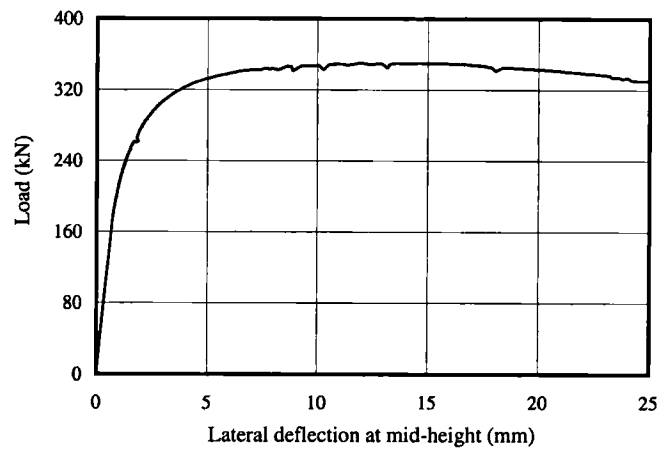
Figure 3.46: *2m SHS 100×100×3 pin-ended column load-lateral deflection curve*
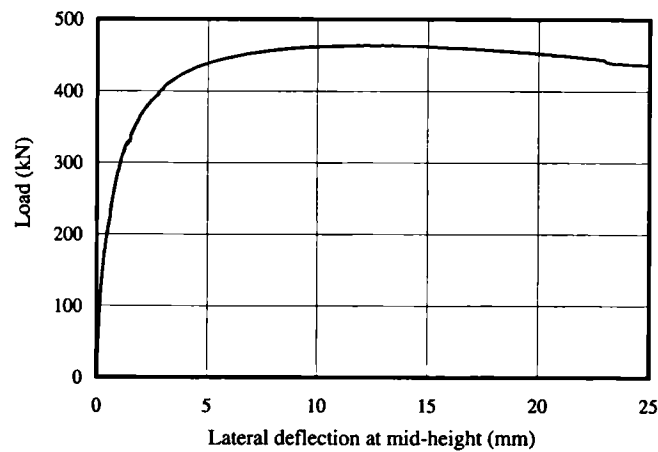
Figure 3.47: *2m SHS 100×100×4 pin-ended column load-lateral deflection curve*
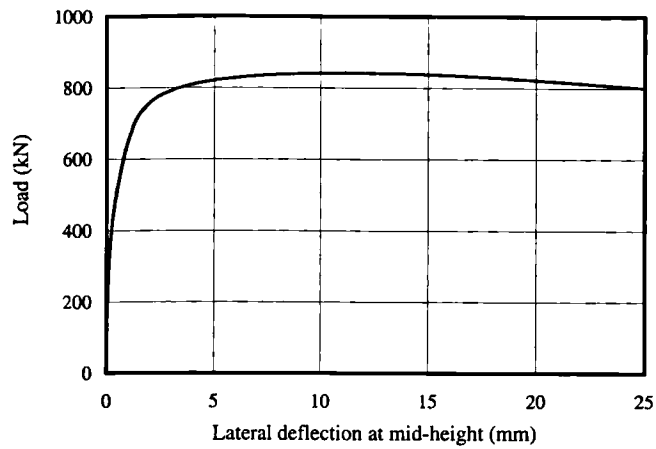
Figure 3.48: *2m SHS 100x100x6 pin-ended column load-lateral deflection curve*
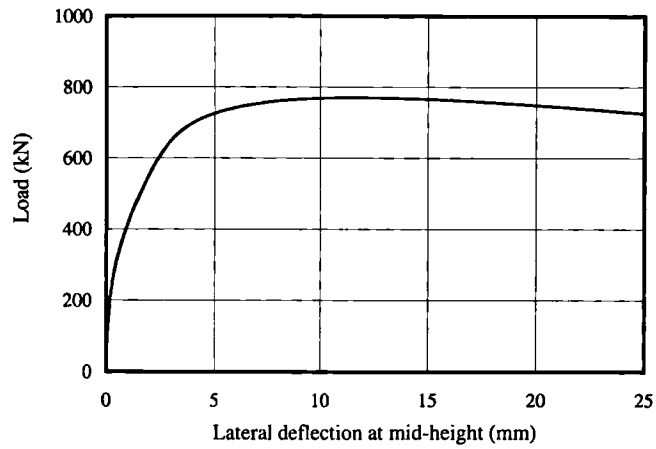
Figure 3.49: *2m SHS 100x100x8 pin-ended column load-lateral deflection curve*
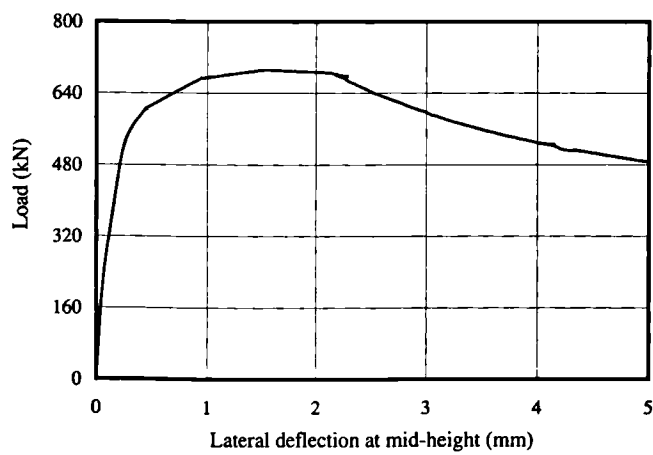
Figure 3.50: *2m SHS 150x150x4 pin-ended column load-lateral deflection curve*
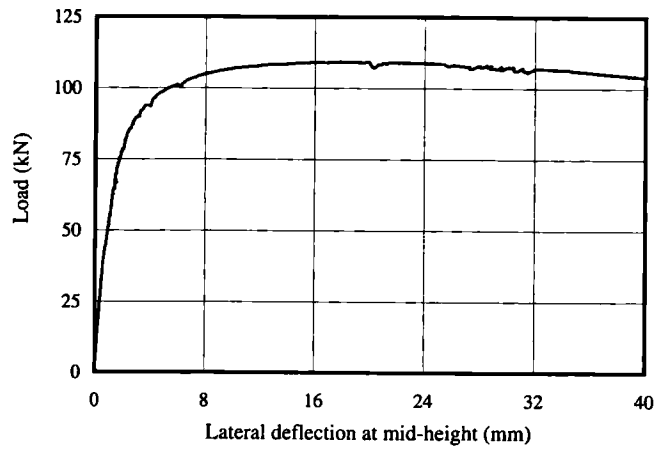
Figure 3.51: *2m RHS 60x40x4 pin-ended column (major) load-lateral deflection curve*
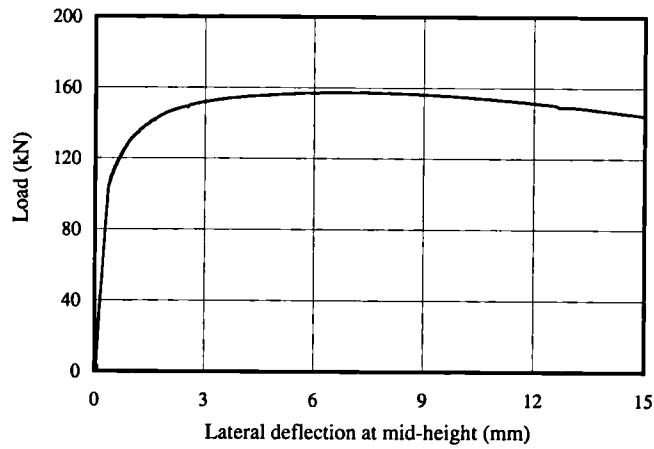
Figure 3.52: *2m RHS 100x50x2 pin-ended column (major) load-lateral deflection curve*
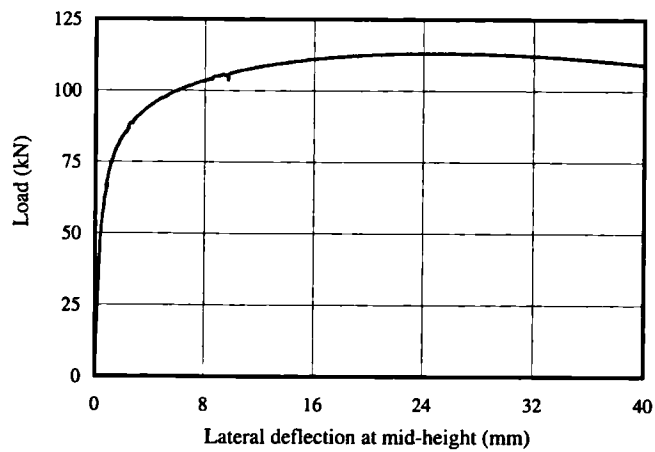
Figure 3.53: *2m RHS 100x50x3 pin-ended column (minor) load-lateral deflection curve*
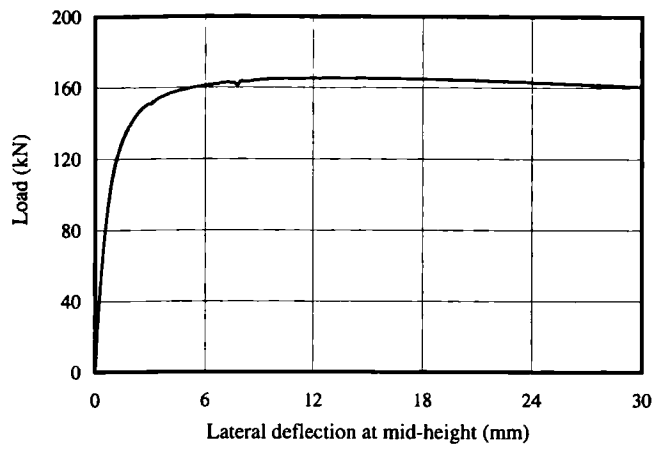
Figure 3.54: *2m RHS 100x50x4 pin-ended column (minor) load-lateral deflection curve*
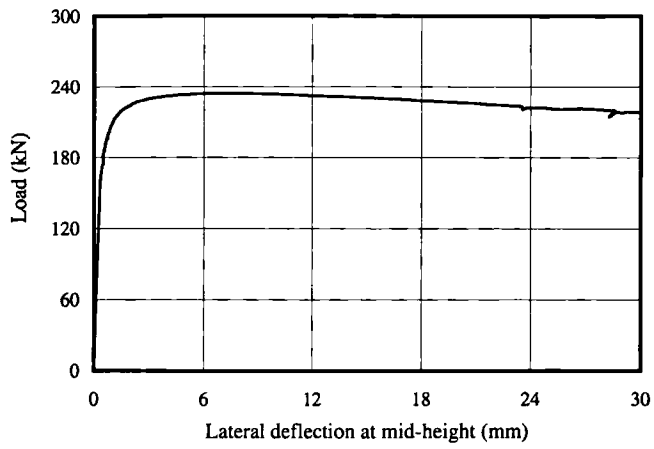
Figure 3.55: *2m RHS 100x50x6 pin-ended column (minor) load-lateral deflection curve*
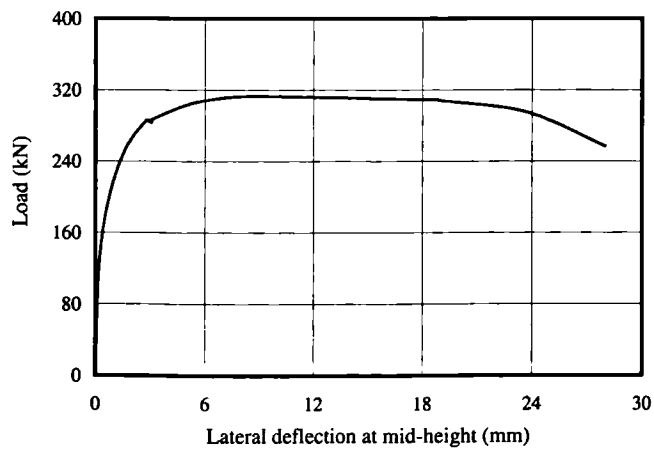
Figure 3.56: *2m RHS 120x80x3 pin-ended column (minor) load-lateral deflection curve*
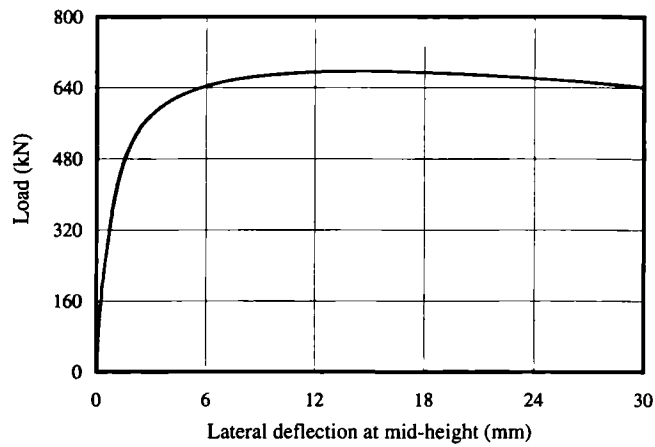
Figure 3.57: *2m RHS 120x80x6 pin-ended column (minor) load-lateral deflection curve*
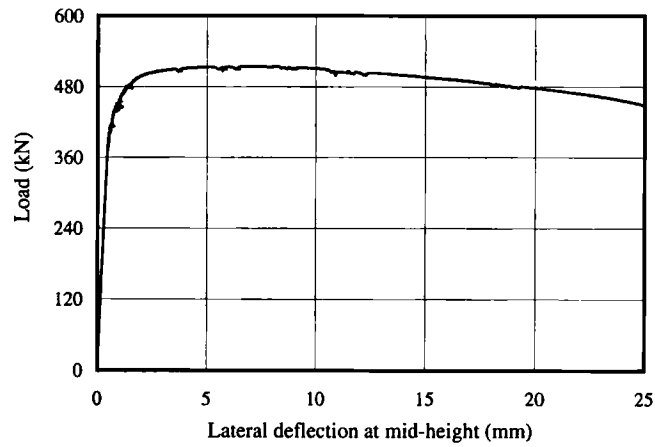
Figure 3.58: *2m RHS 150x100x4 pin-ended column (minor) load-lateral deflection curve*
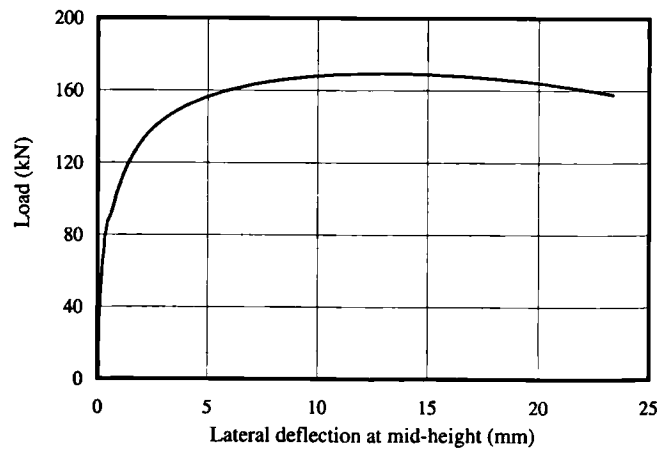
Figure 3.59: *1m RHS 60x40x4 pin-ended column (minor) load-lateral deflection curve*
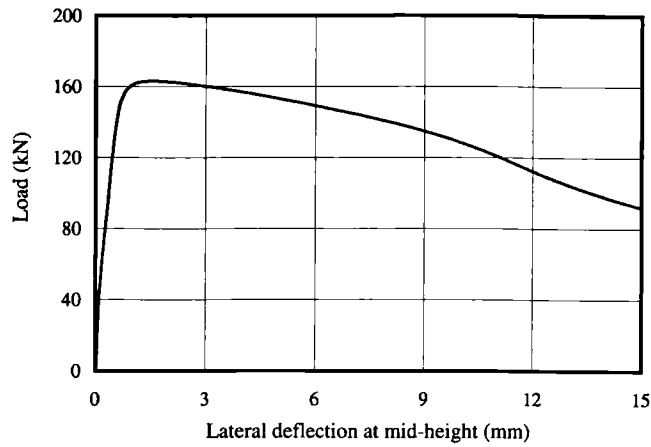
Figure 3.60: *1m RHS 100x50x2 pin-ended column (minor) load-lateral deflection curve*
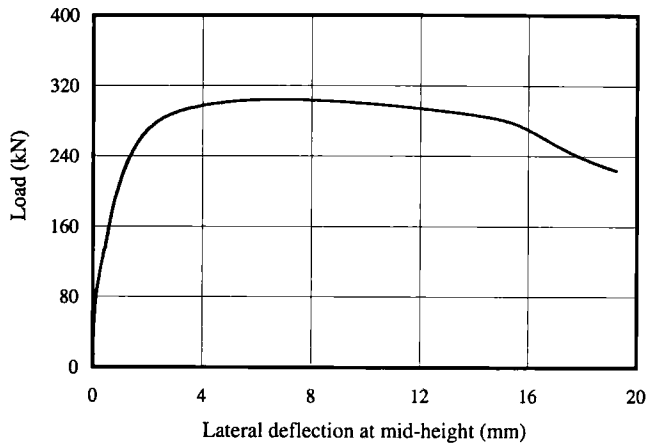
Figure 3.61: *1m RHS 100x50x3 pin-ended column (minor) load-lateral deflection curve*
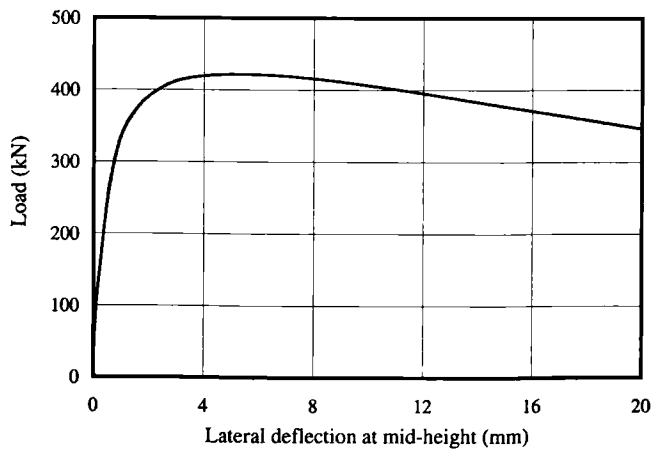
Figure 3.62: *1m RHS 100x50x4 pin-ended column (minor) load-lateral deflection curve*
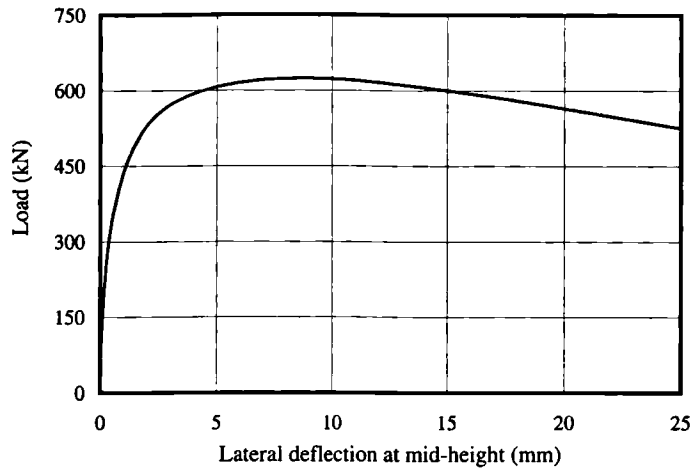
Figure 3.63: *1m RHS 100x50x6 pin-ended column (minor) load-lateral deflection curve*
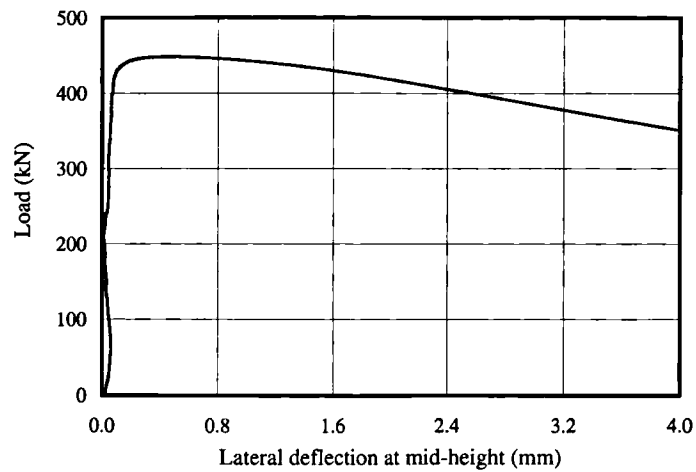
Figure 3.64: *1m RHS 120x80x3 pin-ended column (minor) load-lateral deflection curve*

3.6.5.2 Summary of results

A summary of the results from the pin-ended column tests is given in Tables 3.16 and 3.17. For each test the following results have been tabulated; ultimate load, lateral deflection at ultimate load, end shortening at ultimate load and extreme fibre strains at ultimate load.

Table 3.16: *Results from pin-ended SHS column tests*

Column identification	Ultimate load, F_u (kN)	Lateral deflection at F_u (mm)	End shortening at F_u (mm)	Mid-height outer fibre strains at F_u	
				Max. comp ($\mu\varepsilon$)	Min. comp. ($\mu\varepsilon$)
SHS 80×80×4-LC-2m	293	13.8	4.9	3360	600
SHS 80×80×4-LC-1.9m	307	-	-	-	-
SHS 100×100×2-LC-2m	176	1.0	4.2	1870	1680
SHS 100×100×3-LC-2m	350	11.9	6.7	4190	1470
SHS 100×100×4-LC-2m	464	12.3	6.6	4070	1320
SHS 100×100×6-LC-2m	842	11.1	8.4	4120	1800
SHS 100×100×8-LC-2m	770	11.5	6.2	3500	910
SHS 150×150×4-LC-2m	692	1.9	9.0	3450	3140

Table 3.17: Results from pin-ended RHS column tests

Column identification	Buckling axis	Ultimate load, F_u (kN)	Lateral deflection at F_u (mm)	End shortening at F_u (mm)	Mid-height outer fibre strains at F_u	
					Max. comp ($\mu\varepsilon$)	Min. comp. ($\mu\varepsilon$)
RHS 60×40×4-LCJ-2m	major	109	18.8	3.3	2500	-210
RHS 100×50×2-LCJ-2m	major	157	7.2	5.0	2910	1360
RHS 100×50×3-LC-2m	minor	113	25.5	3.6	2720	-520
RHS 100×50×4-LC-2m	minor	165	13.2	2.6	1760	190
RHS 100×50×6-LC-2m	minor	234	7.0	2.3	1390	340
RHS 120×80×3-LC-2m	minor	313	16.1	5.9	4100	940
RHS 120×80×6-LC-2m	minor	677	13.7	6.2	3400	920
RHS 150×100×4-LC-2m	minor	515	6.7	6.7	3550	1950
RHS 60×40×4-LC-1m	minor	169	13.0	3.1	5150	-580
RHS 100×50×2-LC-1m	minor	163	1.6	2.6	2470	1730
RHS 100×50×3-LC-1m	minor	304	6.9	3.9	5050	1740
RHS 100×50×4-LC-1m	minor	422	5.3	4.0	4440	1960
RHS 100×50×6-LC-1m	minor	624	8.6	4.2	5030	1020
RHS 120×80×3-LC-1m	minor	448	0.5	4.8	3870	3870

3.7 SHS AND RHS BEAM TESTS

9 tests were conducted on SHS and RHS simply-supported beams, 5 of which were SHS and 4 RHS. The aim of the tests was to determine member capacities and to investigate deflections.

3.7.1 Testing Procedure

3.7.1.1 Preparation of beam specimens

The beam specimens were cut roughly to length using a rotary hacksaw. Accurate end preparation was not required. The beams extended approximately 100 mm beyond the points of support. Prior to testing, measurements of geometry were taken.

3.7.1.2 Test set-up and loading rates

The SHS and RHS bending tests were conducted in a 350 kN Amsler hydraulic testing machine. The set-up was load-controlled though an Amsler control cabinet. A general view of the test set-up is shown in Figure 3.65. The beams were simply supported with a span of 1000 mm or 1100 mm. The load was applied at mid-span, and bending was about the major axis.
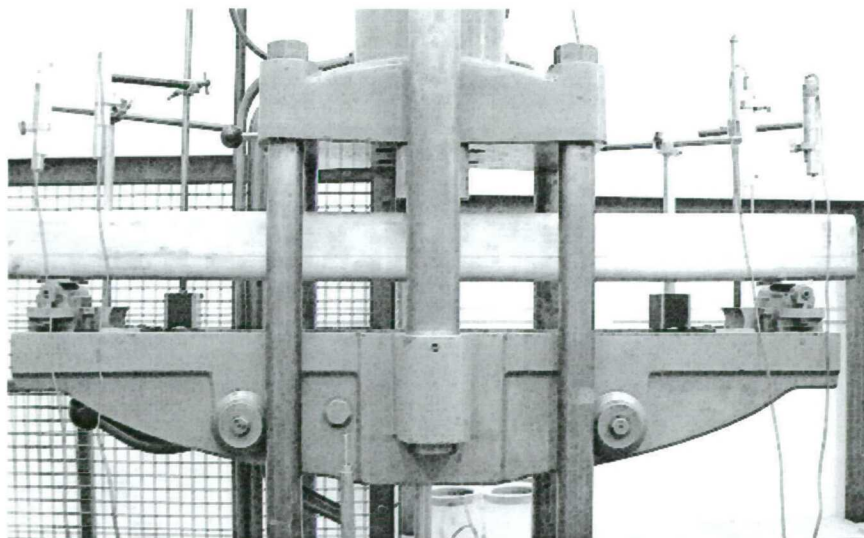
Figure 3.65: *General view of bending test set-up*

Simply-supported end conditions were achieved using rollers, as shown in Figure 3.66. Plates were used to distribute the load and prevent local bearing failure of the cross-sections.
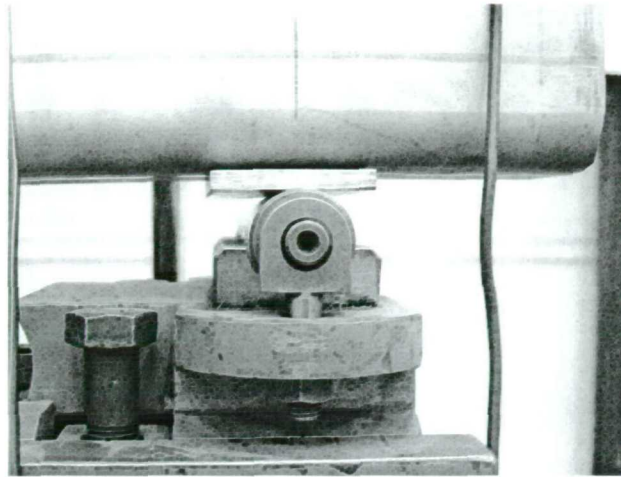
Figure 3.66: *Roller support in bending tests*

Loading rates were set such that the ultimate moment resistance of the beam would be reached after 30-45 minutes, and the test would be completed following an appropriate amount of unloading after 60-80 minutes.

3.7.2 Instrumentation

Five linear displacement transducers were employed to measure the deformation of the beams during testing. The locations of the displacement transducers are shown in Figure 3.67. LVDT 1 measured the mid-span deflection. LVDTs 2 and 3 and LVDTs 4 and 5 were used to determine the rotation of the beams at the supports.
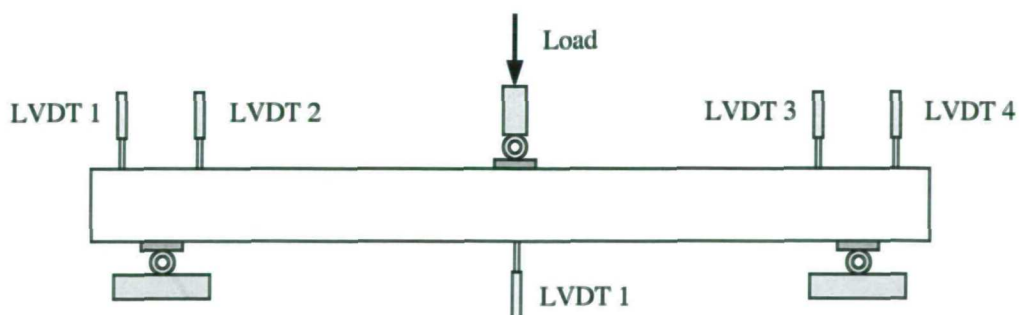
Figure 3.67: *Location of displacement transducers for bending tests*

3.7.3 Measured Dimensions

The average measured dimensions for the beam specimens are presented in Table 3.18. No imperfection measurements were taken, though imperfection magnitudes would be expected to be similar to those measured for the corresponding stub column specimens, since all material originated from one 6 m length.

3.7.4 Beam Results

37.4.1 General

Failure of the simply-supported beams was due to local buckling of the compression flange and upper portion of the webs.

3.7.4.2 Bending moment-vertical mid-span deflection curves

Bending moment-vertical mid-span deflection curves for the simply-supported beam tests are shown in Figures 3.68 to 3.76.
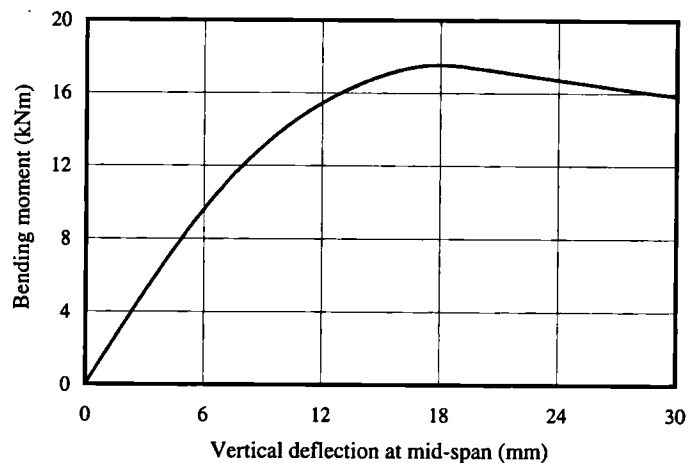
Figure 3.68: *SHS 80x80x4 beam bending moment-vertical deflection curve*

Table 3.18: *Measured dimensions for SHS and RHS simply-supported beams*

Specimen identification	Length between supports, L_s (mm)	Overall length, L (mm)	Depth, D (mm)	Breadth, B (mm)	Thickness, t (mm)	Internal corner radius, r_i (mm)	Area, A (mm²)
SHS 80×80×4- B1	1100.0	1290.0	79.6	79.7	3.75	4.4	1099
SHS 100×100×2- B1	1000.0	1148.3	99.9	99.9	1.84	1.3	715
SHS 100×100×3- B1	1100.0	1299.8	100.1	100.3	2.84	1.5	1091
SHS 100×100×4- B1	1100.0	1300.0	99.8	99.8	3.79	4.5	1415
SHS 100×100×8-B1	1100.0	1299.4	100.7	100.2	7.92	8.0	2768
RHS 60×40×4- B1	1100.0	1298.8	59.9	39.9	3.79	2.9	669
RHS 100×50×2- B1	1000.0	1222.2	99.7	49.8	1.79	2.3	514
RHS 100×50×3- B1	1100.0	1296.6	100.1	50.0	2.88	3.2	810
RHS 100×50×4- B1	1100.0	1299.8	99.7	49.9	3.68	3.6	1014
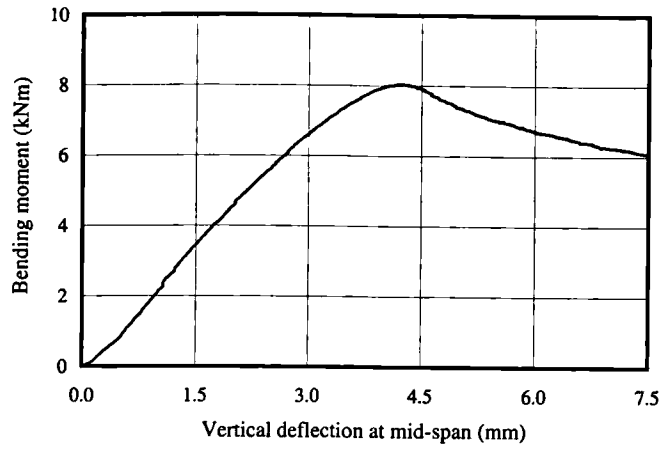
Figure 3.69: *SHS 100x100x2 beam bending moment-vertical deflection curve*
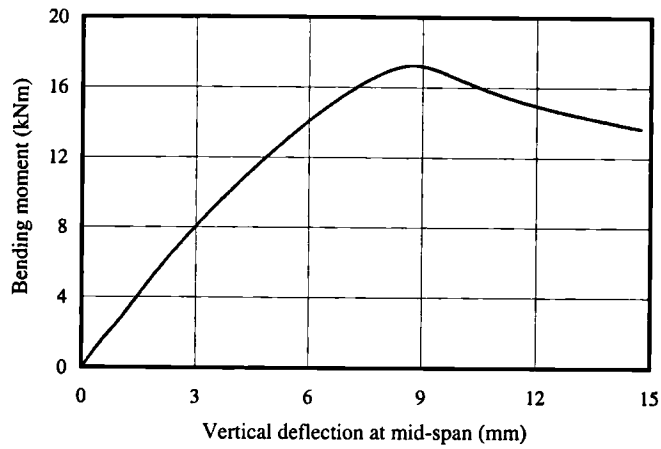
Figure 3.70: *SHS 100x100x3 beam bending moment-vertical deflection curve*
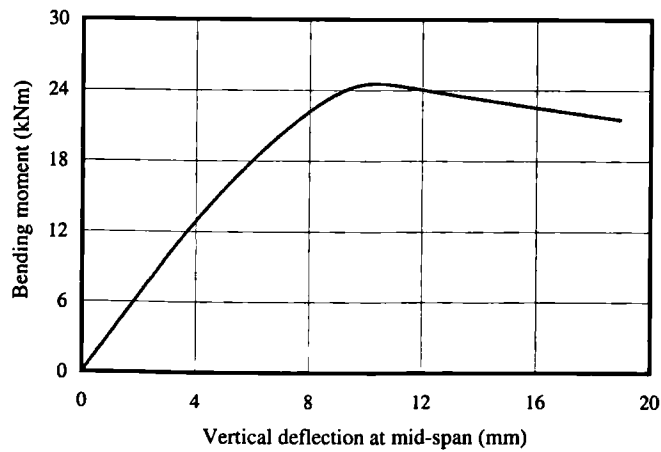
Figure 3.71: *SHS 100x100x4 beam bending moment-vertical deflection curve*
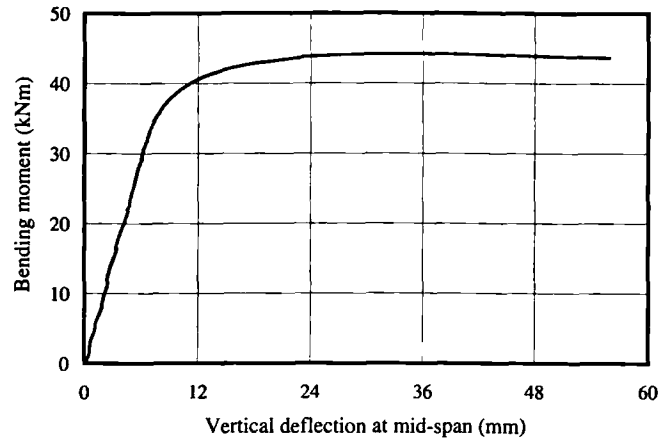
Figure 3.72: *SHS 100x100x8 beam bending moment-vertical deflection curve*
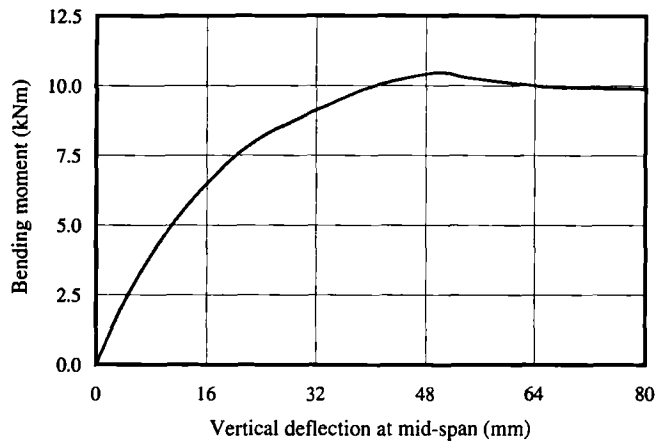
Figure 3.73: *RHS 60x40x4 beam bending moment-vertical deflection curve*
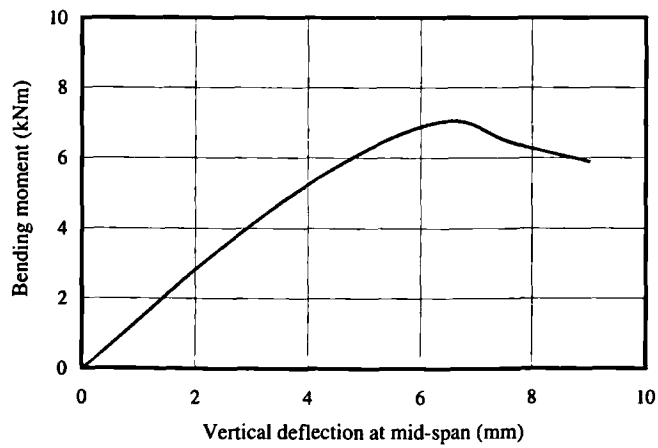
Figure 3.74: *RHS 100x50x2 beam bending moment-vertical deflection curve*
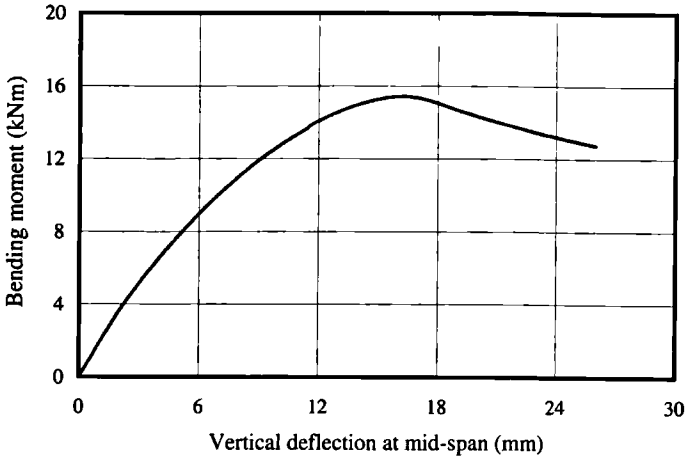
Figure 3.75: *RHS 100x50x3 beam bending moment-vertical deflection curve*
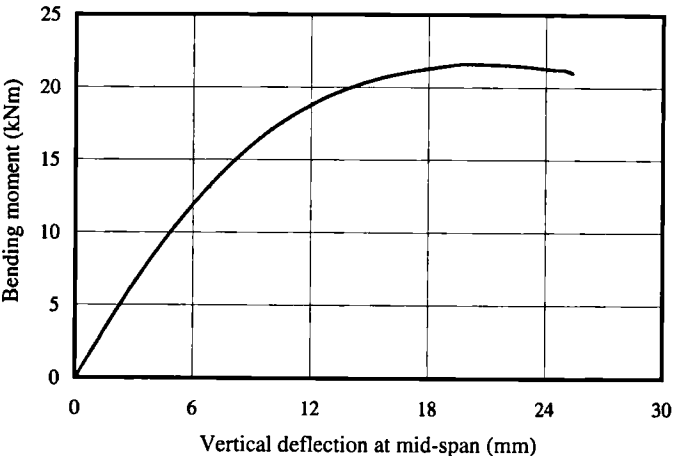
Figure 3.76: *RHS 100x50x4 beam bending moment-vertical deflection curve*

3.7.4.3 Deformed beams

All beams failed by in-plane bending, with local buckling of the compression flange and the top portion of the web. A typical deformed beam (SHS 100×100×3) is shown in elevation in Figure 3.77.
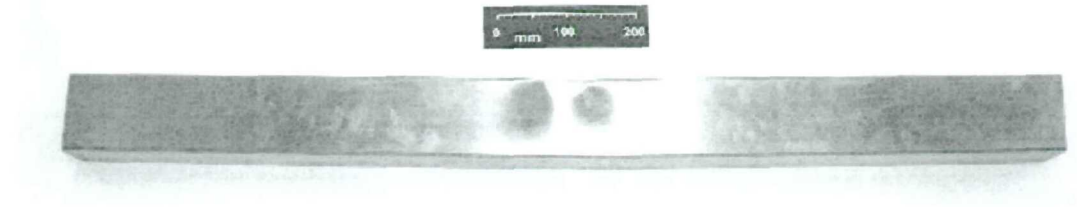
Figure 3.77: *Elevation of deformed SHS 100×100×3 simply-supported beam*

3.7.4.4 Summary of results

A summary of the results from the simply-supported beam tests is presented in Table 3.19. For each test, values of ultimate bending moment and the corresponding mid-span deflection at ultimate bending moment are provided.

Table 3.19: *Summary of results from simply-supported beam tests*

Specimen identification	Ultimate bending moment, M_u (kNm)	Mid-span deflection at M_u (mm)
SHS 80×80×4- B1	17.5	17.9
SHS 100×100×2- B1	8.0	4.2
SHS 100×100×3- B1	17.2	8.7
SHS 100×100×4- B1	24.5	10.3
SHS 100×100×8-B1	44.2	34.8
RHS 60×40×4- B1	10.5	49.4
RHS 100×50×2- B1	7.1	6.6
RHS 100×50×3- B1	15.4	16.2
RHS 100×50×4- B1	21.6	20.0

3.8 CONCLUDING REMARKS

A total of 33 stub column tests, 22 pin-ended column tests, 9 simply-supported beam tests and numerous tensile and compression coupon tests have been conducted. Many of the tests are simulated in Chapter 4 and used to develop accurate FE models. All of the test results are used in Chapter 6 (in conjunction with all other available test results) for comparison with predicted results from the proposed design method and the ENV 1993-1-4 (1996) design method.

CHAPTER 4

NUMERICAL MODELLING

4.1 INTRODUCTION

Owing to the expense and impracticality of generating comprehensive data on the behaviour of stainless steel structures through experimentation, a numerical modelling study was undertaken in parallel with the laboratory testing programme described in Chapter 3. The general-purpose finite element (FE) software package ABAQUS (1999) was employed throughout the study.

This chapter describes the development of the FE models, including the modelling of material stress-strain behaviour, residual stresses and initial geometric imperfections. Validation of the models is made against existing test data, and parametric studies are conducted to investigate the influence of key variables and to generate further results.

4.2 MATERIAL MODELLING

Material modelling generally represents one of the most important aspects of an FE simulation. Inaccurate or inappropriate modelling of the basic material behaviour of a structure will overshadow the performance of even the most refined FE models.

Stainless steel exhibits a rounded stress-strain curve, with no sharp yield point. The degree of roundedness varies from grade to grade, with the austenitic grades demonstrating the greatest non-linearity and strain hardening. Further complications exist due to the presence of anisotropy and non-symmetry of stress-strain behaviour in tension and compression.

4.2.1 Constitutive modelling

Constitutive models in structural steel design are generally based on plasticity theory, with the most commonly used one being the von Mises isotropic hardening model. In this model, the yield surface is expanded in response to post-yield straining. Another important model is that of kinematic hardening whereby the yield surface is translated in order to preserve consistency. Both of these concepts give good predictions for material response under monotonic loading, but not for subsequent loadings, as shown in Figure 4.1.
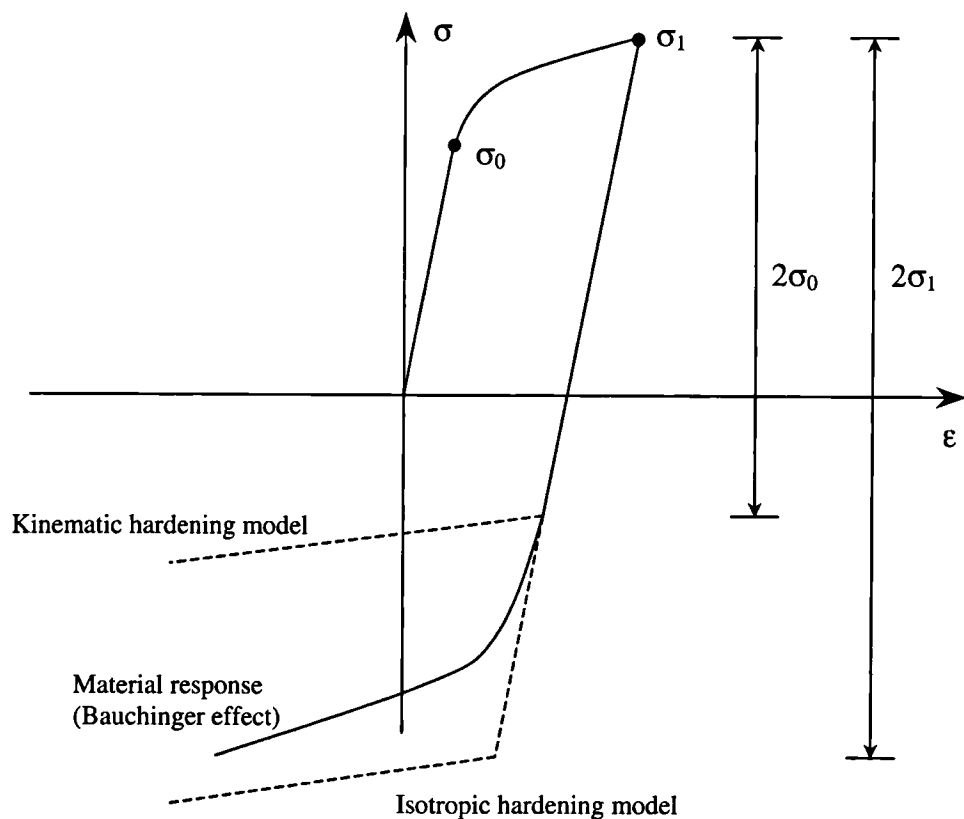
Figure 4.1: *Material behaviour under load reversal*

Models capable of describing material stress-strain response under load reversal have to take due account of phenomena such as the Bauchinger effect, and have in general to be two or multi

surface models. Olsson (2001) used the multi surface concept to develop a model for application to stainless steel. The model is able to predict the phenomenological features that were observed in a prior experimental programme, whilst retaining relative simplicity.

For the purposes of static structural design and the numerical modelling of members subjected to quasi-static loading, however, an expression to describe stainless steel stress-strain behaviour under monotonic loading is required. Existing material models are reviewed in Section 4.2.3.

4.2.2 Anisotropy and non-symmetry of stress-strain behaviour in tension and compression

Anisotropy and non-symmetry of stress-strain behaviour in tension and compression have been observed in numerous experimental studies on stainless steel materials, for example by Johnson & Winter (1966).

In the current study, material tests (on coupons cut from SHS and RHS) were carried out in tension and compression, but loading was only applied in the longitudinal direction (parallel to the direction of rolling). Anisotropy was therefore not investigated, but some clear differences were observed between the tensile and the compressive material behaviour. The following statements summarise these differences, based on mean measurements.

- Young's modulus was 1% higher in compression than in tension
- $\sigma_{0.2}$ was 5% lower in compression than in tension
- $\sigma_{1.0}$ was 4% higher in compression than in tension
- n was 21% lower in compression than in tension
- $n'_{0.2, 1.0}$ was 18% lower in compression than in tension

where $\sigma_{0.2}$ and $\sigma_{1.0}$ are the material proof strengths at 0.2% and 1.0% offset strain, respectively, and n and $n'_{0.2,1.0}$ are strain hardening exponents, described in detail in Section 4.2.4.

Overall, the variation between tensile and compression properties is relatively small, with the primary difference being that the material begins to yield at a lower stress in compression, but continues to strain harden to a higher degree than the tensile material. Figure 4.2 illustrates this fundamental difference in behaviour.
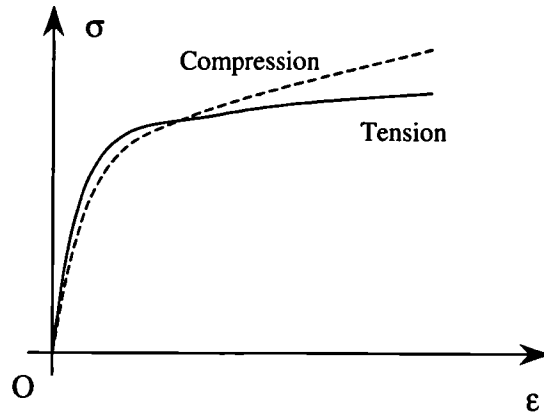
Figure 4.2: *Comparison between average stress-strain behaviour in tension and compression for coupons cut from SHS and RHS*

4.2.3 Appraisal of existing material models

This section describes existing functions that have been applied to the modelling of non-linear behaviour, and discusses their suitability for describing stainless steel material stress-strain response. Section 4.2.3.1 describes models comprising solely linear regions. Models in Section 4.2.3.2 include power functions, models in Section 4.2.3.3 include exponential functions, and other models are described in Section 4.2.3.4.

4.2.3.1 Models comprising linear functions

The material model adopted for carbon steel in all major structural design codes is an idealised elastic, perfectly-plastic relationship. This assumes linear behaviour until the yield stress, σ_y is reached, followed by a flat yield plateau (see Figure 4.3). This model also forms the basis for the current European stainless steel structural design code, ENV 1993-1-4 (1996), despite stainless steels exhibiting no sharply defined yield point and significant strain hardening.
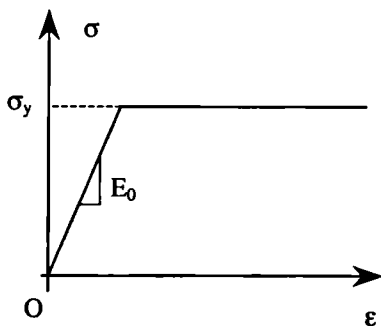
Figure 4.3: *Elastic, perfectly-plastic model*
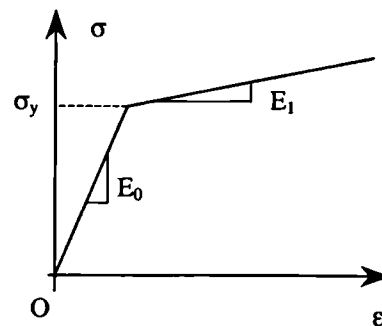
Figure 4.4: *Elastic, linear hardening model*

Multi-linear models can be used to represent strain hardening behaviour to a varying degree of sophistication. The crudest representation is an elastic, linear-hardening model, as shown in Figure 4.4, where there is a reduced stiffness, E_1 above the yield stress. Figure 4.5 shows how increased accuracy can be achieved with an increase in the number of linear parts.

4.2.3.2 Models comprising power functions

The simplest power relationship is of the form $\sigma = C_1\varepsilon^m$, where C_1 and m are constants, and is in fact a special case of the Ludwik expression described in the next paragraph. Clearly, in order to have a diminishing slope with increasing strains, the value of m must be such that $0 < m < 1$, (see Figure 4.6). This model is commonly used to represent material stress-strain behaviour, because it is a simple, continuous function that is explicitly solvable for stress. However, at low strains the model is inaccurate because the function is tangential to the stress axis.
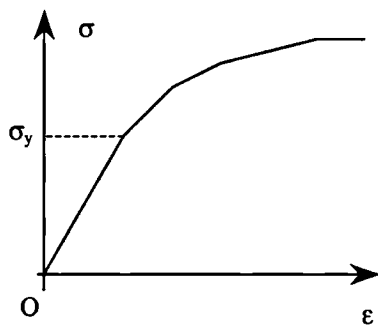
Figure 4.5: *Elastic, multi-linear hardening model*   **Figure 4.6:** *Simple power model*
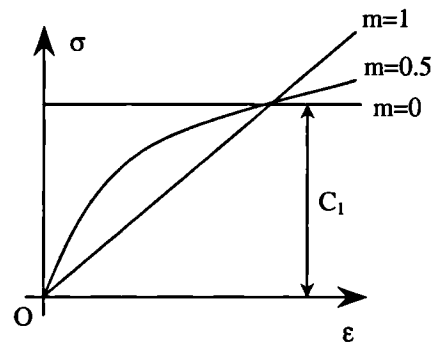
Improvements to overall modelling accuracy can be achieved by adopting expressions of the form given by Equations 4.1 or 4.2, where C_2, C_3, C_4, C_5, p and q are constants, but inaccuracies at low strains remain. Equation 4.1 was originally proposed by Ludwik in 1909, and Equation 4.2 by Swift. Both expressions were described by Slater (1977).

$$\sigma = C_2 + C_3\varepsilon^p \tag{4.1}$$

$$\sigma = C_4(C_5 + \varepsilon)^q \tag{4.2}$$

An elastic, power hardening model can be employed to overcome inaccuracies at low strains, but creates a discontinuity of stiffness at σ_y. The model assumes linear elastic response until σ_y

is reached, upon which a power relationship is adopted. This is mathematically described by Equations 4.3a and 4.3b, and represented in Figure 4.7.

$$\sigma = E_0 \varepsilon \qquad (\sigma \leq \sigma_y) \qquad (4.3a)$$

$$\sigma = C_6 \varepsilon^r \qquad (\sigma \geq \sigma_y) \qquad (4.3b)$$

where E_0 is Young's modulus, and C_6 and r are constants.
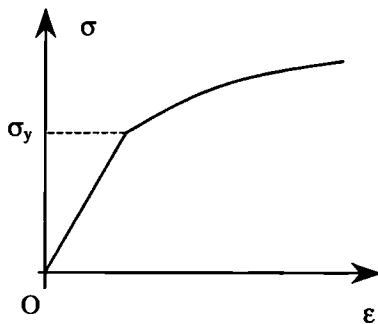
Figure 4.7: *Elastic, power hardening model*

An odd power polynomial model was adopted by Frye & Morris in 1976 for the prediction of the moment-rotation behaviour of several types of connection (Chen & Lui, 1991). The model is described in stress-strain notation by Equation 4.4, where C_7, C_8 and C_9 are constants.

$$\varepsilon = C_7 \sigma + C_8 \sigma^3 + C_9 \sigma^5 \qquad (4.4)$$

Chryssanthopoulos & Low (2001) also adopted a power polynomial for the description of stainless steel stress-strain behaviour, of the form given in Equation 4.5, where K_1 to K_N are constants and N is the order of the polynomial. It was suggested that a sixth order polynomial was sufficient to achieve good fit to experimental stress-strain data.

$$\sigma = K_1 \varepsilon + K_2 \varepsilon^2 + K_3 \varepsilon^3 + \ldots + K_N \varepsilon^N \qquad (4.5)$$

The drawback to these polynomial models is that the constants have no physical significance, and the fluctuating nature of the curves means that there are points of increasing stiffness with increasing strains.

Ramberg & Osgood (1943) proposed the expression given in Equation 4.6 for the description of material stress-strain behaviour, where E_0 is Young's modulus and K and n are constants.

$$\varepsilon = \frac{\sigma}{E_0} + K\left(\frac{\sigma}{E_0}\right)^n \tag{4.6}$$

This basic expression was modified by Hill (1944) to give Equation 4.7, where R_p is a proof stress and c is the offset (plastic) strain at this proof stress.

$$\varepsilon = \frac{\sigma}{E_0} + c\left(\frac{\sigma}{R_p}\right)^n \tag{4.7}$$

In both expressions, (Equations 4.6 and 4.7), the elastic and plastic strains are treated separately. The power function is applied solely to the plastic strains, and the total strain is acquired by means of a summation. The Ramberg-Osgood expression is a popular material model because the constants have physical significance and it provides a smooth curve for all values of strain, with no discontinuities. A drawback to this relationship is that it is not explicitly solvable for stress. Its solution can of course be found by numerical means, but this would ideally be avoided in a structural design procedure.

The Ramberg-Osgood expression, as modified by Hill, appears in an informative Annex of ENV 1999-1-1 (1998), for the description of aluminium stress-strain behaviour. The adopted proof stress, R_p is almost exclusively that at 0.2% offset strain, which leads to the most familiar form of the Ramberg-Osgood expression, given by Equation 4.8.

$$\varepsilon = \frac{\sigma}{E_0} + 0.002\left(\frac{\sigma}{\sigma_{0.2}}\right)^n \tag{4.8}$$

4.2.3.3 Models comprising exponential functions

Slater (1977) described an expression proposed by Voce in 1948, of the form given in Equation 4.9, where C_{10}, C_{11} and k are constants. It has been shown to give good fit to engineering material stress-strain data, particularly for commercially pure aluminium. The current study has

found less good agreement for stainless steel stress-strain behaviour, because of the higher initial stiffness of the material.

$$\sigma = C_{10} + C_1\{1 - \exp(-k\varepsilon)\}$$ (4.9)

Chen & Lui (1991) described models based on exponential functions that have been applied to the prediction of the non-linear moment-rotation behaviour of connections. Presented in terms of stress and strain, Equation 4.10 was proposed by Yee & Melchers in 1986 where C_{12}, C_{13} and C_{14} are constants, and Equation 4.11 was proposed by Wu & Chen in 1990 where C_{15}, C_{16} and C_{17} are constants.

$$\sigma = C_{12}\left(1 - \exp\left(\frac{-(C_{13} + C_{14}\varepsilon)\varepsilon}{C_{12}}\right)\right)$$ (4.10)

Both Equations 4.10 and 4.11 produce continuous curves, but have insufficient constants to be able to achieve good fit to experimental data over a broad range of strains.

$$\sigma = C_{15}C_{16}\left[\ln\left(1 + \frac{\varepsilon}{C_{16}C_{17}}\right)\right]$$ (4.11)

4.2.3.4 Other models

Slater (1977) described a two-parameter hyperbolic tangent expression that was proposed by Prager for material stress-strain modelling. The expression is given in Equation 4.12 where C_{18} is a constant.

$$\sigma = C_{18}\tanh\left(\frac{E_0\varepsilon}{C_{18}}\right)$$ (4.12)

The model produces a continuous stress-strain curve that approaches C_{18} asymptotically with an initial gradient E_0, though there are too few constants to achieve good agreement with experimental data.

Although the degree of non-linearity and strain hardening is more pronounced for stainless steel, aluminium exhibits similar stress-strain behaviour but with generally lower strength, stiffness

and ductility. Annex E of the European design code for aluminium structures, ENV 1999-1-1 (1998) presents a stress-strain model of the form $\sigma = \sigma(\varepsilon)$, containing three distinct behavioural regions. Region 1 exhibits elastic behaviour up to the proportional limit. Region 2 exhibits inelastic behaviour from the proportional limit to the elastic limit. Finally Region 3 exhibits strain-hardening behaviour. A different expression is applied to each region, whilst continuity between regions is maintained.

4.2.3.5 Summary

The models outlined above have been evaluated for their applicability to the description of stainless steel stress-strain behaviour on the basis of five key points:

- Continuity
- Number of parameters
- Accuracy of stress-strain description at low strains
- Overall accuracy of stress-strain description
- Explicit solvability for stress

For agreement with experimental data, the Ramberg-Osgood model is superior to other models, and is particularly accurate at low strains. It is not explicitly solvable for stress, but this is inconsequential for numerical modelling, and for design procedures where the designer is not directly exposed to the material model. Ideally the model should have as few parameters as possible, without compromising accuracy, though perhaps of greater importance than number is that the parameters have physical meaning. The basic Ramberg-Osgood model is considered to meet the requirements most closely, and is developed in Section 4.2.4 to achieve improved overall agreement with experimental data.

4.2.4 Investigation and extension of the Ramberg-Osgood model

The basic Ramberg-Osgood formulation (Equation 4.8) gives excellent agreement with experimental stress-strain data up to $\sigma_{0.2}$. At higher strains however, the model generally over estimates the stress corresponding to a given level of strain (Gardner & Nethercot, 2001a).

Consider initially the basic Ramberg-Osgood expression up to $\sigma_{0.2}$. In order to calibrate the expression to experimental stress-strain data, the values of E_0 and $\sigma_{0.2}$ need to be defined. In addition to this, the strain hardening exponent, n, which characterises the degree of non-linearity of the stress-strain curve has to be determined. This requires the definition of two fixed points on the curve, and the subsequent evaluation of n through Equation 4.13.

$$ n = \frac{\log(\varepsilon_2/\varepsilon_1)}{\log(\sigma_2/\sigma_1)} \tag{4.13} $$

The choice of which two points to use as the basis for evaluating n depends largely on the application of the expression. The stress-strain description will be most accurate close to the regions in which the two points are defined. For typical structural applications, strains beyond about 5% are of limited importance, whereas the accuracy of stress-strain description at lower strains is paramount. Use of the 0.2% proof stress as one of the points is common, as this value is recorded in mill tests, and is readily available in material specification standards. Comparison of the Ramberg-Osgood expression with experimental stress-strain data shows that with the evaluation of n based on the 0.01%, 0.05% or 0.1% strains (three frequently selected second points), good agreement is achieved below the 0.2% proof stress. The absence of a commonly accepted second point indicates that neither one demonstrates persuasively better agreement.

Recent proposals to achieve improved modelling accuracy at strains above $\sigma_{0.2}$ have been made by Mirambell & Real (2000), Macdonald et al. (2000) and Olsson (2001). Olsson's work has a firm theoretical basis, but was concerned with the overall stress-strain description, whereas Mirambell and Real and Macdonald et al. placed more emphasis on strains concurrent with structural applications.

Macdonald et al. (2000) conducted a series of tensile tests on material cut from cold-formed (Grade 1.4301) stainless steel lipped channel cross-sections. The inaccuracies of the basic Ramberg-Osgood expression at high strains were observed, and Equation 4.14 was proposed to achieve better fit with experimental stress-strain data.

$$\varepsilon = \frac{\sigma}{E_0} + 0.002\left(\frac{\sigma}{\sigma_1}\right)^{\left(i+j\left(\frac{\sigma}{\sigma_1}\right)^k\right)}$$

(4.14)

where σ_1 is the stress at offset strain, ε_1 and i, j and k are constants that may be derived from experimental stress-strain data. The expression was shown to be very accurate, though the study was limited to a particular grade of stainless steel, a particular thickness, and in a particular loading direction.

Mirambell & Reals's proposal was to use two adjoining Ramberg-Osgood curves. The basic Ramberg-Osgood expression, repeated in Equation 4.15, is used up to the 0.2% proof stress, and a modified Ramberg-Osgood expression, given in Equation 4.16, beyond the 0.2% proof stress. The modified expression re-defines the origin for the second curve as the point of 0.2% proof stress, and ensures continuity of the gradients.

$$\varepsilon = \frac{\sigma}{E_0} + 0.002\left(\frac{\sigma}{\sigma_{0.2}}\right)^n$$ $(\sigma \le \sigma_{0.2})$ (4.15)

$$\varepsilon = \frac{(\sigma - \sigma_{0.2})}{E_{0.2}} + \varepsilon_{pu}\left(\frac{\sigma - \sigma_{0.2}}{\sigma_u - \sigma_{0.2}}\right)^{n'_{0.2,u}} + \varepsilon_{t0.2}$$ $(\sigma \ge \sigma_{0.2})$ (4.16)

where σ_u is the ultimate material strength, ε_{pu} is the plastic strain at ultimate strength, $\varepsilon_{t0.2}$ is the total strain at the 0.2% proof stress, $n'_{0.2,u}$ is a strain hardening exponent that can be determined from the ultimate strength and another intermediate point, and $E_{0.2}$ is the stiffness at the 0.2% proof stress, and can be determined from Equation 4.17.

$$E_{0.2} = \frac{\sigma_{0.2} E_0}{\sigma_{0.2} + 0.002 \, n \, E_0}$$

(4.17)

It is worth noting that the curve defined by Equation 4.16 produces a slight inconsistency in that it does not pass through the point of σ_u at ε_{tu}, (where ε_{tu} is the total strain at ultimate stress).

However, due to the high ductility of stainless steels, the errors incurred are negligible. For mathematical consistency Equation 4.16 would be replaced by Equation 4.18.

$$\varepsilon = \frac{(\sigma - \sigma_{0.2})}{E_{0.2}} + \left(\varepsilon_{tu} - \frac{\sigma_u - \sigma_{0.2}}{E_{0.2}} - \varepsilon_{t0.2} \right) \left(\frac{\sigma - \sigma_{0.2}}{\sigma_u - \sigma_{0.2}} \right)^{n'_{0.2,u}} + \varepsilon_{t0.2} \qquad (\sigma \geq \sigma_{0.2}) \qquad (4.18)$$

Figure 4.8 demonstrates the improved accuracy at higher strains of the compound Ramberg-Osgood expression, given in Equation 4.16, over the basic Ramberg-Osgood expression, given in Equation 4.8, for describing a typical experimental stainless steel stress-strain curve.
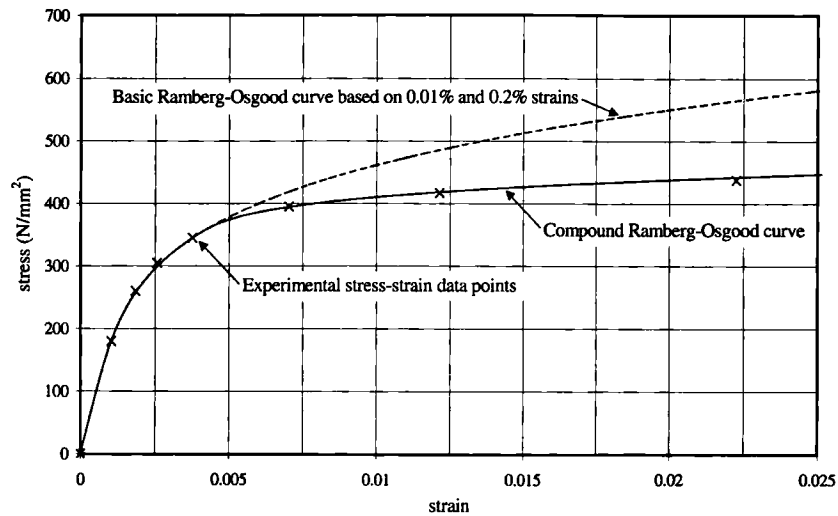
Figure 4.8: *Comparison between compound and basic Ramberg-Osgood models*

For the description of compressive stress-strain behaviour, Equations 4.16 and 4.18 encounter difficulty because there is no ultimate stress in compression due to the absence of the necking phenomenon. It was initially proposed simply to adopt the ultimate tensile strengths and corresponding strains to represent the compressive behaviour (Gardner & Nethercot, 2001a). In general this was an acceptable solution though increased deviation (between experimental and modelled material behaviour) was observed. It was therefore subsequently proposed to use the 1% proof stress instead of the ultimate stress to describe compressive stress-strain behaviour, and Equation 4.19 was derived. Equation 4.15 continued to apply for stresses up to $\sigma_{0.2}$.

$$\varepsilon = \frac{(\sigma - \sigma_{0.2})}{E_{0.2}} + \left(0.08 - \frac{\sigma_{1.0} - \sigma_{0.2}}{E_{0.2}}\right)\left(\frac{\sigma - \sigma_{0.2}}{\sigma_{1.0} - \sigma_{0.2}}\right)^{n'_{0.2,1.0}} + \varepsilon_{t0.2} \qquad (\sigma \geq \sigma_{0.2}) \qquad (4.19)$$

where $n'_{0.2, 1.0}$ is a strain hardening coefficient representing a curve that passes through $\sigma_{0.2}$ and $\sigma_{1.0}$.

Equation 4.19 was found to give excellent agreement with experimental stress-strain data, both in compression and tension, up to strains of approximately 10%.

4.2.5 Corner properties

4.2.5.1 General

The properties of the corner regions in cold-formed stainless steel cross-sections differ from the properties of the flat regions due to the material's response to deformation. Stainless steel exhibits pronounced strain hardening, resulting in corner regions of cold-formed SHS and RHS having 0.2% proof strengths commonly between 20% and 100% higher than the 0.2% proof strengths of the flat regions, accompanied by a corresponding loss in ductility.

4.2.5.2 Previous work

Karren (1967) carried out an extensive study into the corner properties of cold-formed carbon steel cross-sections. It was stated that the yield strength of cold-worked carbon steel can be considerably in excess of the ultimate strength of the original material. The corner regions represent between about 10% and 40% of the total area for typical structural cross-sections, so their influence can be important.

Abdel-Rahman & Sivakumaran (1997) stated that the Karren model can only be used to predict the yield strength in the curved corner portions of cross-sections, and it is not valid for the areas immediately adjacent to the corners (which also showed strength enhancements). The Karren model was revised by multiplying the increase in yield strength in the corner regions by a factor of 0.6, and applying this increased yield strength to a region extending to $0.5\pi r_i$, where r_i is the internal corner radius, beyond the curved corner portions of cross-sections.

Based largely upon the research carried out by Karren (1967), Van den Berg & Van der Merwe (1992) calibrated an expression to predict the corner mechanical properties of cold-formed stainless steel material. Tensile corner coupons were prepared by bending strips of the virgin material to different internal corner radii.

Equation 4.20 is given in the AISI Cold-Formed Steel Design Manual (AISI, 1986) to evaluate the 0.2% proof strength of corner material, $\sigma_{0.2,c}$. Symbols have been harmonised with those adopted in the remainder of this thesis.

$$\sigma_{0.2,c} = \frac{B_c\, \sigma_{0.2}}{(r_i/t)^m} \qquad (4.20)$$

where $\sigma_{0.2}$ is the 0.2% proof strength of the virgin material, t is the thickness of the material, r_i is the internal corner radius, and m and B_c are constants, found by Van den Berg and Van der Merwe by means of a linear regression analysis of experimental results to be given by Equations 4.21 and 4.22 respectively.

$$m = 0.060\frac{\sigma_u}{\sigma_{0.2}} + 0.031 \qquad (4.21)$$

$$B_c = 3.289\frac{\sigma_u}{\sigma_{0.2}} - 0.861\left(\frac{\sigma_u}{\sigma_{0.2}}\right)^2 - 1.340 \qquad (4.22)$$

The results of the formulations apply to uniaxial tensile properties in the longitudinal direction of the corner material. The linear regression analysis was based on a limited number of results, and would benefit from comparison with further tests.

A study was carried out to determine whether these formulations could be applied to the prediction of the corner material strength in cold-formed stainless steel SHS and RHS. Table 4.1 displays the results from six tests conducted on flat and corner material cut from cold-formed stainless steel SHS and RHS. One of the tests was performed by Rasmussen & Hancock (1993a) on material from a Grade 1.4306 SHS. The remaining five tests were conducted as part of the current investigation, where all material was Grade 1.4301. It should be noted that the six cross-sections were not fabricated by direct bending from a flat sheet, but instead by first forming the material into a CHS, and then shaping it into an SHS or RHS.

Table 4.1: Results from tensile tests conducted on flat and corner regions of cold-formed SHS and RHS

Section size	r_i/t	Flat tensile properties		Corner tensile properties			Corner/flat values			
		$\sigma_{0.2}$ (N/mm²)	σ_u (N/mm²)	$\sigma_{0.2,c}$ (N/mm²)	$\sigma_{1.0,c}$ (N/mm²)	$\sigma_{u,c}$ (N/mm²)	$\sigma_{0.2,c}/\sigma_{0.2}$	$\sigma_{0.2,c}/\sigma_u$	$\sigma_{1.0,c}/\sigma_u$	$\sigma_{u,c}/\sigma_u$
SHS 80×80×3[1]	0.84	408	695	580	-	805	1.42	0.83	-	1.16
SHS 80×80×4[2]	1.18	457	706	594	723	820	1.30	0.84	1.02	1.16
SHS 100×100×2[2]	0.68	382	675	587	745	820	1.54	0.87	1.10	1.21
SHS 150×150×4[2]	1.57	314	659	563	649	844	1.79	0.85	0.98	1.28
RHS 100×50×6[2]	0.93	605	754	631	773	802	1.04	0.84	1.03	1.06
RHS 150×100×4[2]	1.46	297	663	572	690	809	1.93	0.86	1.04	1.22
						Mean:	1.50	0.85	1.04	1.18

Notes: [1]   Tests conducted by Rasmussen & Hancock (1993a)
        [2]   Tests conducted by Gardner & Nethercot

Unlike the fabrication method of directly bending flat sheet to form the SHS or RHS, which produces essentially unchanged properties in the flat regions, with large strength enhancements at the corners, the method of first forming a CHS, and then shaping into an SHS or RHS appears to produce moderate strength enhancements in the flat regions, and greater enhancements in the corners, (beyond the strengths of the direct fabrication method).

Table 4.2 compares the measured corner material properties with those predicted by the Equations 4.20 to 4.22. It should be noted that the predictions are based on the average properties of material cut from the flat faces of the cross-sections. Material properties of the flat sheet (prior to fabrication into SHS and RHS) are not known with any degree of accuracy.

Table 4.2: *Comparison between Van den Berg & Van der Merwe (1992) model and test results for corner material properties*

Section size	r_i/t	Flat tensile properties		Corner tensile properties		
		$\sigma_{0.2}$ (N/mm^2)	σ_u (N/mm^2)	Test $\sigma_{0.2,c}$ (N/mm^2)	Pred $\sigma_{0.2,c}$ (N/mm^2)	Test $\sigma_{0.2,c}$ / Pred $\sigma_{0.2,c}$
SHS 80×80×3[1]	0.84	408	695	580	737	1.27
SHS 80×80×4[2]	1.18	457	706	594	755	1.27
SHS 100×100×2[2]	0.68	382	675	587	718	1.22
SHS 150×150×4[2]	1.57	314	659	563	518	0.92
RHS 100×50×6[2]	0.93	605	754	631	867	1.37
RHS 150×100×4[2]	1.46	297	663	572	478	0.84
					MEAN:	**1.15**
					ST DEV:	**0.22**

Notes: [1] Tests conducted by Rasmussen & Hancock (1993a)
[2] Tests conducted by Gardner & Nethercot (Chapter 3)

It can been seen from Table 4.2 that (based on the material properties from the flat regions of the cross-section) the corner material properties of cold-formed stainless steel SHS and RHS are not well predicted by the Van den Berg & Van der Merwe (1992) model. Attempts to re-calibrate the model against the test results from Table 4.1 improved the mean prediction, but the scatter remained large.

4.2.5.3 Proposal

Following further analysis of the available test data in Table 4.1, it was found that the 0.2% proof strength of the corner material, $\sigma_{0.2,c}$ could be accurately described as a fixed percentage of the ultimate strength of the flat material, σ_u. It is therefore proposed that $\sigma_{0.2,c}$ be evaluated through Equation 4.23.

$$\sigma_{0.2,c} = 0.85\sigma_u \tag{4.23}$$

Explanation of the expression is as follows: Corner material is work hardened to strains between about 10% and 20%. This region of the stress-strain curve is relatively flat, so the stress is not sensitive to the exact level of applied strain. Between 10% and 20% strain, the stress is approximately 85% of the ultimate material strength.

Despite the simplicity of Equation 4.23, excellent agreement with the test results in Table 4.1 is achieved. The mean test $\sigma_{0.2,c}$ is predicted exactly, with a standard deviation of 2%. Equation 4.23 will therefore be used for generating the corner material properties in the FE models described throughout this chapter.

4.3 RESIDUAL STRESSES

4.3.1 Introduction

Residual stresses are introduced into cold-formed stainless steel members as a result of the deformations during the cold-forming fabrication process, and due to the thermal gradients that are induced during welding.

Measurements of residual stresses in cold-formed stainless steel cross-sections are scarce. Knowledge of the magnitude and distribution of residual stresses within a cold-formed stainless steel cross-section is therefore speculative. Some measurements were taken by Rasmussen & Hancock (1993a) as part of an experimental programme on cold-formed stainless steel tubular members.

Due to the inherent uncertainty associated with residual stress magnitudes and distributions, their effect is often taken into account in numerical models with an appropriate increase in the magnitude of initial geometric imperfection. For this study, an approximate, though representative solution to the modelling of residual stresses in cold-formed stainless steel CHS, SHS and RHS is adopted.

4.3.2 Deformationally induced residual stresses

Residual stress distributions arising from the cold-forming of carbon steel cross-sections have been investigated analytically and experimentally by Ingvarsson (1975, 1979). Weng & Peköz (1988) concluded that membrane residual stresses in cold-formed carbon steel lipped channel sections were negligible, and proposed an idealised bending residual stress distribution. The proposal comprised uniform compressive residual stress of magnitude $0.5\sigma_y$, where σ_y is the material yield strength, on the inner surface of the section, with tensile residual stress on the outer surface of equal magnitude. A linear distribution was assumed through the plate thickness. Further work was reported by Schafer & Peköz (1998), proposing the bending residual stresses shown in Figure 4.9 (a) and (b). Figure 4.9 (a) is for a roll-formed section and Figure 4.9 (b) is for a press-braked section. Mean membrane residual stresses of $6.8\%\sigma_y$ (tension) in the corners, and $1.7\%\sigma_y$ (compression) in the stiffened elements were found for roll-formed sections. Additional independent experimentation conducted by Abdel-Rahman & Sivakumaran (1997) led to the proposed distribution in Figure 4.9 (c) for a roll-formed section.

(a) Roll-formed   (b) Press-braked   (c) Roll-formed
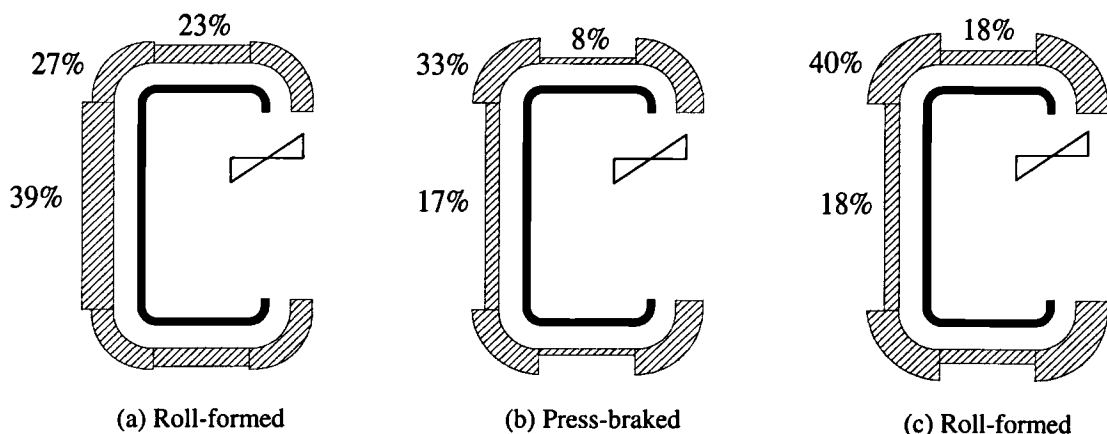
Figure 4.9: *Idealised bending residual stress distributions due to cold-forming*

Analysis of the residual stress measurements recorded by Rasmussen & Hancock (1993a) on a stainless steel (Grade 1.4306) SHS was carried out. The fabrication route for the cross-section

involved first forming into a CHS, followed by welding, and finally shaping into an SHS. Measurements were taken from the centre of one of the flat faces of the cross-section, away from the weld line, and yielded negligible membrane residual stresses, but considerable bending residual stresses. Equal and opposite extreme fibre strains corresponding to approximately 75% of the yield strain were observed. Due to the gradually yielding nature of the material, this corresponds to residual stresses of approximately 85% of the yield stress, (taken as the 0.2% proof stress). Higher residual stresses than observed in the carbon steel channel sections are expected, because the manufacturing route of the stainless steel SHS involved a greater degree of cold-working. With the absence of further experimental results, the uniform bending residual stress distribution in Figure 4.10 can be assumed for cold-formed stainless steel SHS and RHS that have followed the described fabrication route. It may also be assumed that a press-braked cross-section will contain residual stresses of a somewhat lower magnitude.

$$\sigma_r = 0.85\sigma_{0.2}$$
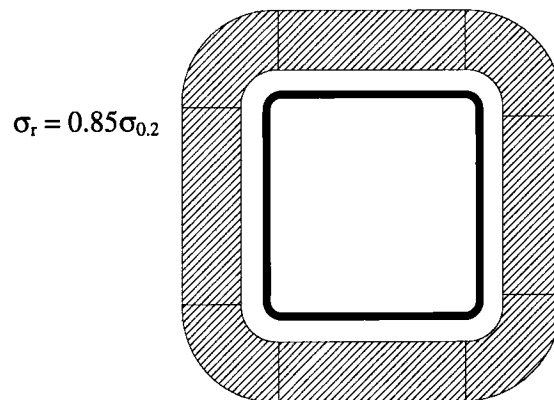
Figure 4.10: *Proposed through-thickness bending residual stress distribution for cold-formed stainless steel SHS and RHS*

4.3.3 Thermally induced residual stresses

Thermally induced residual stresses resulting from welding have been thoroughly investigated in the past. A detailed account of their formation and effects on carbon steel cross-sections has been given by Lay & Ward (1969). Stainless steel has a higher coefficient of thermal expansion, and a lower value of thermal conductivity than carbon steel. It is therefore expected that thermal residual stresses would be greater in stainless steel cross-sections. Bredenkamp et al. (1992) found that the magnitudes of residual stresses in built up stainless

steel I-sections were of the same order as in an equivalent carbon steel section, whilst Lagerqvist & Olsson (2001) carried out a similar study and observed considerably higher residual stresses in the stainless steel sections.

For the modelling of welding residual stresses in cold-formed SHS and RHS stainless steel cross-sections, it is proposed to apply the simplified distribution shown in Figure 4.11 to the welded face of the cross-section.
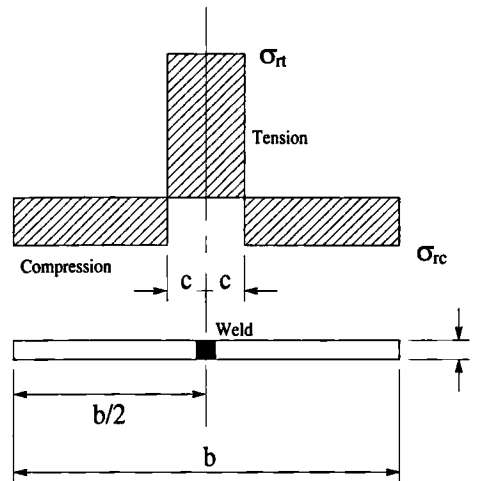
Figure 4.11: *Idealised weld-induced residual stress distribution for SHS and RHS*

The half width, c of the tension area for a single continuous weld was given by Young (1974), following tests on Grade 43 carbon steel as Equation 4.24.

$$c = 50\alpha \frac{A}{\Sigma t} \frac{235}{\sigma_y} \tag{4.24}$$

where A is the cross-sectional area of added metal, Σt is the sum of the plate thicknesses meeting at the weld, and α is the process efficiency factor, suggested as 0.90 for submerged arc welding, 0.80 for manual welding and 0.62 for MIG (spray) welding. In the absence of the weld details, a width of b/5 can be assigned to the tensile residual stress area (Masubuchi, 1980).

Assuming the magnitude of the tensile residual stress area is taken as yield (or the 0.2% proof stress), self-equilibrium of axial forces requires Equation 4.25 to hold, where σ_{rt} and σ_{rc} are the tensile and compressive residual stresses respectively.

$$\sigma_{rc} = \sigma_{rt} \frac{2c}{b-2c} \tag{4.25}$$

Measurements of weld-induced residual stresses in carbon steel CHS have been made by Chen & Ross (1977) and Ostapenko (1977). Typical results from the Chen and Ross study are shown in Figure 4.12, where the dashed line (described by Table 4.3) represents their proposed linear residual stress pattern. No measurements of weld-induced residual stresses are available for stainless steel CHS.

Table 4.3: *Chen & Ross proposed linear weld-induced residual stress pattern*

Angle from weld, θ (radians)	Residual stress, σ_r
0.0	σ_y
0.3	$-0.3\sigma_y$
1.0	0
1.2	$0.1\sigma_y$
> 2.0	0

Note: Tensile residual stresses are positive
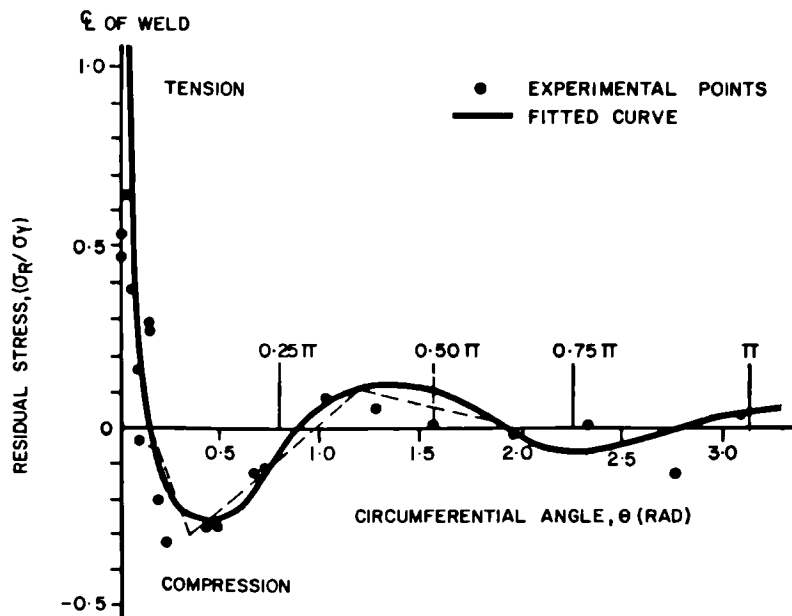
Figure 4.12: *Residual stress measurements in welded carbon steel CHS (Chen & Ross, 1977)*

Based on the measurements taken by Chen and Ross, Gao et al. (1998) proposed a simpler stress-block model, which was successfully applied to the FE modelling of short steel cylinders in compression and bending. Their proposed projected residual stress distribution is shown in Figure 4.13.
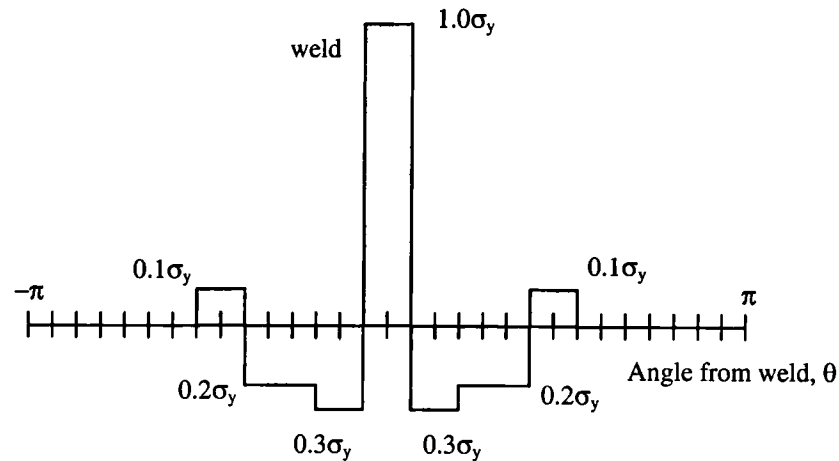
Figure 4.13: *Projected CHS residual stress model proposed by Gao et al. (1998)*

This distribution shall be adopted for the modelling of weld-induced residual stresses in cold-formed stainless steel CHS (with $\sigma_{0.2}$ used in place of σ_y).

4.3.4 Discussion

Having proposed bending and membrane residual stress distributions for application to the numerical modelling of cold-formed stainless steel SHS and RHS, it is only the membrane stresses introduced through welding, that need to be explicitly defined in an FE model. Rasmussen & Hancock (1993a) observed that the tension and compression coupons cut from finished tubes curved longitudinally as a result of the through-thickness bending residual stresses. This same phenomenon was observed in the current study (see Section 3.3.1). However, elastic straightening of the coupons as part of the testing procedure approximately re-introduces the bending residual stresses. Therefore, provided that material properties are established from coupons cut from within the cross-section, the effects of bending residual stresses will be inherently present, and do not have to be explicitly defined in the FE model.

4.4 INITIAL IMPERFECTIONS

For close replication of observed structural behaviour, accurate knowledge of both the distribution and magnitude of cross-sectional and member imperfections is required. This is a complex function of the rolling and fabrication process, with sufficient variability between cross-sections to have precluded their definitive characterisation. Very close agreement between the behaviour of FE models and experiments can be achieved by the superposition of imperfection modes, with the magnitudes determined by means of parametric studies. Sully & Hancock (1999) described how sympathetic and unsympathetic local imperfections were combined with an overall imperfection, to calibrate an FE model to experiments on cold-formed tubular cross-sections.

However, for the generation of further results from parametric studies, and to investigate trends in areas that are not supported by experimental results, a general imperfection that is representative of cold-formed stainless steel hollow sections is sought. Its suitability can be established through comparison with available experimental data.

4.4.1 Local imperfection mode

4.4.1.1 SHS and RHS

For convenience in both hand and numerical analyses, the shape of a local initial geometric imperfection is often assumed to be the same as that of the lowest buckling mode, or eigenmode (Dawson & Walker, 1972). This shape of imperfection, given in Equation 4.26 for a flat plate, is also the most severe in terms of local buckling behaviour, so long as the amplitude of imperfection is sufficiently small, since it coincides with the deflected shape that would occur in a buckled perfect plate. For larger imperfections, the most severe shape is governed by the post-buckling, rather than the critical buckling, behaviour (Wadee, 2000). The lowest buckling mode, generated from an elastic eigenmode analysis of each of the cold-formed stub columns, was therefore used as the initial imperfection mode. It should be noted that no clear local imperfection mode emerged from the experimental data.

$$\omega = \omega_0 \sin\left(\frac{m\pi x}{l}\right)\cos\left(\frac{\pi y}{b}\right) \quad , m = 1, 2, .. \quad (4.26)$$

The four lowest buckling modes from an eigenmode analysis of SHS 80×80×3- SC1 are shown in Figure 4.14 (a) to (d).

(a) Eigenmode 1   (b) Eigenmode 2   (c) Eigenmode 3   (d) Eigenmode 4
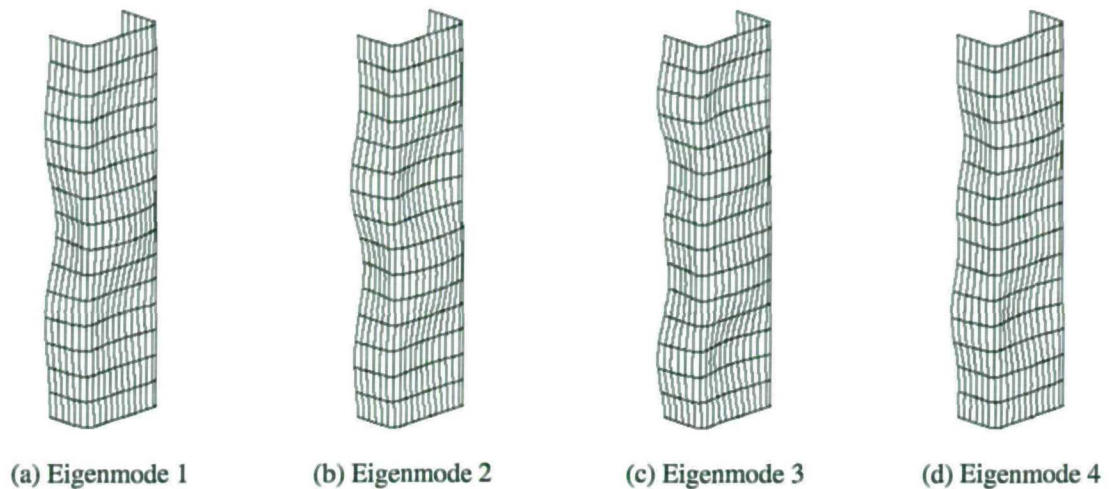
Figure 4.14: *Four lowest eigenmodes for SHS 80×80×3- SC1*

4.4.1.2 CHS

As for the SHS and RHS, the local imperfection shape for the CHS stub columns was taken as the lowest buckling mode from an eigenmode analysis. For all modelled cases the lowest eigenmode comprised a sinusoidal curve in both the longitudinal and circumferential directions. Wheeler & Bridge (2000) conducted a detailed analysis of the effect of imperfection modes and magnitudes on the behaviour of thin-walled steel CHS filled with concrete. Their total imperfection included local and global components generated from eigenmode buckling analyses.

4.4.2 Global imperfection mode

For the FE modelling of pin-ended columns that fail by overall flexural buckling, a global imperfection that corresponded to the lowest buckling mode (generated from an elastic eigenmode analysis) was adopted. For a column where the ends are free to rotate this is a single half-sine wave. The complete initial imperfection field comprised a superposition of the local and global modes.

4.4.3 SHS and RHS local imperfection amplitude

The amplitude of local plate imperfection has a significant influence on the behaviour of stub columns, though measurements of initial imperfections are commonly omitted from

experimental programmes. Analysis was therefore conducted on local imperfection amplitudes measured in the current study (described in Section 3.4.4), and an investigation into the prediction of imperfection amplitudes was carried out.

4.4.3.1 Observations

As noted in Section 3.4.4, towards the ends of the stub columns the faces of the cross-sections were distorted by bending residual stresses. The magnitudes of initial imperfection in these end regions are consequently relatively high, though they are not representative of the overall out-of-flatness of the faces of the stub columns. By adopting imperfections of the magnitude observed at the stub column ends it was found that the FE models consistently under-predicted the strength and deformation capacity of the corresponding test. It was therefore decided to investigate the initial imperfections that were present over the less distorted central three-quarter portion of the stub columns. Figure 4.15 shows a schematic imperfection profile and defines $u_{1,max}$ as the maximum initial imperfection from the line connecting the stub column ends and $u_{2,max}$ as the maximum initial imperfection from the line connecting the 3/4 points of the stub column.
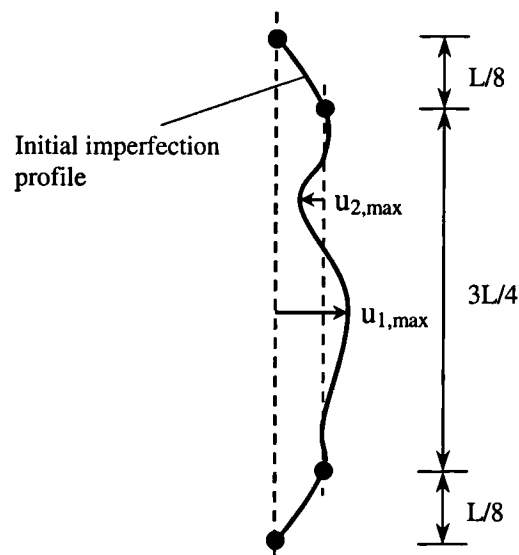
Figure 4.15: *Definition of initial imperfection amplitudes ($u_{1,max}$ and $u_{2,max}$)*

Table 4.4 gives the mean maximum initial imperfection amplitudes $u_{1,max}$ and $u_{2,max}$ for each of the tested SHS stub column specimens with comparison to predicted values. Table 4.5 presents

the same comparison for RHS stub columns, where $u_{1,max}$ and $u_{2,max}$ are the mean maximum initial imperfection amplitudes for the two wider faces of the cross-section. Consistently higher imperfection magnitudes were observed on the wider faces of the RHS cross-sections than on the narrow ones, indicating that the plate width is an important parameter in their formation.

For each cross-section size, imperfection measurements were generally conducted on two independent specimens. Although imperfection data exhibits notoriously high scatter, Figure 4.16 shows that there is a good degree of consistency between the independent measurements. The tendency for specimen 2 imperfections to be higher than specimen 1 imperfections has no significance.

Imperfection amplitudes from Specimen 1 samples (mm)
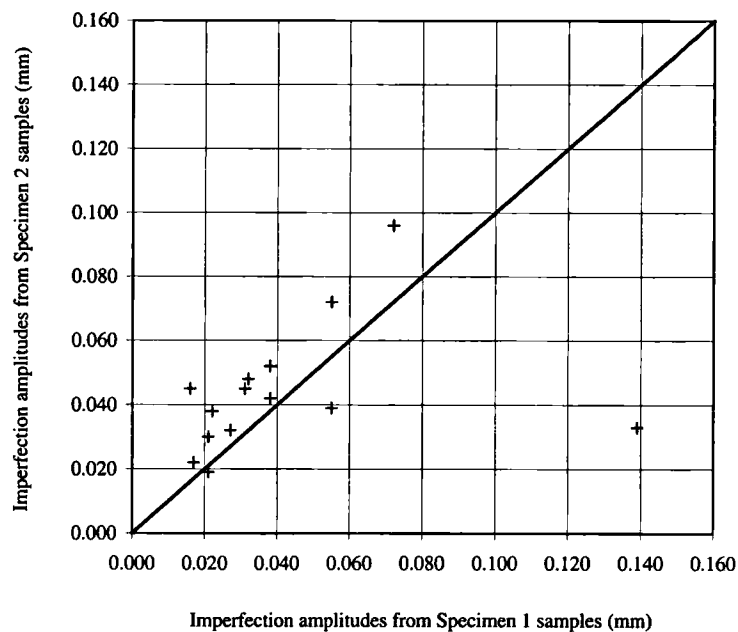
Figure 4.16: *Comparison of imperfection amplitudes from independent specimens*

4.4.3.2 Prediction of imperfection amplitude

The simplest means of predicting the amplitude of an initial plate imperfection, ω_0 is as a fixed multiple of the plate thickness, i.e. $\omega_0 = Kt$, where K is a constant. Dawson & Walker (1972) showed that an adequately conservative fit to test data on cold-formed steel cross-sections could be achieved with an imperfection amplitude of 0.2t, though they recognised that an imperfection amplitude defined as a fixed multiple of the plate thickness is unsuitable as a general parameter for all plates. A further expression given in Equation 4.27 was also shown to be unsuitable as a general parameter. It was concluded that an imperfection amplitude of the form given in

Equation 4.28 was more rational than the previous two expressions, and was in agreement with current rolling practice. It should be noted that the 0.2% proof stress, $\sigma_{0.2}$ has been used in place of the yield stress, σ_y in Equations 4.27 and 4.28 to enable application to stainless steel. Dawson and Walker found that a value of $\gamma = 0.2$ gave reasonable fit to test data for simply-supported plates, and square hollow sections. Square hollow sections produce no constraining moments between the elements of the cross-section due to their symmetrical nature. Their behaviour therefore closely corresponds to an assemblage of simply-supported plates (Timoshenko & Gere, 1985).

$$\omega_0 / t = \alpha(\sigma_{0.2} / \sigma_{cr})^{0.5} \qquad (4.27)$$

$$\omega_0 / t = \gamma(\sigma_{0.2} / \sigma_{cr}) \qquad (4.28)$$

where ω_0 is the initial imperfection amplitude, t is the plate thickness, $\sigma_{0.2}$ is the material 0.2% proof stress, σ_{cr} is the plate critical buckling stress and α and γ are constants. Chou et al. (2000) conducted FE modelling of cold-formed lipped channel and hat-section carbon steel stub columns with varying imperfection amplitudes. The study showed that Equation 4.28 yielded the most accurate and consistent prediction of experimental behaviour as compared to three other imperfection amplitudes of 0.1, 0.5 and 1.0 times the material thickness.

Schafer & Peköz (1998) presented some rules of thumb for the prediction of the maximum local imperfection in a stiffened element that apply for a width-to-thickness ratio less than 200, and a material thickness of less than 3 mm. A simple linear regression analysis based on plate width, w yielded Equation 4.29, and an alternative rule based on an exponential fit to the thickness was given as Equation 4.30, where ω_0 is the amplitude of the initial imperfection, w is the width of the plate, and t is the thickness of the plate in mm.

$$\omega_0 \approx 0.006w \qquad (4.29)$$

$$\omega_0 \approx 6te^{-2t} \qquad (4.30)$$

Based on observations, Schafer & Peköz (1998) also applied a probabilistic approach to the characterisation of imperfection amplitudes. For a stiffened element, a mean imperfection of 0.50 times the material thickness was generated, with a standard deviation of 0.66. This is, however, too simple an analysis to have general applicability.

The suitability of applying Equations 4.27 and 4.28 to the prediction of imperfection amplitudes in cold-formed stainless steel members (measured in the current study) was assessed. The values of α and γ were adjusted to fit the experimental results. Figures 4.17 and 4.18 show plots of predicted versus measured imperfections for Equation 4.27 and 4.28 respectively.
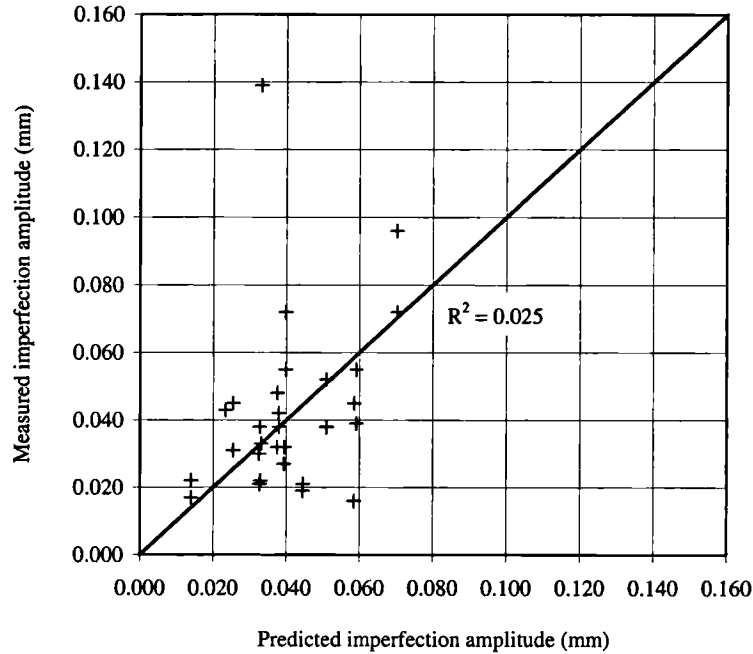
Figure 4.17: *Measured versus predicted imperfection amplitudes for $\omega_0/t = 7.3\times10^{-6}(\sigma_{0.2}/\sigma_{cr})^{0.5}$*

As Dawson and Walker found for cold-formed carbon steel members, Equation 4.27 was also found to be unsuitable for the prediction of imperfection amplitudes in cold-formed stainless steel members. A linear regression analysis revealed that best fit is achieved with $\alpha = 7.3 \times 10^{-6}$ with a corresponding coefficient of determination R^2 equal to 0.025. The R^2 parameter is a sound indicator of whether a postulated relationship gives a good approximation to observed data. The closer the R^2 value is to unity the better the prediction. A similar linear regression analysis was conducted based on Equation 4.28, revealing that best fit is achieved with $\gamma = 0.023$ (leading to Equation 4.31), with a corresponding R^2 value of 0.22. The annealed specimens contained high local imperfections (believed to have been induced by temperature gradients arising during the annealing process) and were therefore not included in the regression analyses.

$$\omega_0/t = 0.023(\sigma_{0.2}/\sigma_{cr}) \qquad (4.31)$$
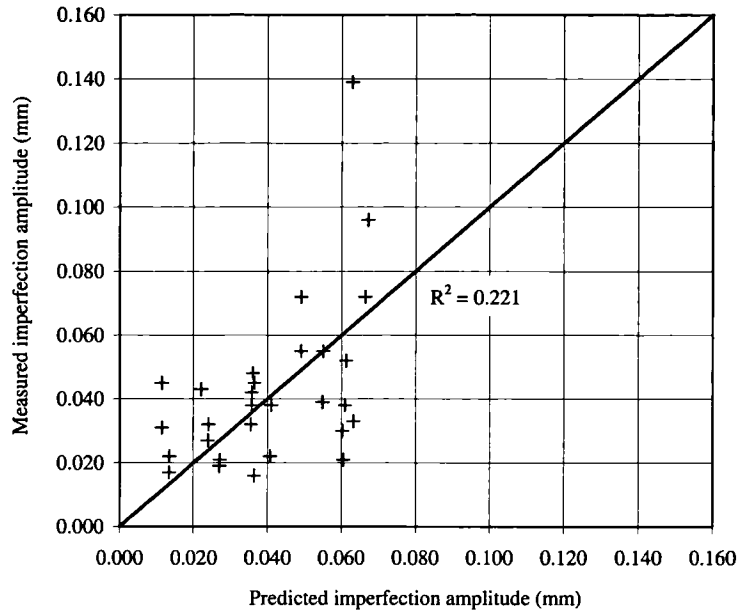
Figure 4.18: *Measured versus predicted imperfection amplitudes for* $\omega_0/t = 0.023(\sigma_{0.2}/\sigma_{cr})$

Since the two wider faces of RHS possess a higher level of edge restraint (provided by the two shorter, stiffer sides of the cross-sections) it would be expected that the amplitude of imperfections would be lower than for a corresponding face of an SHS. Figure 4.19 shows a plot of predicted versus measured imperfection amplitudes, distinguishing between SHS, RHS with aspect ratios of 0.67 and RHS with aspect ratios of 0.5.
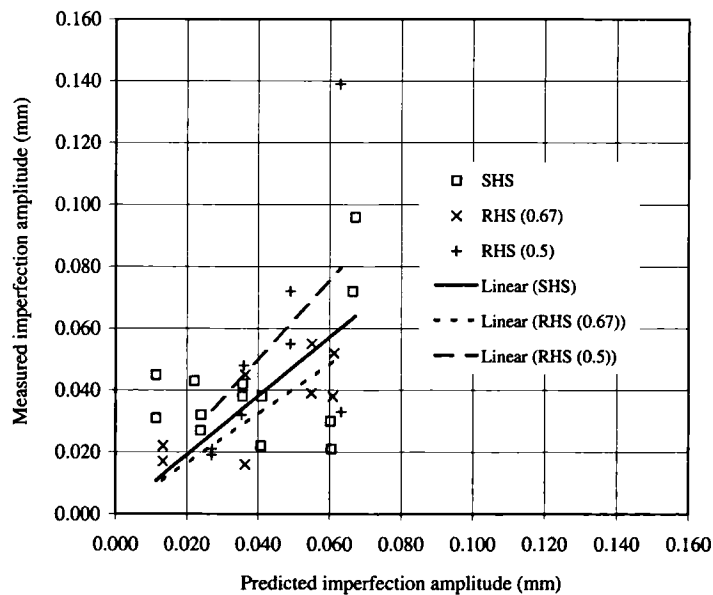
Figure 4.19: *Measured versus predicted imperfection amplitudes for different levels of edge restraint*

The data points, however, demonstrate little justification for including edge restraint in the predictive model. Equation 4.31 will therefore be adopted in the remainder of this chapter for the generation of local imperfection amplitudes in numerical models.

Tables 4.4 and 4.5 compare predicted values of maximum imperfection amplitude with measured values for SHS and RHS specimens respectively. The mean of the tensile and compressive values for E_0 and $\sigma_{0.2}$ have been adopted for each cross-section.

Table 4.4: *Measured and predicted maximum initial imperfection amplitudes for SHS stub columns*

Specimen identification	Measured values (mm)		Predicted values (mm)	Predicted/ $u_{2,max}$
	$u_{1,max}$	$u_{2,max}$	$\omega_0/t = 0.023(\sigma_{0.2}/\sigma_{cr})$	
SHS 60×60×5- SC[1]	-	-	0.011	-
SHS 80×80×3- SC1[1]	-	-	0.027	-
SHS 80×80×3- SC2[1]	-	-	0.027	-
SHS 80×80×4- SC1	-	-	0.023	-
SHS 80×80×4- SC2	-	-	0.022	-
SHS 80×80×4- SC3	0.26	0.043	0.022	0.51
SHS 80×80×4- ASC1[2]	0.34	0.078	0.013	0.16
SHS 80×80×4- ASC2[2]	0.10	0.087	0.013	0.15
SHS 100×100×2- SC1	0.28	0.021	0.060	2.88
SHS 100×100×2- SC2	0.24	0.030	0.060	2.01
SHS 100×100×3- SC1	0.33	0.022	0.041	1.85
SHS 100×100×3- SC2	0.34	0.038	0.041	1.08
SHS 100×100×4- SC1	0.32	0.038	0.036	0.94
SHS 100×100×4- SC2	0.31	0.042	0.036	0.85
SHS 100×100×6- SC1	0.29	0.027	0.024	0.88
SHS 100×100×6- SC2	0.30	0.032	0.024	0.75
SHS 100×100×8- SC1	0.28	0.031	0.011	0.36
SHS 100×100×8- SC2	0.13	0.045	0.011	0.25
SHS 150×150×4- SC1	0.46	0.072	0.066	0.92
SHS 150×150×4- SC2	0.38	0.096	0.067	0.70

Notes: [1] Specimens tested as part of other testing programme

[2] Distortions may have been induced due to thermal gradients during the annealing process

Table 4.5: *Measured and predicted maximum initial imperfection amplitudes for RHS stub columns*

Specimen identification	Measured values (mm)		Predicted values (mm)	Predicted/ $u_{2,max}$
	$u_{1,max}$	$u_{2,max}$	$\omega_0/t = 0.023(\sigma_{0.2}/\sigma_{cr})$	
RHS 60×40×4- SC1	0.23	0.017	0.013	0.78
RHS 60×40×4- SC2	0.23	0.022	0.013	0.61
RHS 120×80×3- SC1	0.70	0.038	0.061	1.60
RHS 120×80×3- SC2	0.73	0.052	0.061	1.18
RHS 120×80×6- SC1	0.45	0.016	0.036	2.27
RHS 120×80×6- SC2	0.49	0.045	0.036	0.81
RHS 150×100×3- SC[1]	-	-	0.073	-
RHS 150×100×4- SC1	0.37	0.055	0.055	1.00
RHS 150×100×4- SC2	0.37	0.039	0.055	1.41
RHS 150×100×6- SC[1]	-	-	0.037	-
RHS 100×50×2- SC1	0.37	0.139	0.063	0.45
RHS 100×50×2- SC2	0.33	0.039	0.063	1.92
RHS 100×50×3- SC1	0.66	0.055	0.049	0.89
RHS 100×50×3- SC2	0.77	0.072	0.049	0.68
RHS 100×50×4- SC1	0.26	0.032	0.035	1.11
RHS 100×50×4- SC2	0.33	0.048	0.036	0.75
RHS 100×50×6- SC1	0.30	0.021	0.027	1.29
RHS 100×50×6- SC2	0.30	0.019	0.027	1.42

Note: [1]   Specimens tested as part of other testing programme

Although the predictions in Tables 4.4 and 4.5 exhibit a high degree of scatter, it is demonstrated in Section 4.5.6 that FE models using the predicted imperfections still produce accurate agreement with test results.

4.4.4 CHS local imperfection amplitude

The available imperfection data for stainless steel CHS are too limited to enable the development of a relationship between initial imperfection amplitude and the geometric and

material properties of a cross-section. The importance of local imperfection amplitude is therefore assessed by means of a parametric study, described in Section 4.6.4, and a suitable imperfection amplitude to use for the generation of further results is presented.

4.4.5 Global imperfection amplitude

The effect of global imperfection amplitude on the flexural buckling of columns is also assessed by means of a parametric study. Details of the study are described in Section 4.7.4.

4.5 SHS AND RHS STUB COLUMN MODELLING

4.5.1 Introduction

As part of the current experimental study, a total of 33 SHS and RHS stub columns were tested to provide data on cross-section deformation capacity over a broad range of cross-sectional slenderness. The purpose of the FE modelling of SHS and RHS stub columns has been to:

- Replicate test behaviour
- Investigate the influence of key parameters
- Establish definitive values/ models for key parameters
- Act as a basis for the modelling of member behaviour.

4.5.2 Development of SHS and RHS FE models

The general-purpose FE package ABAQUS (1999) was employed for all the numerical modelling conducted in this study. Models used measured geometry, measured and predicted initial plate imperfections, assumed residual stresses and measured and predicted material properties, with enhanced material properties employed in the corner regions.

The elements chosen for the stub column models were 9-noded, reduced integration shell elements with five degrees of freedom per node, designated as S9R5 in the ABAQUS element library. This element has been shown to perform well in similar applications involving the modelling of stainless steel SHS and RHS flexural members (Real, 2001) and the buckling

response of mild steel and high performance steel box columns in axial compression (Kiymaz, 1999). S9R5 is characterised as a 'thin' shell element and is not recommended for modelling cases where transverse shear flexibility is important. Transverse shear flexibility is said to become important when the shell thickness is more than about 1/15 of a characteristic length on its surface (ABAQUS, 1999). All bar the stockiest stub column cross-sections that are modelled in this study have width-to-thickness ratios greater than 15. For consistency, the S9R5 shell element has been adopted for all modelled cases, though it is recognised that for the stockiest cross-sections the large strain formulation of the S4R 'thick' shell element may give more reliable results.

The curved geometry at the corners of the cross-sections has been modelled using curved S9R5 shell elements. Convergence studies were conducted to decide upon a suitable mesh density, with the aim of achieving suitably accurate results whilst minimising computational time.

Linear elastic eigenmode simulations were conducted to provide buckling modes to be used as initial imperfections in subsequent non-linear analyses, as described in Section 4.4. The modified Riks method (ABAQUS, 1999) was employed to solve the geometrically and materially non-linear stub column models. The modified Riks method is an algorithm that enables effective solutions to be found to unstable problems (e.g. post-ultimate response of stub columns), and adequately traces non-linear unloading paths.

For each stub column, the full length and half of the cross-section was modelled, with symmetry boundary conditions prescribed along the vertical edges. The ends of the stub columns were fixed against all degrees of freedom except for vertical displacement at the loaded end. All boundary conditions are depicted in Figure 4.20. Equations were used to constrain the nodes at the loaded end of the stub columns to move vertically in unison. Nodal loads were applied to the constrained node set.

ABAQUS requires that material behaviour is specified by means of a multi-linear stress-strain curve, defined in terms of true stress and log plastic strain. The relationships between true stress and engineering stress, σ_{true} and σ_{nom}, respectively, and log plastic strain and engineering strain, ε_{ln}^{pl} and ε_{nom}, respectively, are given in Equations 4.32 and 4.33 respectively. Engineering stress and strain are of course the nominal values that are recorded from a uniaxial stress-strain coupon test.

Loaded end fixed against all degrees of freedom except vertical displacement

Symmetry boundary conditions

Fixed against all degrees of freedom
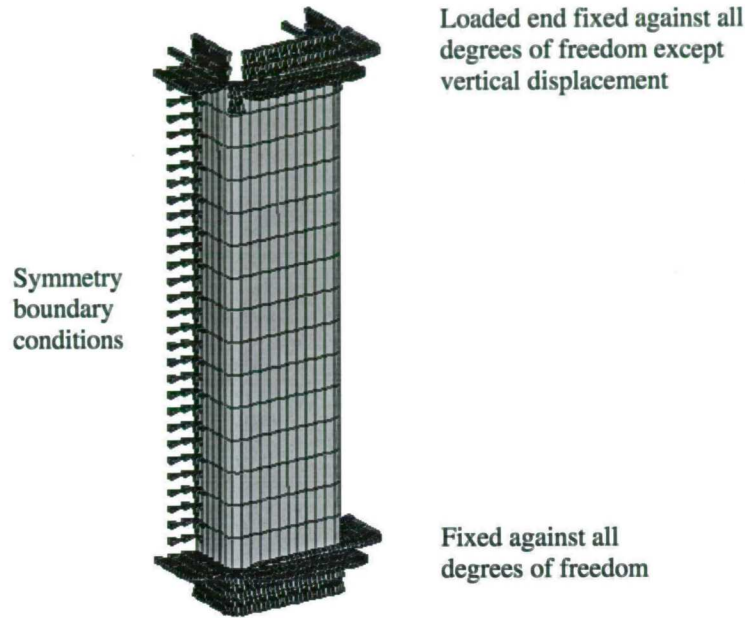
Figure 4.20: *Boundary conditions applied to SHS and RHS stub column FE models*

$$\sigma_{true} = \sigma_{nom} (1 + \varepsilon_{nom}) \tag{4.32}$$

$$\varepsilon_{ln}^{pl} = \ln (1 + \varepsilon_{nom}) - \frac{\sigma_{true}}{E} \tag{4.33}$$

Average measured compressive properties are used for the flat regions of the cross-sections, and average measured tensile corner properties for the corner regions (since no tests were conducted on corner coupons in compression).

For some of the stub column tests conducted as part of other laboratory testing programmes values for $\sigma_{1.0}$ and $n'_{0.2,1.0}$ in compression were not available. In these cases the value of $\sigma_{1.0}$ is taken as a multiple of $\sigma_{0.2}$, found from the mean of all other available test data to be $\sigma_{1.0} = 1.26\sigma_{0.2}$, and similarly $n'_{0.2,1.0}$ is taken as 2.7, which is the absolute mean value from all other available test data.

Where no measurements of corner properties were taken, predicted values (from Equation 4.31) were adopted. In the absence of strain hardening parameters for corner material n_c (equivalent

to n for flat material) and $n'_{0.2,1.0,c}$ (equivalent to $n'_{0.2,1.0}$ for flat material), absolute mean values from all other available test data were used. This provided $n_c = 4.3$ and $n'_{0.2,1.0,c} = 4.6$.

4.5.3 Extent of corner regions

The degree to which the enhanced corner properties extend beyond the curved corner portions of the cross-sections is unclear. Karren (1967) found that for carbon steel sections the effect of cold-forming extends beyond the corner to a distance approximately equal to the material thickness, t. However, stainless steels exhibit far more pronounced strain hardening than carbon steels so it may be assumed that extension to a distance t is a lower bound. Abdel-Rahman & Sivakumaran (1997) observed increased yield strengths at a distance of $0.5\pi r_i$ from the curved corner portions of cold-formed carbon steel cross-sections, though of lower magnitude than in the curved portions themselves.

A parametric study was conducted to investigate the behaviour of cold-formed stainless steel stub columns with enhanced strength regions extending to t and 2t beyond the curved corner portions, as shown in Figure 4.21. For the annealed specimens uniform flat material properties were assumed around the whole cross-section. Ultimate load-carrying capacity, F_u and deformation at ultimate load, δ_u for each model are given in Tables 4.6 and 4.7, and compared to the test values. For each comparison the measured stub column geometry, measured initial imperfections and assumed residual stresses remained constant.

(a) Corner properties extended to a distance t beyond curved portion

(b) Corner properties extended to a distance 2t beyond curved portion
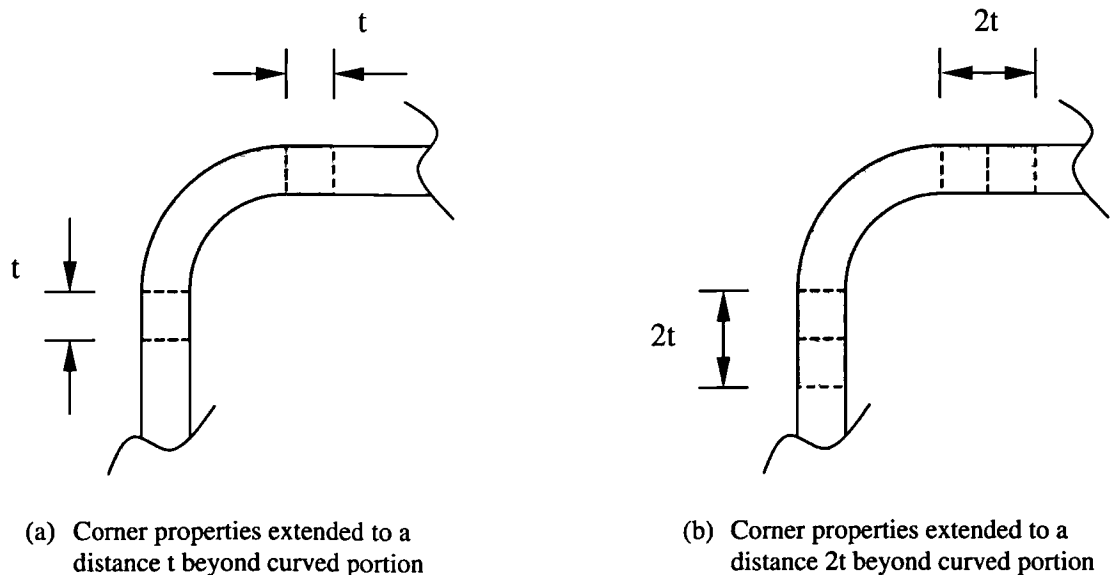
Figure 4.21: *Extents of corner regions in FE models*

Table 4.6: *Comparison between FE results using measured imperfections (with varying corner properties) and test results for SHS stub columns*

Section size	Test		FE - corner properties extended to t				FE - corner properties extended to $2t$			
	Test F_u (kN)	Test δ_u (mm)	FE F_u (kN)	FE δ_u (mm)	FE F_u/ Test F_u	FE δ_u/ Test δ_u	FE F_u (kN)	FE δ_u (mm)	FE F_u/ Test F_u	FE δ_u/ Test δ_u
SHS 60×60×5- SC[1]	801	9.3	-	-	-	-	-	-	-	-
SHS 80×80×3- SC1[2]	485	2.0	-	-	-	-	-	-	-	-
SHS 80×80×3- SC2[2]	471	2.2	-	-	-	-	-	-	-	-
SHS 80×80×4- SC1	727	7.4	620	5.1	0.85	0.69	636	5.1	0.87	0.68
SHS 80×80×4- SC2	714	7.2	648	5.6	0.91	0.78	666	5.6	0.93	0.77
SHS 80×80×4- SC3	711	7.7	648	5.6	0.91	0.73	664	5.5	0.93	0.72
SHS 80×80×4- ASC1[3]	309	8.6	368	6.9	1.19	0.80	368	6.9	1.19	0.80
SHS 80×80×4- ASC2[3]	335	7.1	352	6.2	1.05	0.87	352	6.2	1.05	0.87
SHS 100×100×2- SC1	197	1.1	185	1.5	0.94	1.32	199	2.0	1.01	1.77
SHS 100×100×2- SC2	187	0.9	185	1.5	0.99	1.64	199	2.0	1.06	2.19
SHS 100×100×3- SC1	489	2.2	452	1.8	0.92	0.81	460	1.8	0.94	0.80
SHS 100×100×3- SC2	496	2.3	430	1.6	0.87	0.70	444	1.6	0.90	0.70

Table 4.6 (continued): *Comparison between FE results using measured imperfections (with varying corner properties) and test results for SHS stub colum.*

Section size	Test		FE - corner properties extended to t				FE - corner properties extended to $2t$			
	Test F_u (kN)	Test δ_u (mm)	FE F_u (kN)	FE δ_u (mm)	FE F_u / Test F_u	FE δ_u / Test δ_u	FE F_u (kN)	FE δ_u (mm)	FE F_u / Test F_u	FE δ_u / Test δ_u
SHS 100x100x4- SC1	779	4.0	796	3.5	1.02	0.87	820	3.5	1.05	0.88
SHS 100x100x4- SC2	774	4.0	790	3.4	1.02	0.85	812	3.4	1.05	0.85
SHS 100x100x6- SC1	1513	13.4	1432	13.6	0.95	1.01	1450	13.4	0.96	1.00
SHS 100x100x6- SC2	1507	13.5	1422	12.8	0.94	0.94	1442	12.7	0.96	0.94
SHS 100x100x8- SC1	1630	29.0	1470	22.6	0.90	0.78	1502	20.3	0.92	0.70
SHS 100x100x8- SC2	1797	38.2	1466	22.2	0.82	0.58	1498	19.9	0.83	0.52
SHS 150x150x4- SC1	726	1.7	686	1.6	0.94	0.94	724	1.7	1.00	0.97
SHS 150x150x4- SC2	713	1.6	658	1.5	0.92	0.96	694	1.6	0.97	1.02
SHS MEAN:					**0.95**	**0.90**			**0.98**	**0.95**
SHS ST DEV:					**0.09**	**0.25**			**0.09**	**0.41**

Notes: [1] Test conducted by Talja & Salmi (1995)

[2] Tests conducted by Rasmussen & Hancock (1990)

Remaining tests conducted by Gardner & Nethercot (Chapter 3)

[3] Uniform properties applied over entire (annealed) cross-section

Table 4.7: *Comparison between FE results using measured imperfections (with varying corner properties) and test results for RHS stub columns*

Section size	Test		FE - corner properties extended to t				FE - corner properties extended to 2t			
	Test F_u (kN)	Test δ_u (mm)	FE F_u (kN)	FE δ_u (mm)	FE F_u/ Test F_u	FE δ_u/ Test δ_u	FE F_u (kN)	FE δ_u (mm)	FE F_u/ Test F_u	FE δ_u/ Test δ_u
RHS 60×40×4- SC1	492	6.7	472	7.1	0.96	1.05	474	7.0	0.96	1.05
RHS 60×40×4- SC2	497	6.7	470	7.3	0.95	1.09	474	7.1	0.95	1.07
RHS 120×80×3- SC1	452	1.6	466	1.5	1.03	0.96	484	1.6	1.07	1.01
RHS 120×80×3- SC2	447	1.6	458	1.5	1.02	0.95	474	1.6	1.06	1.00
RHS 120×80×6- SC1	1459	7.8	1354	8.3	0.93	1.06	1376	8.2	0.94	1.05
RHS 120×80×6- SC2	1465	7.9	1348	7.7	0.92	0.98	1370	7.6	0.94	0.96
RHS 150×100×3- SC[1]	372	3.6	-	-	-	-	-	-	-	-
RHS 150×100×4- SC1	660	2.5	668	2.1	1.01	0.83	702	2.2	1.06	0.89
RHS 150×100×4- SC2	659	2.3	676	2.2	1.03	0.95	712	2.3	1.08	0.99
RHS 150×100×6- SC[1]	1292	12.0	-	-	-	-	-	-	-	-

Table 4.7 (continued): *Comparison between FE results using measured imperfections (with varying corner properties) and test results for RHS sub column.*

Section size	Test		FE - corner properties extended to t				FE - corner properties extended to 2t			
	Test F_u (kN)	Test δ_u (mm)	FE F_u (kN)	FE δ_u (mm)	FE F_u/Test F_u	FE δ_u/Test δ_u	FE F_u (kN)	FE δ_u (mm)	FE F_u/Test F_u	FE δ_u/Test δ_u
RHS 100×50×2- SC1	182	1.2	165	1.3	0.90	1.10	176	1.4	0.97	1.13
RHS 100×50×2- SC2	181	1.3	166	1.1	0.92	0.83	174	1.1	0.96	0.87
RHS 100×50×3- SC1	407	1.8	408	1.7	1.00	0.92	418	1.7	1.03	0.92
RHS 100×50×3- SC2	415	1.8	404	1.6	0.97	0.90	416	1.7	1.00	0.92
RHS 100×50×4- SC1	626	3.5	594	3.4	0.95	0.97	610	3.4	0.97	0.97
RHS 100×50×4- SC2	627	3.7	578	3.0	0.92	0.81	594	3.0	0.95	0.82
RHS 100×50×6- SC1	1217	9.3	1128	11.3	0.93	1.22	1138	11.3	0.94	1.21
RHS 100×50×6- SC2	1217	9.8	1130	11.4	0.93	1.16	1140	11.3	0.94	1.15
RHS MEAN:					0.96	0.98			0.99	1.00
RHS ST DEV:					0.04	0.12			0.05	0.11

Notes: [1] Test conducted by Talja & Salmi (1995)

Remaining tests conducted by Gardner & Nethercot (Chapter 3)

Table 4.8 presents a summary of the comparison between FE results and test results for all SHS and RHS stub columns, and demonstrates satisfactory overall agreement. The influence of the corner properties can also be seen. It can be concluded that FE models with corner properties extending to 2t beyond the curved portions of the cross-sections gives better agreement with test results than FE models with corner properties extending only to a distance t. FE models with no allowance for corner strength enhancements produce average under-predictions of strength of around 8%.

Table 4.8: *Summary of comparison between FE results and test results for SHS and RHS stub columns*

Cross-section type	Corner properties extended to t		Corner properties extended to 2t	
	$FE\ F_u/Test\ F_u$	$FE\ \delta_u/Test\ \delta_u$	$FE\ F_u/Test\ F_u$	$FE\ \delta_u/Test\ \delta_u$
SHS MEAN:	0.95	0.90	0.98	0.95
SHS ST DEV:	0.09	0.25	0.09	0.41
RHS MEAN:	0.96	0.98	0.99	1.00
RHS ST DEV:	0.04	0.12	0.05	0.11
OVERALL MEAN:	**0.96**	**0.94**	**0.98**	**0.98**
OVERALL ST DEV:	**0.07**	**0.20**	**0.07**	**0.30**

4.5.4 Influence of residual stresses

Residual stresses of magnitude and distribution as described in Section 4.3 were implemented into the stub column models using the ABAQUS *INITIAL CONDITIONS command. Prior to the application of external loading, a preliminary load step to allow equilibration of the residual stresses was defined. No residual stresses were included in the models of the annealed specimens because it was assumed that any residual stresses due to welding would have been relieved during the annealing process. However, it is recognised that thermal residual stresses due to non-uniform cooling of the cross-sections may have been introduced.

A study into the sensitivity of the stub column models to residual stresses was conducted. Simulations were run with and without residual stresses whilst other parameters remained constant. Figures 4.22 and 4.23 show typical load versus end shortening curves.
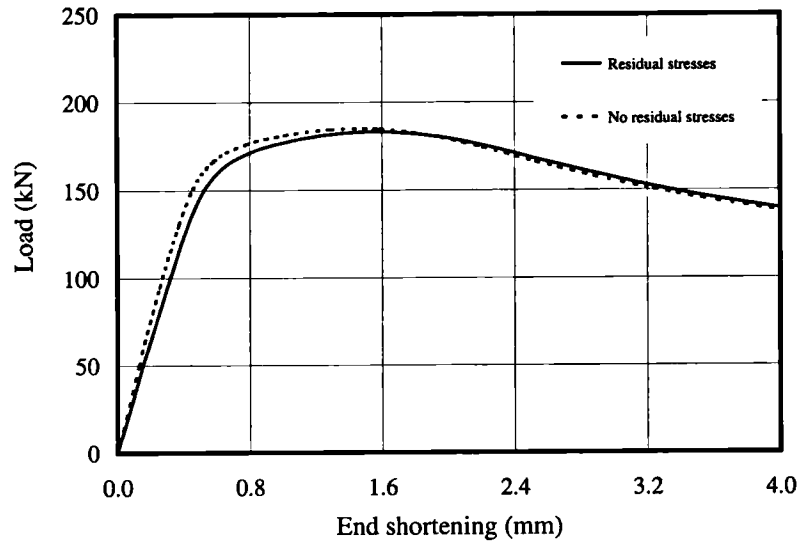
Figure 4.22: *Effect of residual stresses on 100x100x2 stub column FE model*
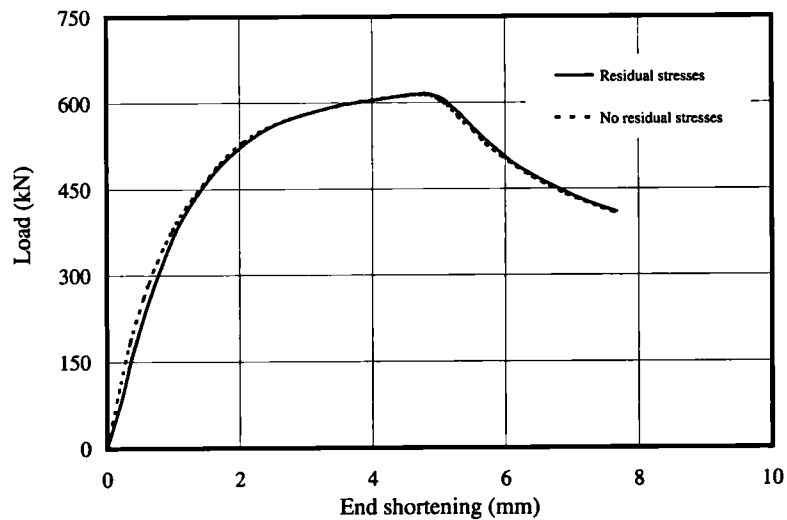
Figure 4.23: *Effect of residual stresses on 80x80x4 stub column FE model*

The effect of the residual stresses is clear, causing a small reduction in stiffness of the stub columns but having little influence on their overall behaviour or ultimate load carrying capacities.

4.5.5 FE model response using predicted local imperfection amplitudes

The results presented in Table 4.8 show that, using measured initial imperfection amplitudes, the load-carrying capacity and deformation response of cold-formed stainless steel SHS and

RHS can be accurately simulated. However, in the absence of measured initial imperfection data, predicted values must be utilised. This section investigates the imperfection sensitivity of the stub column FE models by simulating all tests conducted on stainless steel SHS and RHS stub columns using predicted imperfection amplitudes from Equation 4.31.

Results from FE models using the predicted imperfections are given in Tables 4.9 and 4.10. Ultimate load-carrying capacity, F_u and deformation at ultimate load, δ_u for each FE model are compared to the corresponding test values. Besides initial imperfection amplitude, all parameters are consistent with those in the FE models whose results are presented in Tables 4.6 and 4.7.

A comparison of mean results generated using measured and predicted initial imperfection amplitudes is presented in Table 4.11.

From Table 4.11 it may be seen that results generated using predicted initial imperfection amplitudes do not differ significantly from those generated using measured amplitudes. With predicted imperfections the mean ultimate strength shows an increase of approximately 1.5%, and the mean deformation at ultimate strength shows an increase of approximately 7%. The stub column ultimate strength exhibits less variability than the deformation at ultimate strength (reflected by the lower standard deviation). This is therefore perhaps a better measure of the integrity of the models.

It can be concluded that results generated from the FE stub column models using the predicted initial imperfection amplitudes (defined by Equation 4.31) still demonstrate accurate agreement with test results.

4.5.6 Failure modes

Observed failure modes from the test programme are described in Section 3.4.5.5. All stub columns failed with the same characteristic failure mode whereby the four faces of the cross-sections buckled locally alternately outwards and inwards. Similar failure modes were observed in the FE models. Figure 4.24 shows a typical failed stub column with its corresponding FE model, and a comparison between the test and FE model load-end shortening response.

Table 4.9: *Comparison between FE results using predicted imperfections (with varying corner properties) and test results for SHS stub columns*

Section size	Test		FE - corner properties extended to t				FE - corner properties extended to 2t			
	Test F_u (kN)	Test δ_u (mm)	FE F_u (kN)	FE δ_u (mm)	FE F_u/ Test F_u	FE δ_u/ Test δ_u	FE F_u (kN)	FE δ_u (mm)	FE F_u/ Test F_u	FE δ_u/ Test δ_u
SHS 60×60×5- SC[1]	801	9.3	636	8.9	0.79	0.96	694	16.1	0.87	1.73
SHS 80×80×3- SC1[2]	485	2.04	496	2.6	1.02	1.28	516	2.6	1.06	1.25
SHS 80×80×3- SC2[2]	471	2.18	494	2.6	1.05	1.21	512	2.6	1.09	1.18
SHS 80×80×4- SC1	727	7.4	626	5.9	0.86	0.79	642	5.9	0.88	0.80
SHS 80×80×4- SC2	714	7.2	654	6.7	0.92	0.93	670	6.5	0.94	0.90
SHS 80×80×4- SC3	711	7.7	656	6.7	0.92	0.87	672	6.7	0.95	0.86
SHS 80×80×4- ASC1[3]	309	8.6	414	10.8	1.34	1.25	414	10.8	1.34	1.25
SHS 80×80×4- ASC2[3]	335	7.1	398	9.8	1.19	1.39	398	9.8	1.19	1.39
SHS 100×100×2- SC1	197	1.1	185	1.6	0.94	1.46	199	2.0	1.01	1.77
SHS 100×100×2- SC2	187	0.9	185	1.5	0.99	1.63	198	2.0	1.06	2.18
SHS 100×100×3- SC1	489	2.2	438	1.6	0.90	0.73	452	1.7	0.92	0.77
SHS 100×100×3- SC2	496	2.3	428	1.6	0.86	0.70	442	1.6	0.89	0.70

Table 4.9 (continued): *Comparison between FE results using predicted imperfections (with varying corner properties) and test results for SHS stub columns*

Section size	Test		FE - corner properties extended to t				FE - corner properties extended to 2t			
	Test F_u (kN)	Test δ_u (mm)	FE F_u (kN)	FE δ_u (mm)	FE F_u/ Test F_u	FE δ_u/ Test δ_u	FE F_u (kN)	FE δ_u (mm)	FE F_u/ Test F_u	FE δ_u/ Test δ_u
SHS 100×100×4- SC1	779	4.0	798	3.6	1.02	0.89	820	3.6	1.05	0.90
SHS 100×100×4- SC2	774	4.0	796	3.5	1.03	0.88	818	3.5	1.06	0.89
SHS 100×100×6- SC1	1513	13.4	1434	14.0	0.95	1.04	1452	13.7	0.96	1.02
SHS 100×100×6- SC2	1507	13.5	1430	13.9	0.95	1.03	1448	13.4	0.96	0.99
SHS 100×100×8- SC1	1630	29.0	1470	22.7	0.90	0.78	1502	20.4	0.92	0.70
SHS 100×100×8- SC2	1797	38.2	1468	22.3	0.82	0.58	1498	20.1	0.83	0.52
SHS 150×150×4- SC1	726	1.7	688	1.6	0.95	0.94	726	1.7	1.00	1.00
SHS 150×150×4- SC2	713	1.6	672	1.5	0.94	0.96	708	1.6	0.99	1.02
SHS MEAN:					**0.97**	**1.01**			**1.00**	**1.09**
SHS ST DEV:					**0.12**	**0.27**			**0.12**	**0.41**

Notes: [1] Test conducted by Talja & Salmi (1995)

[2] Tests conducted by Rasmussen & Hancock (1990)

Remaining tests conducted by Gardner & Nethercot (Chapter 3)

[3] Uniform properties applied over entire (annealed) cross-section

Table 4.10: *Comparison between FE results using predicted imperfections (with varying corner properties) and test results for RHS sub columns*

Section size	Test		FE - corner properties extended to t				FE - corner properties extended to 2t			
	Test F_u (kN)	Test δ_u (mm)	FE F_u (kN)	FE δ_u (mm)	FE F_u / Test F_u	FE δ_u / Test δ_u	FE F_u (kN)	FE δ_u (mm)	FE F_u / Test F_u	FE δ_u / Test δ_u
RHS 60×40×4- SC1	492	6.7	472	7.2	0.96	1.07	474	7.2	0.96	1.07
RHS 60×40×4- SC2	497	6.7	470	7.3	0.95	1.09	474	7.1	0.95	1.07
RHS 120×80×3- SC1	452	1.6	464	1.5	1.03	0.94	480	1.6	1.06	0.99
RHS 120×80×3- SC2	447	1.6	458	1.5	1.02	0.94	474	1.6	1.06	0.99
RHS 120×80×6- SC1	1459	7.8	1352	8.2	0.93	1.04	1374	8.1	0.94	1.03
RHS 120×80×6- SC2	1465	7.9	1352	8.2	0.92	1.04	1374	8.1	0.94	1.02
RHS 150×100×3- SC[1]	372	3.6	372	3.2	1.00	0.90	394	3.9	1.06	1.08
RHS 150×100×4- SC1	660	2.5	668	2.1	1.01	0.83	702	2.2	1.06	0.89
RHS 150×100×4- SC2	659	2.3	670	2.1	1.02	0.90	706	2.2	1.07	0.97
RHS 150×100×6- SC[1]	1292	12.0	1284	15.0	0.99	1.25	1338	14.3	1.04	1.19

Table 4.10 (continued): *Comparison between FE results using predicted imperfections (with varying corner properties) and test results for RHS sub columns*

Section size	Test		FE - corner properties extended to t				FE - corner properties extended to 2t			
	Test F_u (kN)	Test δ_u (mm)	FE F_u (kN)	FE δ_u (mm)	FE F_u/ Test F_u	FE δ_u/ Test δ_u	FE F_u (kN)	FE δ_u (mm)	FE F_u/ Test F_u	FE δ_u/ Test δ_u
RHS 100x50x2- SC1	182	1.2	165	1.3	0.91	1.07	176	1.4	0.97	1.18
RHS 100x50x2- SC2	181	1.3	165	1.1	0.91	0.81	174	1.3	0.96	0.98
RHS 100x50x3- SC1	407	1.8	408	1.7	1.00	0.92	420	1.7	1.03	0.93
RHS 100x50x3- SC2	415	1.8	408	1.7	0.98	0.92	420	1.7	1.01	0.93
RHS 100x50x4- SC1	626	3.5	592	3.3	0.95	0.95	608	3.3	0.97	0.95
RHS 100x50x4- SC2	627	3.7	582	3.2	0.93	0.85	596	3.1	0.95	0.83
RHS 100x50x6- SC1	1217	9.3	1126	11.2	0.93	1.20	1136	11.2	0.93	1.20
RHS 100x50x6- SC2	1217	9.8	1128	11.3	0.93	1.15	1138	11.2	0.94	1.14
RHS MEAN:					**0.96**	**0.99**			**1.00**	**1.02**
RHS ST DEV:					**0.04**	**0.13**			**0.05**	**0.10**

Notes: [1]   Test conducted by Talja & Salmi (1995)

         Remaining tests conducted by Gardner & Nethercot (Chapter 3)

Table 4.11: *Summary of comparison between FE results and test results for SHS and RHS stub columns using measured and predicted initial imperfection amplitudes*

	Corner properties extended to t		Corner properties extended to 2t	
	FE F_u / Test F_u	FE δ_u / Test δ_u	FE F_u / Test F_u	FE δ_u / Test δ_u
MEAN (using measured imperfections amplitudes):	0.96	0.94	0.98	0.98
ST DEV (using measured imperfection amplitudes):	0.07	0.20	0.07	0.30
MEAN (using predicted imperfections amplitudes):	0.97	1.00	1.00	1.06
ST DEV (using predicted imperfection amplitudes):	0.09	0.21	0.09	0.30
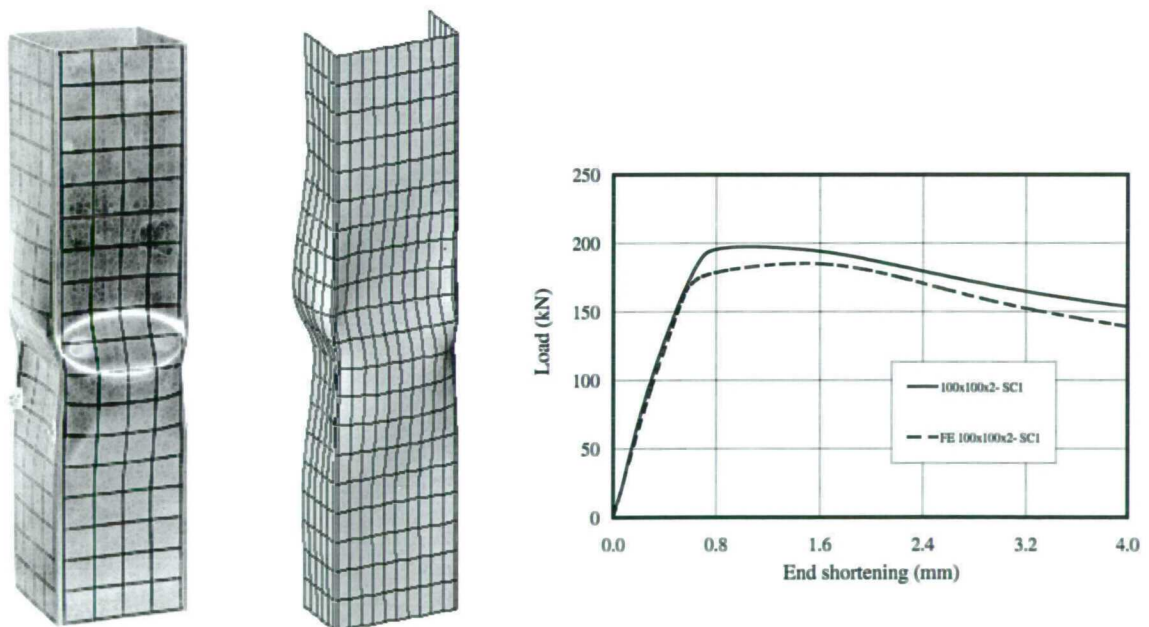
Figure 4.24: *Failure mode and load-end shortening response from SHS 100×100×2- SC1 stub column test and corresponding FE model*

One exception to the typical failure mode was observed for the FE model of the SHS 60×60×5 stub column tested by Talja and Salmi. This FE model exhibited overall out-of-plane deformation (see Figure 4.25), thus inducing second-order bending moments into the column, and negating the intended load case of pure compression.

Figure 4.25: *Failure mode of SHS 60×60×5 stub column FE model*

This may explain why the SHS 60×60×5 is the only stub column test result to lie below the elastic critical plate buckling curve shown in Figure 5.4. However, no such behaviour was mentioned in the test report, and the length of the stub column is within the limit of 20 times the least radius of gyration, prescribed by Structural Stability Research Council (Galambos, 1998) to preclude overall buckling.

4.5.7 Discussion

In general, good agreement between test and FE model behaviour has been displayed. Figures 4.26 and 4.27 show the variation in FE and test results for a range of cross-section slendernesses, β (defined by Equation 5.3). It can be seen that the greatest discrepancies between observed and modelled behaviour occur at the extremities of the tested range of slenderness, and that the prediction of deformations shows the greater variation. At low

slenderness, the discrepancies are believed due to inaccuracies generated by the large plastic strains. This may be overcome, as described in Section 4.5.2, by employing 'thick' shell elements. At high slenderness, it is believed that the imperfection sensitivity associated with the post-buckling response of slender compression elements produces the large scatter of results.
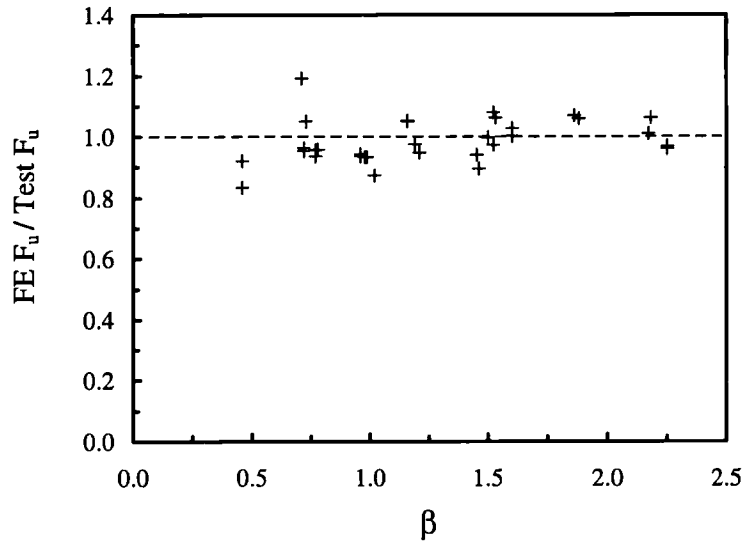
Figure 4.26: *Stub column FE ultimate load divided by test ultimate load versus cross-section slenderness, β*
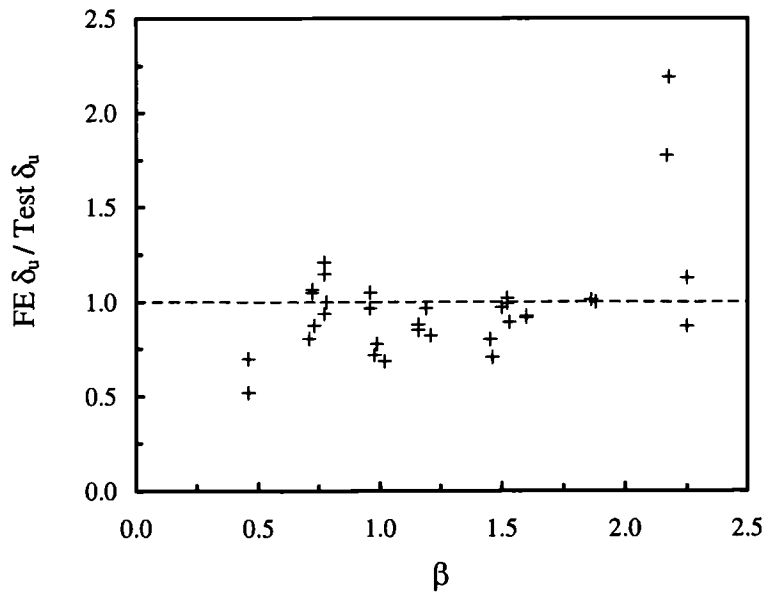
Figure 4.27: *Stub column FE deformation at ultimate load divided by test deformation at ultimate load versus cross-section slenderness, β*

Before modelling more complex overall member behaviour, which involves an interaction between local (cross-sectional) effects and global (member) effects, it is important to first achieve successful replication of the cross-section behaviour. This section has demonstrated that by using a consistent approach to the numerical modelling of stainless steel SHS and RHS stub columns, accurate agreement between FE model and test results has been achieved.

4.6 CHS Stub Column Modelling

4.6.1 Background

As for the SHS and RHS, results from CHS stub column tests form the basis of the proposed design method. However, results from tests on CHS stub columns loaded in pure compression are relatively scarce. The purpose of the FE modelling of CHS stub columns is therefore to replicate the available test results and to generate further load-deformation data by means of parametric studies.

4.6.2 Development of FE models

Development of the CHS stub column FE models was similar to that for the SHS and RHS stub columns described in Section 4.5.2, with a few exceptions. Element choice, material modelling, boundary conditions, generation of initial geometric imperfection modes, and analysis types were as for the SHS and RHS models. A typical CHS stub column FE model is shown in Figure 4.28.

Material properties were assumed to be uniform around the cross-section, since test results for material extracted from different parts of the cross-sections exhibited little variation, and with no discernible pattern. The assumed weld-induced residual stress distribution described in Section 4.3.3 was adopted, and the effect of these residual stresses is demonstrated in Section 4.6.3. The influence of initial geometric imperfection amplitudes was investigated in a parametric study described in Section 4.6.4.
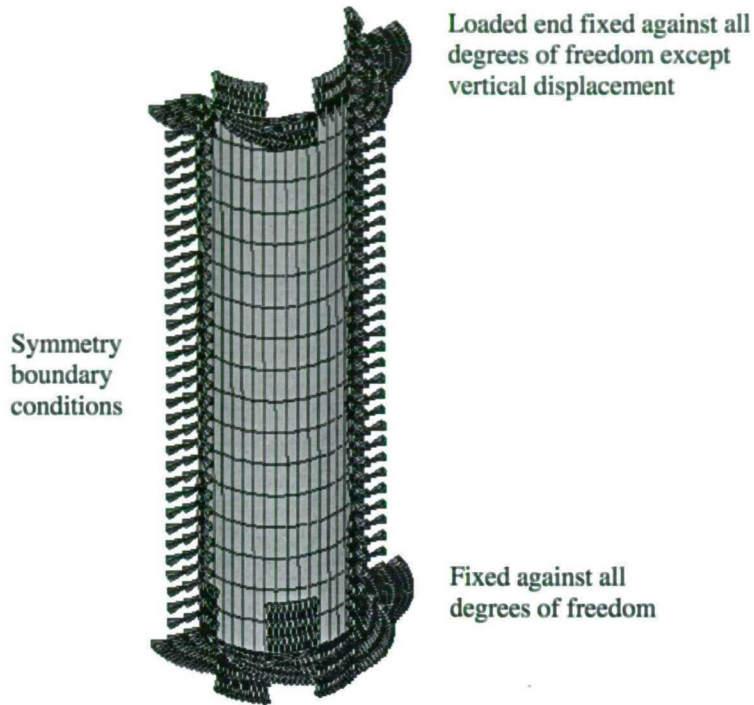
Figure 4.28: *Typical CHS stub column FE model with boundary conditions*

4.6.3 Influence of residual stresses

Residual stresses of magnitude and distribution as described in Section 4.3.3 were implemented into the CHS stub column models in the same manner as for the SHS and RHS stub columns. Simulations were run with and without residual stresses to assess the sensitivity of the models to their presence. Typical results are shown in Figure 4.29 for a CHS 100×1.0.
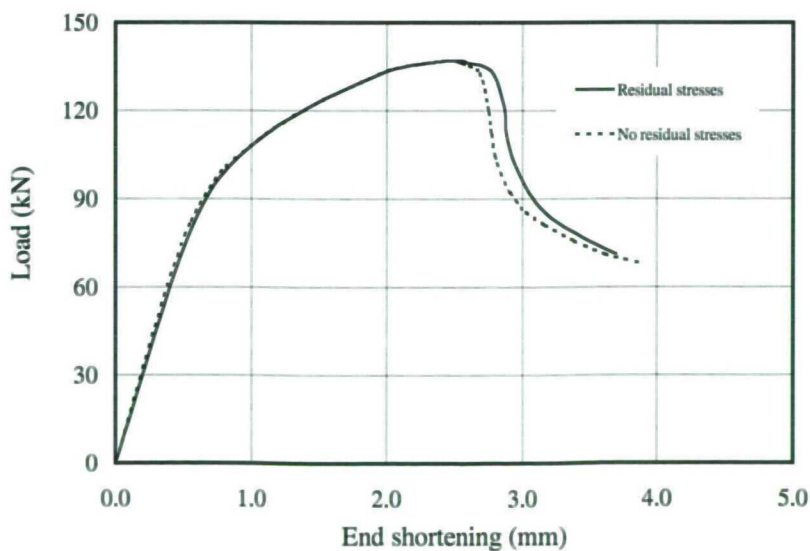
Figure 4.29: *Effect of residual stresses on CHS 100×1.0 stub column FE model*

As expected, the effect of the residual stresses on the CHS stub column models is similar to the SHS and RHS case, causing a small reduction in initial stiffness but having little influence on overall behaviour or ultimate load carrying capacities.

4.6.4 Influence of initial geometric imperfection amplitude

Cylinders with relatively low diameter-to-thickness (D/t) ratios are generally referred to as tubes or pipes, whereas those with relatively high D/t ratios are referred to as shells. Shells subjected to axial compression buckle chiefly in the elastic material range and are often extremely sensitive to the presence of imperfections. CHS used for structural applications (and examined in the current study) have relatively low D/t ratios and failure is largely controlled by the (gradual) material yielding. For such cases, sensitivity to changes in geometric imperfections is significantly lessened.

A parametric study was conducted to determine a suitable geometric imperfection amplitude for stainless steel CHS. FE simulations of all stainless steel CHS stub column tests were conducted with four different levels of imperfection amplitude, specified as a proportion of the material thickness. The four imperfection amplitudes, ω_0 were 0.01t, 0.1t, 0.2t and 0.5t. The results of the study are presented in Table 4.12.

From Table 4.12 it can be concluded that the CHS stub column behaviour is most accurately replicated with an initial geometric imperfection amplitude of 0.2t. The stub column deformation capacity at ultimate load, which is the key parameter of interest, has been shown to be well predicted with a standard deviation comparable to that which exists between repeated laboratory test results.

4.6.5 Generation of further results

With satisfaction in the ability of the FE models to replicate test results, a parametric study was conducted to generate results over a range of cross-sectional slendernesses to support the test data. A CHS with an outer diameter of 100 mm, a length of 350 mm, material stress-strain properties as for the CHS 101.6×2.85 (tested by Rasmussen and Hancock), and an initial geometric imperfection amplitude of 0.2t was chosen as the basis for the parametric study.

Table 4.12: Comparison between CHS stub column tests and FE models with different levels of local geometric imperfection amplitude

Specimen identification	$\beta = (R/t)\dfrac{\sigma_{0.2}}{E_0}$	$\omega_0 = 0.01t$		$\omega_0 = 0.1t$		$\omega_0 = 0.2t$		$\omega_0 = 0.5t$	
		$\dfrac{Test\ F_u}{FE\ F_u}$	$\dfrac{Test\ \delta_u}{FE\ \delta_u}$	$\dfrac{Test\ F_u}{FE\ F_u}$	$\dfrac{Test\ \delta_u}{FE\ \delta_u}$	$\dfrac{Test\ F_u}{FE\ F_u}$	$\dfrac{Test\ \delta_u}{FE\ \delta_u}$	$\dfrac{Test\ F_u}{FE\ F_u}$	$\dfrac{Test\ \delta_u}{FE\ \delta_u}$
CHS 103×1.5- SC1	0.074	1.09	0.91	1.09	0.94	1.10	0.96	1.04	0.71
CHS 103×1.5- SC2	0.074	1.06	0.88	1.05	0.91	1.04	0.90	1.01	0.69
CHS 101.6×2.85- SC1	0.032	1.09	1.29	1.09	1.30	1.10	1.21	1.00	0.96
CHS 101.6×2.85- SC2	0.032	1.09	1.10	1.09	1.10	1.10	1.15	0.99	0.81
CHS 101.6×2.85- SC3	0.035	1.08	0.89	1.08	0.91	1.08	0.93	1.01	0.71
CHS 140×2- SC	0.055	1.05	0.83	1.05	0.83	1.05	0.90	0.96	0.54
CHS 140×3- SC	0.044	0.87	0.54	0.87	0.55	0.87	0.60	0.83	0.41
CHS 140×4- SC	0.026	0.98	0.98	0.98	0.99	0.98	1.18	0.93	0.65
CHS 153×1.5- SC1	0.115	0.98	0.91	0.98	0.92	0.98	1.07	0.93	0.60
CHS 153×1.5- SC2	0.114	0.99	1.18	0.99	1.18	0.99	1.21	0.96	0.85
MEAN:		1.03	0.95	1.03	0.96	1.03	1.01	0.97	0.69
ST DEV:		0.07	0.21	0.07	0.21	0.07	0.19	0.06	0.16

These parameters were fixed, and variation in cross-section slenderness was achieved through variation in material thickness. The essential results from the study are included in Table 4.13.

Table 4.13: *Results from parametric study on CHS stub columns*

Specimen identification	D/t	$\beta = (R/t)\dfrac{\sigma_{0.2}}{E_0}$	F_u (kN)	δ_u (mm)
CHS 100×0.8- SC1	125.0	0.120	106	1.6
CHS 100×1.0- SC1	100.0	0.096	137	2.0
CHS 100×1.2- SC1	83.3	0.079	167	2.4
CHS 100×1.4- SC1	71.4	0.068	198	2.9
CHS 100×1.6- SC1	62.5	0.059	230	3.3
CHS 100×1.8- SC1	55.6	0.053	260	3.7
CHS 100×2.0- SC1	50.0	0.047	290	4.1
CHS 100×2.4- SC1	41.7	0.039	352	4.8
CHS 100×2.8- SC1	35.7	0.034	414	6.1
CHS 100×3.2- SC1	31.3	0.029	476	7.1
CHS 100×3.6- SC1	27.8	0.026	534	7.7
CHS 100×4.0- SC1	25.0	0.023	594	8.2
CHS 100×4.4- SC1	22.7	0.021	652	8.5
CHS 100×4.8- SC1	20.8	0.019	726	11.4

These results are examined in Chapter 5 and used in conjunction with test results to generate a relationship between cross-sectional slenderness and cross-sectional deformation capacity for stainless steel CHS.

4.7 SHS AND RHS PIN-ENDED COLUMN MODELLING

4.7.1 Background

In Section 4.5 it was shown that the behaviour of stainless steel SHS and RHS stub columns can be accurately replicated using the described modelling techniques and assumptions. This

demonstrates the ability to predict the load-carrying and deformation response to variation in cross-sectional slenderness. The behaviour of pin-ended columns is more complex and is dependant upon overall member slenderness, cross-sectional slenderness and the interaction between local and global phenomena.

4.7.2 Development of FE models

Development of the FE models for pin-ended columns was similar to that for stub columns. Models included measured geometry, measured and predicted initial plate imperfections and initial overall members imperfections, assumed residual stresses and measured and predicted material properties, with enhanced material properties applied to the corner regions. The same 9-noded, reduced integration shell elements, S9R5 were adopted for the modelling of the stainless steel members.

The cross-sectional parameters were selected based on the findings from the stub column FE modelling study. Curved S9R5 shell elements were used to model the curved corner regions of the cross-sections, and enhanced corner material properties were assumed to extend to a distance of 2t (two times the material thickness) beyond the curved regions. The incorporation of residual stresses and initial plate imperfections followed the stub column assumptions. Where measurements of local plate imperfection amplitude were not available, predicted amplitudes (given by Equation 4.31) were adopted.

Linear elastic eigenmode simulations were conducted to generate both the local and global imperfection modes, and a superposition of the two gave the final imperfection pattern. The lowest local and global buckling modes generally appeared in the first few eigenmodes. Figure 4.30 shows the two lowest eigenmodes for a 1m pin-ended RHS 100×50×3. Non-linear analyses employed the modified Riks method.

Column end plates were modelled using the ABAQUS multi-purpose C3D20 20-node quadratic brick elements. Nodes along one centreline of the outer surfaces of both end plates were fixed against all degrees of freedom, except for minor axis rotation at both ends and vertical displacement at the loaded end. This provided pin-ended conditions in the minor axis buckling direction. Similar boundary conditions were used across the perpendicular centrelines to model major axis buckling. Constraint equations were employed to ensure that there were no end

rotations about the non-buckling axis, and loads were introduced through the constrained node sets.

<div align="center">

(a) Eigenmode 1:

Global buckling mode

(b) Eigenmode 2:

Local buckling mode

</div>

Figure 4.30: *Two lowest eigenmodes for 1m pin-ended RHS 100×50×3*

4.7.3 Effect of residual stresses

Residual stresses were included in the pin-ended column FE models in the same manner as for the stub columns (as described in Section 4.5.4).

A parametric study to investigate the sensitivity of the pin-ended column models to residual stresses was conducted. Simulations were run with and without residual stresses whilst other parameters remained constant. Figures 4.31 shows the resulting load versus lateral deflection curves for a 2m pin-ended SHS 100×100×4 column.
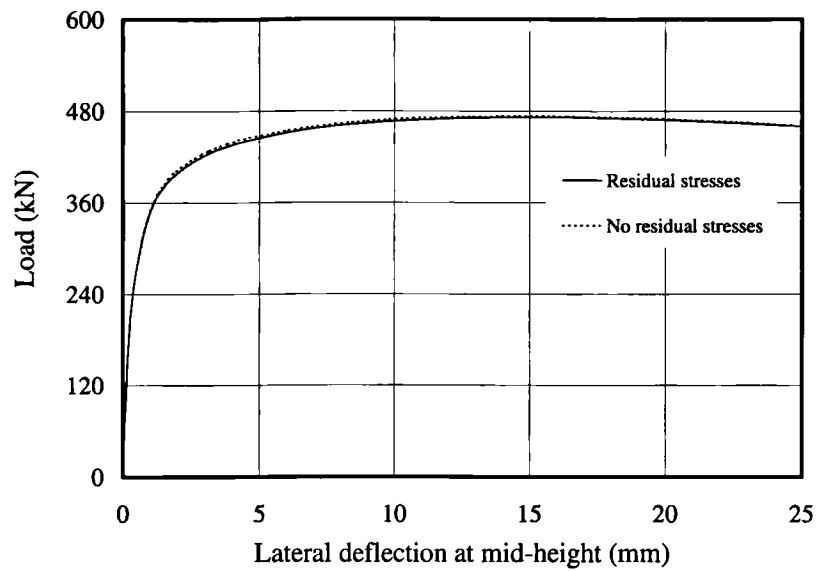
Figure 4.31: *Effect of residual stresses on SHS 100×100×4 pin-ended column FE model*

The influence of residual stresses on pin-ended column SHS flexural buckling behaviour can be seen from Figure 4.31 to be relatively insignificant. A small reduction in stiffness can be observed prior to ultimate load, but the ultimate load carrying capacity itself is unaffected.

4.7.4 Sensitivity of FE models to global imperfection amplitude

A parametric study was also conducted to assess the sensitivity of the pin-ended column FE models to variation in global imperfection amplitude. In this study, the cross-sectional and material properties (SHS 80×80×4) and local imperfection amplitude (measured from the SHS 80×80×4 stub columns) were kept constant. Variation in non-dimensional slenderness, $\overline{\lambda}$, defined by Equation 4.34, was achieved through variation in column length. Three column lengths were used: 1m, 2m and 3m. The 2m column was a replication of a laboratory test.

$$\overline{\lambda} = \frac{L_E}{i} \sqrt{\frac{\sigma_{0.2}}{\pi^2 E_0}} \tag{4.34}$$

where L_E is the effective column length, i is the (minor axis) radius of gyration and $\sigma_{0.2}$ and E_0 are the material 0.2% proof strength and Young's modulus in compression respectively.

Three different levels of imperfection, expressed as a function of the column length, L were considered: L/1000, L/2000, and L/5000. The results are shown in Figure 4.32. The vertical axis in Figure 4.32 is the ultimate strength of the column (ultimate load, F_u × cross-sectional area, A) normalised by the material 0.2% proof strength in compression, $\sigma_{0.2}$). The Euler critical buckling curve and material 0.2% proof strength lines are also shown.
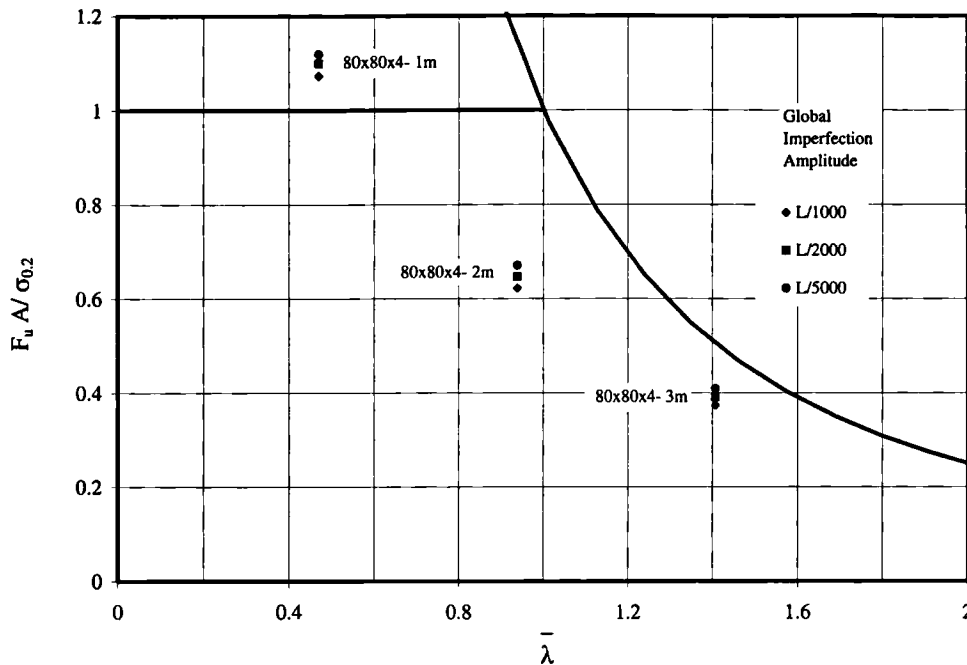
Figure 4.32: *Normalised column strength versus non-dimensional slenderness, $\overline{\lambda}$ for three levels of global imperfection amplitude (L/1000, L/2000 and L/5000)*

The largest magnitude of scatter in normalised ultimate stress was observed for the 2m column that is closest to the imperfection sensitive region where $\overline{\lambda}$ is equal to 1.0, though the largest percentage variation ($\approx$ 9%) was found for the 3m column.

A further study was conducted to investigate the imperfection sensitivity of the 2m SHS 80×80×4 pin-ended column for a range of global imperfection amplitudes from L/100 to L/10000. The results are shown in Figure 4.33.

From Figure 4.33 it can be seen that for global imperfection amplitudes of less than L/1000, the variation in ultimate load carrying capacity is relatively small ($\approx$10%). However, for higher imperfection amplitudes the ultimate load carrying capacity begins to drop off much more sharply.

Overall imperfection amplitude as a proportion of column length
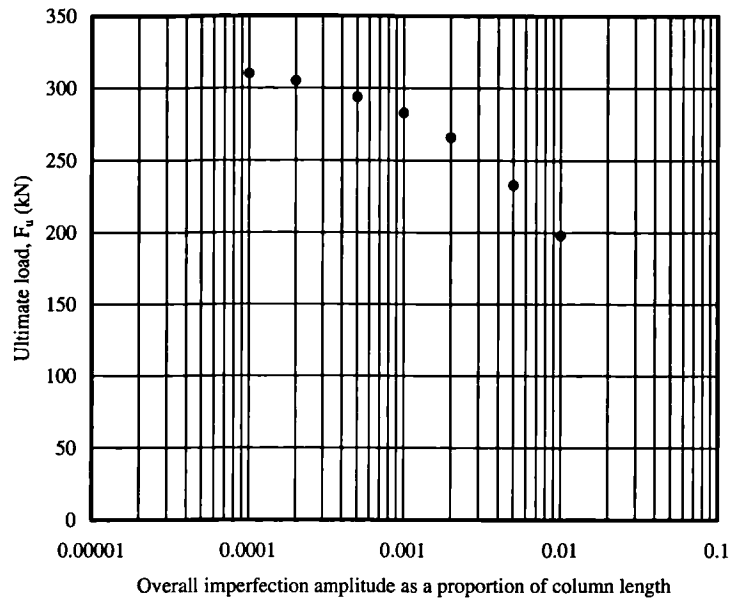
Figure 4.33: *Imperfection sensitivity of 2m SHS 80×80×4 pin-ended column for global imperfection amplitudes ranging from L/100 to L/10000*

To establish a representative global imperfection amplitude, a parametric study was conducted. Eight pin-ended columns, tested as part of the current investigation and covering a range of cross-sectional slendernesses, β and non-dimensional global slendernesses, $\bar{\lambda}$, were modelled using three imperfection amplitudes: L/1000, L/2000 and L/5000. Comparisons of ultimate load carrying capacity from the tests and FE models are given in Table 4.14.

Mean values of FE F_u/Test F_u were 0.96, 0.99 and 1.02 for global imperfections amplitudes of L/1000, L/2000 and L/5000 respectively. The standard deviation was similar for each case with a value of 0.07. Global imperfection amplitudes of L/2000 are therefore adopted for the modelling of the remainder of the test specimens, and for additional parametric studies.

4.7.5 Comparison between test and FE results

A comparison of ultimate load carrying capacity for all tests and FE models of pin-ended SHS columns is presented in Table 4.15. Similarly, comparisons for all pin-ended RHS columns buckling about the minor and the major axis are presented in Tables 4.16 and 4.17 respectively.

Table 4.14: Comparison between pin-ended column test results and FE results for three levels of global imperfection amplitude

Specimen identification	β	$\bar{\lambda}$	Test F_u (kN)	FE (L/1000)		FE (L/2000)		FE (L/5000)	
				FE F_u (kN)	FE F_u / Test F_u	FE F_u (kN)	FE F_u / Test F_u	FE F_u (kN)	FE F_u / Test F_u
SHS 80×80×4-LC1	0.91	0.89	307	301	0.98	313	1.02	324	1.06
SHS 80×80×4-LC2	0.92	0.94	293	283	0.97	294	1.00	305	1.04
SHS 100×100×2-LC1	2.23	0.67	176	164	0.93	167	0.95	169	0.96
SHS 100×100×3-LC1	1.46	0.68	350	317	0.91	328	0.94	338	0.97
SHS 100×100×4-LC1	1.18	0.76	464	456	0.98	472	1.02	485	1.05
SHS 100×100×6-LC1	0.78	0.82	842	728	0.86	755	0.90	777	0.92
SHS 100×100×8-LC1	0.46	0.69	770	839	1.09	871	1.13	896	1.16
RHS 100×50×4-LC1	1.20	1.45	165	152	0.92	160	0.97	167	1.01
MEAN:					0.96		0.99		1.02
ST DEV:					0.07		0.07		0.07

Table 4.15: *Comparison between all SHS pin-ended column test results and FE results for a global imperfection amplitude of L /2000*

Specimen identification	β	$\bar{\lambda}$	Test F_u (kN)	FE F_u (kN)	Test F_u/FE F_u
SHS 40×40×4- LC1	0.51	1.07	184	171	0.93
SHS 40×40×4- LC2	0.51	1.07	184	168	0.91
SHS 60×60×5- LC1	0.57	0.75	417	397	0.95
SHS 60×60×5- LC2	0.57	1.22	235	229	0.97
SHS 60×60×5- LC3	0.57	1.68	137	138	1.01
SHS 80×80×3-LC1	1.18	0.47	390	401	1.03
SHS 80×80×3-LC2	1.18	0.94	193	242	1.25
SHS 80×80×3-LC3	1.18	1.42	96	143	1.49
SHS 80×80×4-LC1	0.91	0.89	307	313	1.02
SHS 80×80×4-LC2	0.92	0.94	293	294	1.00
SHS 100×100×2-LC1	2.23	0.67	176	167	0.95
SHS 100×100×3-LC1	1.46	0.68	350	328	0.94
SHS 100×100×4-LC1	1.18	0.76	464	472	1.02
SHS 100×100×6-LC1	0.78	0.82	842	755	0.90
SHS 100×100×8-LC1	0.46	0.69	770	871	1.13
SHS 150×150×4- LC1	1.51	0.42	692	-[1]	-
MEAN:					**1.03**
ST DEV:					**0.16**

Notes: [1] Convergence problems prevented solution

4.7.6 Discussion

Overall the agreement between test and FE results for flexural column buckling is satisfactory. An obvious exception to this is the SHS 80×80×3-LC3 (tested by Rasmussen and Hancock) with an FE F_u/Test F_u ratio of 1.49, and to a lesser extent the SHS 80×80×3-LC2 (tested by Rasmussen and Hancock) with a FE F_u/Test F_u ratio of 1.25. In both cases, the test failure loads are significantly below those predicted by the FE models.

In Section 6.3.3 there is a comparison between the test failure loads and those predicted by Eurocode 3 and the proposed design method. Both design methods predict failure loads in close agreement with the FE results, and therefore showing similarly large deviation from the test results. No problems with the testing procedure or the test results were reported by Rasmussen and Hancock. Other than erroneous conduct of these tests, no explanation for this large deviation can be suggested.

Table 4.16: *Comparison between all RHS minor axis buckling pin-ended column test results and FE results for a global imperfection amplitude of L /2000*

Specimen identification	β	$\bar{\lambda}$	Test F_u (kN)	FE F_u (kN)	Test F_u/FE F_u
RHS 60×40×4-LC1	0.72	1.02	169	188	1.11
RHS 100×50×2-LC1	2.28	0.64	163	132	0.81
RHS 100×50×3-LC1	1.62	0.73	304	286	0.94
RHS 100×50×4-LC1	1.19	0.72	422	364	0.86
RHS 100×50×6-LC1	0.77	0.80	624	603	0.97
RHS 120×80×3-LC1	1.91	0.45	448	427	0.95
RHS 100×50×3-LC1	1.61	1.46	113	135	1.19
RHS 100×50×4-LC1	1.20	1.45	165	160	0.97
RHS 100×50×6-LC1	0.77	1.61	234	219	0.94
RHS 120×80×3-LC1	1.88	0.90	313	310	0.99
RHS 120×80×6-LC1	0.96	0.99	677	612	0.90
RHS 150×100×4-LC1	1.54	0.62	515	501	0.97
MEAN:					**0.97**
ST DEV:					**0.10**

4.8 SHS AND RHS BEAM MODELLING

4.8.1 Introduction

Sufficient test results for stainless steel beams failing by in-plane bending are available to preclude the need for extensive FE modelling in this area. However, no test results are available

on RHS beams either where the proportions of the cross-section are such that local buckling occurs in the web, or where the beam is subject to lateral torsional buckling. The proportions of structural hollow sections are such that both of these cases are unusual. Nonetheless, for completeness, a study was conducted to investigate the applicability of Eurocode buckling coefficients to the inelastic local buckling of the webs of stainless steel beams of extreme proportions. However, it was decided not to model stainless steel RHS beams with proportions and loading conditions conducive to lateral torsional buckling, since the structural behaviour is complex and there are no supporting test data to use for validation.

Table 4.17: *Comparison between all RHS major axis buckling pin-ended column test results and FE results for a global imperfection amplitude of L /2000*

Specimen identification	β	$\bar{\lambda}$	Test F_u (kN)	FE F_u (kN)	Test F_u/FE F_u
RHS 60×40×4-LC1	0.72	1.47	109	118	1.08
RHS 100×50×2-LC1	2.27	0.75	157	141	0.90
RHS 150×100×3- LC1	1.96	0.58	349	357	1.02
RHS 150×100×3- LC2	1.96	0.94	254	253	1.00
RHS 150×100×3- LC3	1.96	1.29	189	176	0.93
RHS 150×100×6- LC1	0.93	0.59	830	860	1.04
RHS 150×100×6- LC2	0.95	0.95	488	535	1.10
RHS 150×100×6- LC3	0.95	1.31	306	340	1.11
MEAN:					**1.02**
ST DEV:					**0.08**

4.8.2 Investigation into local web buckling in pure bending

4.8.2.1 Hypothesis

Comprehensive results describing the behaviour of SHS and RHS plate elements loaded in pure compression have been generated through experimentation. This behaviour has also been successfully replicated numerically, as described in Section 4.5. However, the behaviour of plate elements subjected to non-uniform compression has not been investigated experimentally.

Eurocode 3 presents buckling coefficients that are used to determine the local slenderness of Class 4 plate elements. The coefficients were generated by finding approximate energy solutions to plate buckling problems with various in-plane loading conditions. The purpose of this investigation is to establish whether these buckling coefficients can be applied to the inelastic buckling of stainless steel web elements subjected to pure bending. If the buckling coefficients are shown to be acceptable for the case of pure bending, it will be assumed that the coefficients for intermediate cases (between pure compression and pure bending) are also acceptable.

4.8.2.2 Description of FE model

The buckling coefficient for a simply supported plate element in pure bending (k=23.9) is approximately six times that for a simply supported plate element in pure compression (k=4.0). Thus, an RHS beam of aspect ratio greater than $1:\sqrt{6}$ (i.e. $\approx 1:2.4$) would be required before the beam web would become the critical element in the cross-section. A RHS beam model with an aspect ratio of 1:4 was therefore developed.

S9R5 shell elements that had performed well in the stub column and pin-ended column models were employed again. The material stress-strain curve was defined using mean parameters from the compressive coupon tests conducted in this study. The initial geometric imperfection mode was taken as the lowest eigenmode in pure compression, shown in Figure 4.34. The amplitude of the imperfection was determined from Equation 4.31. No residual stresses were specified. Three different material thicknesses were considered to achieve a range of cross-section slendernesses.
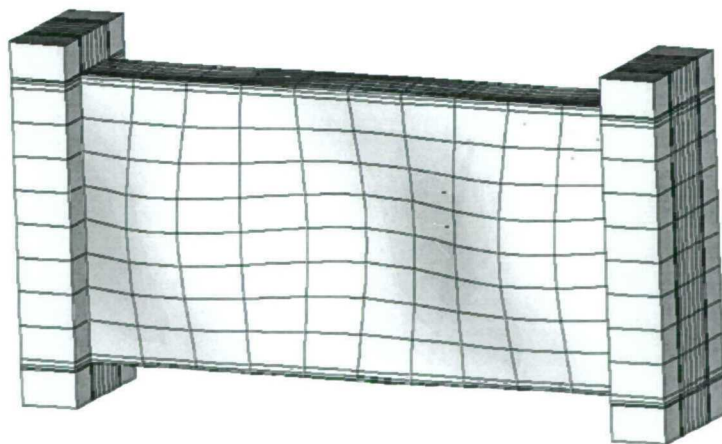
Figure 4.34: *Initial imperfection mode for RHS web buckling study*

Equal and opposite forces were applied at the level of the upper and lower flanges to create a load case of pure bending.

4.8.2.3 Results

Figure 4.35 shows a typical contour plot of out-of-plane deflection highlighting the web buckling mode.
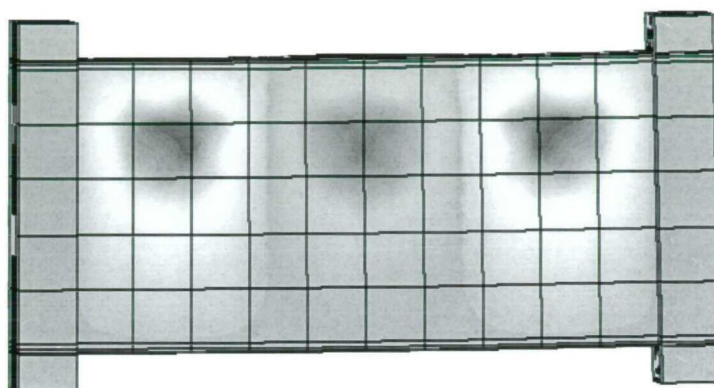
Figure 4.35: *Contour plot of out-of-plane deflection highlighting the web buckling mode*

The average axial strain in the compression flange at ultimate load, ε_{LB} was determined (reported in Table 4.18), and used as the basis of comparison with the pure compression case modified by the Eurocode buckling coefficients.

Table 4.18: *Results from numerical study on RHS in pure bending*

Cross-section	FE ε_{LB}
RHS 160×40×1.5	0.0045
RHS 160×40×2	0.0062
RHS 160×40×3	0.0160
RHS 160×40×4	0.0280

Analysis of the results and comparison with predicted failure strains using the Eurocode buckling coefficients is reported in Section 5.8.3.

4.9 SHS AND RHS PIN-ENDED BEAM-COLUMN MODELLING

4.9.1 Introduction

Beam-columns are members subjected to a combination of applied axial loads plus applied bending moments (about either or both of the principal axes). The design of such members involves consideration of the individual loading components

No tests on beam-columns were conducted in the current study, but a total of 12 tests were reported by Talja & Salmi (1995). FE modelling of these tests is conducted using the parameters found from the stub column and pin-ended column modelling.

4.9.2 Development of FE models

The SHS and RHS beam-column FE models were similar to the pin-ended column models, with the exception of the point of load introduction. For the beam-columns, the load was applied eccentrically, through the centreline of the wall thickness of the cross-section. Figure 4.36 shows the restraints adopted to create pin-ended boundary conditions.
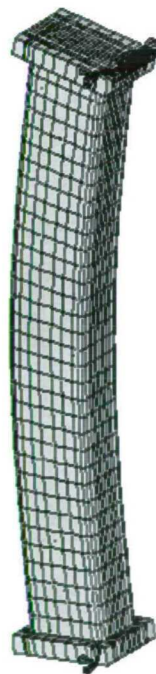
All translational degrees of freedom, except vertical displacement, fixed on a line of nodes adjacent to centreline of wall thickness.

All translational degrees of freedom fixed on a line of nodes adjacent to centreline of wall thickness.

Figure 4.36: *Deformed RHS 150×100×6 (length = 1050 mm) beam-column*

FE model with boundary conditions

4.9.3 Comparison with test results

A comparison of ultimate load carrying capacity for all tests and FE models of pin-ended SHS and RHS beam-columns is presented in Table 4.19. It should be noted that for all tested RHS beam-columns, bending was about the major axis.

Table 4.19: *Comparison between all SHS and RHS beam-column test results and FE results for a global imperfection amplitude of L/2000*

Specimen identification	β	$\bar{\lambda}$	Test F_u (kN)	FE F_u (kN)	Test F_u/FE F_u
SHS 60×60×5- BC1	0.72	1.47	322	290	0.90
SHS 60×60×5- BC2	2.27	0.75	210	196	0.93
SHS 60×60×5- BC3	1.96	0.58	125	122	0.98
SHS 60×60×5- BC4	1.96	0.94	83	82	0.99
RHS 150×100×3- BC1	1.96	1.29	209	202	0.97
RHS 150×100×3- BC2	0.93	0.59	173	171	0.99
RHS 150×100×3- BC3	0.95	0.95	134	126	0.94
RHS 150×100×3- BC4	1.96	0.58	95	93	0.98
RHS 150×100×6- BC1	1.96	0.94	569	577	1.01
RHS 150×100×6- BC2	1.96	1.29	403	400	0.99
RHS 150×100×6- BC3	0.93	0.59	267	272	1.02
RHS 150×100×6- BC4	0.95	1.31	192	194	1.01
MEAN:					**0.98**
ST DEV:					**0.04**

4.9.4 Discussion

The results exhibit excellent agreement between test and FE behaviour. This confirms that the parameters derived from the stub column and pin-ended column models are equally applicable to the modelling of stainless steel SHS and RHS beam-columns.

4.10 SHS AND RHS BI-AXIAL BENDING MODELLING

4.10.1 Introduction

A member subjected to bending moments about both of its principal axes is said to be in bi-axial bending. It may also be viewed as a special case of beam-column loading where the axial load is absent. No tests have been conducted on stainless steel SHS or RHS subjected to bi-axial moments.

4.10.2 Development of FE models

Bi-axial bending is more difficult to achieve in laboratory conditions than the other load cases examined in previous sections. Ultimate load carrying capacity for a series of members subjected to bi-axial bending will therefore be generated using numerical methods. The results will be used to validate the proposed design method for the special load case of bi-axial bending.

FE models were developed using the parameters shown to be applicable for other load cases in previous sections. The boundary conditions for the bi-axial bending models were such that the ends of the members were free to rotate in any direction about a central node. Rigid body rotation was prevented with a torsional restraint at one end. Equal and opposite bending moments were applied at each end of the member and about both of the principal axes. The investigation considered SHS members of fixed length (1000 mm), fixed cross-sectional dimensions (80×80 mm) and fixed material properties (as for the SHS 80×80×4 tested as part of the current study), but with varying wall thickness to create a series of cross-sectional slendernesses. A typical bi-axial bending model is shown in Figure 4.37.

4.10.3 Results

The results are shown in Table 4.20, and compared with the predicted resistances for the Eurocode and proposed design method in Chapter 6.

All translational degrees of freedom
fixed on central node, plus torsional
restraint to prevent rigid body
rotation

All translational degrees of freedom,
except axial displacement, fixed on
central node
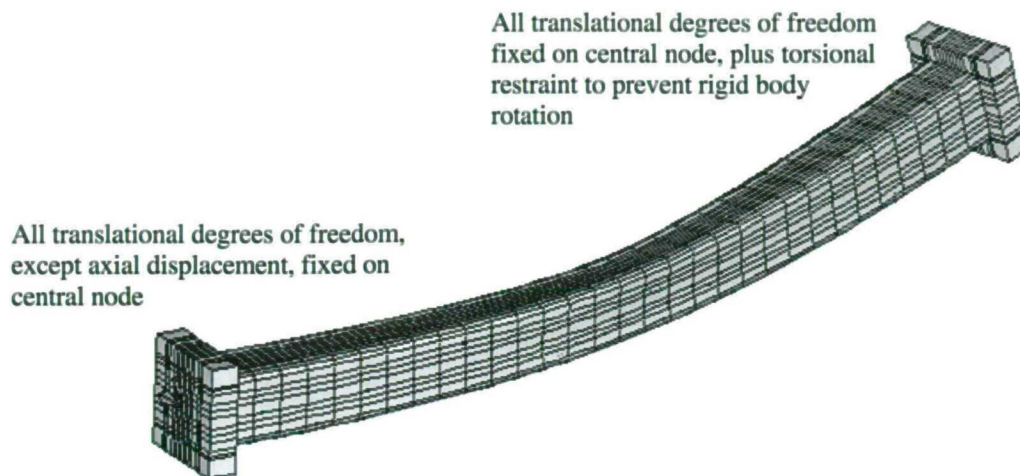
Figure 4.37: *Deformed FE model of SHS 80×80×5 member subjected*
to bi-axial bending with boundary conditions

Table 4.20: *FE results for bi-axial bending models with a global imperfection amplitude of L/2000*

Model identification	β	FE M_u (kNm)
SHS 80×80×2- BB1 (FE)	1.76	3.5
SHS 80×80×3- BB1 (FE)	1.16	6.7
SHS 80×80×4- BB1 (FE)	0.86	9.4
SHS 80×80×5- BB1 (FE)	0.68	11.7
SHS 80×80×6- BB1 (FE)	0.56	15.7

Notes: β is a measure of cross-section slenderness. [$\beta = (b/t)(\sigma_{0.2}/E_0)^{0.5}$].

M_u refers to the moment applied about each of the principal axes

4.11 CONCLUDING COMMENTS

This chapter has described the FE modelling of stainless steel CHS, SHS and RHS members subjected to a variety of loading arrangements. Key parameters and methods have been defined

through examination of experimental data and through carefully conducted parametric studies to achieve a consistent approach to the modelling. A summary of the findings is listed below:

- Material stress-strain properties are defined by means of a compound (two-stage) Ramberg-Osgood formulation (defined by Equation 4.19).

- Enhanced corner material properties in SHS and RHS are defined in Section 4.2.5, and found (by means of parametric studies) to extend to a distance of 2t beyond the curved portions of the cross-sections.

- A suitable amplitude of local initial geometric imperfections was found to be defined by Equation 4.31 for SHS and RHS (determined from analysis of imperfection data, and by comparison of stub column test and FE results), and taken as 0.2t for CHS (following parametric studies with varying imperfection amplitude and comparison with stub column test results).

- Initial member out-of-straightness was taken as L/2000 following parametric studies and comparison with test results.

- Representative residual stress distributions are defined in Section 4.3 for CHS, SHS and RHS sections, but parametric studies showed their influence to be relatively insignificant.

- For all problem types (stub columns, pin-ended columns and beam-columns), for which reliable test data exists, the numerical predictions of the key performance measures demonstrated a high degree of accuracy: On average, ultimate load was predicted to within 3% and with a low standard deviation; deformation at ultimate load was within 6%, but exhibited a higher standard deviation; and the general form of the load-deformation response and the failure modes were similar.

CHAPTER 5

ANALYSIS OF RESULTS & DEVELOPMENT OF DESIGN METHOD

5.1 INTRODUCTION

A detailed account of the proposed design approach for stainless steel structures is given in Chapter 6, where comparison is made between all available test results and predicted resistances according to ENV 1993-1-4 (1996) and the proposed design method. This chapter presents an overview of the method, and describes how test and FE results have been used for its development, calibration and initial validation. Results from other laboratory testing programmes are introduced and analysed in conjunction with those generated as part of the current study (described in Chapter 3).

5.2 OVERVIEW OF DESIGN METHOD

5.2.1 Background

An important step towards the enhancement of understanding and use of stainless steel in structures has been the development of the design guidance given in the European pre-Standard,

ENV 1993-1-4 (1996) and provided by The Steel Construction Institute (Baddoo & Burgan, 2001). However, one of the principal drawbacks to these is that they were based on the rather limited amount of structural performance data available. Additionally, since they were 'first generation' design guides, an important factor in their development was to ensure that a designer familiar with the carbon steel rules would be able to make a straightforward transition to stainless steel structural design. As a result, the authors were obliged to use a simplified elastic, perfectly plastic material model. This model is acceptable for carbon steel that exhibits a sharply defined yield point, followed by a plastic yield plateau. For stainless steel, though, where there is no sharply defined yield point and substantial strain hardening is possible, this model leads to overly conservative designs.

5.2.2 Objectives for proposed new design method

The primary objective of this study has been to develop a design approach to allow structural stainless steel members to be designed safely and efficiently. Where possible and appropriate it is intended that the method should be consistent with the carbon steel rules, but not at the expense of economy. It is clear that a compromise between simplicity and accuracy of design procedure has to be reached.

The proposed method is limited in scope to the classification and design of circular, square and rectangular hollow sections, CHS, SHS and RHS respectively, due to the constraints of time and lack of suitable experimental data, though in principle, the design method can be extended to cover all types of cross-sections. It should also be noted that hollow sections are the most widely used type of structural stainless steel cross-section in construction.

5.2.3 Proposed design method

In view of the continuous nature of the stainless steel stress-strain curve, it seemed rational that a continuous, rather than a discretised section classification system should be adopted. Development of this idea was the focal point of the research. The design procedure was reported at various stages of advancement by Gardner & Nethercot (2001b, 2001c and 2002).

Eurocode 3 defines four discrete behavioural classes of cross-sections, as shown in Figure 5.1. Cross-sections with very high deformation capacity are classified as Class 1. Class 1 cross-

sections are fully effective under pure compression and capable of reaching and maintaining their full plastic moment in bending. Class 2 cross-sections have a somewhat lower deformation capacity, but are also fully effective in pure compression and capable of reaching their full plastic moment in bending. Class 3 cross-sections are fully effective in pure compression, but local buckling prevents attainment of the full plastic moment in bending. Bending moment resistance is therefore limited to the yield moment. For Class 4 cross-sections, local buckling occurs in the elastic range. An effective cross-section is therefore defined based on the width-to-thickness ratios of individual plate elements, and this is used to determine the cross-sectional resistance.
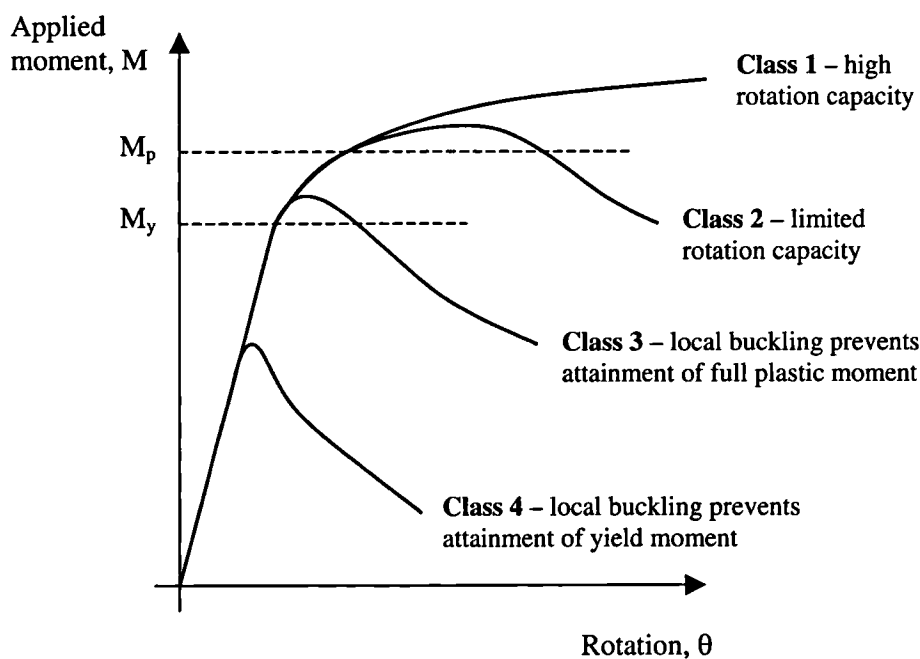
Figure 5.1: *Four behavioural classes of cross-section defined by Eurocode 3*

For the proposed design method, these four behavioural classes are to be replaced by a numerical value that is a measure of the deformation capacity of the cross-section. The deformation capacity is based upon the slenderness of the individual plate elements that make up the cross-section, and the interaction between them. These data are generated by means of stub column tests.

Member resistances are determined using the cross-section deformation capacity, in conjunction with a material model appropriate for stainless steels. A compound Ramberg-Osgood model was devised in Chapter 4 and was shown to be capable of achieving excellent replication of

stainless steel stress-strain behaviour. This model will be utilised in the proposed design method. For members in bending, the concept of a generalised shape factor is adopted, into which material as well as geometric properties of a cross-section are incorporated. For cases of instability, member resistance is determined from revised buckling curves, and modified by a factor derived from the cross-section deformation capacity.

Figure 5.2 shows a schematic representation of the design procedure, where b and t are internal element width and thickness respectively, A is the cross-sectional area, W_{el} is the elastic section modulus, $\sigma_{0.2}$ is the material 0.2% proof strength in compression and E_0 is the material Young's modulus.
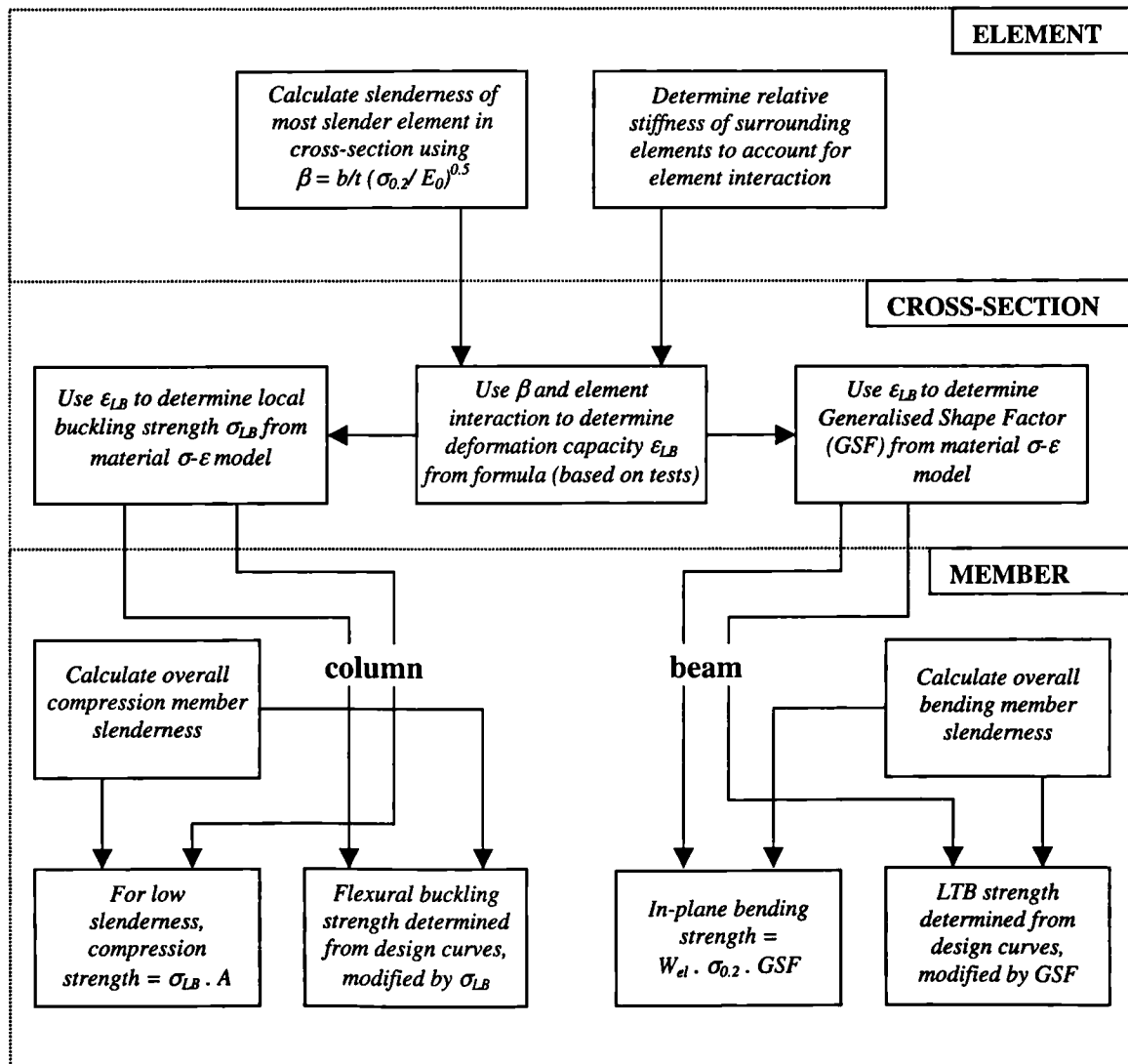
Figure 5.2: *Schematic representation of proposed design procedure*

The resistance of members subjected to a combination of axial load plus bending moments may be determined through an interaction of the component load cases.

5.3 MATERIAL STRESS-STRAIN CHARACTERISTICS

5.3.1 Background

The proposed design method implements a more complex material model than ENV 1993-1-4 (1996) and other current stainless steel structural design codes. In addition to $\sigma_{0.2}$ and E_0 that are required by the elastic, perfectly-plastic material model, the compound Ramberg-Osgood model (described in Section 4.2.4) also requires values for $\sigma_{1.0}$ (or σ_u and ε_{pu}), n and $n'_{0.2,1.0}$ (or $n'_{0.2,u}$). Therefore, working with the same input parameters as ENV 1993-1-4 (1996), representative values for these additional parameters should be defined.

5.3.2 Tensile, compressive and stub column material properties

Analysis of stainless steel material stress-strain data has shown divergence between tensile, compressive and stub column properties. For consistency it should be decided which stress-strain curve the proposed design procedure shall be based upon. Since cross-section deformation capacity is defined by the compressive behaviour of plate elements and the primary structural components (beams and columns) act largely in compression, it seems most rational that the compressive stress-strain curve be used.

Stub column stress-strain curves differ from compressive coupon stress-strain curves due to the presence of residual stresses, weld material and (for SHS and RHS) enhanced strength corner regions. Weld-induced residual stresses have been shown to have little influence on stub column behaviour (Section 4.5.4) and through-thickness residual stresses are also present in tensile and compressive coupons. The weld material makes up a small percentage of the total cross-sectional area (approximately 1 – 2% for a typical hollow section). It is believed that any material strength loss due to the annealing effect of the weld heat is fairly localised and relatively insignificant, and may often be offset by the increase in area due to the weld material. Enhanced strength corner regions in SHS and RHS however have been shown to have an

important influence on stub column behaviour (Section 4.5.3). For CHS no such corner regions exist and material properties are approximately uniform around the cross-section.

Compression stress-strain properties will therefore be used as the basis for the design procedure, though in the absence of compressive properties, tensile properties will be used for SHS and RHS, and stub column properties will be used for CHS. It will be noted when properties other than compression ones are used.

5.3.3 Results from other laboratory testing programmes

Results from the material stress-strain tests carried out in the current study have been presented in Chapter 3. Results from other studies where stress-strain tests were conducted on material cut from cold-formed austenitic stainless steel SHS and RHS are given in Table 5.1. Similarly results from tests conducted on cold-formed stainless steel CHS material are presented in Table 5.2.

5.3.3.1 Rasmussen and Hancock (1990)

Rasmussen & Hancock (1990) conducted tensile and compressive tests on material cut from cold-formed stainless steel SHS and CHS. All specimens were Grade 1.4306. For the SHS, material was cut from two flat faces (one adjacent to the weld and one opposite the weld) and one corner region. For the CHS, material was taken from one location, at 90° to the weld. Mean tensile and compressive stress-strain results are presented in Tables 5.1 and 5.2.

5.3.3.2 Talja and Salmi (1995)

Talja & Salmi (1995) conducted a total of 39 tests on cold-formed stainless steel SHS and RHS members, in a variety of loading configurations. All material was Grade 1.4301. Tensile and compressive coupon tests were carried out on material cut from the flat faces of the cross-sections. In some instances compressive coupon tests were omitted. Weighted average results are presented in Table 5.1.

5.3.3.3 Talja (1997)

Talja (1997) reported on tests conducted on stainless steel welded I-section and CHS beams, columns and beam-columns. Tensile tests were conducted on material cut from the cross-

sections at two locations: opposite the weld and at 90° to the weld. Three CHS sizes were tested. The CHS 140×4 was Grade 1.4541, and the CHS 140×3 and CHS 140×2 were Grade 1.4435. Mean results from the tensile tests are presented in Table 5.2.

5.3.3.4 Chryssanthopoulos and Kiymaz (1998)

Chryssanthopoulos & Kiymaz (1998) conducted eight bending tests on stainless steel CHS, four of which were Grade 1.4301. Tensile tests were carried out on material cut from the cross-sections at three locations: near to the weld, at 90° to the weld and opposite the weld. Mean values are presented in Table 5.2.

5.3.3.5 Mirambell and Real (2001)

Mirambell & Real (2001) conducted bending tests on six simply supported beams and six continuous beams. Measured tensile material properties for the SHS and RHS (Grade 1.4301) are presented in Table 5.1. It was reported that coupons were extracted from the cross-sections and tested by the stainless steel producers. No information regarding the location of the extracted material was available (Real, 2001).

5.3.3.6 Young and Hartono (2002)

Young & Hartono (2002) performed a series of tests on cold-formed stainless steel CHS columns compressed between fixed ends. Failure of the columns was primarily due to overall flexural buckling. Tensile and stub column tests were conducted to determine material stress-strain behaviour. Mean results are presented in Table 5.2. All material was Grade 1.4301.

5.3.3.7 Young and Liu (2002)

Young & Liu (2002) described an experimental investigation into the strength of cold-formed RHS columns compressed between fixed ends. Test strengths were compared to strengths predicted by various design codes, and it was concluded that the design strengths were generally conservative. Material properties were obtained by means of tensile coupon tests and stub column tests. The tensile coupon test results are presented in Table 5.1. All material was Grade 1.4301.

5.3.3.8 Liu and Young (2002)

Liu & Young (2002) conducted a series of tests on cold-formed stainless SHS columns subjected to pure compression, with fixed-ended boundary conditions and the primary failure mode being overall flexural buckling. Material properties were measured by means of tensile coupon tests and stub column tests. Results from the tensile coupon tests are presented in Table 5.1. All material was Grade 1.4301.

5.3.4 Representative compound Ramberg-Osgood parameters

On the basis of the material stress-strain tests conducted as part of the current study and as part of all other suitable studies, the following values are proposed for use in the compound (2-stage) Ramberg-Osgood formulation described in Section 4.2.4. The proposed values are for material removed from cold-formed austenitic SHS, RHS and CHS and are based on mean test results. Other stress-strain data that exist for flat sheet material have not been considered. Values for $\sigma_{1.0}$ have been expressed as a multiple of $\sigma_{0.2}$, whereas σ_u and ε_{pu} have been expressed as absolute values since there is less inherent absolute variation.

For flat material in cold-formed (austenitic) stainless steel SHS and RHS:

- $\sigma_{1.0}$ (tensile) $= 1.15\sigma_{0.2}$ N/mm^2 (tensile)
- $\sigma_{1.0}$ (comp.) $= 1.26\sigma_{0.2}$ N/mm^2 (comp.)
- σ_u $= 694$ N/mm^2 $(= 1.61\sigma_{0.2})$
- ε_{pu} $= 0.50$

For cold-formed (austenitic) stainless steel CHS:

- $\sigma_{1.0}$ (tensile) $= 1.20\sigma_{0.2}$ (tensile)
- $\sigma_{1.0}$ (comp.) $= 1.20\sigma_{0.2}$ (comp.)[1]
- σ_u $= 661$ N/mm^2 $(= 1.77\sigma_{0.2})$
- ε_{pu} $= 0.55$

---

[1] It should be noted that since there are no test values of $\sigma_{1.0}$ for CHS material in compression, $\sigma_{1.0}$ (comp.) has been taken as $1.20\sigma_{0.2}$ (comp.), assuming an analogy with the tensile behaviour.

Table 5.1: SHS and RHS measured material properties from other laboratory test programmes

Coupons	Tested by	E_0 (N/mm²)	$\sigma_{0.2}$ (N/mm²)	$\sigma_{1.0}$ (N/mm²)	σ_u (N/mm²)	ε_{pu}	Modified R-O coefficients		
							n	$n'_{0.2,u}$	$n'_{0.2,1.0}$
SHS 80×80×3- TF	Rasmussen & Hancock	194000	408	-	695	0.50	-	-	-
SHS 80×80×3- TC		190000[1]	580	-	805	0.29	-	-	-
SHS 80×80×3- CF		196000	415	-	-	-	-	-	-
SHS 80×80×3- CC		213000[1]	645	-	-	-	-	-	-
SHS 60×60×5-a- TF	Talja & Salmi	185000	566	-	753	0.42	4.8	-	-
SHS 60×60×5-a- CF		186500	463	-	-	-	3.2	-	-
SHS 60×60×5-b- TF		181000	530	-	669	0.45	4.1	-	-
SHS 60×60×5-c- TF		184000	544	-	761	0.48	4.7	-	-
RHS 150×100×3- TF[2]	Talja & Salmi	197200	294	-	626	0.66	5.9	-	-
RHS 150×100×3- CF[2]		206600	305	-	-	-	4.8	-	-
RHS 150×100×6-a- TF	Talja & Salmi	193600	339	-	651	0.59	7.1	-	-
RHS 150×100×6-a- CF		240800	345	-	-	-	3.2	-	-
RHS 150×100×6-b- TF		198200	320	-	668	0.66	5.1	-	-
SHS 80×80×3- TF	Mirambell & Real	165600	422	-	658	-	4.8	-	-
RHS 120×80×4- TF		161200	442	-	661	-	6.2	-	-

Table 5.1 (continued): *SHS and RHS measured material properties from other laboratory test programmes*

Coupons	Tested by	E_0 (N/mm^2)	$\sigma_{0.2}$ (N/mm^2)	$\sigma_{1.0}$ (N/mm^2)	σ_u (N/mm^2)	ε_{pu}	Modified R-O coefficients		
							n	$n'_{0.2,u}$	$n'_{0.2,1.0}$
SHS 70×70×2- TF	Liu & Young	195000	337	-	636	0.60	4.0	-	-
SHS 70×70×5- TF		194000	444	-	688	0.61	5.0	-	-
RHS 120×40×2- TF	Young & Liu	198000	350	-	649	0.72	5.0	-	-
RHS 120×40×5.3- TF		194000	424	-	676	0.61	5.0	-	-
RHS 120×80×2.8- TF		193000	366	-	648	0.68	5.0	-	-
RHS 120×80×6- TF		194000	443	-	678	0.61	5.0	-	-

Notes: 1   Rasmussen & Hancock reported that bracketed values may have been affected by initial bending of the coupons

2   Formed from flat sheet directly into RHS. All other cross-sections are believed to have been formed firstly into a CHS and then into an SHS or RHS

Key: TF – Tension Flat
  TC – Tension Corner
  CF – Compression Flat
  CC – Compression Corner

Table 5.2: CHS measured material properties from other laboratory test programmes

Coupons	Tested by	E_0 (N/mm^2)	$\sigma_{0.2}$ (N/mm^2)	$\sigma_{1.0}$ (N/mm^2)	σ_u (N/mm^2)	ε_{pu}	Modified R-O coefficients		
							n	$n'_{0.2,u}$	$n'_{0.2,1.0}$
CHS 103×1.5- Tensile	Chryssanthopoulos & Kiymaz	214000	461	554	783	-	4.3	-	-
CHS 103×1.5- Stub Col.		206000	368	-	-	-	4.6	-	-
CHS 153×1.5- Tensile		211000	456	547	800	-	4.9	-	-
CHS 153×1.5- Stub Col.		203000	405	-	-	-	4.2	-	-
CHS 203×1.5- Tensile		200000	370	434	744	-	6.3	-	-
CHS 219×2.0- Tensile		211000	332	404	623	-	5.0	-	-
CHS 101.6×2.85- Tensile	Rasmussen & Hancock	198000	390	-	640	0.49	-	-	-
CHS 101.6×2.85- Comp.		202000	390	-	-	-	-	-	-
CHS 101.6×2.85- Tensile		202000	405	-	630	0.58	7.3	-	-
CHS 101.6×2.85- Comp.		-	405	-	-	-	5.5	-	-

Table 5.2 (continued): *CHS measured material properties from other laboratory test programmes*

Coupons	Tested by	E_0 (N/mm²)	$\sigma_{0.2}$ (N/mm²)	$\sigma_{1.0}$ (N/mm²)	σ_u (N/mm²)	ε_{pu}	Modified R-O coefficients n	$n'_{0.2,u}$	$n'_{0.2,1.0}$
CHS 140x2- Tensile	Talja	201000	318	-	598	0.51	5.7	-	-
CHS 140x2- Stub col.		200000	294	-	-	-	5.2	-	-
CHS 140x3- Tensile		190500	352	-	577	0.59	4.9	-	-
CHS 140x3- Stub col.		192000	317	-	-	-	4.7	-	-
CHS 140x4- Tensile		193000	295	-	520	0.59	5.5	-	-
CHS 140x4- Stub col.		197000	309	-	-	-	5.5	-	-
CHS 89x2.78 – Tensile	Young & Hartono	190000	270	-	690	0.60	4.0	-	-
CHS 89x2.78 – Stub col.		190000	242	-	-	-	9.0	-	-
CHS 168.7x3.34- Tensile		195000	288	-	690	0.59	7.0	-	-
CHS 168.7x3.34- Stub col.		195000	247	-	-	-	7.0	-	-
CHS 324.3x4.32- Tensile		202000	261	-	616	0.65	5.0	-	-
CHS 324.3x4.32- Stub col.		202000	248	-	-	-	9.0	-	-

For completeness, though not required by the proposed design method, for corner material in cold-formed (austenitic) stainless steel SHS and RHS:

- $\sigma_{1.0,c}$ (tensile)   = $1.84\sigma_{0.2}$ (tensile)
- $\sigma_{1.0,c}$ (comp.)   = $1.84\sigma_{0.2}$ (comp.)[2]
- $\sigma_{u,c}$ = $817 \, N/mm^2$ ($= 2.11\sigma_{0.2}$)
- $\varepsilon_{pu,c}$ = 0.23

[2] It should be noted that since there are no test values of $\sigma_{1.0,c}$ for SHS and RHS corner material in compression, $\sigma_{1.0,c}$ (comp.) has been taken as $1.84\sigma_{0.2}$ (comp.), assuming an analogy with the tensile behaviour.

Mean measured values for the strain hardening exponents n, $n'_{0.2,u}$ and $n'_{0.2,1.0}$ for different cross-section types in longitudinal tension and compression are given in Table 5.3. Material testing in the current study was limited to the longitudinal direction since this is the primary direction of material straining during structural service. No tests were performed in the transverse direction.

Table 5.3: *Mean measured values for Ramberg-Osgood strain hardening exponents*

Cross-section type	Loading direction	n	$n'_{0.2,u}$	$n'_{0.2,1.0}$
SHS & RHS – flat	Tension	5.5	3.2	3.4
	Compression	4.2	-	2.7
SHS & RHS - corner	Tension	4.3	5.9	4.6
	Compression	-	-	-
CHS	Tension	5.5	-	-
	Compression	5.5	-	-

Codified values of n tend to be based on the stress-strain behaviour of flat sheet material (prior to its shaping into final products). Values of n from ENV 1993-1-4 (1996) have been presented in Table 5.4 for comparison with those in Table 5.3, though it is not deemed that these values are suitable for the description of the material behaviour of cold-formed structural stainless steel hollow sections.

Table 5.4: *Codified values for the Ramberg-Osgood strain hardening exponent, n*

Strength Class	Coefficient n	
	Longitudinal direction	Transverse direction
S 220 (inc. Grade 1.4301)	5.5	7.5
S 240 (inc. Grade 1.4401)	6.0	8.0
S 480	4.0	4.0

Note: No distinction is made is ENV 1993-1-4 (1996) between
tensile and compressive material behaviour.

5.4 SHS AND RHS STUB COLUMNS

5.4.1 Background

The behaviour of plate elements within a cross-section loaded in pure compression forms the basis of the proposed design method. The purpose of the stub column tests in the current study was to develop a relationship between cross-section slenderness and deformation capacity.

5.4.2 SHS and RHS stub column test results from other test programmes

Full details of SHS and RHS stub column tests conducted in the current study are presented in Chapter 3. Geometrical measurements of SHS and RHS stub columns from other laboratory test programmes are presented in Table 5.5, and corresponding load-end shortening details are provided in Table 5.6. All available austenitic stainless steel SHS and RHS stub column test results, where sufficient details have been reported, are included in Tables 5.5 and 5.6.

5.4.3 Relationship between cross-section slenderness and deformation capacity

The starting point for deriving the relationship between the slenderness of stainless steel SHS and RHS cross-sections and their corresponding deformation capacities was to consider the elastic critical buckling of a compressed plate element.

Table 5.5: Measured dimensions for SHS and RHS stub columns from other test programmes

Specimen identification	Tested by	Depth, D (mm)	Breadth, B (mm)	Thickness, t (mm)	Length, L (mm)	Internal corner radius, r_i (mm)	Area, A (mm²)
SHS 80×80×3- SC1	Rasmussen & Hancock	80.4	80.4	3.00	300	5.5	908
SHS 80×80×3- SC2		79.7	79.7	3.00	298	5.5	900
RHS 60×60×5- SC1	Talja & Salmi	59.6	59.8	4.77	399	3.5	999
RHS 150×100×3- SC1		150.7	100.5	2.89	1048	3.0	1397
RHS 150×100×6- SC1		150.5	100.7	5.77	1049	5.5	2683

Table 5.6: Results for SHS and RHS stub columns from other test programmes

Specimen identification	Ultimate load, F_u (kN)	End shortening at F_u (mm)
SHS 80×80×3- SC1	485	2.0
SHS 80×80×3- SC2	471	2.2
RHS 60×60×5- SC	801	9.4
RHS 150×100×3- SC	372	3.7
RHS 150×100×6- SC	1292	12.0

5.4.3.1 Definition of cross-section slenderness, β

The elastic critical buckling strain, ε_{cr} of a perfect, uniformly compressed plate, where buckling occurs in the elastic range, is given by Equation 5.1.

$$\varepsilon_{cr} = \frac{k\pi^2}{12(1-v^2)(b/t)^2} \qquad (5.1)$$

in which v is Poisson's ratio, b is plate width, t is plate thickness and k is the buckling coefficient dependent upon edge restraint conditions. The elastic critical buckling strain can be normalised by the elastic strain at the material compressive 0.2% proof stress, defined as $\varepsilon_0 = \sigma_{0.2}/E_0$, to give Equation 5.2.

$$\frac{\varepsilon_{cr}}{\varepsilon_0} = \frac{E_0 k\pi^2}{12\sigma_{0.2}(1-v^2)(b/t)^2} = \frac{k\pi^2}{12(1-v^2)} \frac{1}{\beta^2} \qquad (5.2)$$

in which the geometrical and material property variables of the plate have been grouped into the single slenderness parameter, β given by Equation 5.3. The plate width b will be measured between the centrelines of the adjoining plates, (i.e. (D-t) or (B-t), where t is the material thickness). The value of β for the most slender plate in the cross-section will be used as the basic measure of slenderness. The parameters $\sigma_{0.2}$ and E_0 will be based on material stress-strain behaviour in compression.

$$\beta = (b/t)\sqrt{\sigma_{0.2}/E_0} \qquad (5.3)$$

Plate buckling, however, only occurs wholly in the elastic range for slender plates, and Equation 5.2 has to be modified to allow for effects including inelastic plate buckling, though the definition of β will remain unchanged.

Allowance for varying edge restraint conditions of the plate is made by considering the geometry of the cross-section. Square hollow sections produce no constraining moments between the elements of the cross-section due to their symmetrical nature. Their behaviour therefore closely corresponds to an assemblage of simply-supported plates (Timoshenko and Gere, 1985), and a buckling coefficient, $k = 4.0$ is therefore appropriate. In the case of

rectangular hollow sections however, greater edge restraint is applied to the more slender sides of the cross-section by the less slender sides. As a result, higher buckling curves can be applied to the more slender sides of rectangular hollow sections, and clearly an increase in aspect ratio produces an increase in edge restraint, tending towards the limit of fixed edge restraint where $k = 6.97$.

5.4.3.2 Definition of cross-section deformation capacity

The basic measure of cross-section deformation capacity will be defined as the strain at ultimate load, ε_{LB} (local buckling strain) determined from the stub column load-end shortening curves, as shown in Figure 5.3. For each cross-section ε_{LB} is determined by dividing the end shortening at ultimate load, δ_u by the stub column length, L.
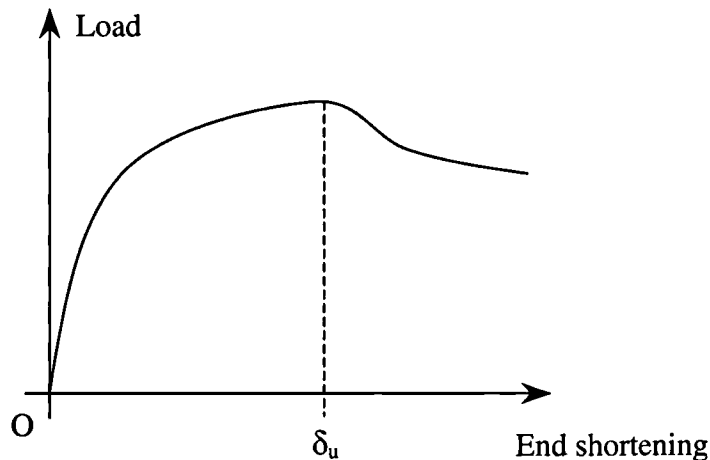
Figure 5.3: *Determination of cross-section deformation capacity*

The raw SHS and RHS stub column test results from the current study (given in Tables 3.10 and 3.11) and from all other studies (given in Table 5.6) have been manipulated and assembled in Tables 5.7 to 5.9, and plotted in Figure 5.4. Figure 5.4 shows a graph of normalised local buckling strain ($=\varepsilon_{LB}/\varepsilon_0$), where ε_0 is the elastic strain at the material compressive 0.2% proof stress, versus cross-section slenderness, β. The elastic critical buckling curve for a simply-supported plate element in pure compression (with the buckling coefficient, k set equal 4.0, and Poisson's ratio taken as 0.3) has been added.

Table 5.7: *Cross-section slenderness and deformation capacity for SHS stub columns*

Specimen identification	$\beta = b/t(\sigma_{0.2}/E_0)^{0.5}$	$\varepsilon_0 = \sigma_{0.2}/E_0$	ε_{LB}	$\varepsilon_{LB}/\varepsilon_0$
SHS 60×60×5- SC[1]	0.57	0.0025	0.0236	9.50
SHS 80×80×3- SC1[1]	1.19	0.0021	0.0068	3.21
SHS 80×80×3- SC2[1]	1.18	0.0021	0.0073	3.45
SHS 80×80×4- SC1	1.02	0.0024	0.0184	7.52
SHS 80×80×4- SC2	0.99	0.0024	0.0180	7.33
SHS 80×80×4- SC3	0.98	0.0024	0.0193	7.86
SHS 80×80×4- ASC1	0.71	0.0013	0.0214	16.90
SHS 80×80×4- ASC2	0.73	0.0013	0.0179	14.12
SHS 100×100×2- SC1	2.17	0.0018	0.0027^2	1.50^2
SHS 100×100×2- SC2	2.18	0.0018	0.0022^2	1.26^2
SHS 100×100×3- SC1	1.45	0.0018	0.0056	3.09
SHS 100×100×3- SC2	1.46	0.0018	0.0057	3.14
SHS 100×100×4- SC1	1.16	0.0021	0.0100	4.67
SHS 100×100×4- SC2	1.16	0.0021	0.0100	4.65
SHS 100×100×6- SC1	0.78	0.0024	0.0335	14.00
SHS 100×100×6- SC2	0.77	0.0024	0.0337	14.11
SHS 100×100×8- SC1	0.46	0.0016	0.0726	45.14
SHS 100×100×8- SC2	0.46	0.0016	0.0954	59.31
SHS 150×150×4- SC1	1.50	0.0015	0.0037	2.48
SHS 150×150×4- SC2	1.52	0.0015	0.0036	2.37

Notes: [1] Results obtained from other test programmes

[2] Peaks of load-end shortening curves dominated by post buckling effects (revised values for ε_{LB} presented in Table 5.10)

Table 5.8: *Cross-section slenderness and deformation capacity for RHS stub columns with aspect ratios of 0.67*

Specimen identification	$\beta = b/t(\sigma_{0.2}/E_0)^{0.5}$	$\varepsilon_0 = \sigma_{0.2}/E_0$	ε_{LB}	$\varepsilon_{LB}/\varepsilon_0$
RHS 60×40×4- SC1	0.72	0.0024	0.0370	15.25
RHS 60×40×4- SC2	0.72	0.0024	0.0371	15.29
RHS 120×80×3- SC1	1.86	0.0022	0.0045^2	2.06^2
RHS 120×80×3- SC2	1.88	0.0022	0.0044^2	2.03^2
RHS 120×80×6- SC1	0.96	0.0024	0.0218	8.98
RHS 120×80×6- SC2	0.96	0.0024	0.0218	9.00
RHS 150×100×3- SC[1]	1.98	0.0015	0.0035^1	2.37^1
RHS 150×100×4- SC1	1.53	0.0016	0.0055	3.43
RHS 150×100×4- SC2	1.52	0.0016	0.0051	3.20
RHS 150×100×6- SC[1]	0.96	0.0015	0.0114	7.77

Notes: [1] Results obtained from other test programmes

[2] Peaks of load-end shortening curves dominated by post buckling effects (revised values for ε_{LB} presented in Table 5.10)

Table 5.9: *Cross-section slenderness and deformation capacity for RHS stub columns with aspect ratios of 0.50*

Specimen identification	$\beta = b/t(\sigma_{0.2}/E_0)^{0.5}$	$\varepsilon_0 = \sigma_{0.2}/E_0$	ε_{LB}	$\varepsilon_{LB}/\varepsilon_0$
RHS 100×50×2- SC1	2.25	0.0018	0.0040^2	2.22^2
RHS 100×50×2- SC2	2.25	0.0018	0.0042^2	2.32^2
RHS 100×50×3- SC1	1.60	0.0023	0.0060	2.66
RHS 100×50×3- SC2	1.60	0.0023	0.0059	2.62
RHS 100×50×4- SC1	1.19	0.0022	0.0116	5.38
RHS 100×50×4- SC2	1.21	0.0022	0.0124	5.76
RHS 100×50×6- SC1	0.77	0.0024	0.0309	12.92
RHS 100×50×6- SC2	0.77	0.0024	0.0327	13.64

Note: [2] Peaks of load-end shortening curves dominated by post buckling effects (revised values for ε_{LB} presented in Table 5.10)
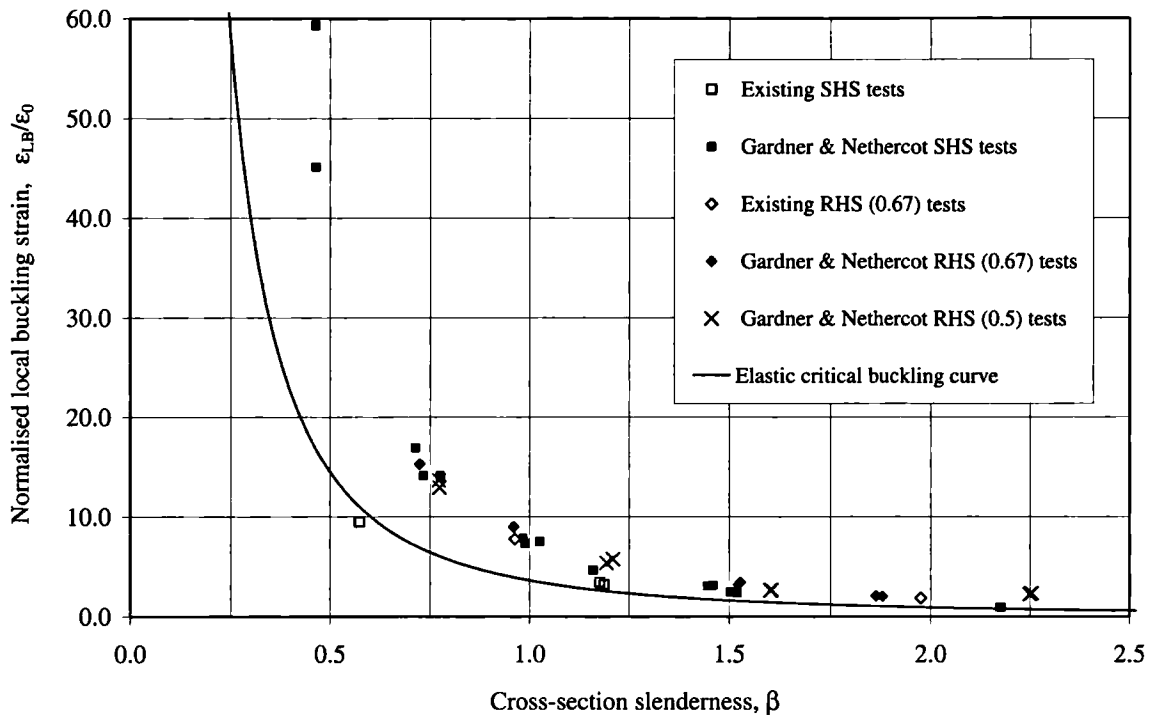
Figure 5.4: *Normalised local buckling strain versus cross-section slenderness*

From Figure 5.4 it can be seen that all bar one test result lie above the elastic critical buckling curve. Deviation of the test results from the elastic critical buckling curve is due to several effects including inelastic material behaviour, geometric imperfections, residual stresses, and post buckling response.

5.4.3.3 Modified definition of deformation capacity for slender cross-sections

For slender cross-sections, where β is greater than about 1.6, it was observed that the deformation capacity at ultimate load, δ_u becomes increasingly dominated by post-buckling response. Figure 5.5 compares the load-deformation behaviour of stub columns with slender and non-slender cross-sections.

For the non-slender case, deviation from the material σ-ε curve occurs approximately at ultimate load where there is the onset of local buckling. Therefore, using ε_2 in conjunction with the material stress-strain curve, the predicted design strength, $\sigma_{2,\ pred}$ is close to the actual strength of the stub column, $\sigma_{2,actual}$. However, for the slender case (where β is greater than about 1.6), local buckling occurs in the elastic range, and deviation from the stress-strain curve

may be followed by considerable post-buckling deformation. Therefore, using ε_1 would result in an over-prediction of the actual stub column strength by the proposed design method. Thus, for cross-sections where β is greater than 1.6, deformation capacity is redefined at an empirically-derived proportion of the ultimate load. The linear reduction given in Equation 5.4 was derived from the test results.
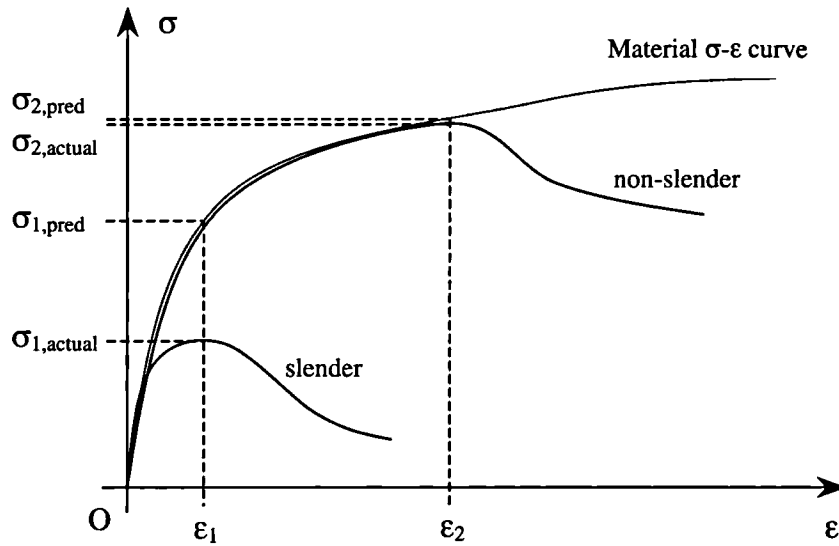
Figure 5.5: *Behaviour of stub columns with slender and non-slender cross-sections*

$$\varphi = -0.0833\beta + 1.133 \qquad \text{for } \beta > 1.6 \qquad (5.4)$$

where φ is the proportion of ultimate load at which deformation capacity is defined.

Revised values of ε_{LB} and $\varepsilon_{LB}/\varepsilon_0$ for cross-sections where $\beta > 1.6$ are given in Table 5.10.

5.4.3.4 Generation of mean (design) curves

To describe the local buckling behaviour of aluminium plate elements, Faella et al (1999) proposed an expression of the general form given in Equation 5.5. The constants C_1, C_2, and C_3 were determined from a regression analysis of experimental points.

$$\frac{\varepsilon_{LB}}{\varepsilon_0} = \frac{C_1}{\beta^{C_2 + C_3\beta}} \qquad (5.5)$$

Table 5.10: *Cross-section slenderness and revised deformation capacity for stub columns with $\beta > 1.6$*

Specimen identification	$\beta = b/t(\sigma_{0.2}/E_0)^{0.5}$	$\varepsilon_0 = \sigma_{0.2}/E_0$	φ	ε_{LB}	$\varepsilon_{LB}/\varepsilon_0$
SHS 100×100×2- SC1	2.17	0.0018	0.95	0.0017	0.94
SHS 100×100×2- SC2	2.18	0.0018	0.95	0.0016	0.92
RHS 120×80×3- SC1	1.86	0.0022	0.98	0.0038	3.43
RHS 120×80×3- SC2	1.88	0.0022	0.98	0.0038	3.20
RHS 150×100×3- SC[1]	1.98	0.0015	0.97	0.0027	1.84
RHS 100×50×2- SC1	2.25	0.0018	0.95	0.0025	1.39
RHS 100×50×2- SC2	2.25	0.0018	0.95	0.0025	1.38

Note: [1] Results obtained from other test programmes

The right hand side of the Equation 5.5 was multiplied by χ^{C_4} by Faella et al (1999), where χ is the ratio of slenderness of the least slender element to that of the most slender element in the cross-section, (i.e. for a RHS of constant thickness and material properties, the aspect ratio of the cross-section), and C_4 was another constant that was determined experimentally to account for the greater edge restraint that the two longer faces of an RHS cross-section receive from the two shorter ones. With increasing cross-section aspect ratio there is clearly an increasingly level of restraint.

A regression analysis of the results from Table 5.7 to 5.9 and Table 5.10 (for the revised values for cross-sections where $\beta > 1.6$) yielded $C_1 = 7.07$, $C_2 = 2.13$ and $C_3 = 0.21$ for SHS. The experimental results indicated that the increased deformation capacity for the two longer faces of RHS was less significant for sections with lower cross-section slenderness. To reflect this behaviour, it was therefore decided to multiply the right hand side of Equation 5.5 by $\chi^{C_4 \beta^{0.5}}$, where the constant $C_4 = -0.30$ was determined based on the experimental results for RHS with aspect ratios of 0.67 and 0.50. Substituting the derived constants into Equation 5.5 and including the modification factor for RHS therefore yields Equation 5.6.

$$\frac{\varepsilon_{LB}}{\varepsilon_0} = \frac{7.07}{\beta^{2.13+0.21\beta}} \chi^{-0.3\beta^{0.5}}$$ (5.6)

The resulting curves are plotted in Figure 5.6 for $\chi = 1.0$ (SHS), $\chi = 0.67$ and $\chi = 0.50$. It is worth noting that although the effect of the increased edge restraint for the RHS appears to be relatively small, it can lead to increases in cross-section compressive resistance of up to 10%.
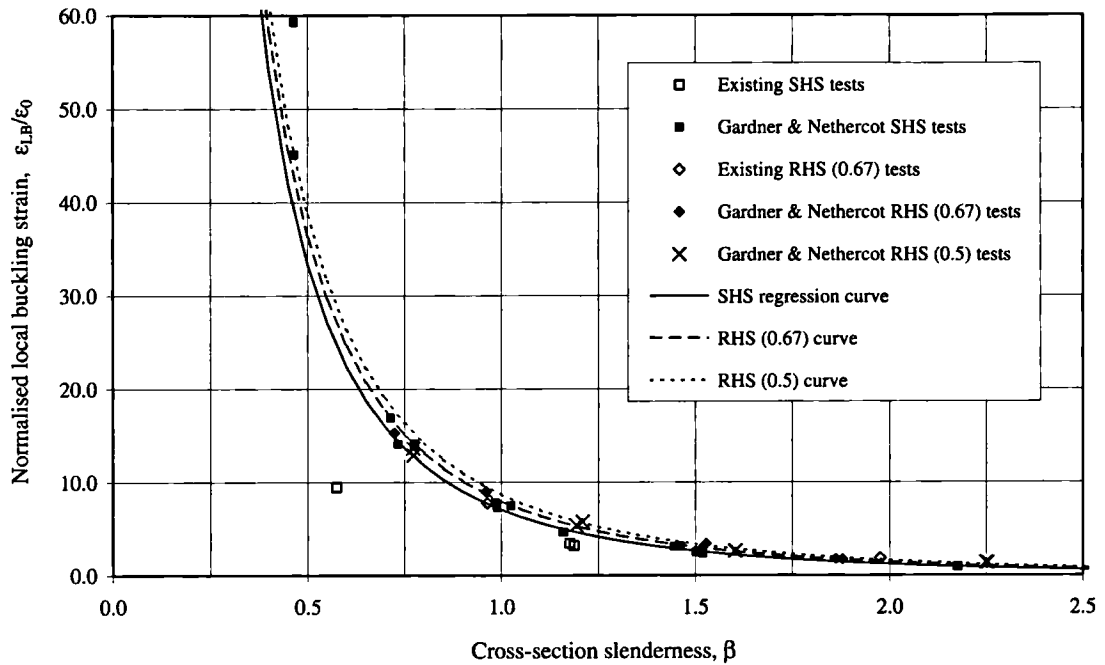
Figure 5.6: *SHS and RHS cross-section deformation capacity versus cross-section slenderness*

For all cases other than pure compression the degree of plate element edge restraint becomes less clear (due to the more complex loading arrangement). It is thus proposed to use the simply supported (SHS) buckling curve for all such cases.

5.4.3.5 Cross-section compressive resistance

With knowledge of the deformation capacity of the cross-section, its ultimate compressive resistance may hence be determined with reference to the material stress-strain curve, defined by means of the compound Ramberg-Osgood expression. For design purposes, values may be tabulated so direct use of the material model is avoided.

5.5 CHS STUB COLUMNS

5.5.1 Background

As with the SHS and RHS stub columns, CHS stub column test results have been used to develop a relationship between cross-section slenderness and deformation capacity.

5.5.2 CHS stub column test results from other test programmes

Full details of CHS stub column tests conducted in the current study have been presented in Chapter 3. Geometrical measurements and load-end shortening details for CHS stub columns from other laboratory test programmes are given in Tables 5.11 and 5.12 respectively. All available stainless steel CHS stub column test results, where sufficient details have been reported, are included in the tables.

5.5.3 Relationship between cross-section slenderness and deformation capacity

The relationship between CHS cross-section slenderness and deformation capacity was derived in a similar way to the SHS and RHS, by looking initially at the elastic critical buckling of a perfect, uniformly compressed cylinder.

5.5.3.1 Definition of cross-section slenderness, β

The elastic critical buckling strain of a perfect, uniformly compressed cylinder, where buckling occurs in the elastic range, is given by Equation 5.7.

$$\varepsilon_{cr} = \frac{1}{\sqrt{3(1-v^2)}} \frac{t}{R} \tag{5.7}$$

in which v is Poisson's ratio, t is the wall thickness of the cross-section, and R is the radius of the cross-section.

The elastic critical buckling strain can be normalised by the elastic strain at the compressive 0.2% proof stress, $\varepsilon_0 = \sigma_{0.2}/E_0$, where $\sigma_{0.2}$ is the material 0.2% proof stress in compression, and E_0 is the initial tangent modulus, to give Equation 5.8.

Table 5.11: *Measured dimensions for CHS stub columns from other laboratory test programmes*

Specimen identification	Tested by	Outer diameter, D_o (mm)	Thickness, t (mm)	Length, L (mm)	Area, A (mm^2)
CHS 101.6×2.85- SC1	Rasmussen & Hancock	101.5	2.96	350	916
CHS 101.6×2.85- SC2		101.5	2.96	350	916
CHS 101.6×2.85- SC3		102.1	2.77	350	864
CHS 140×2- SC	Talja	139.4	1.97	499	851
CHS 140×3- SC		139.4	2.87	498	1231
CHS 140×4- SC		138.7	3.99	499	1689

Table 5.12: *Results for CHS stub columns from other test programmes*

Specimen identification	Ultimate load, F_u (kN)	End shortening at F_u (mm)
CHS 101.6×2.85- SC1	426	5.7
CHS 101.6×2.85- SC2	425	6.0
CHS 101.6×2.85- SC3	391	3.9
CHS 140×2- SC	278	4.5
CHS 140×3- SC	468	6.0
CHS 140×4- SC	665	12.8

$$\frac{\varepsilon_{cr}}{\varepsilon_0} = \frac{E_0}{\sigma_{0.2}\sqrt{3(1-v^2)}}\frac{t}{R} = \frac{1}{\sqrt{3(1-v^2)}}\frac{1}{\beta} \qquad (5.8)$$

in which the geometrical and material property variables of the cross-section have been grouped into the single slenderness parameter, β given in Equation 5.9.

$$\beta = (R/t)(\sigma_{0.2}/E_0) \qquad (5.9)$$

The radius R will be measured to the centreline of the wall thickness, (i.e. R = $(D_0 -t)/2$, where D_0 is the outside diameter of the cross-section). The value of β will be used as the measure of cross-section slenderness. Where available the parameters $\sigma_{0.2}$ and E_0 will be based on material stress-strain behaviour in compression. In the absence of compressive stress-strain data stub column, values will be adopted instead.

The raw CHS stub column test results from the current study (given in Table 3.13) and from all other studies (given in Table 5.12) have been manipulated and assembled in Table 5.13, and plotted in Figure 5.7. Results from numerical simulations of tests (described in Section 4.6) have been assembled in Table 5.14, and also plotted in Figure 5.7. Figure 5.7 shows a graph of normalised local buckling strain ($=\varepsilon_{LB}/\varepsilon_0$), where ε_0 is the elastic strain at the material compressive (or stub column in the absence of compressive stress-strain data) 0.2% proof stress, versus cross-section slenderness, β. The elastic critical buckling curve for a perfect cylinder in pure compression (with Poisson's ratio taken as 0.3) has been added to Figure 5.7.

5.5.3.2 Generation of mean (design) curve

The general expression given in Equation 5.5 (and used to generate the SHS and RHS stub column curves) will also form the basis for the generation of the CHS mean design curve. However, since CHS are axisymmetric, no modification to the right hand side of the expression is necessary. A regression analysis of the results from Table 5.13 (experimentally generated) and Table 5.14 (numerically generated simulations of tests), plus further results presented in Table 5.15 (generated from a parametric study described in Section 4.6.5) was conducted.

Table 5.13: *Cross-section slenderness and deformation capacity from CHS stub column tests*

Specimen identification	$\beta = (R/t)(\sigma_{0.2}/E_0)$	$\varepsilon_0 = \sigma_{0.2}/E_0$	ε_{LB}	$\varepsilon_{LB}/\varepsilon_0$
CHS 103×1.5- SC1[2]	0.060	0.0018	0.008	4.53
CHS 103×1.5- SC2[2]	0.061	0.0018	0.008	4.64
CHS 101.6×2.85- SC1[1]	0.032	0.0019	0.016	8.44
CHS 101.6×2.85- SC2[1]	0.032	0.0019	0.017	8.88
CHS 101.6×2.85- SC3[1]	0.035	0.0019	0.011	5.77
CHS 140×2- SC[1,2]	0.051	0.0015	0.009	6.13
CHS 140×3- SC[1,2]	0.039	0.0017	0.012	7.30
CHS 140×4- SC[1,2]	0.026	0.0016	0.026	16.35
CHS 153×1.5- SC1[2]	0.106	0.0020	0.004	2.18
CHS 153×1.5- SC2[2]	0.105	0.0020	0.005	2.58

Notes: [1] Results obtained from other test programmes

[2] No material coupon tests conducted in compression. Values based on stub column curves.

Table 5.14: *Cross-section slenderness and numerically generated deformation capacity for CHS stub columns (FE models of tests)*

Specimen identification	$\beta = (R/t)(\sigma_{0.2}/E_0)$	$\varepsilon_0 = \sigma_{0.2}/E_0$	ε_{LB}	$\varepsilon_{LB}/\varepsilon_0$
CHS 103×1.5- SC1	0.060	0.0018	0.008	4.35
CHS 103×1.5- SC2	0.061	0.0018	0.007	4.16
CHS 101.6×2.85- SC1	0.032	0.0019	0.019	9.92
CHS 101.6×2.85- SC2	0.032	0.0019	0.018	9.47
CHS 101.6×2.85- SC3	0.035	0.0019	0.013	6.98
CHS 140×2- SC	0.051	0.0015	0.008	5.68
CHS 140×3- SC	0.039	0.0017	0.011	6.54
CHS 140×4- SC	0.026	0.0016	0.015	9.78
CHS 153×1.5- SC1	0.106	0.0020	0.005	2.65
CHS 153×1.5- SC2	0.105	0.0020	0.006	2.97
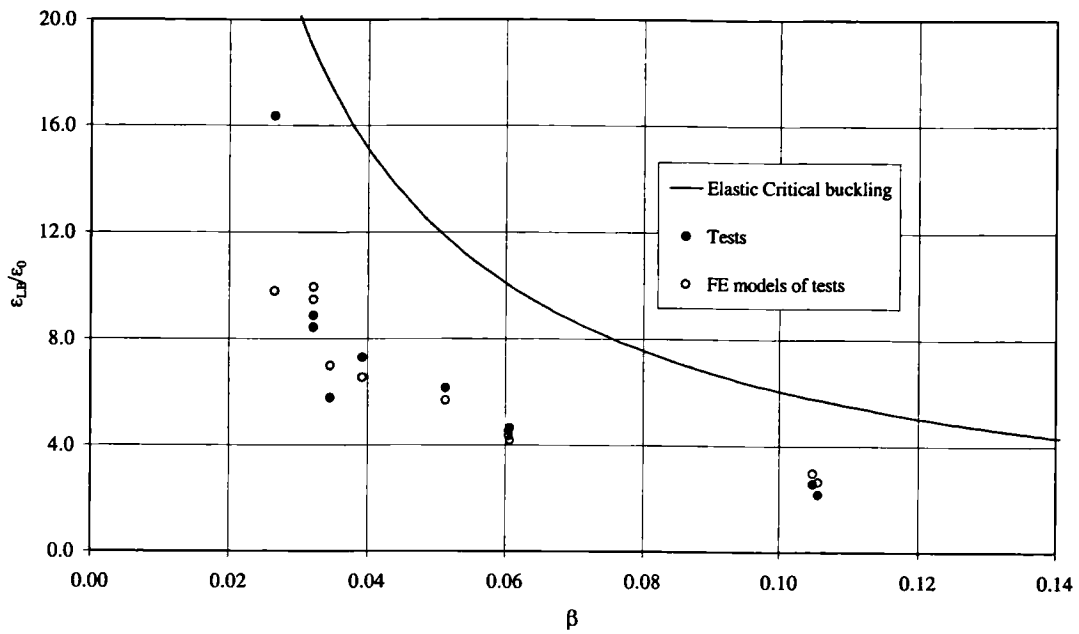
Figure 5.7: *CHS stub column test results and FE simulations of test results*

Table 5.15: *Cross-section slenderness and deformation capacity for CHS stub columns generated by means of a parametric FE study*

Specimen identification	$\beta = (R/t)(\sigma_{0.2}/E_0)$	$\varepsilon_0 = \sigma_{0.2}/E_0$	ε_{LB}	$\varepsilon_{LB}/\varepsilon_0$
CHS 100×0.8- SC	0.120	0.0019	0.005	2.46
CHS 100×1.0- SC	0.096	0.0019	0.006	3.14
CHS 100×1.2- SC	0.079	0.0019	0.007	3.77
CHS 100×1.4- SC	0.068	0.0019	0.009	4.47
CHS 100×1.6- SC	0.059	0.0019	0.010	5.18
CHS 100×1.8- SC	0.053	0.0019	0.011	5.57
CHS 100×2.0- SC	0.047	0.0019	0.012	6.04
CHS 100×2.4- SC	0.039	0.0019	0.014	7.13
CHS 100×2.8- SC	0.034	0.0019	0.017	9.00
CHS 100×3.2- SC	0.029	0.0019	0.021	10.76
CHS 100×3.6- SC	0.026	0.0019	0.022	11.39
CHS 100×4.0- SC	0.023	0.0019	0.023	12.13
CHS 100×4.4- SC	0.021	0.0019	0.024	12.63
CHS 100×4.8- SC	0.019	0.0019	0.032	16.80

Figure 5.7 shows that, unlike for the results for SHS and RHS, the CHS stub column results lie significantly below the elastic critical buckling curve, indicating a higher sensitivity to imperfections.

The regression analysis of all results yielded the constants $C_1 = 0.116$, $C_2 = 1.21$ and $C_3 = 1.69$. Substituting the derived constants into Equation 5.5 results in Equation 5.10.

$$\frac{\varepsilon_{LB}}{\varepsilon_0} = \frac{0.116}{\beta^{1.21+1.69\beta}}$$
(5.10)

Figure 5.8 shows the experimentally and numerically generated CHS stub column results and the normalised local buckling curve defined by Equation 5.10. For comparison, the regression curve for the CHS test results alone is also shown in Figure 5.8.
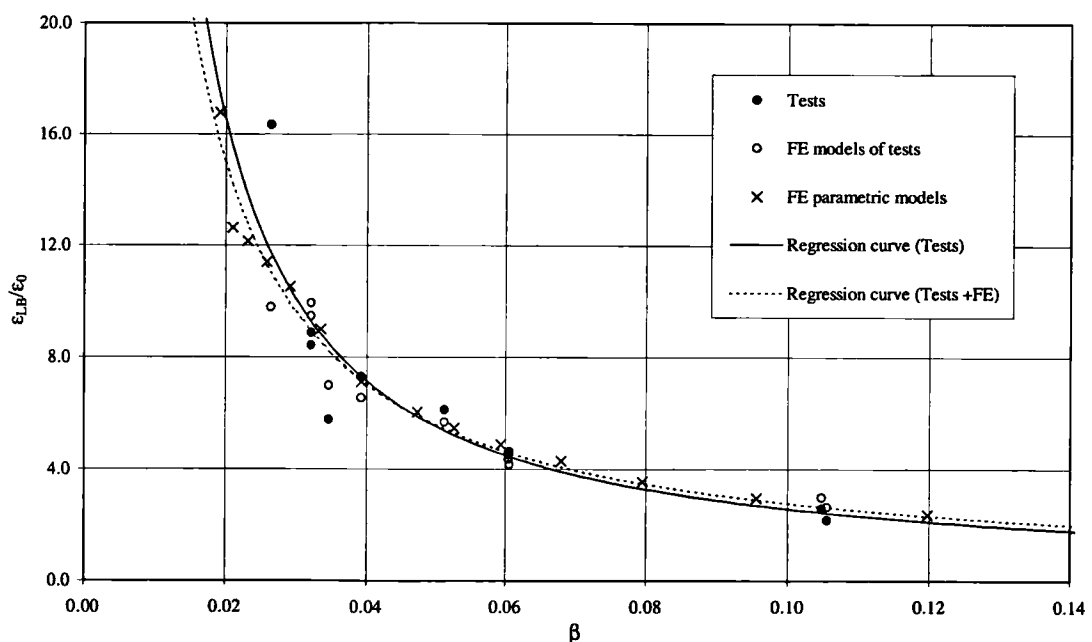
Figure 5.8: *CHS deformation capacity versus cross-section slenderness*

5.5.3.3 Cross-section compressive resistance

With knowledge of the deformation capacity of the cross-section, its ultimate compressive resistance may hence be determined with reference to the material (compound Ramberg-Osgood) stress-strain curve. As for SHS and RHS, values may be tabulated to avoid direct use of the material model.

5.6 SHS AND RHS FLEXURAL BUCKLING

5.6.1 Background

Flexural buckling of stainless steel structural members involves an interaction between overall member buckling and local plate buckling. In Eurocode 3, the structural steel and stainless steel design rules account for this interaction through cross-section classification. For members with Class 1-3 cross-sections, flexural buckling resistance is given by a single Perry based buckling curve. Since the constituent plate elements are capable of reaching the full material yield stress (or 0.2% proof stress) in pure compression before local buckling occurs, no reduction is made to the basic flexural buckling strength. For members with Class 4 cross-sections local buckling of the constituent plate elements occurs below the material yield stress (or 0.2% proof stress) and an effective area is therefore used to reduce the basic flexural buckling strength.

In the proposed design method the interaction between global member buckling and local plate buckling is to be governed by the continuous cross-section slenderness parameter, β defined by Equation 5.3. Therefore, in addition to reducing the basic flexural buckling resistance for cross-sections that buckle locally in the elastic range, an increase in basic flexural buckling resistance shall also be possible, should the local buckling resistance of the cross-section exceed the material 0.2% proof stress.

5.6.2 SHS and RHS flexural buckling results from other test programmes

A total of 22 tests on pin-ended SHS and RHS columns were carried out as part of the current study. Full details of these are provided in Chapter 3. Geometrical measurements and ultimate load carrying capacity for pin-ended SHS and RHS columns from other laboratory test programmes are given in Table 5.16. Geometrical measurements and ultimate load carrying capacity for fixed-ended SHS columns from other laboratory test programmes, all tested by Liu & Young (2002), are given in Table 5.17. Likewise, results for fixed-ended RHS columns from other test programmes, all tested by Young & Liu (2002), are presented in Table 5.18.

5.6.3 Proposed method for the determination of flexural buckling resistance

In Eurocode 3 the determination of flexural buckling resistance is based upon the Perry formula, whereby a compression member fails when the maximum stress at some point along the length

Table 5.16: Measured dimensions and ultimate load carrying capacity for pin-ended SHS and RHS columns from other test programmes

Specimen identification	Length, L (mm)	Depth, D (mm)	Breadth, B (mm)	Thickness, t (mm)	Internal corner radius, r_i (mm)	Area, A (mm^2)	Ultimate load, F_u (kN)
SHS 40×40×4 (AO)	889	39.9	39.8	3.88	-	519[1]	184
SHS 40×40×4 (AO)	888	39.9	39.8	3.88	-	519[1]	184
SHS 60×60×5 (TS)	1050	59.8	59.6	4.77	3.0	999	417
SHS 60×60×5 (TS)	1700	59.8	59.6	4.77	3.0	999	235
SHS 60×60×5 (TS)	2350	59.8	59.6	4.77	3.0	999	137
SHS 80×80×3 (RH)	1001	80.5	80.5	2.90	3.1	900	390
SHS 80×80×3 (RH)	2000	80.4	80.4	2.99	3.0	900	193
SHS 80×80×3 (RH)	3002	80.7	80.7	2.95	2.6	900	96
RHS 150×100×3 (TS)	2700	150.4	100.3	2.89	3.0	1397	349
RHS 150×100×3 (TS)	4350	150.4	100.3	2.89	3.0	1397	254
RHS 150×100×3 (TS)	6000	150.4	100.3	2.89	3.0	1397	189
RHS 150×100×6 (TS)	2700	149.8	100.2	5.85	5.0	2683	830
RHS 150×100×6 (TS)	4350	150.6	100.6	5.77	6.0	2683	488
RHS 150×100×6 (TS)	6000	150.6	100.6	5.77	6.0	2683	306

Notes: [1] Area calculated assuming internal corner radii equal to material thickness (no measurements taken)

(OA) Ala-Outinen and Oksanen (1997)
(RH) Rasmussen and Hancock (1993a)
(TS) Talja and Salmi (1995)

Table 5.17: Measured dimensions and ultimate load carrying capacity for fixed-ended SHS columns tested by Liu & Young (2002)

Specimen identification	Length, L (mm)	Depth, D (mm)	Breadth, B (mm)	Thickness, t (mm)	Internal corner radius, r_i (mm)	Area, A (mm^2)	Ultimate load, F_u (kN)
SHS 70×70×2- LC1 (LY)	1199.0	69.9	70.0	1.92	1.9	513	190
SHS 70×70×2- LC2 (LY)	2000.0	69.9	70.1	1.95	1.9	522	188
SHS 70×70×2- LC3 (LY)	2800.5	69.9	70.2	1.92	1.9	515	159
SHS 70×70×2- LC4 (LY)	3599.0	70.0	70.1	1.93	1.9	516	115
SHS 70×70×5- LC1 (LY)	1199.0	70.0	69.9	4.90	4.1	1212	669
SHS 70×70×5- LC2 (LY)	2000.0	70.0	70.0	4.90	4.1	1223	510
SHS 70×70×5- LC3 (LY)	2799.0	69.9	70.0	4.90	4.1	1222	407
SHS 70×70×5- LC4 (LY)	3600.0	70.0	69.9	4.90	4.1	1212	281

Note: (LY) All fixed-ended SHS column tests were conducted by Liu & Young (2002)

Table 5.18: *Measured dimensions and ultimate load carrying capacity for fixed-ended RHS columns tested by Young & Liu (2002)*

Specimen identification	Length, L (mm)	Depth, D (mm)	Breadth, B (mm)	Thickness, t (mm)	Internal corner radius, r_i (mm)	Area, A (mm^2)	Ultimate load, F_u (kN)
RHS 120×40×2- LC1 (YL)	1198.5	120.1	40.1	1.94	3.1	593	167
RHS 120×40×2- LC2 (YL)	2000.0	120.2	40.0	1.95	3.1	596	141
RHS 120×40×2- LC3 (YL)	2800.0	120.2	40.0	1.97	3.1	602	96
RHS 120×40×2- LC4 (YL)	3600.0	120.2	40.0	1.96	3.1	599	84
RHS 120×40×5.3- LC1 (YL)	1200.0	119.7	39.9	5.31	3.7	1524	717
RHS 120×40×5.3- LC2 (YL)	2000.0	119.7	40.1	5.27	3.7	1516	417
RHS 120×40×5.3- LC3 (YL)	2801.0	119.8	40.0	5.29	3.7	1521	261
RHS 120×40×5.3- LC4 (YL)	3600.0	119.7	40.1	5.27	3.7	1516	164
RHS 120×80×3- LC1 (YL)	1199.5	119.9	80.1	2.82	3.9	1071	398
RHS 120×80×3- LC2 (YL)	2000.0	120.0	80.0	2.80	3.9	1063	394
RHS 120×80×3- LC3 (YL)	2799.5	119.4	79.9	2.92	3.9	1103	337
RHS 120×80×3- LC4 (YL)	3598.5	119.7	80.1	2.90	3.9	1099	311
RHS 120×80×6- LC1 (YL)	1199.5	120.1	80.2	6.01	6.5	2165	1222
RHS 120×80×6- LC2 (YL)	2000.0	120.1	80.4	6.02	6.5	2171	970
RHS 120×80×6- LC3 (YL)	2800.0	120.3	80.6	5.96	6.5	2156	860
RHS 120×80×6- LC4 (YL)	3600.0	120.2	80.5	6.11	6.5	2203	612

Note: (YL) All fixed-ended RHS column tests were conducted by Young & Liu (2002)

reaches the material yield strength (or 0.2% proof strength) due to a combination of axial load plus bending moment (Ayrton & Perry, 1886). However, with no sharply defined yield point, the approach is less valid for stainless steel than for carbon steel. With the aim of achieving a general approach to the design of metallic columns, Rasmussen & Rondal (1997) proposed a more complex imperfection parameter that could be used in conjunction with the Perry curve. The imperfection included the Ramberg-Osgood parameters, $\sigma_{0.2}$, E_0 and n. Finite element results were used to calibrate column curves. No comparisons were made with test results and it is not clear whether a more complex imperfection parameter is justified given the degree of scatter associated with column buckling behaviour.

The Eurocode 3 flexural buckling resistance is given by Equation 5.11, with the Class 4 cross-section reduction factor and material safety factor removed, where χ is the buckling reduction factor.

$$N_{b.Rd} \quad = \quad \chi A \sigma_{0.2} \tag{5.11}$$

The initial proposal was to replace $\sigma_{0.2}$ in the buckling formula with σ_{LB}. However, a direct replacement would generally lead to an over-prediction of member resistance, since the Perry formula is based on elastic material response, and (particularly for stocky cross-sections) σ_{LB} may only be reached following significant plastic straining. Following analysis of test results, it was found that modifying basic flexural buckling strengths by a factor of $(\sigma_{LB}/\sigma_{0.2})^{0.32}$ gave best agreement between test and predicted values. The proposed formula for determining the flexural buckling resistance of stainless steel SHS and RHS members is therefore given by Equation 5.12.

$$N_{b.Rd} \quad = \quad \chi A \sigma_{0.2} \left(\frac{\sigma_{LB}}{\sigma_{0.2}} \right)^{0.32} \tag{5.12}$$

5.6.4 Modification to basic flexural buckling curve parameters

ENV 1993-1-4 (1996) offers three flexural buckling curves defined by the imperfection factor, α and the limiting slenderness, $\overline{\lambda}_0$. The selection of buckling curve is dependent upon the type of cross-section, as explained by Table 5.19.

Table 5.19: *Parameters for ENV 1993-1-4 (1996) flexural buckling curves*

Cross-section type	α	$\overline{\lambda}_0$
Cold-formed open section	0.49	0.40
Cold-formed rolled hollow section	0.49	0.40
Welded open section	0.76	0.20

The parameters α and $\overline{\lambda}_0$, have been fixed so that the buckling curves predict the mean buckling strength for members with Class 1-3 cross-sections. For the proposed design method, however, the basic flexural buckling curves are required to predict the mean buckling strength for members whose cross-sections fail locally at the material 0.2% proof stress. For this purpose, best fit to appropriate SHS and RHS column buckling test results was achieved with $\alpha = 0.70$ and $\overline{\lambda}_0 = 0.44$. The revised basic buckling curve is shown with all SHS and RHS column buckling test results in Figure 5.9.
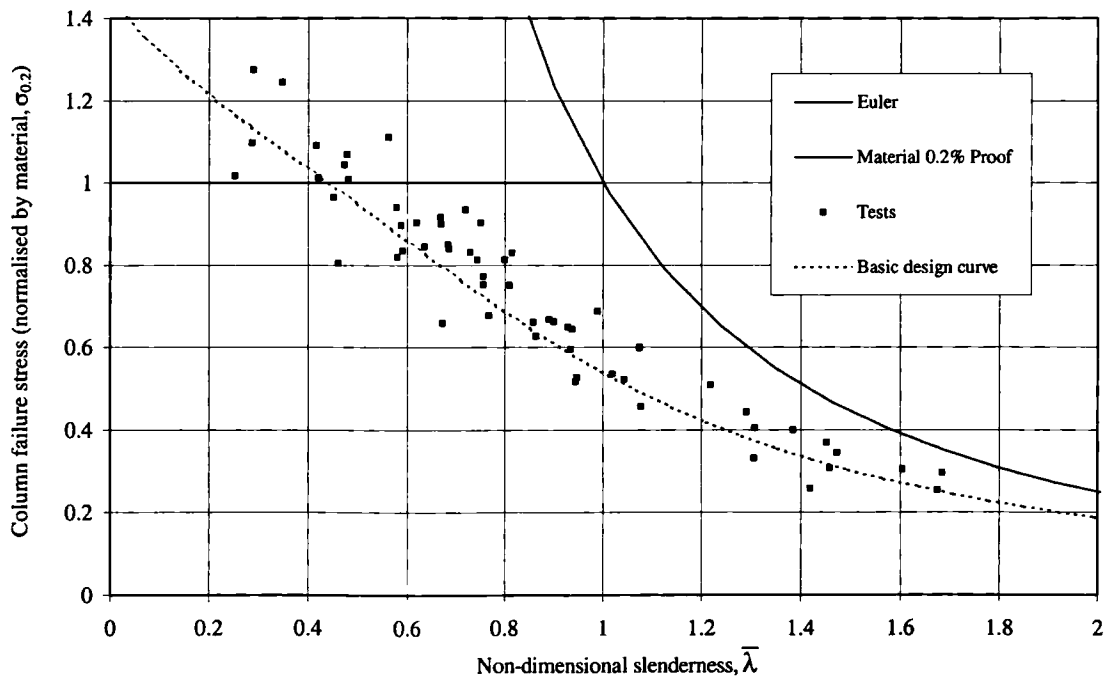
Figure 5.9: *SHS and RHS flexural buckling test results and basic design curve*

For clarification, the flexural buckling test data have been assembled into three groups based upon cross-section slenderness and presented in Figure 5.10.
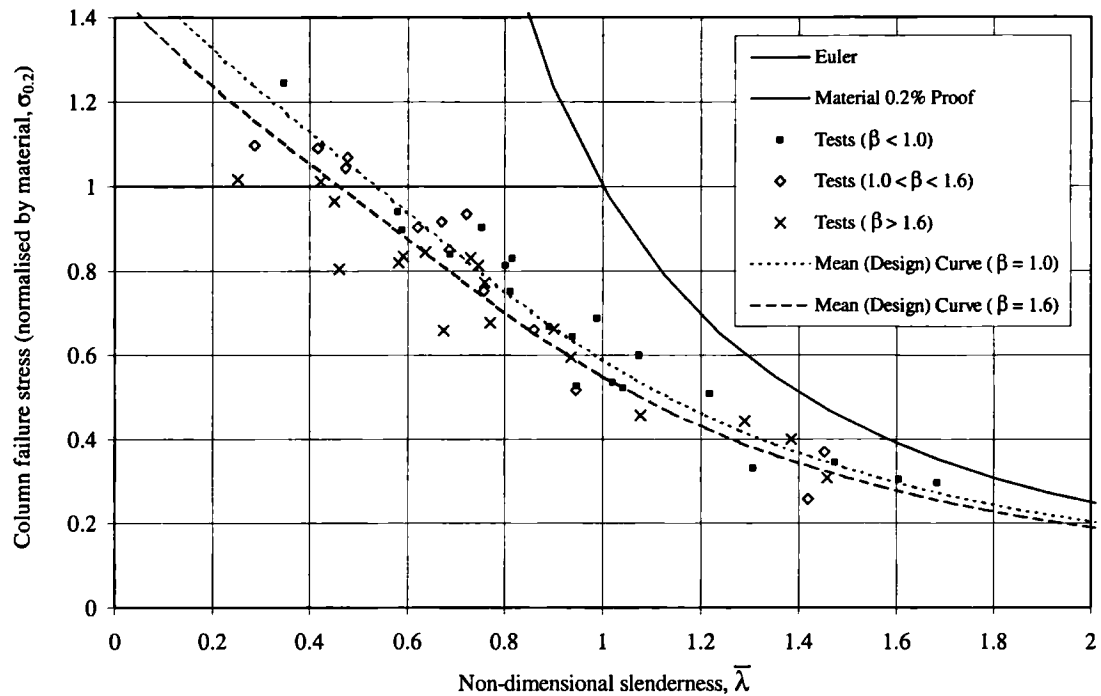
Figure 5.10: *SHS and RHS flexural buckling test results and mean (design) curves for β=1.0 and β=1.6*

A detailed comparison between test and predicted results for SHS and RHS members subject to flexural buckling is given in Section 6.3.

5.7 CHS FLEXURAL BUCKLING

5.7.1 Introduction

The rationale behind the determination of flexural buckling resistance for CHS members is the same as for SHS and RHS members.

5.7.2 CHS flexural buckling results from other test programmes

No tests on the flexural buckling of CHS members were conducted as part of the current study. However, 4 compression tests were carried out on pin-ended CHS members by Rasmussen & Hancock (1993a) and 6 by Talja (1997), the results of which are given in Table 5.20, and 12 compression tests were conducted on fixed-ended CHS columns by Young & Hartono (2002), the results of which are given in Table 5.21.

Table 5.20: *Measured dimensions and ultimate load carrying capacities for pin-ended CHS columns from other test programmes*

Specimen identification	Length, L (mm)	Outer diameter, D_o (mm)	Thickness, t (mm)	Area, A (mm^2)	Ultimate load, F_u (kN)
CHS 101.6×2.85 (RH)	1000	101.4	2.98	921	328
CHS 101.6×2.85 (RH)	2001	101.5	2.95	913	241
CHS 101.6×2.85 (RH)	3000	101.4	2.93	906	171
CHS 101.6×2.85 (RH)	4000	101.3	2.96	915	113
CHS 140×2 - C1 (T)	2250	139.8	1.95	845	202
CHS 140×2 - C2 (T)	3350	139.8	1.95	845	156
CHS 140×2 - C3 (T)	4449	139.9	1.97	854	122
CHS 140×4 - C1 (T)	2251	140.0	3.99	1705	437
CHS 140×4 - C2 (T)	3350	139.1	3.99	1694	330
CHS 140×4 - C3 (T)	4450	140.1	3.98	1702	278

Notes: (RH) Tests performed by Rasmussen & Hancock (1993a)

         (T)   Tests performed by Talja (1997)

Table 5.21: *Measured dimensions and ultimate load carrying capacities for fixed-ended CHS columns from other test programmes*

Specimen identification	Length, L (mm)	Outer diameter, D_o (mm)	Thickness, t (mm)	Area, A (mm^2)	Ultimate load, F_u (kN)
CHS 89×2.78 - LC1	1000	89.0	2.71	735	198
CHS 89×2.78 - LC2	1500	89.2	2.83	768	177
CHS 89×2.78 - LC3	2001	89.0	2.78	753	165
CHS 89×2.78 - LC4	2499	88.9	2.78	752	152
CHS 89×2.78 - LC5	3001	88.9	2.68	726	133
CHS 168.7×3.34- LC1	999	168.5	3.31	1718	475
CHS 168.7×3.34- LC2	1500	168.8	3.37	1751	461
CHS 168.7×3.34- LC3	2004	168.7	3.26	1694	432
CHS 324.3×4.32- LC1	1499	322.5	4.25	4249	1120
CHS 324.3×4.32- LC2	1999	320.4	4.48	4446	1088
CHS 324.3×4.32- LC3	2498	324.1	4.24	4261	1046
CHS 324.3×4.32- LC4	2998	324.3	4.38	4402	1010

Note: All fixed-ended CHS column tests were conducted by Young & Hartono (2002)

5.7.3 Proposed method for determination of CHS flexural buckling resistance

As for the SHS and RHS members, the basic flexural buckling curve in the proposed design method is required to predict the mean buckling strength for members whose cross-sections fail locally at the material 0.2% proof stress. For this purpose, best fit to appropriate CHS column buckling test results was achieved with $\alpha = 0.50$ and $\overline{\lambda}_0 = -0.10$. The fact that $\overline{\lambda}_0$ is negative for the basic buckling curve is of no real significance; it simply reflects the buckling behaviour of CHS members whose cross-sections fail locally at the material 0.2% proof stress. Following analysis of the CHS test results, a suitable modification factor to the basic flexural buckling curve to account for variation in cross-section slenderness was found to be $(\sigma_{LB}/\sigma_{0.2})^{0.80}$. CHS flexural buckling resistance is therefore determined from Equation 5.13. Tests results are presented in Figure 5.11 with corresponding mean (design) curves.

$$N_{b.Rd} = \chi A \sigma_{0.2} \left(\frac{\sigma_{LB}}{\sigma_{0.2}} \right)^{0.80} \tag{5.13}$$
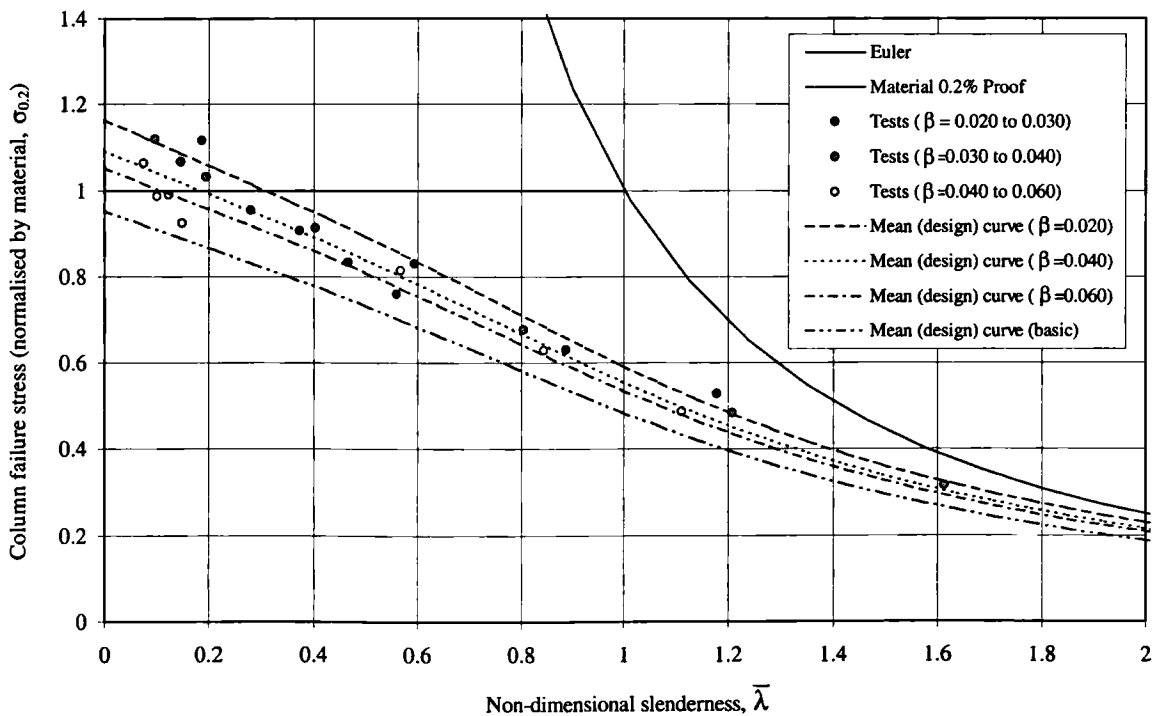
Figure 5.11: *CHS flexural buckling test results and corresponding mean (design) curves*

A detailed comparison between test and predicted results for CHS members subject to flexural buckling is given in Section 6.3.

5.8 SHS AND RHS BEAMS

5.8.1 Background

The compression flange of an SHS or RHS beam behaves in much the same way as the compression elements within an SHS or RHS stub column. Furthermore, in the same way as stub column strength is governed by the local buckling resistance of its constituent elements, also the in-plane bending strength of a beam is controlled by the local buckling resistance of its compression flange and the compressed portion of its web. These ideas form the basis for the proposed method for the determination of in-plane bending strength.

5.8.2 SHS and RHS beam results from other test programmes

A total of 9 tests on simply-supported SHS and RHS beams were carried out as part of the current study. Full details of these are provided in Chapter 3. Geometrical measurements and ultimate bending moment resistance with corresponding deflections for SHS and RHS beams from other laboratory test programmes are given in Tables 5.22 and 5.23 respectively.

5.8.3 Local buckling in flange and web elements

In many structural configurations the plate elements within a cross-section are subjected to non-uniform stress conditions; Figure 5.12 shows the cases of pure compression (stub column) and pure bending (beam). The proportions of cold-formed SHS and RHS are such that local buckling rarely occurs in the web when the cross-sections are subjected to pure bending. According to plate buckling theory (Bulson, 1970), the aspect ratio of the cross-section would have to be around 0.41 (1:2.4) for local buckling to occur simultaneously in the uniformly compressed flange and the web subjected to pure bending. Nonetheless for general applicability allowance should be made for all common in-plane element loading conditions.

Table 5.22: *Measured dimensions for SHS and RHS simply-supported beams from other test programmes*

Specimen identification	Overall span length, L (mm)	Distance between loading points, L_1 (mm)	Depth, D (mm)	Breadth, B (mm)	Thickness, t (mm)	Internal corner radius, r_i (mm)	Area, A (mm^2)
SHS 60×60×5- B1 (TS)	900	300	59.9	59.6	4.77	3.5	1000
SHS 60×60×5- B2 (TS)	900	300	59.5	59.3	4.89	3.0	1021
SHS 60×60×5- B3 (TS)	900	300	59.8	59.5	4.77	3.0	1003
SHS 80×80×3- B1 (MR)	1800	-	80.0	80.0	2.89	-	870[1]
SHS 80×80×3- B2 (MR)	1800	-	80.0	80.0	2.89	-	870[1]
SHS 80×80×3- B3 (RH)	1000	500	80.0	80.0	2.98	3.0	895
RHS 120×80×4- B1 (MR)	2800	-	120.0	80.0	3.69	-	1379[1]
RHS 120×80×4- B2 (MR)	2800	-	120.0	80.0	3.69	-	1379[1]
RHS 150×100×3- B1 (TS)	4000	1000	150.6	100.2	2.89	3.0	1394
RHS 150×100×3- B2 (TS)	4000	1000	150.4	100.3	2.89	3.0	1394
RHS 150×100×3- B3 (TS)	4000	1000	150.6	100.2	2.89	3.0	1394
RHS 150×100×6- B1 (TS)	2200	550	149.9	100.2	5.85	4.5	2715
RHS 150×100×6- B2 (TS)	2200	550	149.9	100.2	5.85	4.5	2715
RHS 150×100×6- B3 (TS)	2200	550	149.8	100.1	5.85	4.5	2713

Notes: [1]   Area calculated assuming internal corner radii equal to material thickness (no measurements taken)

(MR) Tests conducted by Mirambell & Real (2000) – all tests 3 point bending

(RH) Tests conducted by Rasmussen & Hancock (1992) – 4 point bending test

(TS) Tests conducted by Talja & Salmi (1995) – all tests 4 point bending

Table 5.23: *Summary of results for simply-supported beams from other test programmes*

Specimen identification	Ultimate bending moment, M_u (kNm)	Mid-span deflection at M_u (mm)
SHS 60×60×5- B1 (TS)	15.0	59
SHS 60×60×5- B2 (TS)	13.5	55
SHS 60×60×5- B3 (TS)	15.2	55
SHS 80×80×3- B1 (MR)	13.5	55
SHS 80×80×3- B2 (MR)	12.9	50
SHS 80×80×3- B3 (RH)	15.4	-
RHS 120×80×4- B1 (MR)	31.9	95
RHS 120×80×4- B2 (MR)	31.4	95
RHS 150×100×3- B1 (TS)	26.3	108
RHS 150×100×3- B2 (TS)	26.3	112
RHS 150×100×3- B3 (TS)	26.3	108
RHS 150×100×6- B1 (TS)	70.5	87
RHS 150×100×6- B2 (TS)	70.4	90
RHS 150×100×6- B3 (TS)	70.2	80

Notes: (MR) Tests conducted by Mirambell & Real (2000) – all tests 3 point bending
(RH) Tests conducted by Rasmussen & Hancock (1992) – 4 point bending test
(TS) Tests conducted by Talja & Salmi (1995) – all tests 4 point bending

(a) RHS stub column (b) RHS beam
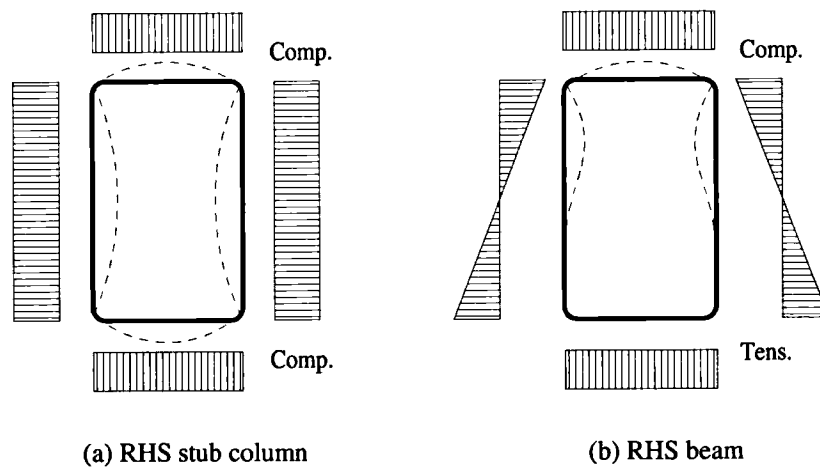
Figure 5.12: *Compression elements within a RHS stub column and beam*

217

Figure 5.13 shows a graph produced by Bulson (1970) giving buckling coefficients, k for simply supported plate elements subjected to different linearly varying loading. The curves were derived by employing the principle of conservation of energy since there is no exact analytical solution.
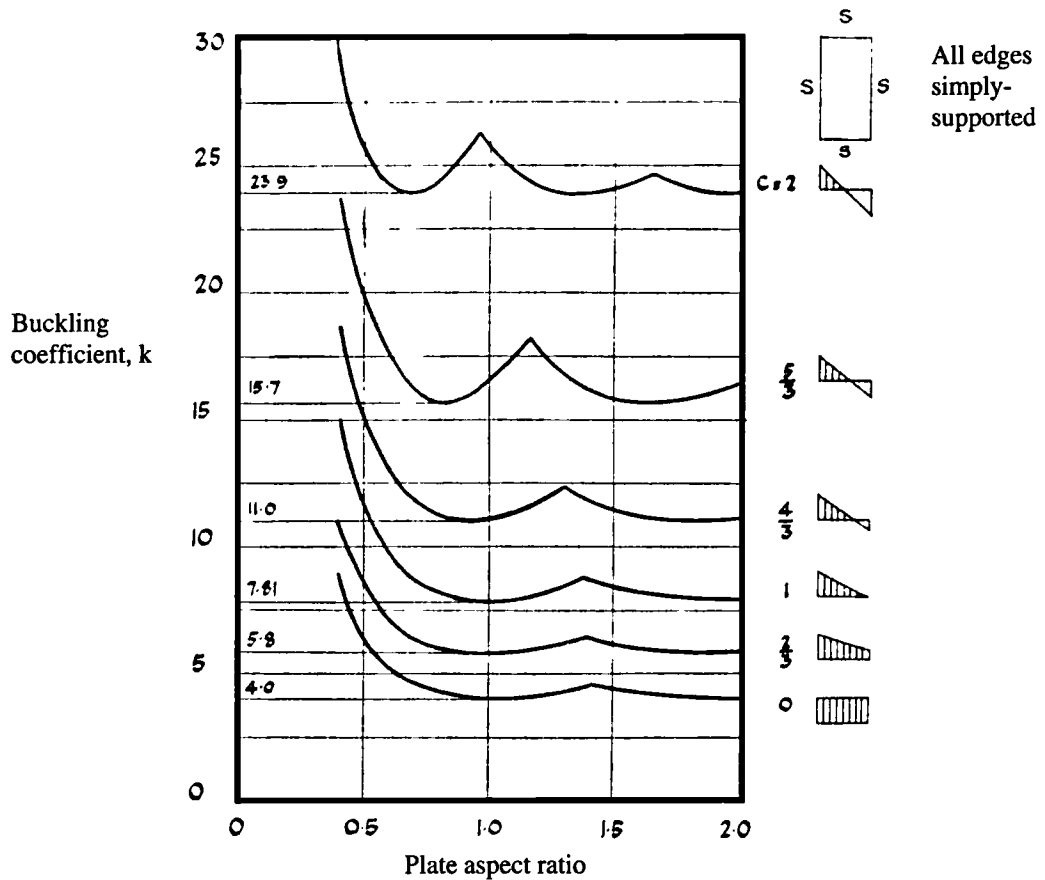
Figure 5.13: *Buckling coefficients for simply supported plates with linearly varying edge loading (Bulson, 1970)*

From Figure 5.13 it can be seen that for a perfect simply supported plate element subjected to pure bending, and buckling in the elastic range, the buckling coefficient k is equal to 23.9 (as compared to the pure compression case where k is equal to 4.0).

Table 5.24 is presented in ENV 1993-1-1 (1992) and used to modify the local slenderness of Class 4 elements depending upon their in-plane loading conditions. The formulations are applied to stainless steel, directed from ENV 1993-1-4 (1996), and carbon steel cross-sections.

The same expressions (using the alternative formulation for $1 \geq \psi \geq -1$) are also adopted in the structural stainless steel design guidance produced by the UK Steel Construction Institute (Baddoo & Burgan, 2001).

Table 5.24: *Buckling coefficients presented in ENV 1993-1-1(1992)*

$\psi = \sigma_1/\sigma_2$	1	$1 > \psi > 0$	0	$0 > \psi > -1$	-1	$-1 > \psi > -2$
Buckling Coefficent, k	4.0	$\dfrac{8.2}{1.05 + \psi}$	7.81	$7.81 - 6.29\psi + 9.78\psi^2$	23.9	$5.98(1-\psi)^2$

Alternatively, for $1 \geq \psi \geq -1$:

$$k = \frac{16}{[(1+\psi)^2 + 0.112(1-\psi)^2]^{0.5} + (1+\psi)}$$

Note: ψ is the ratio of end stresses (compression positive) for compression element.

Subject to experimental or numerical confirmation, it is therefore recommended that the buckling coefficients presented in Table 5.24 be adopted in the proposed design procedure to account for non-uniformly loaded elements, resulting in the general definition of element slenderness given in Equation 5.14. It is however recognised that the assumption of elastic material behaviour becomes increasingly tenuous for increasingly stocky plate elements.

$$\beta = \left(\frac{b}{t}\right)\sqrt{\frac{\sigma_{0.2}}{E_0}}\sqrt{\frac{4.0}{k}} \tag{5.14}$$

where k is taken from Table 5.24.

For an RHS in pure bending, the slenderness of the compression flange would therefore be calculated by Equation 5.15 and the slenderness of the web by Equation 5.16. The deformation capacity of the cross-section would be defined by the most slender element.

$$\beta = \left(\frac{b}{t}\right)\sqrt{\frac{\sigma_{0.2}}{E_0}}\sqrt{\frac{4.0}{4.0}} \tag{5.15}$$

$$\beta \;=\; \left(\frac{b}{t}\right)\sqrt{\frac{\sigma_{0.2}}{E_0}}\sqrt{\frac{4.0}{23.9}} \tag{5.16}$$

No experimental data for RHS with high aspect ratios in pure bending are available to confirm the applicability of Table 5.24 to the inelastic buckling of stainless elements. A parametric numerical study, described in Section 4.8.2, was therefore conducted. RHS with aspect ratios of 0.25 (1:4) were modelled in pure bending. Four different material thicknesses were modelled to investigate the behaviour over a range of cross-section slendernesses. The results are presented in Table 5.25, and compared to the values predicted using Equation 5.16 (in conjunction with Equation 5.6).

Table 5.25: *Comparison between predicted deformation capacities of RHS beam webs and results from a numerical study*

Cross-section	β_{flange}	β_{web}	Predicted $\varepsilon_{LB}/\varepsilon_0$	FE $\varepsilon_{LB}/\varepsilon_0$
RHS 160×40×1.5	1.15	1.93	1.3	2.3
RHS 160×40×2	0.85	1.45	2.9	3.1
RHS 160×40×3	0.55	0.96	7.8	8.0
RHS 160×40×4	0.40	0.71	15.4	14.0

β_{flange} is the slenderness of the compression flange (Equation 5.15)

β_{web} is the slenderness of the web in bending (Equation 5.16)

$\varepsilon_{LB}/\varepsilon_0$ is the normalised local buckling strain (a measure of deformation capacity)

Table 5.25 demonstrates that for pure bending, satisfactory prediction of FE results can be achieved by adopting the buckling coefficients presented in Table 5.24. It may also be assumed that Table 5.24 can be applied to the intermediate load cases of combined compression plus bending. Cases where ψ is less than -1 have not been considered, though it is not envisaged that there would be any significant behavioural changes. Deviation between the predicted and FE results may be due to inelastic material behaviour, differences in boundary conditions, assumed imperfection modes and amplitudes and FE modelling inaccuracies (since there is no supporting experimental data). Residual stresses were not incorporated into these FE models.

5.8.4 Generalised shape factors

To determine the bending moment resistance of a cross-section formed from material with non-linear stress-strain characteristics, the concept of a generalised shape factor, a_g was proposed by Mazzolani (1995). The generalised shape factor is essentially a means by which the material characteristics, as well as the geometric characteristics of a cross-section can be incorporated into a single numerical value. Increasing deformation capacity, $\varepsilon_{LB}/\varepsilon_0$ (governed by the most slender compression element) clearly brings about a higher generalised shape factor. Additionally higher generalised shape factors are synonymous with materials that possess a high degree of strain hardening.

The geometric shape factor, a_p of a cross-section is the ratio of its plastic modulus, W_{pl} to its elastic modulus, W_{el}. For a given material model the generalised shape factor can be calculated in terms of the geometric shape factor and the limiting outer-fibre cross-section deformation capacity, $\varepsilon_{LB}/\varepsilon_0$ and presented to a designer in tabular or graphical form. Direct use of the material model is not necessary. Ultimate bending moment resistance is therefore defined by Equation 5.17.

$$M_u = a_g \, \sigma_{0.2} \, W_{el} \qquad\qquad (5.17)$$

Figure 5.14 shows a typical graph of bending moment versus outer-fibre strain. The generalised shape factor is represented by the factor $M_u/M_{0.2}$, where $M_{0.2} = \sigma_{0.2} \, W_{el}$.
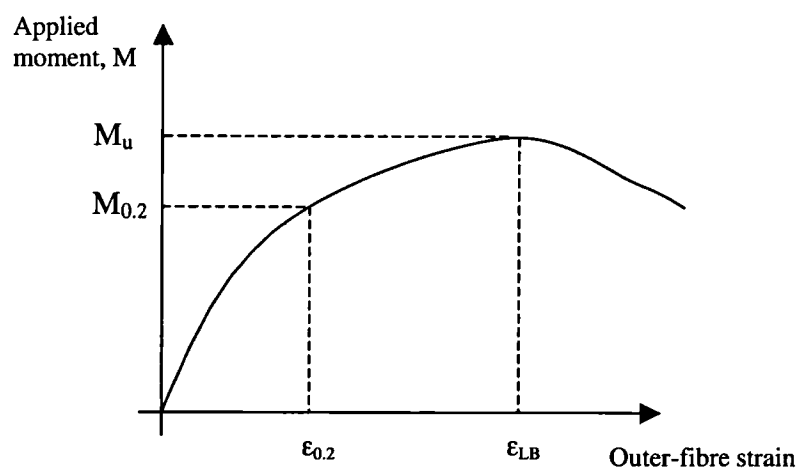
Figure 5.14: *Typical graph of bending moment versus outer-fibre strain*

There is no closed-form analytical solution to the compound Ramberg-Osgood expression over a linearly varying strain gradient. Generalised shape factors must therefore be generated for a series of outer-fibre strain limits by means of numerical integration. A typical non-linear bending stress distribution generated from the compound Ramberg-Osgood expression is shown in Figure 5.15.
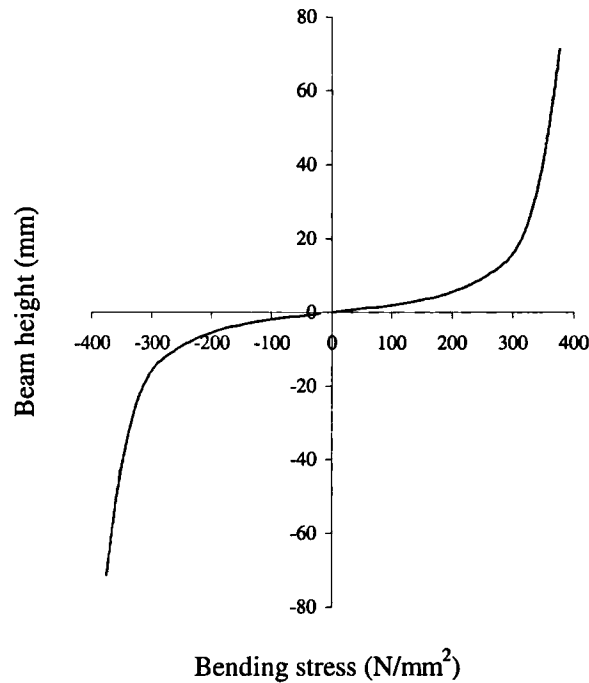
Figure 5.15: *Typical non-linear bending stress distribution from compound Ramberg-Osgood material model*

Figure 5.16 shows a graphical means of determining the generalised shape factor of a cross-section (with $E_0 = 200000$ N/mm^2 and $\sigma_{0.2} = 400$ N/mm^2), for limiting outer-fibre strains of 0.5%, 1.0%, 2.0%, and 3.0%. The generalised shape factor curves for SHS and RHS have been produced with the following material parameters: $\sigma_{1.0} = 1.26\sigma_{0.2}$, $n = 4.2$ and $n'_{0.2,1.0} = 2.7$. The lines labelled 'Plastic' and 'Elastic' represent the discretised classification system given in ENV 1993-1-4 (1996), whereby Class 1-2 cross-sections are able to attain their full plastic moment capacity, Class 3 cross-sections are able to attain their elastic moment capacity, and the capacity of Class 4 cross-sections is limited by local buckling in the elastic range.
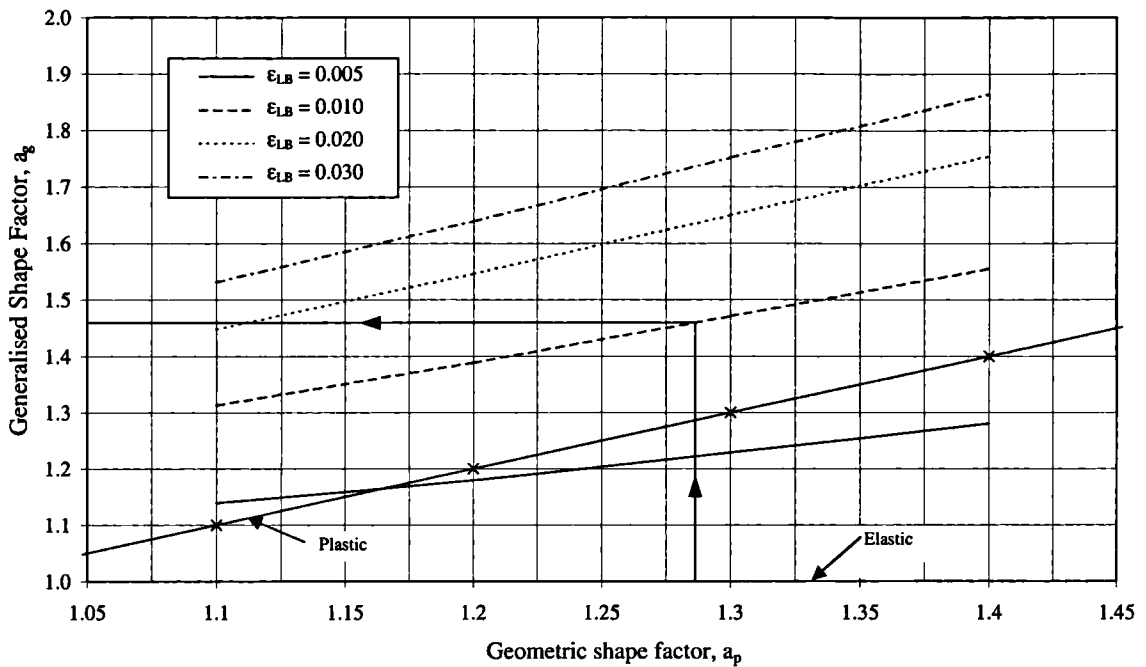
Figure 5.16: *Generalised shape factor versus geometric shape factor*

The generalised shape factor, a_g of a cross-section may hence be used (in conjunction with $\sigma_{0.2}$ in compression and W_{el}) to determine its ultimate bending resistance from Equation 5.17.

5.8.5 Lateral torsional buckling

SHS and CHS beams are not affected by lateral torsional buckling since their stiffness about both principal axes is equal. However, unrestrained RHS members may be affected by lateral torsional buckling, with increasing cross-section aspect ratio and increasing buckling length bringing increased susceptibility to the phenomenon.

The SCI structural stainless steel design guidance (Baddoo & Burgan, 2001) does not include lateral torsional buckling curves for RHS. ENV 1993-1-4 (1996) does define a curve for rolled hollow sections, though it is believed that this was mistakenly included since there is an absence of suitable test data upon which to base it. However, Baddoo & Burgan (2001) do supply an expression to calculate a buckling length below which a member will not be prone to lateral

torsional effects. The proposed method for determining the lateral torsional buckling resistance of stainless steel beams is analogous to the case of flexural buckling:

- A basic buckling curve would be calibrated for members with cross-sections that buckle locally at the material 0.2% proof stress

- Lateral torsional buckling resistance would then be calculated by modifying the basic curve depending upon the deformation capacity of the cross-section.

However, with the current absence of suitable test data, no firm design rules will be presented for RHS beams subject to lateral torsional buckling.

5.9 CHS Beams

5.9.1 Introduction

The deformation behaviour of a CHS in bending is less clear than for an SHS or RHS, where failure is generally governed by the local buckling resistance of the uniformly loaded compression flange. ENV 1993-1-4 (1996) employs the same cross-section slenderness limits for all CHS, whether under pure compression, pure bending or any other intermediate case. It will therefore be assumed in the proposed design method that the outer fibre deformation capacity of a CHS in bending (and combined compression plus bending) is as for the case of pure compression. It was initially expected that this may lead to conservative solutions, though analysis of test data showed this not to be the case.

5.9.2 CHS beam results from other test programmes

No tests on CHS members in bending were conducted as part of the current study, though a total of 8 tests have been carried out by other researchers. Geometrical measurements and ultimate bending moment resistance with corresponding deflections for CHS beams from other laboratory test programmes are given in Table 5.26.

Table 5.26: *Measured dimensions and ultimate test bending moment for CHS simply-supported beams from other test programmes*

Specimen identification	Overall span length, L (mm)	Distance between loading points, L₁ (mm)	Outer diameter, D₀ (mm)	Thickness, t (mm)	Area, A (mm²)	M_{u,test} (kNm)	δ_u (mm)
CHS 101.6×2.85- B1 (RH)	1000	500	102.1	2.84	886	13.0	-
CHS 103×1.5- B1 (CK)	2000	500	103.3	1.40	448	6.5	57
CHS 153×1.5- B1 (CK)	2000	500	152.6	1.30	618	13.4	33
CHS 203×1.5- B1 (CK)	2000	500	202.9	1.40	886	17.7	17
CHS 219×2.0- B1 (CK)	2000	500	218.4	1.80	1225	27.6	20
CHS 140×2- B1 (T)	2031	501	140.2	2.00	868	11.6	41
CHS 140×3- B1 (T)	2030	500	139.0	2.87	1227	19.7	60
CHS 140×4- B1(T)	2031	500	139.6	4.00	1704	26.0	83

Notes: (RH) Tests conducted by Rasmussen & Hancock (1992) – 4 point bending

   (CK) Tests conducted by Chryssantopoulos & Kiymaz (1998) – all tests 4 point bending

   (T) Tests conducted by Talja (1997) – all tests 4 point bending

5.9.3 Generalised shape factors

In principle, generalised shape factors are independent of cross-section type. However since average material properties tend to vary between cross-section types, (due to the different manufacturing routes and hence level of cold-working), so revised generalised shape factor curves may be required. The generalised shape factor curves for CHS have been produced with the following material parameters: $\sigma_{1.0} = 1.20\sigma_{0.2}$, $n = 4.2$ and $n'_{0.2,1.0} = 2.7$. (Values of n and $n'_{0.2,1.0}$ have been taken as for the SHS and RHS due to a lack of compressive CHS stress-strain test data).

As for SHS and RHS, the generalised shape factor, a_g of a CHS may hence be used (in conjunction with $\sigma_{0.2}$ in compression and W_{el}) to determine its ultimate bending resistance through Equation 5.17

5.10 PRESENTATION OF GENERALISED SHAPE FACTORS

For a particular material model (i.e. a fixed factor to which $\sigma_{1.0}$ exceeds $\sigma_{0.2}$ and fixed values for n and $n'_{0.2,1.0}$), the generalised shape factor, a_g varies in response to changes in geometric shape factor, a_p, elastic strain at the material compressive 0.2% proof stress, defined as $\varepsilon_0 = \sigma_{0.2}/E_0$, and the outer fibre local buckling strain limit, ε_{LB}. This information may be presented as a series of graphs (each similar to Figure 5.16) or tables, with a separate graph or table for different values of ε_0. However, since the generalised shape factor, a_g is linearly proportional to both geometric shape factor and ε_0, it is described by a flat plane. The equation of a plane contains four constants. Therefore, for each value of ε_{LB} the generalised shape factor may be determined through Equation 5.18.

$$a_g = A_1 + A_2\varepsilon_0 + A_3a_p + A_4\varepsilon_0a_p \qquad (5.18)$$

The constants can be determined by numerical integration of the compound Ramberg-Osgood material over the depth of a beam, for a series of values of a_p and ε_0. The generalised shape factors will be presented in the design method set out in Chapter 6 in the form given in Equation 5.18.

5.11 SHS AND RHS SUBJECTED TO COMBINED AXIAL LOAD PLUS (BI-AXIAL) BENDING

5.11.1 Introduction

The most general member loading condition is that of combined axial load plus bending moment (about either or both of the principal axes).

5.11.2 Results from other laboratory testing programmes

No tests were conducted on members subjected to combined loadings as part of the current study. However, 12 eccentric compression tests on SHS and RHS pin-ended columns were conducted by Talja & Salmi (1995). The results of these tests are given in Table 5.27. Load eccentricity was created by applying the load through the centreline of the cross-section wall.

5.11.3 Proposed design method

To determine the resistance of stainless steel members subjected to combined compression and bending ENV 1993-1-4 (1996) directs the designer towards the provisions given in ENV 1993-1-1 (1992) or ENV 1993-1-3 (1996). The interaction expression given in ENV 1993-1-3 (1996) for cross-section resistance (with the modifications for additional moments due to shifts in the centroidal axes removed), similar to that given in ENV 1993-1-1 (1992) for Class 4 cross-sections, shall be adopted as the basis for the proposed design method. Similarly, the interaction expression for buckling resistance given in ENV 1993-1-3 (1996), similar to that given in ENV 1993-1-1 (1992) shall be adopted as the basis for the proposed design method.

The Eurocode expressions for cross-section resistance and for buckling resistance (without lateral torsional buckling) are given in Equations 5.19 and 5.20 respectively. Material safety factors have been omitted.

$$\frac{N_{Sd}}{f_y A_{eff}} + \frac{M_{y,Sd}}{W_{eff,y} f_y} + \frac{M_{z,Sd}}{W_{eff,z} f_y} \leq 1 \tag{5.19}$$

Table 5.27: *Measured dimensions and ultimate load carrying capacity for pin-ended SHS and RHS beam-columns tested by Talja and Salmi (1995)*

Specimen identification	Length, L (mm)	Depth, D (mm)	Breadth, B (mm)	Thickness, t (mm)	Internal corner radius, r_i (mm)	Area, A (mm^2)	Ultimate load, F_u (kN)
SHS 60×60×5-BC1 (TS)	400	59.8	59.6	4.77	3.0	1004	322
SHS 60×60×5-BC2 (TS)	1050	59.8	59.6	4.77	3.0	1004	210
SHS 60×60×5-BC3 (TS)	1700	59.7	59.4	4.71	3.0	990	125
SHS 60×60×5-BC4 (TS)	2350	59.7	59.4	4.71	3.0	990	83
RHS 150×100×3- BC1 (TS)	1050	150.4	100.3	2.89	3.0	1394	209
RHS 150×100×3- BC2 (TS)	2700	150.4	100.3	2.89	3.0	1394	173
RHS 150×100×3- BC3 (TS)	4350	150.4	100.3	2.89	3.0	1394	134
RHS 150×100×3- BC4 (TS)	6000	150.4	100.3	2.89	3.0	1394	95
RHS 150×100×6- BC1 (TS)	1050	150.6	100.6	5.77	6.0	2678	569
RHS 150×100×6- BC2 (TS)	2700	149.8	100.2	5.85	5.0	2709	403
RHS 150×100×6- BC3 (TS)	4350	150.6	100.6	5.77	6.0	2678	267
RHS 150×100×6- BC4 (TS)	6000	150.6	100.6	5.77	6.0	2678	192

Note: (TS)   All tests conducted by Talja & Salmi (1995)

$$\frac{N_{Sd}}{\chi_{min} f_{yb} A_{eff}} + \frac{\kappa_y M_{y,Sd}}{W_{eff,y} f_{yb}} + \frac{\kappa_z M_{z,Sd}}{W_{eff,z} f_{yb}} \leq 1 \tag{5.20}$$

The parameters, κ_y and κ_z (and μ_y and μ_z) are defined in Equations 5.21 to 5.24. It should be noted that the definition of μ_y and μ_z is based on the ENV 1993-1-1 (1992) rules for Class 1-2 cross-sections.

$$\kappa_y = 1 - \frac{\mu_y N_{Sd}}{\chi_y A_{eff} f_y} \qquad \text{but } \kappa_y \leq 1.5 \tag{5.21}$$

$$\mu_y = \overline{\lambda}_y (2\beta_{My} - 4) + \left[\frac{W_{pl,y} - W_{el,y}}{W_{el,y}}\right] \qquad \text{but } \mu_y \leq 0.90 \tag{5.22}$$

$$\kappa_z = 1 - \frac{\mu_z N_{Sd}}{\chi_z A_{eff} f_y} \qquad \text{but } \kappa_z \leq 1.5 \tag{5.23}$$

$$\mu_z = \overline{\lambda}_z (2\beta_{Mz} - 4) + \left[\frac{W_{pl,z} - W_{el,z}}{W_{el,z}}\right] \qquad \text{but } \mu_z \leq 0.90 \tag{5.24}$$

β_{My} and β_{Mz} are equivalent uniform moment factors for flexural buckling. For uniform moment along the member $\beta_M = 1.1$.

For the proposed design method, the Eurocode cross-section and member resistances will be replaced by those determined using the proposed design procedures described in previous sections. The interaction expression will otherwise remain unaltered. This leads to Equation 5.25 for cross-section resistance and Equation 5.26 for member resistance. Note that due to an absence of tests on RHS members subjected to lateral torsional buckling, the major axis bending resistance is simply taken as the in-plane bending strength.

$$\frac{N_{Sd}}{\sigma_{LB} A} + \frac{M_{y,Sd}}{W_{el,y} \sigma_{0.2} a_{gy}} + \frac{M_{z,Sd}}{W_{el,z} \sigma_{0.2} a_{gz}} \leq 1 \tag{5.25}$$

$$\frac{N_{Sd}}{\chi_{min} \sigma_{0.2} A(\sigma_{LB}/\sigma_{0.2})^{0.32}} + \frac{\kappa_y M_{y,Sd}}{W_{el,y} \sigma_{0.2} a_{gy}} + \frac{\kappa_z M_{z,Sd}}{W_{el,z} \sigma_{0.2} a_{gz}} \leq 1 \tag{5.26}$$

Since the concept of a plastic modulus is not to be used in the proposed design method, the definitions of μ_y and μ_z will be altered to those given in Equation 5.27 and 5.28. Additionally, the denominators in Equations 5.21 and 5.23 are replaced by $N_{b,Rd,y}$ and $N_{b,Rd,z}$ (which are the buckling resistances about each of the two principal axes according to proposed approach), respectively, in the proposed design method.

$$\mu_y = \overline{\lambda}_y (2\beta_{My} - 4) + (a_{gy} - 1) \qquad \text{but } \mu_y \le 0.90 \qquad (5.27)$$

$$\mu_z = \overline{\lambda}_z (2\beta_{Mz} - 4) + (a_{gz} - 1) \qquad \text{but } \mu_z \le 0.90 \qquad (5.28)$$

Figure 5.17 presents a comparison between the SHS and RHS test ultimate loads from Table 5.27, and those predicted by the Eurocode design method and the proposed design method, where $F_{Applied}$ and $F_{u, Res}$ are the applied axial load and axial (compression) resistance, respectively, and $M_{Applied}$ and $M_{u, Res}$ are the applied bending moment and bending moment resistance, respectively.
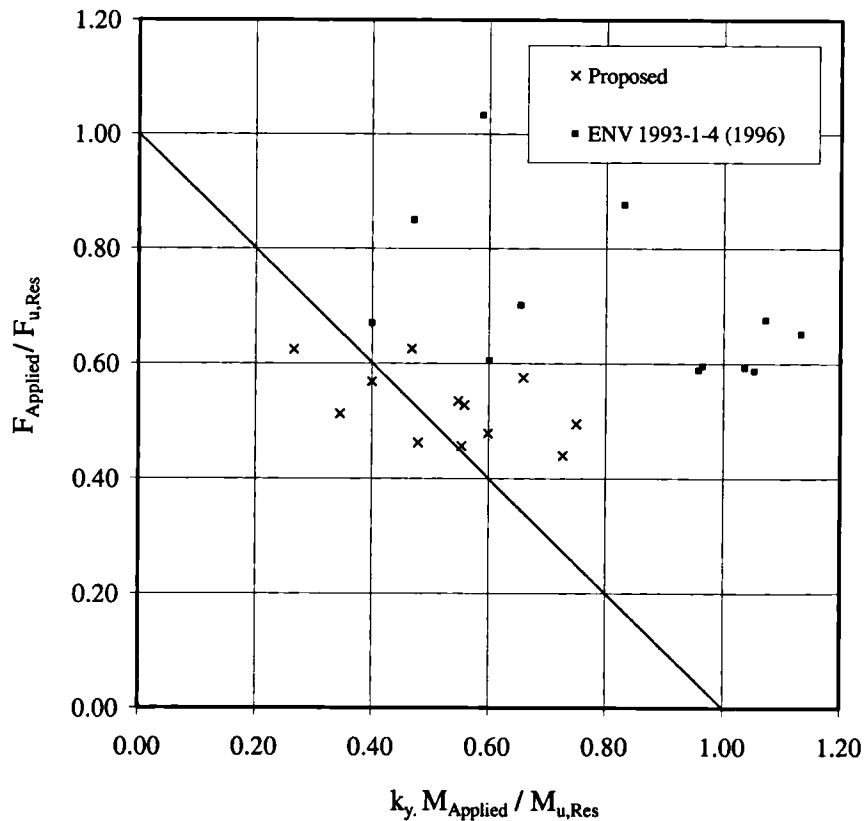
Figure 5.17: *Interaction diagram for SHS and RHS members subjected to combined axial load plus bending moment*

The graphical comparison given in Figure 5.17 demonstrates that the proposed design method predicts the behaviour of stainless steel SHS and RHS members subjected to combined axial load plus bending moment more accurately, and with less variability, than the Eurocode design method. A more detailed numerical comparison is presented in Chapter 6.

5.12 CHS SUBJECTED TO COMBINED AXIAL LOAD PLUS (BI-AXIAL) BENDING

5.12.1 Results from other laboratory testing programmes

No tests were conducted on CHS beam-columns in the current study, though a total of 8 were tested by Talja (1997), and reported in detail by Way (2000). Two cross-section sizes were investigated, CHS 140×2 (Grade 1.4435) and CHS 140×4 (Grade 1.4541). The results are presented in Table 5.28. The columns were pin-ended with loading applied through the centreline of the wall thickness to create the eccentricity.

5.12.2 Proposed design method

The proposed design method for CHS subjected to combined compression and bending is the same as for SHS and RHS members. The interaction expression for cross-section resistance remains as Equations 5.25, where the Eurocode member resistances have been replaced by those determined through the proposed design procedures. For CHS member resistance the axial compression component of the interaction given in Equation 5.26 has to be modified in accordance with Equation 5.13, leading to Equation 5.29.

$$\frac{N_{Sd}}{\chi_{min}\,\sigma_{0.2}\,A(\sigma_{LB}\,/\,\sigma_{0.2})^{0.80}} + \frac{\kappa_y\,M_{y,Sd}}{W_{el,y}\,\sigma_{0.2}\,a_{gy}} + \frac{\kappa_z\,M_{z,Sd}}{W_{el,z}\,\sigma_{0.2}\,a_{gz}} \leq 1 \qquad (5.29)$$

The parameters, κ_y, κ_z, μ_y and μ_z are defined as for SHS and RHS by Equations 5.21, 5.23, 5.27 and 5.28 respectively.

Figure 5.18 presents a comparison between the CHS test ultimate loads from Table 5.28, and those predicted by the Eurocode design method and the proposed design method, where $F_{Applied}$

Table 5.28: Measured dimensions and ultimate load carrying capacity CHS beam-columns from other test programmes

Specimen identification	Length, L (mm)	Outer diameter, D_o (mm)	Thickness, t (mm)	Area, A (mm²)	Ultimate load, F_u (kN)
CHS 140x2- BC1 (T)	550	139.9	1.97	854	122
CHS 140x2- BC2 (T)	2251	139.6	1.95	84	89
CHS 140x2- BC3 (T)	3351	139.8	1.95	845	73
CHS 140x2- BC4 (T)	4451	139.8	1.96	849	58
CHS 140x4- BC1 (T)	550	139.1	3.99	1694	297
CHS 140x4- BC2 (T)	2250	139.2	3.98	1691	202
CHS 140x4- BC3 (T)	3351	140.1	3.98	1702	155
CHS 140x4- BC4 (T)	4451	140.2	3.99	1707	121

Note: (T)   All tests conducted by Talja (1997)

and $F_{u, Res}$ are the applied axial load and axial (compression) resistance, respectively, and $M_{Applied}$ and $M_{u, Res}$ are the applied bending moment and bending moment resistance, respectively.
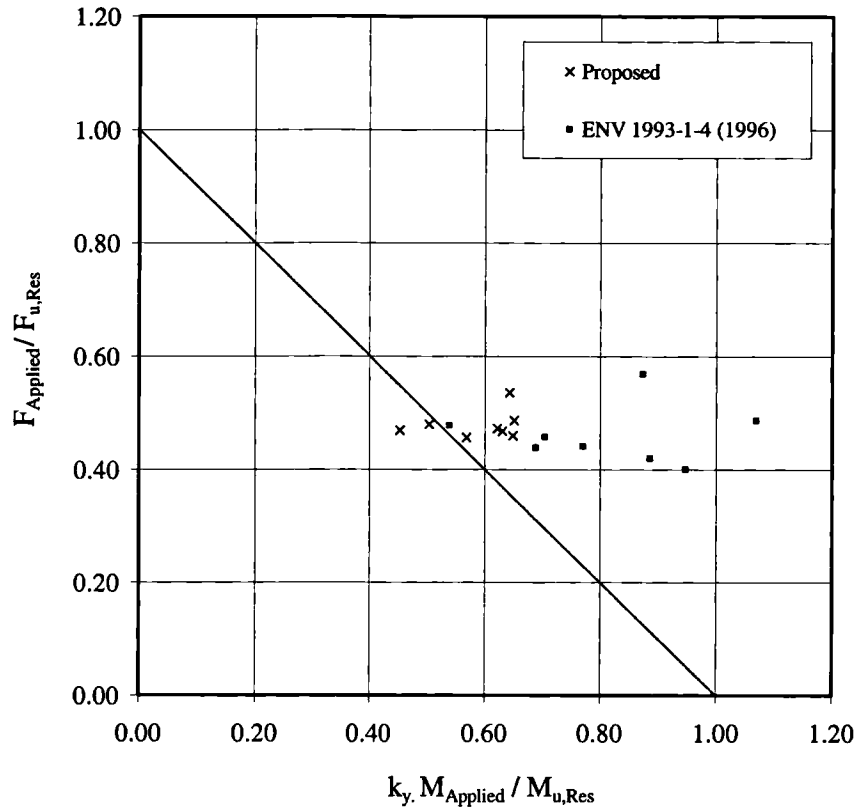
Figure 5.18: *Interaction diagram for CHS members subjected to combined axial load plus bending moment*

Similarly to the SHS and RHS case, the graphical comparison given in Figure 5.18 demonstrates that the proposed design method predicts the behaviour of stainless steel CHS members subjected to combined axial load plus bending moment more accurately, and with less variability, than the Eurocode design method. A more detailed numerical comparison is presented in Chapter 6.

5.13 CONCLUDING COMMENTS

This chapter has described the development of a new approach to structural stainless steel design. The following points describe the key components of the design method and summarise the important findings of this chapter:

- The new design approach adopts a continuous, rather than a discretised, system of cross-section classification and member design, in view of the rounded nature of the stainless steel stress-strain curve.

- Test results from the current study and all suitable test results from other studies have been analysed together to develop and calibrate the new design method.

- Relationships between cross-section slenderness and cross-section deformation capacity have been derived from the results of tests on stub columns loaded in pure compression.

- Cross-section compression resistance is determined by using the deformation capacity in conjunction with an accurate compound (2-stage) Ramberg-Osgood material model.

- Additional benefit is achieved by taking account of the interaction between the individual compression elements within a cross-section.

- In-plane bending strength is based upon the most critical element within the cross-section, (generally the uniformly loaded compression flange, but in extreme cases the web in bending). The concept of a generalised shape factor is adopted to determine bending moment resistance, with values presented in tabular form for design purposes.

- The prediction of flexural buckling resistance has been improved by using new Perry-based buckling curves, modified by a factor dependent upon cross-section deformation capacity.

- Members subjected to combined axial load plus (bi-axial) bending are designed by means of the same interaction expression provided by ENV 1993-1-3 (1996), except with the Eurocode resistances replaced by those given by the proposed design method.

The design method is presented in a straightforward format in Chapter 6 and validated against all available test data. Comparison is made with the ENV 1993-1-4 (1996) design rules. Worked examples are presented to clarify the proposed design procedure.

CHAPTER 6

DESIGN METHOD

6.1 INTRODUCTION

Development of the proposed design approach for stainless steel hollow sections is described in Chapter 5. This Chapter presents the proposed design rules in a straightforward format. It should be noted that the design expressions currently predict mean failure loads. Clearly safety factors and load factors need to be incorporated into the method to achieve the required level of reliability, though this will not be performed as part of the current study.

6.2 DESIGN METHOD

6.2.1 Cross-section slenderness, β

Cross-section slenderness, β shall be determined for all internal elements from Equation 6.1 (for SHS and RHS) and Equation 6.2 (for CHS).

$$\text{For SHS and RHS,} \qquad \beta = \left(\frac{b}{t}\right)\sqrt{\frac{\sigma_{0.2}}{E_0}}\sqrt{\frac{4.0}{k}} \qquad (6.1)$$

$$\text{For CHS,} \qquad \beta = \left(\frac{R}{t}\right)\left(\frac{\sigma_{0.2}}{E_0}\right) \qquad (6.2)$$

where $\sigma_{0.2}$ is the material 0.2% proof stress in compression

E_0 is the material Young's modulus

b is the flat face width measured between centrelines of adjacent faces

R is the radius of the CHS measured to the centreline of the wall thickness

t is the wall thickness of the cross-section

k is the buckling coefficient from Table 6.1

Table 6.1: *Buckling coefficients for compressed plate elements*

$\psi = \sigma_1/\sigma_2$	1	$1 > \psi > 0$	0	$0 > \psi > -1$	-1	$-1 > \psi > -2$
Buckling Coefficent, k	4.0	$\dfrac{8.2}{1.05 + \psi}$	7.81	$7.81 - 6.29\psi + 9.78\psi^2$	23.9	$5.98(1-\psi)^2$

Alternatively, for $1 \geq \psi \geq -1$:

$$k = \frac{16}{[(1+\psi)^2 + 0.112(1-\psi)^2]^{0.5} + (1+\psi)}$$

Note: ψ is the ratio of end stresses (compression positive) for the compression element

6.2.2 Cross-section deformation capacity, ε_{LB}

Based on β for the most slender element, cross-section deformation capacity, ε_{LB} may be determined from Equation 6.3 (SHS and RHS) or Equation 6.4 (CHS). For RHS subjected to pure compression only, allowance may be made for enhanced element edge restraint by taking χ equal to the aspect ratio of the cross-section. Strictly χ is the ratio of the stiffness of the longer face of the RHS to the stiffness of the shorter face, but for uniform material properties and thickness, this simplifies to the aspect ratio. For all other cases, χ should be taken as 1.0.

$$\text{SHS and RHS,} \qquad \frac{\varepsilon_{LB}}{\varepsilon_0} = \frac{7.07}{\beta^{2.13+0.21\beta}} \chi^{-0.30\beta^{0.5}} \qquad (6.3)$$

$$\text{CHS,} \qquad \frac{\varepsilon_{LB}}{\varepsilon_0} = \frac{0.116}{\beta^{1.21+1.69\beta}} \tag{6.4}$$

where χ is the cross-section aspect ratio for RHS subjected to pure compression and is taken as 1.0 for all other cases

ε_0 is the elastic strain at the material compressive 0.2% proof stress = $\sigma_{0.2}/E_0$

ε_{LB} is the cross-section local buckling strain

6.2.3 Local buckling stress, σ_{LB}

Local buckling stress, σ_{LB} is determined from Table 6.2 (SHS and RHS) or Table 6.3 (CHS).

6.2.4 Cross-section resistance

6.2.4.1 Compression

Compression resistance, $N_{c,Rd}$, is given by Equation 6.5.

$$N_{c,Rd} = A\sigma_{LB} \tag{6.5}$$

where A is the gross area of the cross section

σ_{LB} is the local buckling stress (from Table 6.2 or 6.3)

6.2.4.2 Bending

In-plane bending resistance, $M_{c,Rd}$, is given by Equation 6.6.

$$M_{c,Rd} = W_{el} \, \sigma_{0.2} \, a_g \tag{6.6}$$

where W_{el} is the elastic section modulus

a_g is the generalised shape factor (from Table 6.4 or 6.5 and Equation 6.7)

Table 6.2: *Local buckling stress for SHS and RHS*

ε_{LB} \ $\sigma_{0.2}$	200 N/mm²	220 N/mm²	240 N/mm²	280 N/mm²	320 N/mm²	360 N/mm²	400 N/mm²	440 N/mm²	480 N/mm²
0.001	131	140	148	161	171	179	184	188	192
0.002	174	189	203	229	252	274	292	309	324
0.003	200	218	235	268	299	328	356	381	405
0.004	216	236	256	295	332	367	400	431	461
0.005	225	247	268	310	351	391	430	468	504
0.006	232	254	276	320	364	407	448	489	530
0.007	237	260	283	328	373	418	461	505	547
0.008	241	265	288	335	381	426	472	516	560
0.009	245	269	293	340	387	434	480	526	572
0.010	248	273	297	345	393	441	488	535	581
0.012	254	279	304	354	403	452	501	549	598
0.014	259	285	310	361	412	461	511	561	611
0.016	263	289	316	367	419	470	521	572	622
0.018	268	294	320	373	426	478	529	581	632
0.020	271	298	325	378	431	484	537	590	642
0.024	277	305	333	388	442	497	551	605	658
0.028	284	312	340	396	451	508	563	618	673
0.032	289	317	346	403	461	517	574	630	687
0.036	294	323	352	410	468	526	584	641	698
0.040	298	328	357	416	476	534	592	652	710
0.050	308	338	369	430	491	552	613	673	735
0.060	316	348	379	442	505	568	630	693	755
0.080	331	364	397	463	529	594	660	725	791
0.100	344	377	412	480	548	616	685	752	821

$\sigma_{LB}\ (N/mm^2)$

Table 6.3: *Local buckling stress for CHS*

σ_{LB} (N/mm^2)

ε_{LB} \ $\sigma_{0.2}$	200 N/mm^2	220 N/mm^2	240 N/mm^2	280 N/mm^2	320 N/mm^2	360 N/mm^2	400 N/mm^2	440 N/mm^2	480 N/mm^2
0.001	131	140	148	161	171	179	184	188	192
0.002	174	189	203	229	252	274	292	309	324
0.003	200	218	235	268	299	328	356	381	405
0.004	214	234	254	293	331	367	400	431	461
0.005	220	242	263	305	346	387	426	465	502
0.006	225	247	269	313	356	398	440	481	522
0.007	229	251	274	318	362	406	449	492	535
0.008	232	255	278	323	368	413	457	501	544
0.009	235	258	281	327	373	418	463	508	552
0.010	237	261	284	331	377	423	469	514	560
0.012	242	265	289	337	384	431	478	525	571
0.014	245	269	294	342	390	438	486	533	581
0.016	248	273	298	347	396	444	493	541	589
0.018	252	276	301	351	401	450	499	548	597
0.020	254	279	304	355	405	455	505	554	604
0.024	259	285	311	362	413	464	515	566	616
0.028	263	290	316	368	420	472	524	576	627
0.032	267	294	320	374	426	479	532	584	637
0.036	271	298	324	379	432	485	539	592	646
0.040	274	301	328	383	437	492	546	600	654
0.050	281	309	337	393	449	505	561	616	672
0.060	288	316	345	402	460	516	574	631	687
0.080	298	328	358	417	477	536	595	655	714
0.100	308	338	369	430	492	553	614	675	736

The generalised shape factor, a_g may be calculated using Equation 6.7, where the constants A_1 to A_4 may be determined from Table 6.4 for SHS and RHS and Table 6.5 for CHS.

$$a_g = A_1 + A_2\varepsilon_0 + A_3a_p + A_4\varepsilon_0a_p \tag{6.7}$$

where A_1 to A_4 are constants determined from Table 6.4 (SHS & RHS) and Table 6.5 (CHS)

a_p is the geometric shape factor of the cross-section

6.2.4.3 Combined compression and bending

Cross-sections subjected to combined compression and bending should satisfy Equation 6.8.

$$\frac{N_{Sd}}{\sigma_{LB} A} + \frac{M_{y,Sd}}{W_{el,y}\,\sigma_{0.2}\,a_{gy}} + \frac{M_{z,Sd}}{W_{el,z}\,\sigma_{0.2}\,a_{gz}} \leq 1 \tag{6.8}$$

where N_{Sd} is the applied axial compression

$M_{y,Sd}$ is the applied bending moment about the y-axis

$M_{z,Sd}$ is the applied bending moment about the z-axis

$W_{el,y}$ is the elastic modulus about the y-axis

$W_{el,z}$ is the elastic modulus about the z-axis

a_{gy} is the generalised shape factor about the y-axis

a_{gz} is the generalised shape factor about the z-axis

6.2.5 Buckling resistance

6.2.5.1 Compression (flexural buckling)

The buckling resistances of SHS and RHS compression members and CHS compression members are given by Equation 6.9 and 6.10 respectively.

$$\text{SHS and RHS,} \qquad N_{b.Rd} = \chi A\sigma_{0.2}\left(\frac{\sigma_{LB}}{\sigma_{0.2}}\right)^{0.32} \tag{6.9}$$

Table 6.4: *Generalised shape factor calculation constants for SHS and RHS*

ε_{LB}	A_1	A_2	A_3	A_4
0.0015	0.373	35.937	0.559	-193.75
0.0020	0.360	68.187	0.644	-207.92
0.0025	0.336	83.333	0.720	-206.67
0.0030	0.343	80.833	0.761	-193.33
0.0035	0.332	86.250	0.807	-187.50
0.0040	0.307	99.667	0.858	-188.33
0.0045	0.230	125.156	0.937	-196.87
0.0050	0.181	147.634	0.993	-203.31
0.0055	0.152	148.437	1.024	-193.75
0.0060	0.140	136.062	1.046	-175.42
0.0070	0.163	104.375	1.042	-137.50
0.0080	0.164	80.667	1.059	-110.00
0.0090	0.180	63.594	1.061	-90.63
0.0100	0.178	55.771	1.077	-79.58
0.0120	0.188	42.146	1.092	-62.08
0.0140	0.196	31.917	1.107	-50.00
0.0160	0.201	27.083	1.122	-43.33
0.0180	0.207	24.229	1.135	-38.75
0.0200	0.220	18.542	1.141	-32.50
0.0240	0.224	17.854	1.168	-29.58
0.0280	0.238	12.250	1.183	-23.33
0.0320	0.247	11.187	1.199	-21.25
0.0360	0.253	10.042	1.214	-19.17
0.0400	0.261	8.625	1.229	-17.50
0.0500	0.287	4.375	1.253	-12.50
0.0600	0.297	5.625	1.282	-12.50
0.0700	0.310	6.250	1.307	-12.50
0.0800	0.327	3.281	1.324	-9.37
0.1000	0.357	0.312	1.356	-6.25

ε_{LB} is the cross-section local buckling strain

A_1 to A_4 are constants to be used in Equation 6.7

Table 6.5: *Generalised shape factor calculation constants for CHS*

ε_{LB}	A_1	A_2	A_3	A_4
0.0015	0.373	35.937	0.559	-193.75
0.0020	0.346	67.187	0.656	-206.25
0.0025	0.329	83.438	0.726	-206.25
0.0030	0.343	77.969	0.761	-190.62
0.0035	0.308	95.312	0.824	-193.75
0.0040	0.226	127.187	0.911	-206.25
0.0045	0.149	156.094	0.986	-215.62
0.0050	0.097	172.969	1.036	-215.62
0.0055	0.084	163.906	1.052	-196.87
0.0060	0.085	143.281	1.057	-171.87
0.0070	0.108	100.000	1.050	-125.00
0.0080	0.124	70.937	1.049	-93.75
0.0090	0.135	54.375	1.050	-75.00
0.0100	0.134	47.344	1.061	-65.62
0.0120	0.135	38.594	1.078	-53.12
0.0140	0.145	27.344	1.086	-40.62
0.0160	0.151	22.656	1.094	-34.37
0.0180	0.153	20.937	1.106	-31.25
0.0200	0.160	18.594	1.113	-28.12
0.0240	0.173	9.688	1.124	-18.75
0.0280	0.168	15.156	1.147	-21.87
0.0320	0.185	8.594	1.151	-15.63
0.0360	0.186	9.844	1.166	-15.62
0.0400	0.195	6.875	1.172	-12.50
0.0500	0.255	-42.188	1.154	31.25
0.0600	0.263	-37.969	1.177	28.13
0.0700	0.277	-37.969	1.192	28.12
0.0800	0.278	-33.750	1.215	25.00
0.1000	0.295	-29.531	1.243	21.88

ε_{LB} is the cross-section local buckling strain

A_1 to A_4 are constants to be used in Equation 6.7

$$\text{CHS,} \qquad N_{b.Rd} \quad = \quad \chi A\sigma_{0.2}\left(\frac{\sigma_{LB}}{\sigma_{0.2}}\right)^{0.80} \qquad\qquad (6.10)$$

where $\quad \chi \quad$ is the buckling reduction factor given by Equation 6.11 (not limited to ≤ 1.0)

$$\chi \quad = \quad \frac{1}{\phi + [\phi^2 - \overline{\lambda}^2]^{0.5}} \qquad\qquad (6.11)$$

where $\quad \phi \quad = \quad 0.5[1 + \alpha(\overline{\lambda} - \overline{\lambda}_0) + \overline{\lambda}^2]$

$\alpha \quad$ is an imperfection factor (Table 6.6)

$\overline{\lambda}_0 \quad$ is the limiting slenderness (Table 6.6)

$\overline{\lambda} \quad = \quad \lambda/\lambda_1$

$\lambda \quad = \quad L_E/i \quad$ and is the slenderness for the relevant buckling mode

$\lambda_1 \quad = \quad \pi \, [E_0/\sigma_{0.2}]^{0.5}$

$L_E \quad$ is the effective column length

$i \quad$ is the radius of gyration about the relevant axis, determined using the properties of the gross cross-section

Table 6.6: *Parameters for flexural buckling curves*

Cross-section type	α	$\overline{\lambda}_0$
Cold-formed SHS and RHS	0.70	0.44
Cold-formed CHS	0.50	-0.10

6.2.5.2 Bending (lateral torsional buckling)

Clearly SHS, CHS and RHS (bending about the minor axis) are not affected by lateral torsional buckling, so member resistance may be taken as the cross-section in-plane bending resistance.

No design guidance is given for lateral torsional buckling resistance of RHS beams (bending about the major axis) due to an absence of supporting test data.

6.2.5.3 Combined axial load plus bending

The buckling resistance of members subjected to combined axial load plus bending may be evaluated through Equation 6.12 (for SHS and RHS) and Equation 6.13 (for CHS). As described in Section 6.2.4.2 no design guidance is given for lateral torsional buckling. The major axis bending component given in Equations 6.12 and 6.13 therefore only applies to members not affected by lateral torsional buckling.

$$\frac{N_{Sd}}{\chi_{min}\,\sigma_{0.2}\,A(\sigma_{LB}/\sigma_{0.2})^{0.32}} + \frac{\kappa_y\,M_{y,Sd}}{W_{el,y}\,\sigma_{0.2}\,a_{gy}} + \frac{\kappa_z\,M_{z,Sd}}{W_{el,z}\,\sigma_{0.2}\,a_{gz}} \leq 1 \qquad (6.12)$$

$$\frac{N_{Sd}}{\chi_{min}\,\sigma_{0.2}\,A(\sigma_{LB}/\sigma_{0.2})^{0.80}} + \frac{\kappa_y\,M_{y,Sd}}{W_{el,y}\,\sigma_{0.2}\,a_{gy}} + \frac{\kappa_z\,M_{z,Sd}}{W_{el,z}\,\sigma_{0.2}\,a_{gz}} \leq 1 \qquad (6.13)$$

where χ_{min} is the lesser of the buckling reduction factors χ_y and χ_z

κ_y is defined by Equation 6.14

κ_z is defined by Equation 6.16

$$\kappa_y = 1 - \frac{\mu_y\,N_{Sd}}{N_{b,Rd,y}} \qquad \text{but } \kappa_y \leq 1.5 \qquad (6.14)$$

$$\mu_y = \overline{\lambda}_y(2\beta_{My}-4) + (a_{gy}-1) \qquad \text{but } \mu_y \leq 0.90 \qquad (6.15)$$
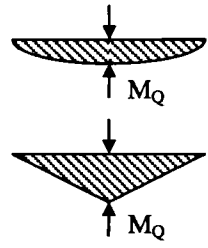
$$\kappa_z = 1 - \frac{\mu_z\,N_{Sd}}{N_{b,Rd,z}} \qquad \text{but } \kappa_z \leq 1.5 \qquad (6.16)$$

$$\mu_z = \overline{\lambda}_z(2\beta_{Mz}-4) + (a_{gz}-1) \qquad \text{but } \mu_z \leq 0.90 \qquad (6.17)$$

where β_{My} is the equivalent uniform moment factor from Table 6.7

Table 6.7 is a reproduction of part of Figure 5.5.3 from ENV 1993-1-1 (1992), providing equivalent uniform moment factors for the most common load cases.

Table 6.7: *Equivalent uniform moment factors*

Moment diagram	*Equivalent uniform moment factor,* β_M
End moments M_1 ▨▨▨▨▨ ψM_1 $-1 \le \psi \le 1$	$\beta_{M,\psi} = 1.8 - 0.7\psi$
Moments due to in-plane lateral loads ↓ ▨▨▨▨▨ ↑ M_Q	$\beta_{M,Q} = 1.3$
↓ ▨▨▨▨▨ ↑ M_Q	$\beta_{M,Q} = 1.4$

M_1 is the applied end bending moment

M_Q is the applied mid-span bending moment

ψ is the ratio of the smaller end moment to the larger end moment

$\beta_{M,\psi}$ is the equivalent uniform moment factor for end moments

$\beta_{M,Q}$ is the equivalent uniform moment factor for moments due to in-plane lateral loads

6.3 VERIFICATION OF DESIGN METHOD AND COMPARISON WITH ENV 1993-1-4 (1996)

6.3.1 Introduction

The purpose of this section is to analyse all available test data and to compare test failure loads and moments with those predicted by ENV 1993-1-4 (1996) and the proposed design method.

For comparison purposes, measured geometric and material properties are adopted, and all safety factors and load factors are set to unity.

6.3.2 Cross-section resistance

6.3.2.1 Compression

Table 6.8 presents a comparison between the Eurocode design procedure and the proposed design method for all tests conducted on SHS stub columns. Similar comparisons are presented for RHS stub columns with an aspect ratio of 0.67 in Table 6.9, RHS stub columns with an aspect ratio of 0.50 in Table 6.10 and CHS stub columns in Table 6.11.

For SHS and RHS compression resistance, the Eurocode design method predicts, on average, 78% of the test failure load with a standard deviation of 13%, whereas the proposed design method predicts 95% of the test failure load with a standard deviation of 8%.

For CHS compression resistance, the Eurocode design method predicts, on average, 80% of the test failure load with a standard deviation of 7%, whereas the proposed design method predicts 101% of the test failure load with a standard deviation of 5%.

A summary of the comparisons for all compression tests is presented in Table 6.12. Overall the proposed design method provides a 25% increase in cross-sectional resistance, with a reduction in scatter (standard deviation) from 12% to 8%.

Table 6.8: *Comparison between ENV 1993-1-4 (1996) and the proposed design method for SHS stub columns*

Cross-section	$F_{u,Test}$ (kN)	$\sigma_{0.2}$ (N/mm²)	E_0 (N/mm²)	ENV 1993-1-4 (1996)			Proposed method			
				Class (1-4)	$F_{u,ENV}$ (kN)	$F_{u,ENV}/F_{u,Test}$	$\varepsilon_{LB}/\varepsilon_0$	$F_{u,Prop}$ (kN)	$F_{u,Prop}/F_{u,Test}$	$F_{u,Prop}/F_{u,ENV}$
SHS 60×60×5- SC (TS)	801	463	186500	1	463	0.58	24.8	731	0.91	1.58
SHS 80×80×3- SC1 (RH)	485	415	196000	4	370	0.76	4.7	451	0.93	1.22
SHS 80×80×3- SC2 (RH)	471	415	196000	4	367	0.78	4.8	448	0.95	1.22
SHS 80×80×4- SC1 (GN)	727	457	186600	3	493	0.68	6.7	641	0.88	1.30
SHS 80×80×4- SC2 (GN)	714	457	186600	2	513	0.72	7.3	675	0.95	1.32
SHS 80×80×4- SC3 (GN)	711	457	186600	2	514	0.72	7.3	677	0.95	1.32
SHS 80×80×4- ASC1 (GN)	309	261	206300	1	288	0.93	15.3	388	1.26	1.35
SHS 80×80×4- ASC2 (GN)	335	261	206300	1	282	0.84	14.3	376	1.12	1.33
SHS 100×100×2- SC1 (GN)	197	370	207100	4	203	1.03	0.9	192	0.97	0.95
SHS 100×100×2- SC2 (GN)	187	370	207100	4	202	1.08	0.9	190	1.02	0.94
SHS 100×100×3- SC1 (GN)	489	379	208800	4	404	0.83	2.9	458	0.94	1.13
SHS 100×100×3- SC2 (GN)	496	379	208800	4	398	0.80	2.8	450	0.91	1.13

Notes: (GN) Gardner and Nethercot (Chapter 3)
  (RH) Rasmussen and Hancock (1993a)
  (TS) Talja and Salmi (1995)

$\varepsilon_{LB}/\varepsilon_0$ is the cross-section normalised local buckling strain
$F_{u,Test}$ is the test ultimate load
$F_{u,ENV}$ is the compression resistance predicted by ENV 1993-1-4 (1996)
$F_{u,Prop}$ is the compression resistance predicted by proposed design method

Table 6.8 (continued): *Comparison between ENV 1993-1-4 (1996) and the proposed design method for SHS stub columns*

Cross-section	$F_{u,Test}$ (kN)	$\sigma_{0.2}$ (N/mm²)	E_0 (N/mm²)	ENV 1993-1-4 (1996)			Proposed method			$F_{u,Prop}/F_{u,ENV}$
				Class (1-4)	$F_{u,ENV}$ (kN)	$F_{u,ENV}/F_{u,Test}$	$\varepsilon_{LB}/\varepsilon_0$	$F_{u,Prop}$ (kN)	$F_{u,Prop}/F_{u,Test}$	
SHS 100×100×4- SC1 (GN)	779	437	203400	4	625	0.80	5.0	769	0.99	1.23
SHS 100×100×4- SC2 (GN)	774	437	203400	4	623	0.80	4.9	765	0.99	1.23
SHS 100×100×6- SC1 (GN)	1513	473	197900	1	1016	0.67	12.7	1441	0.95	1.42
SHS 100×100×6- SC2 (GN)	1507	473	197900	1	1019	0.68	12.7	1448	0.96	1.42
SHS 100×100×8- SC1 (GN)	1630	330	205200	1	919	0.56	39.0	1462	0.90	1.59
SHS 100×100×8- SC2 (GN)	1797	330	205200	1	918	0.51	39.1	1459	0.81	1.59
SHS 150×150×4- SC1 (GN)	726	294	195400	4	604	0.83	2.6	662	0.91	1.10
SHS 150×150×4- SC2 (GN)	713	294	195400	4	592	0.83	2.5	647	0.91	1.09
SHS MEAN:						**0.77**			**0.96**	**1.28**
SHS ST DEV:						**0.14**			**0.09**	

Note: (GN) Gardner and Nethercot (Chapter 3)

$\varepsilon_{LB}/\varepsilon_0$ is the cross-section normalised local buckling strain

$F_{u,Test}$ is the test ultimate load

$F_{u,ENV}$ is the compression resistance predicted by ENV 1993-1-4 (1996)

$F_{u,Prop}$ is the compression resistance predicted by proposed design method

Table 6.9: *Comparison between ENV 1993-1-4 (1996) and the proposed design method for RHS (0.67) stub columns*

Cross-section	$F_{u,Test}$ (kN)	$\sigma_{0.2}$ (N/mm²)	E_0 (N/mm²)	ENV 1993-1-4 (1996)			Proposed method			$F_{u,Prop}/F_{u,ENV}$
				Class (1-4)	$F_{u,ENV}$ (kN)	$F_{u,ENV}/F_{u,Test}$	$\varepsilon_{LB}/\varepsilon_0$	$F_{u,Prop}$ (kN)	$F_{u,Prop}/F_{u,Test}$	
RHS 60×40×4- SC1 (GN)	492	469	193100	1	317	0.64	16.4	468	0.95	1.48
RHS 60×40×4- SC2 (GN)	497	469	193100	1	317	0.64	16.4	467	0.94	1.47
RHS 120×80×3- SC1 (GN)	452	429	197300	4	429	0.95	1.7	456	1.01	1.06
RHS 120×80×3- SC2 (GN)	447	429	197300	4	423	0.95	1.7	448	1.00	1.06
RHS 120×80×6- SC1 (GN)	1459	466	192300	2	982	0.67	8.8	1324	0.91	1.35
RHS 120×80×6- SC2 (GN)	1465	466	192300	2	982	0.67	8.7	1324	0.90	1.35
RHS 150×100×3- SC1 (TS)	372	305	204500	4	372	1.00	1.5	357	0.96	0.96
RHS 150×100×4- SC1 (GN)	660	319	200300	4	553	0.84	2.9	619	0.94	1.12
RHS 150×100×4- SC2 (GN)	659	319	200300	4	555	0.84	2.9	623	0.95	1.12
RHS 150×100×6- SC1 (TS)	1292	345	240800	2	926	0.72	9.0	1178	0.91	1.27
RHS (0.67) MEAN:						0.79			0.95	1.22
RHS (0.67) ST DEV:						0.14			0.04	

Notes: (GN) Gardner and Nethercot (Chapter 3)
(TS) Talja and Salmi (1995)

$\varepsilon_{LB}/\varepsilon_0$ is the cross-section normalised local buckling strain
$F_{u,Test}$ is the test ultimate load
$F_{u,ENV}$ is the compression resistance predicted by ENV 1993-1-4 (1996)
$F_{u,Prop}$ is the compression resistance predicted by proposed design method

Table 6.10: *Comparison between ENV 1993-1-4 (1996) and the proposed design method for RHS (0.50) sub columns*

Cross-section	$F_{u,\,Test}$ (kN)	$\sigma_{0.2}$ (N/mm²)	E_0 (N/mm²)	ENV 1993-1-4 (1996)			Proposed method				$F_{u,Prop}/$ $F_{u,ENV}$
				Class (1-4)	$F_{u,ENV}$ (kN)	$F_{u,ENV}/$ $F_{u,Test}$	$\varepsilon_{LB}/\varepsilon_0$	$F_{u,Prop}$ (kN)	$F_{u,Prop}/$ $F_{u,Test}$		
RHS 100×50×2- SC1 (GN)	182	370	205900	4	159	0.87	1.2	152	0.84		0.96
RHS 100×50×2- SC2 (GN)	181	370	205900	4	159	0.88	1.2	152	0.84		0.96
RHS 100×50×3- SC1 (GN)	407	455	200900	4	348	0.86	2.9	416	1.02		1.20
RHS 100×50×3- SC2 (GN)	415	455	200900	4	349	0.84	2.9	416	1.00		1.19
RHS 100×50×4- SC1 (GN)	626	439	203900	4	450	0.72	5.8	566	0.90		1.26
RHS 100×50×4- SC2 (GN)	627	439	203900	4	445	0.71	5.6	557	0.89		1.25
RHS 100×50×6- SC1 (GN)	1217	494	206300	1	770	0.63	15.3	1124	0.92		1.46
RHS 100×50×6- SC2 (GN)	1217	494	206300	1	770	0.63	15.4	1125	0.92		1.46
RHS (0.50) MEAN:						**0.77**			**0.92**		**1.22**
RHS (0.50) ST DEV:						**0.11**			**0.07**		

Note: (GN) Gardner and Nethercot (Chapter 3)

$\varepsilon_{LB}/\varepsilon_0$ is the cross-section normalised local buckling strain

$F_{u,Test}$ is the test ultimate load

$F_{u,ENV}$ is the compression resistance predicted by ENV 1993-1-4 (1996)

$F_{u,Prop}$ is the compression resistance predicted by proposed design method

Table 6.11: *Comparison between ENV 1993-1-4 (1996) and the proposed design method for CHS stub columns*

Cross-section	$F_{u,Test}$ (kN)	$\sigma_{0.2}$ (N/mm²)	E_0 (N/mm²)	ENV 1993-1-4 (1996)			Proposed method			$\dfrac{F_{u,Prop}}{F_{u,ENV}}$
				Class (1-4)	$F_{u,ENV}$ (kN)	$\dfrac{F_{u,ENV}}{F_{u,Test}}$	$\varepsilon_{LB}/\varepsilon_0$	$F_{u,Prop}$ (kN)	$\dfrac{F_{u,Prop}}{F_{u,Test}}$	
CHS 103×1.5-SC1 (GN)	214	368	206000	4	165	0.77	4.6	203	0.95	1.23
CHS 103×1.5-SC2 (GN)	217	368	206000	4	164	0.76	4.6	202	0.93	1.23
CHS 153×1.5- SC1 (GN)	287	405	203000	4	197	0.69	2.6	298	1.04	1.51
CHS 153×1.5- SC2 (GN)	286	405	203000	4	200	0.70	2.6	301	1.05	1.51
CHS 140×2- SC (T)	278	294	200000	4	250	0.90	5.4	288	1.04	1.15
CHS 140×3- SC (T)	468	317	192000	3	390	0.83	7.2	468	1.00	1.20
CHS 140×4- SC (T)	665	309	197000	2	522	0.78	11.0	650	0.98	1.25
CHS 101.6×2.85- SC1 (RH)	426	390	202000	2	357	0.84	8.9	444	1.04	1.24
CHS 101.6×2.85- SC2 (RH)	425	390	202000	2	357	0.84	8.9	444	1.04	1.24
CHS 101.6×2.85- SC3 (RH)	391	390	202000	2	337	0.86	8.2	415	1.06	1.23
CHS MEAN:						**0.80**			**1.01**	**1.28**
CHS ST DEV:						**0.07**			**0.05**	

Notes: (GN) Gardner and Nethercot (Chapter 3)
(RH) Rasmussen and Hancock (1993a)
(T) Talja (1997)

$\varepsilon_{LB} / \varepsilon_0$ is the cross-section normalised local buckling strain
$F_{u,Test}$ is the test ultimate load
$F_{u,ENV}$ is the compression resistance predicted by ENV 1993-1-4 (1996)
$F_{u,Prop}$ is the compression resistance predicted by proposed design method

Table 6.12: *Summary of comparison between ENV 1993-1-4 (1996) and the proposed design method for compression resistance*

Cross-section type	$F_{u,ENV}/F_{u,Test}$	$F_{u,Prop}/F_{u,Test}$	$F_{u,Prop}/F_{u,ENV}$
SHS & RHS MEAN:	0.78	0.95	1.25
SHS & RHS ST DEV:	0.13	0.08	
CHS MEAN:	0.80	1.01	1.28
CHS ST DEV:	0.07	0.05	
OVERALL MEAN:	**0.78**	**0.96**	**1.25**
OVERALL ST DEV:	**0.12**	**0.08**	

$F_{u,Test}$ is the test ultimate load

$F_{u,ENV}$ is the compression resistance predicted by ENV 1993-1-4 (1996)

$F_{u,Prop}$ is the compression resistance predicted by proposed design method

6.3.2.2 Bending

Table 6.13 presents a comparison between the Eurocode design procedure and the proposed design method for all tests conducted on SHS beams. Similar comparisons are presented for all RHS and CHS beams in Table 6.14 and Table 6.15 respectively. A summary is presented in Table 6.16. It should be noted that ENV 1993-1-4 (1996) contains no guidance on the calculation of effective areas or effective moduli for Class 4 CHS. These are therefore calculated using the expressions provided in BS 5950: Part 1 (2000), and repeated in Equations 6.18 and 6.19.

$$\frac{A_{eff}}{A} = \left[\frac{80}{D/t} \frac{275}{p_y} \right]^{0.5} \tag{6.18}$$

$$\frac{W_{eff}}{W_{el}} = \left[\frac{140}{D/t} \frac{275}{p_y} \right]^{0.25} \tag{6.19}$$

where A is the cross-sectional area, A_{eff} is the effective cross-sectional area, W_{el} is the elastic modulus of the cross-section, W_{eff} is the effective modulus of the cross-section, and p_y is the material design strength, taken as $\sigma_{0.2}$ in this study.

The comparisons demonstrates that the Eurocode design method predicts, on average, 72% of the test bending resistance with a standard deviation of 10%, whereas the proposed design method predicts 94% of the test bending resistance with a standard deviation of 8%. An overall increase in predicted in-plane bending strength of 33% is achieved.

6.3.2.2 Combined compression plus bending

Tests on eccentrically loaded pin-ended columns were conducted by Talja & Salmi (1995). The members were proportioned such that overall flexural buckling was the primary failure mode. These test results will therefore be compared to the buckling resistances predicted by the Eurocode and the proposed design method, in Section 6.3.3.3.

Table 6.13: *Comparison between ENV 1993-1-4 (1996) and the proposed design method for SHS beams*

Cross-section	$M_{u,Test}$ (kNm)	$\sigma_{0.2}$ (N/mm²)	E_0 (N/mm²)	ENV 1993-1-4 (1996)			Proposed method			$M_{u,Prop}/M_{u,ENV}$
				Class[1] (1-4)	$M_{u,ENV}$ (kNm)	$M_{u,ENV}/M_{u,Test}$	$\varepsilon_{LB}/\varepsilon_0$	$M_{u,Prop}$ (kNm)	$M_{u,Prop}/M_{u,Test}$	
SHS 60×60×5-B1 (TS)	15.0	463	186500	1	9.4	0.62	24.9	14.2	0.94	1.51
SHS 60×60×5-B2 (TS)	13.5	463	186500	1	9.5	0.71	26.6	14.5	1.08	1.53
SHS 60×60×5-B3 (TS)	15.2	463	186500	1	9.4	0.62	24.9	14.2	0.93	1.51
SHS 80×80×3 - B1 (MR)	13.5	422	165570	4	9.0	0.67	3.4	11.7	0.87	1.31
SHS 80×80×3 - B2 (MR)	12.9	422	165570	4	9.0	0.70	3.4	11.7	0.91	1.31
SHS 80×80×3- B3 (RH)	15.4	440	196000	4	9.6	0.62	4.4	13.0	0.84	1.35
SHS 80×80×4 - B1 (GN)	17.5	416	203200	1	12.8	0.73	8.7	16.3	0.93	1.27
SHS 100×100×2 - B1 (GN)	8.0	370	207100	4	6.9	0.86	0.9	5.8	0.72	0.84
SHS 100×100×3 - B1 (GN)	17.2	379	208800	4	12.7	0.73	2.8	15.2	0.88	1.20
SHS 100×100×4 - B1 (GN)	24.5	437	203200	3	18.8	0.76	4.8	25.7	1.05	1.37
SHS 100×100×8 - B1 (GN)	44.2	330	205200	1	31.1	0.70	38.5	47.1	1.07	1.52
SHS MEAN:						**0.70**			**0.93**	**1.34**
SHS ST DEV:						**0.07**			**0.11**	

Notes: [1] Taken as the higher of the compression flange under pure compression and web under pure bending

(GN) Gardner and Nethercot (Chapter 3)
(MR) Mirambell and Real (2000)
(RH) Rasmussen and Hancock (1993b)
(TS) Talja and Salmi (1995)

$\varepsilon_{LB}/\varepsilon_0$ is the cross-section normalised local buckling strain
$M_{u,Test}$ is the test ultimate bending moment
$M_{u,ENV}$ is the moment resistance predicted by ENV 1993-1-4 (1996)
$M_{u,Prop}$ is the moment resistance predicted by proposed design method

Table 6.14: Comparison between ENV 1993-1-4 (1996) and the proposed design method for RHS beams

Cross-section	$M_{u,Test}$ (kNm)	$\sigma_{0.2}$ (N/mm²)	E_0 (N/mm²)	ENV 1993-1-4 (1996)			Proposed method			$M_{u,Prop}/M_{u,ENV}$
				Class[1] (1-4)	$M_{u,ENV}$ (kNm)	$M_{u,ENV}/M_{u,Test}$	$\varepsilon_{LB}/\varepsilon_0$	$M_{u,Prop}$ (kNm)	$M_{u,Prop}/M_{u,Test}$	
RHS 60×40×4- B1 (GN)	10.5	469	193100	1	6.0	0.57	38.2	9.6	0.92	1.60
RHS 100×50×2- B1 (GN)	7.1	370	205900	4	5.0	0.70	5.2	7.0	0.99	1.41
RHS 100×50×3- B1 (GN)	15.4	455	200900	1	11.7	0.76	12.5	15.7	1.02	1.35
RHS 100×50×4-B1 (GN)	21.6	439	203900	1	13.9	0.64	24.0	20.4	0.94	1.47
RHS 120×80×4 - B1 (MR)	31.9	442	161160	3	20.3	0.64	5.9	30.3	0.95	1.49
RHS 120×80×4 - B2 (MR)	31.4	442	161160	3	20.3	0.65	5.9	30.3	0.97	1.49
RHS 150×100×3-B1 (TS)	26.3	305	206600	4	18.2	0.69	3.8	23.0	0.87	1.26
RHS 150×100×3-B2 (TS)	26.3	305	206600	4	18.2	0.69	3.8	22.9	0.87	1.26
RHS 150×100×3-B3 (TS)	26.3	305	206600	4	18.2	0.69	3.8	23.0	0.87	1.26
RHS 150×100×6-B1 (TS)	70.5	345	240800	1	46.5	0.66	21.6	64.0	0.91	1.38
RHS 150×100×6-B2 (TS)	70.4	345	240800	1	46.5	0.66	21.6	64.0	0.91	1.38
RHS 150×100×6-B3 (TS)	70.2	345	240800	1	46.5	0.66	21.6	63.9	0.91	1.38
RHS MEAN:						0.67			0.93	1.39
RHS ST DEV:						0.05			0.05	

Notes: [1] Taken as the higher of the compression flange under
pure compression and web under pure bending

(GN)   Gardner and Nethercot (Chapter 3)
(MR)   Mirambell and Real (2000)
(TS)   Talja and Salmi (1995)

$\varepsilon_{LB}/\varepsilon_0$ is the cross-section normalised local buckling strain
$M_{u,Test}$ is the test ultimate bending moment
$M_{u,ENV}$ is the moment resistance predicted by ENV 1993-1-4 (1996)
$M_{u,Prop}$ is the moment resistance predicted by proposed design method

Table 6.15: *Comparison between ENV 1993-1-4 (1996) and the proposed design method for CHS beams*

Cross-section	$M_{u,Test}$ (kNm)	$\sigma_{0.2}$ (N/mm²)	E_0 (N/mm²)	ENV 1993-1-4 (1996)			Proposed method			$M_{u,Prop}/M_{u,ENV}$
				Class[1] (1-4)	$M_{u,ENV}$[2] (kNm)	$M_{u,ENV}/M_{u,Test}$	$\varepsilon_{LB}/\varepsilon_0$	$M_{u,Prop}$ (kNm)	$M_{u,Prop}/M_{u,Test}$	
CHS 103×1.5-B1 (CK)	6.5	368	206000	3	4.2	0.64	4.3	5.7	0.87	1.37
CHS 153×1.5- B1 (CK)	13.4	405	203000	4	8.9	0.66	2.4	11.3	0.84	1.26
CHS 203×1.5- B1 (CK)	17.7	370	200000	4	15.1	0.86	2.1	18.4	1.04	1.22
CHS 219×2.0- B1 (CK)	27.6	332	211000	4	21.6	0.78	2.9	26.9	0.97	1.25
CHS 140×2- B1 (T)	11.6	294	200000	3	9.5	0.82	5.5	12.2	1.06	1.29
CHS 140×3- B1 (T)	19.7	317	192000	2	18.8	0.96	7.2	19.3	0.98	1.02
CHS 140×4- B1 (T)	26.0	309	197000	1	25.1	0.96	10.9	27.1	1.04	1.08
CHS 101.6×2.85- B1 (RH)	13.0	405	202000	1	11.3	0.87	8.1	13.4	1.03	1.18
CHS MEAN:						**0.82**			**0.98**	**1.21**
CHS ST DEV:						**0.12**			**0.08**	

Notes: [1] Taken as the higher of the compression flange under
pure compression and web under pure bending

[2] Effective moduli of Class 4 cross-sections
determined from Equation 6.19

(CK)   Chryssanthopoulos and Kiymaz (1998)
(T)   Talja (1997)
(RH)   Rasmussen and Hancock (1993b)

$\varepsilon_{LB}/\varepsilon_0$ is the cross-section normalised local buckling strain
$M_{u,Test}$ is the test ultimate bending moment
$M_{u,ENV}$ is the moment resistance predicted by ENV 1993-1-4 (1996)
$M_{u,Prop}$ is the moment resistance predicted by proposed design method

Table 6.16: *Summary of comparison between ENV 1993-1-4 (1996) and the proposed design method for in-plane bending resistance*

Cross-section type	$M_{u,ENV}/M_{u,Test}$	$M_{u,Prop}/M_{u,Test}$	$M_{u,Prop}/M_{u,ENV}$
SHS & RHS MEAN:	0.69	0.92	1.37
SHS & RHS ST DEV:	0.06	0.08	
CHS MEAN:	0.82	0.98	1.21
CHS ST DEV:	0.12	0.08	
OVERALL MEAN:	**0.72**	**0.94**	**1.33**
OVERALL ST DEV:	**0.10**	**0.08**	

$M_{u,Test}$ is the test ultimate bending moment

$M_{u,ENV}$ is the moment resistance predicted by ENV 1993-1-4 (1996)

$M_{u,Prop}$ is the moment resistance predicted by proposed design method

6.3.3 Buckling resistance

6.3.3.1 Compression (flexural buckling)

Table 6.17 presents a comparison between buckling resistances predicted by the Eurocode design procedure and the proposed design method for all tests conducted on long pin-ended SHS columns. Similar comparisons are presented for long fixed-ended SHS columns in Table 6.18, long pin-ended RHS columns where buckling is about the minor axis in Table 6.19, long fixed-ended RHS columns where buckling is about the minor axis in Table 6.20, long pin-ended RHS columns where buckling is about the major axis in Table 6.21, long pin-ended CHS columns in Table 6.22 and long fixed-ended CHS columns in Table 6.23. A summary of the comparisons is presented in Table 6.24.

It should be noted that for pin-ended columns, effective lengths have been taken as 1.0 times the actual length, and for fixed-ended columns, effective lengths have been taken as 0.5 times the actual length.

On average, the Eurocode design method predicts 94% of test buckling loads with a standard deviation of 14%, whereas the proposed method predicts 100% of test buckling loads with a standard deviation of 9%. An overall increase in member buckling resistance of 8% is achieved.

6.3.3.2 Bending (lateral torsional buckling)

There are no test results for RHS beams subjected to lateral torsional buckling. All tested beams have failed by in-plane bending, and the resistance is therefore determined on a cross-section level. Comparison between the Eurocode design method and the proposed design method for in-plane bending has been given in Section 6.3.2.2.

Table 6.17: *Comparison between ENV 1993-1-4 (1996) and the proposed design method for flexural buckling of pin-ended SHS columns*

Cross-section	Effective length (mm)	$F_{u,Test}$ (kN)	$\sigma_{0.2}$ (N/mm²)	E_0 (N/mm²)	ENV 1993-1-4 (1996)			Proposed method			
					Class (1-4)	$F_{u,ENV}$ (kN)	$F_{u,ENV}/F_{u,Test}$	$\varepsilon_{LB}/\varepsilon_0$	$F_{u,Prop}$ (kN)	$F_{u,Prop}/F_{u,Test}$	$F_{u,Prop}/F_{u,ENV}$
SHS 40×40×4- LC1 (AO)	889	184	592	197980	1	164	0.89	32.3	179	0.97	1.09
SHS 40×40×4- LC2 (AO)	888	184	592	197980	1	165	0.90	32.3	179	0.97	1.09
SHS 60×60×5- LC1 (TS)	1050	417	463	186500	1	356	0.85	24.7	392	0.94	1.10
SHS 60×60×5- LC2 (TS)	1700	235	463	186500	1	210	0.89	24.7	223	0.95	1.06
SHS 60×60×5- LC3 (TS)	2350	137	463	186500	1	126	0.92	24.7	135	0.99	1.07
SHS 80×80×3- LC1 (RH)	1001	390	415	196000	4	350	0.90	4.8	377	0.97	1.08
SHS 80×80×3- LC2 (RH)	2000	193	415	196000	4	237	1.23	4.8	234	1.21	0.99
SHS 80×80×3- LC3 (RH)	3002	96	415	196000	4	137	1.43	4.8	134	1.40	0.98

Notes:
(GN) Gardner and Nethercot (Chapter 3)
(AO) Ala-Outinen and Oksanen (1997)
(TS) Talja and Salmi (1995)
(RH) Rasmussen and Hancock (1993a)

$\varepsilon_{LB}/\varepsilon_0$ is the cross-section normalised local buckling strain
$F_{u,Test}$ is the test ultimate load
$F_{u,ENV}$ is the flexural buckling resistance predicted by ENV 1993-1-4 (1996)
$F_{u,Prop}$ is the flexural buckling resistance predicted by proposed design method

Table 6.17 (continued): *Comparison between ENV 1993-1-4 (1996) and the proposed design method for flexural buckling of pin-ended SHS columns*

Cross-section	Effective length (mm)	$F_{u,Test}$ (kN)	$\sigma_{0.2}$ (N/mm²)	E_0 (N/mm²)	ENV 1993-1-4 (1996)			Proposed method			$F_{u,Prop}/F_{u,ENV}$
					Class (1-4)	$F_{u,ENV}$ (kN)	$F_{u,ENV}/F_{u,Test}$	$\varepsilon_{LB}/\varepsilon_0$	$F_{u,Prop}$ (kN)	$F_{u,Prop}/F_{u,Test}$	
SHS 80×80×4- LC1 (GN)	1900	307	416	203200	1	304	0.99	8.8	310	1.01	1.02
SHS 80×80×4- LC2 (GN)	2001	293	416	203200	1	286	0.98	8.6	290	0.99	1.01
SHS 100×100×2- LC1 (GN)	2000	176	370	207125	4	125	0.71	0.9	187	1.06	1.50
SHS 100×100×3- LC1 (GN)	2000	350	379	208800	4	315	0.90	2.8	334	0.95	1.06
SHS 100×100×4- LC1 (GN)	2000	464	437	203400	4	469	1.01	4.8	475	1.02	1.01
SHS 100×100×6- LC1 (GN)	2000	842	473	197900	1	730	0.87	12.6	768	0.91	1.05
SHS 100×100×8- LC1 (GN)	2000	770	330	205200	1	748	0.97	39.0	836	1.09	1.12
SHS 150×150×4- LC1 (GN)	2000	692	294	195350	4	566	0.82	2.6	655	0.95	1.16
SHS (PINNED) MEAN:							**0.95**			**1.02**	**1.09**
SHS (PINNED) ST DEV:							**0.17**			**0.12**	

Notes: (GN)   Gardner and Nethercot (Chapter 3)
       (AO)   Ala-Outinen and Oksanen (1997)
       (TS)   Talja and Salmi (1995)
       (RH)   Rasmussen and Hancock (1993a)

$\varepsilon_{LB}/\varepsilon_0$ is the cross-section normalised local buckling strain
$F_{u,Test}$ is the test ultimate load
$F_{u,ENV}$ is the flexural buckling resistance predicted by ENV 1993-1-4 (1996)
$F_{u,Prop}$ is the flexural buckling resistance predicted by proposed design method

Table 6.18: *Comparison between ENV 1993-1-4 (1996) and the proposed design method for flexural buckling of fixed-ended SHS columns*

Cross-section	Effective length (mm)	$F_{u,Test}$ (kN)	$\sigma_{0.2}$ (N/mm²)	E_0 (N/mm²)	ENV 1993-1-4 (1996)			Proposed method			$F_{u,Prop}/F_{u,ENV}$
					Class (1-4)	$F_{u,ENV}$ (kN)	$F_{u,ENV}/F_{u,Test}$	$\varepsilon_{LB}/\varepsilon_0$	$F_{u,Prop}$ (kN)	$F_{u,Prop}/F_{u,Test}$	
SHS 70×70×2- LC1 (LY)	600	190	337	195000	4	159	0.84	2.7	201	1.06	1.26
SHS 70×70×2- LC2 (LY)	1000	188	337	195000	4	157	0.83	2.9	174	0.93	1.11
SHS 70×70×2- LC3 (LY)	1400	159	337	195000	4	133	0.84	2.7	143	0.90	1.08
SHS 70×70×2- LC4 (LY)	1800	115	337	195000	4	112	0.97	2.8	114	0.99	1.02
SHS 70×70×5- LC1 (LY)	600	669	444	194000	1	538	0.80	19.4	661	0.99	1.23
SHS 70×70×5- LC2 (LY)	1000	510	444	194000	1	482	0.94	19.8	544	1.07	1.13
SHS 70×70×5- LC3 (LY)	1400	407	444	194000	1	392	0.96	19.9	421	1.03	1.07
SHS 70×70×5- LC4 (LY)	1800	281	444	194000	1	299	1.06	19.4	313	1.12	1.05
SHS (FIXED) MEAN:							**0.91**			**1.01**	**1.12**
SHS (FIXED) ST DEV:							**0.09**			**0.07**	

Note: (LY) Liu and Young (2002)

$\varepsilon_{LB}/\varepsilon_0$ is the cross-section normalised local buckling strain

$F_{u,Test}$ is the test ultimate load

$F_{u,ENV}$ is the flexural buckling resistance predicted by ENV 1993-1-4 (1996)

$F_{u,Prop}$ is the flexural buckling resistance predicted by proposed design method

Table 6.19: *Comparison between ENV 1993-1-4 (1996) and the proposed design method for minor axis flexural buckling of pin-ended RHS columns*

Cross-section	Effective length (mm)	$F_{u,Test}$ (kN)	$\sigma_{0.2}$ (N/mm²)	E_0 (N/mm²)	ENV 1993-1-4 (1996)			Proposed method			$F_{u,Prop}/F_{u,ENV}$
					Class (1-4)	$F_{u,ENV}$ (kN)	$F_{u,ENV}/F_{u,Test}$	$\varepsilon_{LB}/\varepsilon_0$	$F_{u,Prop}$ (kN)	$F_{u,Prop}/F_{u,Test}$	
RHS 60×40×4-LC1 (GN)	1000	169	469	193100	1	180	1.07	16.4	188	1.11	1.04
RHS 100×50×2-LC1 (GN)	1000	163	370	205900	4	113	0.69	1.1	147	0.90	1.30
RHS 100×50×3-LC1 (GN)	1000	304	455	200900	4	259	0.85	2.8	284	0.93	1.10
RHS 100×50×4-LC1 (GN)	1000	422	439	203900	4	357	0.85	5.8	367	0.87	1.03
RHS 100×50×6-LC1 (GN)	1000	624	494	206267	1	561	0.90	15.2	597	0.96	1.06
RHS 120×80×3-LC1 (GN)	1001	448	429	197300	4	364	0.81	1.6	450	1.00	1.24
RHS 100×50×3-LC1 (GN)	2000	113	455	200900	4	117	1.04	2.8	121	1.07	1.03
RHS 100×50×4-LC1 (GN)	2000	165	439	203900	4	154	0.94	5.7	153	0.93	0.99
RHS 100×50×6-LC1 (GN)	2000	234	494	206267	1	226	0.96	15.4	235	1.00	1.04
RHS 120×80×3-LC1 (GN)	1999	313	429	197300	4	263	0.84	1.7	284	0.91	1.08
RHS 120×80×6-LC1 (GN)	2000	677	466	192300	1	584	0.86	8.8	594	0.88	1.02
RHS 150×100×4-LC1 (GN)	2000	515	319	200260	4	458	0.89	2.9	492	0.96	1.07
RHS MINOR (PINNED) MEAN:							**0.89**			**0.96**	**1.08**
RHS MINOR (PINNED) ST DEV:							**0.10**			**0.08**	

Note: (GN) Gardner and Nethercot (Chapter 3)

$\varepsilon_{LB}/\varepsilon_0$ is the cross-section normalised local buckling strain

$F_{u,Test}$ is the test ultimate load

$F_{u,ENV}$ is the flexural buckling resistance predicted by ENV 1993-1-4 (1996)

$F_{u,Prop}$ is the flexural buckling resistance predicted by proposed design method

Table 6.20: *Comparison between ENV 1993-1-4 (1996) and the proposed design method for minor axis flexural buckling of fixed-ended RHS columns*

Cross-section	Effective length (mm)	$F_{u,Test}$ (kN)	$\sigma_{0.2}$ (N/mm²)	E_0 (N/mm²)	ENV 1993-1-4 (1996)			Proposed method			$F_{u,Prop}/F_{u,ENV}$
					Class (1-4)	$F_{u,ENV}$ (kN)	$F_{u,ENV}/F_{u,Test}$	$\varepsilon_{LB}/\varepsilon_0$	$F_{u,Prop}$ (kN)	$F_{u,Prop}/F_{u,Test}$	
RHS 120×40×2- LC1 (YL)	599	167	350	198000	4	113	0.68	1.0	182	1.09	1.61
RHS 120×40×2- LC2 (YL)	1000	141	350	198000	4	95	0.67	1.0	134	0.95	1.41
RHS 120×40×2- LC3 (YL)	1400	96	350	198000	4	74	0.77	1.0	93	0.97	1.26
RHS 120×40×2- LC4 (YL)	1800	84	350	198000	4	54	0.65	1.0	64	0.76	1.19
RHS 120×40×5.3- LC1 (YL)	600	717	424	194000	3	582	0.81	9.7	636	0.89	1.09
RHS 120×40×5.3- LC2 (YL)	1000	417	424	194000	3	408	0.98	9.5	416	1.00	1.02
RHS 120×40×5.3- LC3 (YL)	1401	261	424	194000	3	262	1.01	9.6	265	1.02	1.01
RHS 120×40×5.3- LC4 (YL)	1800	164	424	194000	3	175	1.07	9.5	179	1.09	1.02
RHS 120×80×3- LC1 (YL)	600	398	366	193000	4	323	0.81	1.9	451	1.13	1.40
RHS 120×80×3- LC2 (YL)	1000	394	366	193000	4	319	0.81	1.8	390	0.99	1.22
RHS 120×80×3- LC3 (YL)	1400	337	366	193000	4	307	0.91	2.1	351	1.04	1.14
RHS 120×80×3- LC4 (YL)	1799	311	366	193000	4	267	0.86	2.0	291	0.94	1.09
RHS 120×80×6- LC1 (YL)	600	1222	443	194000	1	959	0.78	9.9	1199	0.98	1.25
RHS 120×80×6- LC2 (YL)	1000	970	443	194000	1	915	0.94	10.0	1025	1.06	1.12
RHS 120×80×6- LC3 (YL)	1400	860	443	194000	1	789	0.92	9.7	841	0.98	1.07
RHS 120×80×6- LC4 (YL)	1800	612	443	194000	1	666	1.09	10.3	688	1.12	1.03
RHS MINOR (FIXED) MEAN:							**0.86**			**1.00**	**1.18**
RHS MINOR (FIXED) ST DEV:							**0.14**			**0.09**	

Note: (GN) Young and Liu (2002)

Table 6.21: *Comparison between ENV 1993-1-4 (1996) and the proposed design method for major axis flexural buckling of pin-ended RHS columns*

Cross-section	Effective length (mm)	$F_{u,Test}$ (kN)	$\sigma_{0.2}$ (N/mm²)	E_0 (N/mm²)	ENV 1993-1-4 (1996)			Proposed method			$F_{u,Prop}/F_{u,ENV}$
					Class (1-4)	$F_{u,ENV}$ (kN)	$F_{u,ENV}/F_{u,Test}$	$\varepsilon_{LB}/\varepsilon_0$	$F_{u,Prop}$ (kN)	$F_{u,Prop}/F_{u,Test}$	
RHS 60×40×4- LC1 (GN)	2000	109	469	193100	1	107	0.98	17.1	112	1.03	1.05
RHS 100×50×2- LC1 (GN)	2000	157	370	205900	4	105	0.67	1.0	131	0.83	1.25
RHS 150×100×3- LC1 (TS)	2700	349	305	206600	4	298	0.85	1.4	353	1.01	1.18
RHS 150×100×3- LC2 (TS)	4350	254	305	206600	4	220	0.87	1.4	235	0.93	1.07
RHS 150×100×3- LC3 (TS)	6000	189	305	206600	4	149	0.79	1.4	153	0.81	1.03
RHS 150×100×6- LC1 (TS)	2700	830	345	240800	1	823	0.99	9.4	878	1.06	1.07
RHS 150×100×6- LC2 (TS)	4350	488	345	240800	2	575	1.18	9.0	575	1.18	1.00
RHS 150×100×6- LC3 (TS)	6000	306	345	240800	2	376	1.23	9.0	373	1.22	0.99
RHS MAJOR (PINNED) MEAN:							**0.94**			**1.01**	**1.08**
RHS MAJOR (PINNED) ST DEV:							**0.19**			**0.15**	

Notes: (GN) Gardner and Nethercot (Chapter 3)
      (TS) Talja and Salmi (1995)

$\varepsilon_{LB}/\varepsilon_0$ is the cross-section normalised local buckling strain
$F_{u,Test}$ is the test ultimate load
$F_{u,ENV}$ is the flexural buckling resistance predicted by ENV 1993-1-4 (1996)
$F_{u,Prop}$ is the flexural buckling resistance predicted by proposed design method

Table 6.22: *Comparison between ENV 1993-1-4 (1996) and the proposed design method for flexural buckling of pin-ended CHS columns*

Cross-section	Effective length (mm)	$F_{u,Test}$ (kN)	$\sigma_{0.2}$ (N/mm²)	E_0 (N/mm²)	ENV 1993-1-4 (1996)			Proposed method			$F_{u,Prop}/F_{u,ENV}$
					Class (1-4)	$F_{u,ENV}$ (kN)	$F_{u,ENV}/F_{u,Test}$	$\varepsilon_{LB}/\varepsilon_0$	$F_{u,Prop}$ (kN)	$F_{u,Prop}/F_{u,Test}$	
CHS 101.5×2.85- LC1 (RH)	1000	328	390	201000	2	359	1.09	8.9	332	1.01	0.93
CHS 101.5×2.85- LC2 (RH)	2001	241	390	201000	2	259	1.07	8.8	246	1.02	0.95
CHS 101.5×2.85- LC3 (RH)	3000	171	390	201000	2	162	0.95	8.8	166	0.97	1.03
CHS 101.5×2.85- LC4 (RH)	4000	113	390	201000	2	104	0.92	8.9	104	0.92	1.00
CHS 140×2- LC1 (T)	2250	202	319	197000	4	223	1.10	5.3	194	0.96	0.87
CHS 140×2- LC2 (T)	3350	156	319	197500	4	173	1.11	5.3	156	1.00	0.90
CHS 140×2- LC3 (T)	4449	122	318	201000	4	129	1.06	5.4	122	1.00	0.95
CHS 140×4- LC1 (T)	2251	437	293	195000	1	463	1.06	10.8	431	0.99	0.93
CHS 140×4- LC2 (T)	3350	330	293	195000	1	348	1.05	10.8	336	1.02	0.97
CHS 140×4- LC3 (T)	4450	278	294	193000	2	249	0.90	10.6	254	0.91	1.02
CHS (PINNED) MEAN:							**1.03**			**0.98**	**0.95**
CHS (PINNED) ST DEV:							**0.08**			**0.04**	

Notes: (RH) Rasmussen and Hancock (1993a)

(T) Talja (1997)

$\varepsilon_{LB}/\varepsilon_0$ is the cross-section normalised local buckling strain

$F_{u,Test}$ is the test ultimate load

$F_{u,ENV}$ is the flexural buckling resistance predicted by ENV 1993-1-4 (1996)

$F_{u,Prop}$ is the flexural buckling resistance predicted by proposed design method

Table 6.23: *Comparison between ENV 1993-1-4 (1996) and the proposed design method for flexural buckling of fixed-ended CHS columns*

Cross-section	Effective length (mm)	$F_{u, Test}$ (kN)	$\sigma_{0.2}$ (N/mm²)	E_0 (N/mm²)	ENV 1993-1-4 (1996)			Proposed method				$F_{u,Prop}/F_{u,ENV}$
					Class (1-4)	$F_{u,ENV}$ (kN)	$\frac{F_{u,ENV}}{F_{u,Test}}$	$\varepsilon_{LB}/\varepsilon_0$	$F_{u,Prop}$ (kN)	$\frac{F_{u,Prop}}{F_{u,Test}}$		
CHS 89×2.78 - LC1 (YH)	500	198	242	190000	1	178	0.90	14.7	186	0.94		1.05
CHS 89×2.78 - LC2 (YH)	750	177	242	190000	1	186	1.05	15.4	187	1.05		1.01
CHS 89×2.78 - LC3 (YH)	1001	165	242	190000	1	182	1.10	15.2	174	1.05		0.95
CHS 89×2.78 - LC4 (YH)	1250	152	242	190000	1	175	1.15	15.2	164	1.08		0.94
CHS 89×2.78 - LC5 (YH)	1501	133	242	190000	1	159	1.19	14.6	148	1.11		0.93
CHS 168.7×3.34- LC1 (YH)	500	475	247	195000	2	424	0.89	9.1	446	0.94		1.05
CHS 168.7×3.34- LC2 (YH)	750	461	247	195000	2	433	0.94	9.2	445	0.97		1.03
CHS 168.7×3.34- LC3 (YH)	1002	432	247	195000	2	419	0.97	8.9	420	0.97		1.00
CHS 324.3×4.32- LC1 (YH)	750	1120	248	202000	3	1054	0.94	6.1	1082	0.97		1.03
CHS 324.3×4.32- LC2 (YH)	1000	1088	248	202000	3	1103	1.01	6.5	1125	1.03		1.02
CHS 324.3×4.32- LC3 (YH)	1249	1046	248	202000	3	1057	1.01	6.0	1060	1.01		1.00
CHS 324.3×4.32- LC4 (YH)	1499	1010	248	202000	3	1092	1.08	6.3	1085	1.07		0.99
CHS (FIXED) MEAN:							1.02			1.02		1.00
CHS (FIXED) ST DEV:							0.10			0.06		

Note: (YH) Young and Hartono (2002)

$\varepsilon_{LB}/\varepsilon_0$ is the cross-section normalised local buckling strain
$F_{u,Test}$ is the test ultimate load
$F_{u,ENV}$ is the flexural buckling resistance predicted by ENV 1993-1-4 (1996)
$F_{u,Prop}$ is the flexural buckling resistance predicted by proposed design method

Table 6.24: *Summary of comparison between ENV 1993-1-4 (1996) and the proposed design method for flexural buckling resistance*

Cross-section type	$F_{u,ENV} / F_{u,Test}$	$F_{u,Prop} / F_{u,Test}$	$F_{u,Prop} / F_{u,ENV}$
SHS & RHS MEAN:	0.91	1.00	1.11
SHS & RHS ST DEV:	0.14	0.11	
CHS MEAN:	1.02	1.00	0.98
CHS ST DEV:	0.09	0.05	
OVERALL MEAN:	**0.94**	**1.00**	**1.08**
OVERALL ST DEV:	**0.14**	**0.09**	

$F_{u,Test}$ is the test ultimate load

$F_{u,ENV}$ is the flexural buckling resistance predicted by ENV 1993-1-4 (1996)

$F_{u,Prop}$ is the flexural buckling resistance predicted by proposed design method

6.3.3.3 Combined axial load plus bending

SHS and RHS members subjected to axial load plus major axis bending moments were tested by Salmi & Talja (1995). CHS members subjected to axial load plus bending moments were tested by Talja (1997). A comparison between the test failure loads and those predicted by the Eurocode design method and the proposed design method are presented in Table 6.25 (SHS and RHS) and Table 6.26 (CHS). No account for the possibility of lateral torsional buckling has been made, though no such effects were observed in the tests.

Stainless steel hollow section members subjected to bi-axial moments alone have not been investigated experimentally. However, FE results for such members (SHS) were generated as part of the current study, described in Section 4.10. Comparison between the FE failure moments and those predicted by the Eurocode design method and the proposed design method are presented in Table 6.27.

For SHS and RHS members subjected to combined axial load plus bending about one of the principal axes, the Eurocode design method predicts, on average, 68% of the test failure load, with a standard deviation of 12%, whereas the proposed method predicts 98% of the failure load with the same standard deviation.

For CHS members subjected to combined axial load plus bending about a single axis, the Eurocode design method predicts, on average, 79% of the test failure load, with a standard deviation of 11%, whereas the proposed method predicts 94% of the failure load, with a standard deviation of 8%.

For SHS members subjected to equal bi-axial moments, the Eurocode design method predicts, on average, 73% of the FE failure moment, with a standard deviation of 11%, whereas the proposed method predicts 94% of the FE failure moment, with a standard deviation of 3%.

Table 6.25: *Comparison between ENV 1993-1-4 (1996) and the proposed design method for pin-ended SHS and RHS members subjected to axial load plus bending moments*

Cross-section	Effective length (mm)	$F_{u,Test}$ (kN)	$\sigma_{0.2}$ (N/mm²)	E_0 (N/mm²)	ENV 1993-1-4 (1996)			Proposed method			
					Class[1] (1-4)	$F_{u,ENV}$ (kN)	$F_{u,ENV}/F_{u,Test}$	$\varepsilon_{LB}/\varepsilon_0$[1]	$F_{u,Prop}$ (kN)	$F_{u,Prop}/F_{u,Test}$	$F_{u,Prop}/F_{u,ENV}$
SHS 60x60x5-BC1 (TS)	400	322	463	186500	1	189	0.59	24.6	307	0.95	1.62
SHS 60x60x5-BC2 (TS)	1050	210	463	186500	1	141	0.67	24.6	200	0.95	1.42
SHS 60x60x5-BC3 (TS)	1700	125	463	186500	1	107	0.86	24.0	132	1.06	1.23
SHS 60x60x5-BC4 (TS)	2350	83	463	186500	1	79	0.95	24.0	95	1.14	1.20
RHS 150x100x3- BC1 (TS)	1050	209	305	206600	4	126	0.60	1.4	181	0.87	1.44
RHS 150x100x3- BC2 (TS)	2700	173	305	206600	4	99	0.57	1.4	140	0.81	1.41
RHS 150x100x3- BC3 (TS)	4350	134	305	206600	4	78	0.58	1.4	109	0.81	1.40
RHS 150x100x3- BC4 (TS)	6000	95	305	206600	4	58	0.61	1.4	87	0.92	1.50
RHS 150x100x6- BC1 (TS)	1050	569	345	240800	1	348	0.61	9.0	535	0.94	1.54
RHS 150x100x6- BC2 (TS)	2700	403	345	240800	1	263	0.65	9.4	404	1.00	1.54
RHS 150x100x6- BC3 (TS)	4350	267	345	240800	1	199	0.75	9.0	287	1.07	1.44
RHS 150x100x6- BC4 (TS)	6000	192	345	240800	1	146	0.76	9.0	225	1.17	1.54
SHS & RHS MEAN:							**0.68**			**0.98**	**1.44**
SHS & RHS ST DEV:							**0.12**			**0.12**	

Notes: [1] Eurocode cross-section class and the proposed method deformation capacity have been presented based on the pure compression load case

(TS) Talja and Salmi (1995)

$\varepsilon_{LB}/\varepsilon_0$ is the cross-section normalised local buckling strain
$F_{u,Test}$ is the test ultimate load (under concentric compression)
$F_{u,ENV}$ is eccentric compression resistance predicted by ENV 1993-1-4 (1996)
$F_{u,Prop}$ is eccentric compression resistance predicted by proposed design method

Table 6.26: Comparison between ENV 1993-1-4 (1996) and the proposed design method for pin-ended CHS members subjected to axial load plus bending moments

Cross-section	Effective length (mm)	$F_{u,Test}$ (kN)	$\sigma_{0.2}$ (N/mm²)	E_0 (N/mm²)	Class[1] (1-4)	$F_{u,ENV}$ (kN)	$F_{u,ENV}/F_{u,Test}$	$\varepsilon_{LB}/\varepsilon_0$ [1]	$F_{u,Prop}$ (kN)	$F_{u,Prop}/F_{u,Test}$	$F_{u,Prop}/F_{u,ENV}$
					ENV 1993-1-4 (1996)			Proposed method			
CHS 140x2- BC1 (T)	550	122	294	200000	4	78	0.64	5.4	106	0.87	1.36
CHS 140x2- BC2 (T)	2251	89	294	200000	4	65	0.73	5.4	79	0.89	1.22
CHS 140x2- BC3 (T)	3351	73	294	200000	4	55	0.75	5.4	67	0.92	1.22
CHS 140x2- BC4 (T)	4451	58	294	200000	4	49	0.84	5.4	59	1.02	1.20
CHS 140x4- BC1 (T)	550	297	309	197000	1	204	0.69	11.0	251	0.85	1.23
CHS 140x4- BC2 (T)	2250	202	309	197000	1	165	0.82	10.9	184	0.91	1.12
CHS 140x4- BC3 (T)	3351	155	309	197000	1	136	0.88	10.8	152	0.98	1.12
CHS 140x4- BC4 (T)	4451	121	309	197000	1	119	0.98	10.9	131	1.08	1.10
CHS MEAN:							**0.79**			**0.94**	**1.20**
CHS ST DEV:							**0.11**			**0.08**	

Notes: [1] Eurocode cross-section class and the proposed method deformation capacity have been presented based on the pure compression load case

(T) Talja (1997)

$\varepsilon_{LB}/\varepsilon_0$ is the cross-section normalised local buckling strain
$F_{u,Test}$ is the test ultimate load (under concentric compression)
$F_{u,ENV}$ is eccentric compression resistance predicted by ENV 1993-1-4 (1996)
$F_{u,Prop}$ is eccentric compression resistance predicted by proposed design method

Table 6.27: Comparison between ENV 1993-1-4 (1996) and the proposed design method for pin-ended SHS members subjected to equal bi-axial bending moments

Cross-section	$M_{u,Test}$ (kNm)	$\sigma_{0.2}$ (N/mm²)	E_0 (N/mm²)	ENV 1993-1-4 (1996)			Proposed method			$M_{u,Prop}/M_{u,ENV}$
				$Class^1$ (1-4)	$M_{u,ENV}$ (kNm)	$F_{u,ENV}/F_{u,Test}$	$\varepsilon_{LB}/\varepsilon_0{}^1$	$M_{u,Prop}$ (kNm)	$M_{u,Prop}/M_{u,Test}$	
SHS 80×80×2- BB1- FE (GN)	3.5	416	203200	4	3.2	0.91	1.7	3.2	0.91	1.00
SHS 80×80×3- BB1- FE (GN)	6.7	416	203200	3	4.5	0.68	5.0	6.2	0.93	1.37
SHS 80×80×4- BB1- FE (GN)	9.4	416	203200	1	6.8	0.73	10.0	8.9	0.95	1.30
SHS 80×80×5- BB1- FE (GN)	11.7	416	203200	1	8.2	0.70	17.1	11.5	0.99	1.40
SHS 80×80×6- BB1- FE (GN)	15.7	416	203200	1	9.5	0.60	26.3	14.1	0.90	1.49
SHS & RHS MEAN:						0.73			0.94	1.31
SHS & RHS ST DEV:						0.11			0.03	

Notes: ¹ Eurocode cross-section class and the proposed method deformation capacity have been presented based on the pure compression load case

(GN) Gardner and Nethercot (Chapter 4)

$\varepsilon_{LB}/\varepsilon_0$ is the cross-section normalised local buckling strain

$F_{u,Test}$ is the test ultimate load (under concentric compression)

$F_{u,ENV}$ is eccentric compression resistance predicted by ENV 1993-1-4 (1996)

$F_{u,Prop}$ is eccentric compression resistance predicted by proposed design method

6.4 WORKED EXAMPLES

The purpose of this section is to demonstrate the workings of the proposed design method presented in Section 6.2 for different cross-section types (CHS, SHS and RHS) under various loading configurations. The geometric and material properties of the tested specimens will be used to allow comparison with the test results, and demonstrate how the predicted results in Section 6.3 were derived.

6.4.1 Compression resistance

The predicted compression resistance of the RHS 60×40×4- SC1 stub column, tested as part of the current study, was determined as follows:

Cross-section properties:

D	=	$60.0\,mm$	B	= $40.0\,mm$
t	=	$3.83\,mm$	r_i	= $2.9\,mm$
A	=	$675.0\,mm^2$		

Material properties:

$$\sigma_{0.2} = 469\,N/mm^2 \qquad E_0 = 193100\,N/mm^2$$

$$\varepsilon_0 = \sigma_{0.2}/E_0 = 469/193100 = 0.0024$$

Cross-section slenderness, β for longer face in pure compression (Equation 6.1):

$$\beta = \left(\frac{b}{t}\right)\sqrt{\frac{\sigma_{0.2}}{E_0}}\sqrt{\frac{4.0}{k}} = \left(\frac{60.0-3.83}{3.83}\right)\sqrt{\frac{469}{193100}}\sqrt{\frac{4.0}{4.0}} = 0.72$$

Deformation capacity, $\varepsilon_{LB}/\varepsilon_0$ (Equation 6.3):

$$\frac{\varepsilon_{LB}}{\varepsilon_0} = \frac{7.07}{\beta^{2.13+0.21\beta}}\chi^{-0.30\beta^{0.5}} = \frac{7.07}{0.72^{2.13+0.21(0.72)}}0.67^{-0.30\times0.72^{0.5}} = 16.4$$

$$\therefore \quad \varepsilon_{LB} \quad = \quad 16.4 \times 0.0024 \quad = \quad 0.040$$

Local buckling stress, σ_{LB} (Table 6.2):

By linear interpolation, $\sigma_{LB} \quad = \quad 693.4 \ N/mm^2$

Compression resistance (Equation 6.5):

$$N_{c, Rd} \quad = \quad A \ \sigma_{LB} \quad = \quad 675.0 \times 693.4 \times 10^{-3} \quad = \quad 468 \ kN$$

[Eurocode compression resistance = 317 kN; Test ultimate load = 492 kN]

6.4.2 In-plane bending resistance

The predicted in-plane bending resistance of the CHS 101.6×2.85- B1 simply-supported beam, tested by Rasmussen Hancock (1993b), was determined as follows:

Cross-section properties:

D_0	=	*102.1 mm*	t	= *2.84 mm*
A	=	*885.6 mm^2*	W_{el}	= *21383 mm^3*
W_{pl}	=	*27989 mm^3*	a_p	= *1.31*

Material properties:

$$\sigma_{0.2} \quad = \quad 405 \ N/mm^2 \qquad E_0 \quad = \quad 202000 \ N/mm^2$$

$$\varepsilon_0 \quad = \quad \sigma_{0.2}/E_0 \quad = \quad 405/202000 \quad = \quad 0.0020$$

Cross-section slenderness, β (Equation 6.2):

$$\beta = (R/t)(\sigma_{0.2}/E_0) \qquad = \qquad \left(\frac{102.1-2.84}{2\times2.84}\right)\left(\frac{405}{202000}\right) \qquad = \qquad 0.0350$$

Deformation capacity, $\varepsilon_{LB}/\varepsilon_0$ (Equation 6.4):

$$\frac{\varepsilon_{LB}}{\varepsilon_0} = \frac{0.116}{\beta^{1.21+1.69\beta}} = \frac{\varepsilon_{LB}}{\varepsilon_0} = \frac{0.116}{0.035^{1.21+(1.69\times0.035)}} = 8.17$$

$$\therefore \quad \varepsilon_{LB} = 8.17 \times 0.0020 = 0.0163$$

Generalised shape factor (Equation 6.7 and Table 6.5):

$$a_g = A_1 + A_2\varepsilon_0 + A_3a_p + A_4\varepsilon_0 a_p$$

For $\varepsilon_{LB} = 0.016$: $A_1 = 0.151$ $A_2 = 22.66$ $A_3 = 1.09$ $A_4 = -34.37$

$$a_g = 0.151 + (22.66 \times 0.002) + (1.09 \times 1.31) + (-34.37 \times 0.002 \times 1.31) = 1.53$$

For $\varepsilon_{LB} = 0.018$: $A_1 = 0.153$ $A_2 = 20.94$ $A_3 = 1.11$ $A_4 = -31.25$

$$a_g = 0.153 + (20.94 \times 0.002) + (1.11 \times 1.31) + (-31.25 \times 0.002 \times 1.31) = 1.57$$

$\therefore$ *For $\varepsilon_{LB} = 0.0163$, $a_g = 1.54$ (by linear interpolation)*

In-plane bending resistance (Equation 6.6):

$$M_{c,Rd} = W_{el}\,\sigma_{0.2}\,a_g = 21383 \times 405 \times 1.54 \times 10^{-6} = 13.4\ kNm$$

[Eurocode bending resistance = 11.3 kNm; Test ultimate bending moment = 13.0 kNm]

6.4.3 Flexural buckling resistance

The predicted minor axis flexural buckling resistance of the RHS 120×80×6- LC3 fixed-ended column, tested by Young & Liu (2002), was determined as follows:

Cross-section properties:

$D = 120.3\ mm$ $B = 80.6\ mm$

t = $5.96\ mm$ r_i = $6.5\ mm$

L = $2800\ mm$ A = $2155.6\ mm^2$

I_z = $31.76\ mm$

Material properties:

$\sigma_{0.2}$ = $443\ N/mm^2$ E_0 = $194000\ N/mm^2$

ε_0 = $\sigma_{0.2}/E_0$ = $443/194000$ = 0.0023

Cross-section slenderness, β for longer face in compression (Equation 6.1):

$$\beta = \left(\frac{b}{t}\right)\sqrt{\frac{\sigma_{0.2}}{E_0}}\sqrt{\frac{4.0}{k}} = \left(\frac{120.3-5.96}{5.96}\right)\sqrt{\frac{443}{194000}}\sqrt{\frac{4.0}{4.0}} = 0.92$$

Deformation capacity, $\varepsilon_{LB}/\varepsilon_0$ (Equation 6.3):

$$\frac{\varepsilon_{LB}}{\varepsilon_0} = \frac{7.07}{\beta^{2.13+0.21\beta}}\chi^{\frac{-0.30}{\beta^{0.5}}} = \frac{7.07}{0.92^{2.13+0.21(0.92)}}0.67^{-0.30\times0.92^{0.5}} = 9.7$$

$\therefore$ ε_{LB} = 9.7×0.0023 = 0.022

Local buckling stress, σ_{LB} (Table 6.2):

By linear interpolation, σ_{LB} = $602\ N/mm^2$

Flexural buckling resistance (Equation 6.9):

From Table 6.6, a = 0.70, $\overline{\lambda}_0$ = 0.44

λ = L_E/i_z = $(0.5\times2800)/31.76$ = 44.08

$$\lambda_1 = \pi [E_0/\sigma_{0.2}]^{0.5} = \pi [194000/443]^{0.5} = 65.74$$

$$\overline{\lambda} = \lambda/\lambda_1 = 44.08/65.74 = 0.67$$

$$\phi = 0.5[1 + \alpha(\overline{\lambda} - \overline{\lambda}_0) + \overline{\lambda}^2] = 0.5[1 + 0.70(0.67 - 0.44) + 0.67^2] = 0.81$$

$$\chi = \frac{1}{\phi + [\phi^2 - \overline{\lambda}^2]^{0.5}} = \frac{1}{0.81 + [0.81^2 - 0.67^2]^{0.5}} = 0.80$$

$$\therefore N_{b.Rd} = \chi A \sigma_{0.2} \left(\frac{\sigma_{LB}}{\sigma_{0.2}}\right)^{0.32} = 0.80 \times 2155.6 \times 443 \times (602/443)^{0.32} = 841\ kN$$

[Eurocode flexural buckling resistance = 789 kN; Test ultimate load = 860 kN]

6.4.4 Buckling resistance of members subjected to combined axial load plus bending

The predicted member resistance of the pin-ended CHS 140×2- BC3 subjected to combined axial load plus bending moment, tested by Talja (1997), was determined as below. It should be noted that the bending moment was introduced though an eccentricity of loading, e of $(D_0 - t)/2$.

Cross-section properties:

D_0	=	139.8 mm	t = 1.95 mm	
A	=	844.5 mm^2	W_{el} = 28703 mm^3	
W_{pl}	=	37058 mm^3	a_p = 1.29	
L	=	3351 mm	i = 48.74 mm	
e	=	68.93 mm		

Material properties:

$$\sigma_{0.2} = 294\ N/mm^2 \qquad E_0 = 200000\ N/mm^2$$

$$\varepsilon_0 = \sigma_{0.2}/E_0 = 294/200000 = 0.0015$$

Cross-section slenderness, β (Equation 6.2):

For CHS, β is the same in compression and bending.

$$\beta = (R/t)(\sigma_{0.2}/E_0) \qquad = \qquad \left(\frac{139.8-1.95}{2\times1.95}\right)\left(\frac{294}{200000}\right) \qquad = \qquad 0.052$$

Deformation capacity, $\varepsilon_{LB}/\varepsilon_0$ (Equation 6.4):

$$\frac{\varepsilon_{LB}}{\varepsilon_0} = \frac{0.116}{\beta^{1.21+1.69\beta}} \qquad = \qquad \frac{\varepsilon_{LB}}{\varepsilon_0} = \frac{0.116}{0.052^{1.21+(1.69\times0.052)}} \qquad = \qquad 5.39$$

$$\therefore \quad \varepsilon_{LB} \quad = \quad 5.39 \times 0.0015 \quad = \quad 0.0079$$

Local buckling stress, σ_{LB} (Table 6.3):

By linear interpolation, $\sigma_{LB} = 338.2 \ N/mm^2$

Flexural buckling resistance (Equation 6.10):

From Table 6.6, $\quad \alpha = 0.50, \qquad \overline{\lambda}_0 = -0.10$

$$\lambda \quad = \quad L_E/i \qquad = \quad 3351/48.74 \quad = \quad 68.75$$

$$\lambda_1 \quad = \quad \pi [E_0/\sigma_{0.2}]^{0.5} \quad = \quad \pi [200000/294]^{0.5} \quad = \quad 81.98$$

$$\overline{\lambda} \quad = \quad \lambda/\lambda_1 \qquad = \quad 68.75/81.94 \qquad = \quad 0.84$$

$$\phi \quad = \quad 0.5[1 + \alpha(\overline{\lambda} - \overline{\lambda}_0) + \overline{\lambda}^2] \qquad = \qquad 0.5[1 + 0.50(0.84-(-0.10)) + 0.84^2] \qquad = \qquad 1.09$$

$$\chi \quad = \quad \frac{1}{\phi + [\phi^2 - \overline{\lambda}^2]^{0.5}} \qquad \cdot \qquad = \qquad \frac{1}{1.09 + [1.09^2 - 0.84^2]^{0.5}} \qquad = \qquad 0.56$$

$$\therefore \quad N_{b.Rd} \quad = \quad \chi A \sigma_{0.2} \left(\frac{\sigma_{LB}}{\sigma_{0.2}}\right)^{0.80} \quad = \quad 0.56 \times 844.5 \times 294 \times (338/294)^{0.80} \quad = \quad 156 \ kN$$

Generalised shape factor (Equation 6.7 and Table 6.5):

$$a_g = A_1 + A_2\varepsilon_0 + A_3 a_p + A_4\varepsilon_0 a_p$$

For $\varepsilon_{LB} = 0.0070$: $A_1 = 0.108$ $A_2 = 100.00$ $A_3 = 1.05$ $A_4 = -125.00$

$$a_g = 0.108 + (100.00 \times 0.0015) + (1.05 \times 1.29) + (-125.00 \times 0.0015 \times 1.29) = 1.37$$

For $\varepsilon_{LB} = 0.0080$: $A_1 = 0.124$ $A_2 = 70.94$ $A_3 = 1.05$ $A_4 = -93.75$

$$a_g = 0.124 + (70.94 \times 0.0015) + (1.05 \times 1.29) + (-93.75 \times 0.0015 \times 1.29) = 1.40$$

$\therefore$ *For* $\varepsilon_{LB} = 0.0079$, $a_g = 1.40$ *(by linear interpolation)*

In-plane bending resistance (Equation 6.6):

$$M_{c,Rd} = W_{el}\,\sigma_{0.2}\,a_g = 28703 \times 294 \times 1.40 \times 10^{-6} = 11.8\,kNm$$

Interaction between axial load and bending (Equation 6.13):

By trial and error (since applied bending moment is a function of applied axial load),

Take $N_{Sd} = 66.6\,kN$ $\therefore$ $M_{Sd} = 66.6 \times 68.93 = 4.6\,kNm$

$\beta_{My} = 1.1$ *for uniform bending moments (Table 6.7)*

$$\mu_y = \overline{\lambda}_y(2\beta_{My} - 4) + (a_{gy} - 1),\ \ [but\ \leq 0.90] = 0.84((2 \times 1.1) - 4) + (1.40 - 1) = -1.11$$

$$\kappa_y = 1 - \frac{\mu_y N_{Sd}}{N_{b,Rd,y}}\ \ but\ \kappa_y \leq 1.5 = 1 - \frac{-1.11 \times 66.6}{156} = 1.47$$

The following interaction expression should be satisfied:

$$\frac{N_{Sd}}{\chi_{min}\,\sigma_{0.2}\,A(\sigma_{LB}/\sigma_{0.2})^{0.80}} + \frac{\kappa_y\,M_{y,Sd}}{W_{el,y}\,\sigma_{0.2}\,a_{gy}} + \frac{\kappa_z\,M_{z,Sd}}{W_{el,z}\,\sigma_{0.2}\,a_{gz}} \leq 1$$

$$\frac{66.6}{156} + \frac{1.47 \times 4.6}{11.8} + 0 \quad = \quad 0.43 + 0.57 \quad = \quad 1.00$$

∴ Eccentric compression resistance, N_{Sd} = 66.6 kN

[Eurocode eccentric compression resistance = 55 kN; Test ultimate eccentric load= 73 kN]

6.5 CONCLUDING COMMENTS

In this chapter, a new design method for stainless steel hollow section structures loaded in compression, bending and combined compression plus bending has been presented. Worked examples have been included to demonstrate the calculation steps involved in the method.

The approach has been validated against all available test results and compared with the current European design guidance given in ENV 1993-1-4 (1996). A summary of the comparisons is presented in Table 6.28.

Table 6.28: Summary of comparison between ENV 1993-1-4 (1996)
and the proposed design method for all test results

	Configuration	ENV/ Test	Proposed / Test	Proposed / ENV
Cross-section resistance	Compression	78% ± 12%	96% ± 8%	125%
	Bending	72% ± 10%	94% ± 8%	133%
	Compression + bending	-	-	-
	All	76% ± 12%	95% ± 8%	128%
Member resistance	Flexural buckling	94% ± 14%	100% ± 9%	108%
	Bending	72% ± 10%	94% ± 8%	133%
	Flexural buckling + bending	73% ± 13%	96% ± 11%	134%
	All	86% ± 17%	98% ± 10%	117%
Overall	**All**	**82% ± 16%**	**97% ± 9%**	**121%**

In addition to the clear benefit in terms of enhanced strength prediction (21% overall), the reduction in scatter (standard deviation) of the prediction is also advantageous since design curves are typically 2-3 standard deviations below mean curves. The design method represents a considerable material and thus cost saving. It is envisaged that the proposed design method will be considered for incorporation into future revisions of Eurocode 3, bringing greater efficiency to structural stainless steel design and promoting more widespread use of the material.

CHAPTER 7

CONCLUSIONS AND SUGGESTIONS FOR FURTHER WORK

7.1 CONCLUSIONS

This section summarises the important findings from the project and presents the overall conclusions. More detailed concluding comments may be found at the end of each of the individual chapters.

Current structural stainless steel design codes are based largely on assumed analogies with carbon steel behaviour. This is advantageous for designers in terms of ease of transition from carbon steel to stainless steel structural design, but detrimental in terms of making efficient use of the particular behavioural properties exhibited by stainless steel. The primary objective of this study has therefore been to develop a more rational and efficient design method for stainless steel structures, whilst, where possible, maintaining consistency with the carbon steel design approach.

The process of developing the proposed design method has involved; reviewing existing design rules, creating a compilation of available laboratory test data, conducting further laboratory tests in key areas, using FE modelling to investigate the importance of individual parameters and to

generate further results, formulating the design method and validating it against test data. This process has predominantly defined the shape and flow of the thesis. The literature review revealed widespread interest in the subject, though limited laboratory test data existed.

Chapter 3 described a laboratory testing programme conducted as part of the current study. Tensile and compressive coupon tests were conducted to determine the material stress-strain characteristics of the tested cross-sections. Stub column tests were used to calibrate an expression, originally devised for aluminium, defining a relationship between stainless steel cross-section slenderness and cross-section deformation capacity. Member tests were conducted to provide a means of validating the proposed design method.

A total of 33 stub column tests, 22 pin-ended column tests and 9 simply-supported beam tests were performed. The tests were carefully conducted and reported and now represent a major contribution to the pool of available experimental results on stainless steel structures.

Numerical modelling of the structural response of stainless steel hollow sections was described in Chapter 4. The aim of the investigation was to develop a consistent approach to the modelling of stainless steel structures. The developed FE models are more sophisticated than any other reported attempts to model stainless steel structural behaviour, with general expressions defined for material stress-strain behaviour, enhanced strength corner properties, initial geometric imperfection modes and amplitudes (local and global), and residual stresses. The general expressions define a consistent means of describing the key input parameters.

A compound (two-stage) Ramberg-Osgood model was developed to describe stainless steel material stress-strain behaviour. The model provides a very accurate description of observed behaviour, and can be applied equally to the modelling of tensile and compressive stress-strain curves. For the prediction of enhanced strength corner properties, a simple, though accurate model was proposed. Characterisation of local plate imperfection amplitudes in stainless steel SHS and RHS has not previously been attempted. A first attempt is described in Chapter 4, where a model originally devised for hot-rolled carbon steel cross-sections was re-calibrated and applied to stainless steel cross-sections.

Numerical prediction of the key performance measures from tests was achieved with a high degree of accuracy: On average, ultimate load was predicted to within 3% and with a low standard deviation; deformation at ultimate load was within 6%, but exhibited a higher standard

deviation; and the general form of the load-deformation response and the failure modes were similar.

The proposed design method was developed in Chapter 5. Throughout its development thought had to be given to the final form in which the design method would appear. Counter intuitive occurrences, such as effective cross-sectional areas greater than gross cross-sectional areas were avoided. Likewise, procedures requiring iteration were also minimised, and where possible consistency with the carbon steel rules was maintained.

The new design approach recognises that placing cross-sections into discrete behavioural classes is inappropriate for stainless steel, since there is no sharply defined yield point. Instead, with a more appropriate material model, member strengths are assessed using a local buckling strength derived from the deformation capacity of the cross-section. It may therefore be viewed as a continuous method of cross-section classification and member design. Additional refinement has been achieved by taking account of the interaction between the elements that make up a cross-section.

Chapter 6 presented the proposed design method in a straightforward form. Design rules were set out for hollow sections (SHS, RHS and CHS) subjected to compression, bending and combined compression plus bending. No account was made for lateral torsional buckling, though this is rarely a problem for hollow section members. Worked examples were included to demonstrate the design steps involved in the proposed design approach.

In order to verify the method, comparison was made between predicted results and experimental results for all available tests on stainless steel hollow sections. Comparison was also made with the current structural stainless steel design guidance given in ENV 1993-1-4 (1996). The results showed that the ENV 1993-1-4 method predicted, on average, 82% of the test failure load, with a standard deviation of 16%, whereas the proposed method predicted, on average, 97% of the test failure load, with a standard deviation of 9%, providing an average increase in member resistance of 21%. This represents a considerable material and thus cost saving.

Overall, the objective of achieving a more rational and efficient structural design method for stainless steel has been met. The design approach is also more consistent than current stainless steel design methods, in that it applies the same method over the full range of cross-sectional slenderness, and it involves a similar volume of calculations. It is envisaged that the proposed

design method will be considered for incorporation into future revisions of Eurocode 3, bringing greater efficiency to structural stainless steel design and promoting more widespread use of the material.

7.2 SUGGESTIONS FOR FURTHER WORK

The suggestions for further work fall into two main categories; the first relate to the extension of the proposed design method, and the second to more general thoughts that have emerged throughout the course of the investigation.

7.2.1 Extension of the proposed design method

The proposed design method is currently limited to stainless steel hollow sections. Although these represent the most widely used cross-sections for structural applications, extension of the design method to cover the design of open-sections will form an important part of promoting the method for wider use. For acceptance by Standards committees and designers, guidance covering all types of structural cross-sections is more desirable. Additionally, statistical analysis of the proposed method should be conducted in order to derive suitable safety factors for design purposes.

The design of structures at elevated temperatures has attracted increasing attention in recent years, with the current European fire design rules given in ENV 1993-1-2 (1995). Extension of the proposed design method to cover members at the fire limit state could be investigated, with elevated temperature material properties used in place of those at room temperature.

Similarities exist between stainless steel stress-strain behaviour and that of aluminium and high strength carbon steel. All demonstrate a degree of material non-linearity; and this makes the use of the elastic, perfectly-plastic material model questionable. Possible application of the proposed design method to these materials may be investigated.

7.2.2 Other ideas

Stainless steel exhibits a pronounced response to strain hardening. Currently, exploitation of the resulting strength enhancements is minimal. The proposed design approach offers a means of

accounting for the material non-linearity, but minimum specified values of 0.2% proof strength will still need to be taken from a material specification. However, it was shown in Chapter 3 that the 0.2% proof strengths of flat material contained within the cold-formed stainless steel cross-sections tested as part of the current study were in excess of two times those presented in the current material specification.

Clearly large increases in member resistances could be achieved by harnessing these material strength enhancements. It is suggested that a carefully conducted study, in co-operation with material producers and cross-section fabricators, could be conducted in order to derive a relationship between product type, material grade, fabrication method and the material strength of the finished cross-sections.

More ambitious would be to attempt to develop a means of considering the total strain path that a given product follows from the molten material stage, through the rolling of the flat sheet and finally to the shaping into the finished cross-section, with a view to defining parameters to enable the reliable prediction of the material properties for any cross-section with a specified material grade and process route. Strategic modifications of the process route may then be considered to achieve a desired distribution of strength, with the possibility of controlled peening of material to attain localised strength enhancements.

Sustainability and life-cycle costing are important arguments for selecting stainless steel as a constructional material. However, previous comparisons of the relative life-cycle costs of stainless steel with the more traditional structural materials of carbon steel and reinforced concrete have been limited in scope and only semi-quantitative. A more detailed study, including the material cost savings achieved with the proposed design method, could be conducted to demonstrate the level of whole-life cost savings typically attainable for stainless steel structures.

REFERENCES

ABAQUS (1999). ABAQUS/ Standard User's Manual Volumes I-III and ABAQUS Post Manual. Version 5.8. Hibbitt, Karlsson & Sorensen, Inc. Pawtucket, USA.

Abdel-Rahman, N. & Sivakumaran, K. S. (1997). Material properties models for analysis of cold-formed steel members. *Journal of Structural Engineering*, ASCE. **123:9**, 1135-1143.

AISI (1974). Stainless Steel Cold-Formed Structural Design Manual. *American Iron and Steel Institute*. Washington, D.C.

AISI (1986). Cold-formed Steel Design Manual. *American Iron and Steel Institute*. Washington, D.C.

Ala-Outinen, T. (1999). Stainless steel compression members exposed to fire. *Proceedings of the Fourth International Conference on Steel and Aluminium Structures, ICSAS '99*. Edited by Mäkeläinen, P. and Hassinen, P. Espoo, Finland. 523-530.

Ala-Outinen, T. & Oksanen, T. (1997). Stainless steel compression members exposed to fire. *Research Note 1864*, VTT Building Technology, Finland.

American Society for Testing and Materials. (1987). Standard Methods and Definitions for Mechanical Testing of Steel Products. ASTM A370-87a. Annual Book of ASTM Standards.

Aoki, H. (2000). Establishment of design standards and current practice for stainless steel structural design in Japan. *Journal of Constructional Steel Research.* **54**, 191-210.

ASCE (1991). Specification of the Design of Cold-Formed Stainless Steel Structural Members, ANSI/ASCE 8-90. *American Society of Civil Engineers.* New York.

Ayrton, W. E. & Perry, J. (1886). On struts. *The Engineer.* **62**, 464-465 and 513-514.

Aust/NZS. (2001). Cold-formed stainless steel structures. Australian/ New Zealand Standard AS/NZS 4673:2001. Sydney, Australia: Standards Austalia.

Baddoo, N. R. & Gardner, L. (2000). WP5.2: Member behaviour at elevated temperatures. ECSC project – Development of the use of stainless steel in construction. Contract No. 7210 SA/ 842. The Steel Construction Institute, UK.

Baddoo, N. R. & Burgan, B. A. (2001). Structural Design of Stainless Steel (P291). The Steel Construction Institute, UK.

Baddoo, N. R., Burgan, R. & Ogden, R. (1997). Architects' Guide to Stainless Steel. P179. The Steel Construction Institute, UK.

Bredenkamp, P. J. & Van den Berg, G. J. (1995). The strength of stainless steel built-up I-section columns. *Journal of Constructional Steel Research.* **34**, 131-144.

Bredenkamp, P. J., Van den Berg, G. J., & Van der Merwe, P. (1992). Residual stresses and the strength of stainless steel I-section columns. *Proceedings of the Structural Stability Research Council, Annual Technical Session.* Pittsburg, U.S.A. 69-86.

Bulson, P.S. (1970). The stability of flat plates. 63-77. Chatto and Windus, London.

Burgan, B. A. (1992). Concise Guide to the Structural Design of Stainless. The Steel Construction Institute, UK.

BS 5950-1. (1990). Structural use of steelwork in buildings – Part 1: Code of practice for design in simple and continuous construction: hot rolled sections. British Standards Institution.

BS 5950-1. (2000). Structural use of steelwork in buildings – Part 1: Code of practice for design in simple and continuous construction: hot rolled sections. British Standards Institution.

BS EN 10088-1. (1995). Stainless steels – Part 1: List of stainless steels. British Standards Institution.

BS EN 10088-2. (1995). Stainless steels – Part 2: Technical delivery conditions for sheet/plate and strip for general purposes. British Standards Institution.

Centre for Advanced Structural Engineering. (1990). Compression tests of stainless steel tubular columns. Investigation Report S770. University of Sydney.

Chen, W. F. & Lui, E. M. (1991). Stability design of steel frames. CRC Press, Inc. 243-251.

Chen, W. F. & Ross, D. A. (1977). Test of fabricated tubular columns. *Journal of Structural Division*, ASCE. **103:3**, 619-634.

Chou, S.M., Chai, G. B. & Ling, L. (2000). Finite element technique for design of stub columns. *Thin-Walled Structures*. **37**, 97-112.

Chryssanthopoulos, M. K. & Low, Y. M. (2001). A method for predicting the flexural response of tubular members with non-linear stress-strain characteristics. *Journal of Constructional Steel Research*. **57**. 1197-1216.

Chryssanthopoulos, M. K. & Kiymaz, G. (1998). Bending tests of stainless steel circular hollow sections. *CESLIC Report No. OR12*. Engineering Structures Laboratory, Department of Civil Engineering. Imperial College, London.

Coetzee, J. S., Van den Berg, G. J., & Van der Merwe, P. The effect of workhardening and residual stresses due to cold-work of forming on the strength of cold-formed stainless steel

lipped channel sections. *Proceedings of the Tenth International Speciality Conference on Cold-Formed Steel Structures*. St. Louis, Missouri, U.S.A.

Dawson, R. G. & Walker, A. C. (1972). Post-buckling of geometrically imperfect plates. *Journal of the Structural Division*, ASCE. **98: ST1**, 75-94.

Dier, A. (1991). Tests on stainless steel beams and columns. Technical Report No. 29. Document No. SCI-RT-231. The Steel Construction Institute, UK.

Dubuc, J., Krivobok, V. N. & Welter, G. (1956). Studies of type 301 stainless steel columns. *ASTM Special Technical Publication No. 196*. USA.

ENV 1993-1-1 (1992). Eurocode 3: Design of steel structures – Part 1.1: General rules and rules for buildings. CEN.

ENV 1993-1-2 (1995). Eurocode 3: Design of steel structures – Part 1.2: General rules – Structural fire design. CEN.

ENV 1993-1-3. (1996). Eurocode 3: Design of steel structures – Part 1.3: General rules – Supplementary rules for cold formed thin gauge members and sheeting. CEN.

ENV 1993-1-4. (1996). Eurocode 3: Design of steel structures - Part 1.4: General rules - Supplementary rules for stainless steel. CEN.

ENV 1999-1-1. (1998). Eurocode 9: Design of aluminium structures – Part 1.1: General rules – General rules and rules for buildings. CEN.

Euro Inox (1994). Design Manual for Structural Stainless Steel. NiDI. Toronto, Canada.

Euro Inox (2002). Design Manual for Structural Stainless Steel. 2nd Edition. NiDI. Toronto, Canada.

Faella, C., Mazzolani, F. M., Piluso, V. and Rizzano, G. (2000). Local buckling of aluminium members: testing and classification. *Journal of Structural Engineering, ASCE.* **126:3,** 353-360.

Galambos, T. V., Editor. (1998). Guide to stability design criteria for metal structures. 4th Edition. *Structural Stability Research Council.* John Wiley & Sons, Inc. New York.

Gao, S., Usami, T. & Ge, H. (1998). Ductility of steel short cylinders in compression and bending. *Journal of Engineering Mechanics,* ASCE. 124:2, 176-183.

Gardner, L. & Nethercot, D. A. (2001a). Numerical modelling of cold-formed stainless steel sections. *Proceedings of the Ninth Nordic Steel Construction Conference.* Edited by Mäkeläinen et al. Helsinki, Finland. 781-789.

Gardner, L. & Nethercot, D. A. (2001b). Behaviour of stainless steel cross-sections. *Proceedings of the Ninth Nordic Steel Construction Conference.* Edited by Mäkeläinen et al. Helsinki, Finland. 773-780.

Gardner, L. & Nethercot, D. A. (2001c). Towards improved stainless steel structural design. *Festschrift Greiner.* Edited by Ofner, R. and Unterweger, H. TV, Graz. 9-18.

Gardner, L. & Nethercot, D. A. (2002). Improved efficiency for stainless steel structures. *Proceedings of the International Iron and Steel Institute World Conference 2002: Steel in Sustainable Construction.* Edited by Sansom, M. Luxemburg Congrès, Luxemburg. 75-80.

Hammer, E. W. Jr. & Petersen, R. E. (1955). Column curves for type 301 stainless steel. *Aeronautical Engineering Review.* **14:12,** 33-39 and 48.

Hasan, S. W. & Hancock, G. J. (1988). Plastic bending tests of cold-formed rectangular hollow sections. Report No. R568. University of Sydney, Australia.

Hill, H. N. (1944). Determination of stress-strain relations from the offset yield strength values. *Technical Note No. 927, National Advisory Committee for Aeronautics.* Washington, D.C.

Ingvarsson, L. (1975). Cold-forming residual stresses. Effect on buckling. *Proceedings of the Third Speciality Conference on Cold-formed Steel Structures.* 85-119.

Ingvarsson, L. (1977). Cold-forming residual stresses. Bulletin No. 121. Dept. of Building Statics and Structural Engineering. The Royal Institute of Technology, Stockholm.

Ingvarsson, L. (1979). Cold-forming residual stresses in thin-walled structures. *Proceedings of the First International Conference on Thin-Walled Structures.* University of Strathclyde, Glasgow. 575-587.

Johnson, A. L. & Winter, G. (1966). Behaviour of stainless steel columns and beams. *Journal of the Structural Division*, ASCE. **ST5**, 97-118.

Karren, K. W. (1967). Corner properties of cold-formed steel shapes. *Journal of the Structural Division,* ASCE. **93:ST1**, 401-432.

Kemp, A. R., Byfield, M. P. & Nethercot, D. A. (2002). Effect of strain hardening on flexural properties of steel beams. *The Structural Engineer.* **18:8**, 29-35.

Kiymaz, G. (1999). Stability criteria for thin-walled box columns of high performance steel in axial compression. PhD Thesis. Structures Section, Department of Civil Engineering, Imperial College, London.

Kouhi, J., Talja, A., Salmi, P. & Ala-Outinen, T. (2000). Current R&D work on the use of stainless steel in construction in Finland. *Journal of Constructional Steel Research*, **54**, 31-50.

Lagerqvist, O. & Olsson, A. (2001). Residual stresses in welded I-girders made of stainless steel and structural steel. *Proceedings of the Ninth Nordic Steel Construction Conference.* Edited by Mäkeläinen et al. Helsinki, Finland. 737-744.

Lay, M. G., & Ward, R. (1969). Residual stresses in steel sections. *Journal of the Australian Institute of Steel Construction.* **3:3**, 2-21.

Lin, S.-H., Yu, W.-W. & Galambos, T. V. (1992). ASCE LRFD Method for Stainless Steel Structures. *Journal of Structural Engineering, ASCE.* **118: 4**, 1056-1070.

Liu, Y. & Young, B. (2002). Buckling of stainless steel square hollow section compression members. *Journal of Constructional Steel Research.* In press.

Macdonald, M., Rhodes, J. & Taylor, G. T. (2000). Mechanical properties of stainless steel lipped channels. *Fifteenth International Conference on Cold-Formed Steel Structures.* St. Louis, Missouri, USA. 673-686.

Mann, A. P. (1993). The structural use of stainless steel. *The Structural Engineer*, **71:4**, 60-69.

Masubuchi, K. (1980). Analysis of welded structures. Pergamon Press Ltd.

Mazzolani, F. M. (1995). Aluminium Alloy Structures. 2nd Edition. E & FN Spon, An imprint of Chapman and Hall.

Mirambell, E. & Real, E. (2000). On the calculation of deflections in structural stainless steel beams: an experimental and numerical investigation. *Journal of Constructional Steel Research*, **54**, 109-133.

Olsson, A (2001). Stainless steel plasticity – material modelling and structural applications. Luleå University of Technology. Doctoral thesis 2001:19.

Ostapenko, A. (1977). Local buckling of welded tubular columns. Report No. 406.11. Fritz Engineering Laboratory, Lehigh University, Bethlehem, Palestine.

Ramberg, W. & Osgood, W. R. (1943). Description of stress-strain curves by three parameters. *Technical Note No. 902, National Advisory Committee for Aeronautics.* Washington, D.C.

Rasmussen, K. J. R. (2000a). Recent research on stainless steel tubular structures. *Journal of Constructional Steel Research*, **54**, 75-88.

Rasmussen, K. J. R. (2000b). The Development of an Australian Standard for Stainless Steel Structures. *Proceedings of the Fifteenth International Speciality Conference on Cold-formed Steel Structures.* St. Louis, Missouri, USA. 659-671.

Rasmussen, K. J. R. & Hancock, G. J. (1990). Stainless steel tubular columns – tests and design. *Proceedings of the Tenth International Speciality Conference on Cold-formed Steel Structures.* St. Louis, Missouri, U.S.A.

Rasmussen, K. J. R. & Hancock, G. J. (1992). Stainless steel tubular beams – tests and design. *Proceedings of the Eleventh International Speciality Conference on Cold-formed Steel Structures,* 587-609. St. Louis, Missouri, USA.

Rasmussen, K. J. R. & Hancock, G. J. (1993a). Design of cold-formed stainless steel tubular members. I: Columns. *Journal of Structural Engineering,* ASCE. **119: 8,** 2349-2367.

Rasmussen, K. J. R. & Hancock, G. J. (1993b). Design of cold-formed stainless steel tubular members. II: Beams. *Journal of Structural Engineering,* ASCE. **119: 8,** 2368-2386.

Rasmussen, K. J. R. & Rondal, J. (1997a). Strength curves for metal columns. *Journal of Structural Engineering,* ASCE. **123: 6,** 721-728.

Rasmussen, K. J. R. & Rondal, J. (1997b). Explicit approach to design of stainless steel columns. *Journal of Structural Engineering,* ASCE. **123: 7,** 857-863.

Real, E. (2001). Aportaciones al estudio del comportamiento a flexion de estructuras de acero inoxiddable. Tesis Doctoral. Departamento de Ingeniería de la Construcción, Universitat Politècnica de Catalunya. UPC-ETSECCP. Barcelona, Mayo. (In Spanish).

Rhodes, J., Macdonald, M. & McNiff, W. (2000). Buckling of cold formed stainless steel columns under concentric and eccentric loading. Fifteenth International Speciality Conference on Cold-Formed Steel Structures. St Louis, Missouri, USA. 687-699.

Rockey, K. C. & Jenkins, F. (1957). The behaviour of webplates of plate girders subjected to pure bending. *The Structural Engineer.* 35 ,176-189.

SABS (1997). Structural use of steel – Part 4: The design of cold-formed stainless steel structural members. SABS 0162-4:1997.

Sedlacek, G. & Stangenberg, H. (1999). Numerical modelling of the behaviour of stainless steel members in tests. *Proceedings of the Fourth International Conference on Steel and Aluminium Structures, ICSAS '99*. Edited by Mäkeläinen, P. and Hassinen, P. Espoo, Finland. 503-512.

Shafer, B. & Peköz, T. (1998). Computational modelling of cold-formed steel: characterizing geometric imperfections and residual imperfections. *Journal of Constructional Steel Research.* **47**, 193-210.

Slater, R. A. C. (1977). Engineering Plasticity Theory and application to metal forming processes. The Macmillan Press Ltd.

SSBJA (1995). The design and construction specifications for stainless steel structures. Stainless Steel Building Association of Japan. (In Japanese, not seen).

Sully, R. M. & Hancock, G. J. (1999). Stability of cold-formed tubular beam-columns. *Proceedings of the Fourth International Conference on Steel and Aluminium Structures, ICSAS '99*. Edited by Mäkeläinen, P. and Hassinen, P. Espoo, Finland. 141-154.

Talja, A. (1997). Test report on welded I and CHS beams, columns and beam-columns. Report to ECSC. VTT Building Technology, Finland.

Talja, A. (1999). Tests on cold-formed and welded stainless steel members. *Fourth International Conference on Steel and Aluminium Structures*. Espoo, Finland. Edited by Mäkeläinen, P. and Hassinen, P. 531-538.

Talja, A. & Salmi, P. (1995). Design of stainless steel RHS beams, columns and beam-columns. *Research Note 1619*, VTT Building Technology, Finland.

Timoshenko, S. P. & Gere, J. M. (1985). Theory of elastic stability. McGraw-Hill International Book Company, New York.

Truman, J. (1985). The initiation and growth of high alloy (stainless) steel production. *Journal of the Historical Metallurgy Society.* **19:1**, 116-125.

Van den Berg, G. J. (2000). The effect of non-linear stress-strain behaviour of stainless steel on member capacity. *Journal of Constructional Steel Research.* **54**, 135-160.

Van den Berg, G. J. & Van der Merwe, P. (1992). Prediction of corner mechanical properties for stainless steels due to cold forming. *Proceedings of the 11th International Speciality Conference on Cold-Formed Steel Structures.* St. Louis, Missouri, USA.

Wadee, M. A. (2000). Effects of periodic and localized imperfections on struts on nonlinear foundations and compression sandwich panels. *International Journal of Solids and Structures.* **37**, 1191-1209.

Wang, S. T. & Errara, S. J. (1971). Behaviour of cold rolled stainless steel members. *Proceedings of the First Speciality Conference on Cold-formed Steel Structures.* University of Missouri-Rolla, Rolla, Mo.

Way, J. (2000). WP2, 3.1, 3.2 and 3.3: Cross-sections, beams, columns and beam-columns – circular hollow sections. ECSC project – Development of the use of stainless steel in construction. Contract No. 7210 SA/ 842. The Steel Construction Institute, UK.

Weng, C. C. & Pekoz, T. (1988). Residual stresses in cold-formed steel members. *Proceedings of the Ninth International Speciality Conference on Cold-Formed Steel Structures.* St. Louis, Missouri, U.S.A. 167-189.

Wheeler, A. T. & Bridge, R. Q. (2000). Thin-walled steel tubes filled with high strength concrete in bending. *Proceedings of the Composite Construction IV Conference.* Alberta, Canada.

Yamada, S. & Kato, T. (1988). Strength and deformation of H-shaped stainless steel beams. *Japanese Institution of Architecture. Journal of the Kanto branch.*

Young, B. W. (1974). The effect of process efficiency on the calculation of weld shrinkage forces. *Proceedings of the Institution of Civil Engineers,* Part 2. **57**, 685-692.

Young, B. & Hartono, W. (2002). Compression tests of stainless steel tubular members. *Journal of Structural Engineering, ASCE.* **128:6**, 754-761.

Young, B. & Liu, Y. (2002). Experimental investigation of cold-formed stainless steel columns. *Journal of Structural Engineering, ASCE.* In press.

APPENDIX A

CORRELATION BETWEEN STAINLESS STEEL DESIGNATIONS

There are a number of different stainless steel designation systems. The system adopted in this thesis is the 'steel number' given in the European material standard BS EN 10088-1 (1995). Correlations between BS EN 10088, German, UK, French, Italian, Swedish, Spanish and US designation systems are presented in Table A.1. Table A.1 was reproduced from the Euro Inox 'Design Manual for Structural Stainless Steel' (Euro Inox, 2002).

Table A.1: Correlation between stainless steel designations

| Steel Grade to BS EN 10088 | | Germany (DIN) | | UK | France | Italy | Sweden | Spain | USA | |
Name	No.	Name	No.	BSI	AFNOR	UNI	SIS	UNE	AISI	UNS
X5CrNi18-10	1.4301	X5 CrNi 18 10	1.4301	304 S 15 304 S 16 304 S 31	Z 6 CN 18-09	X5 CrNi 18 10	2332 2333	3504	304	S 30400
X2CrNi19-11	1.4306	X2 CrNi 19 11	1.4306	304 S 11	Z 2 CN 18-10	X2 CrNi 18 11	2352	3503	304 L	S 30403
X2CrNi18-9	1.4307	-	-	-	-	-	-	-	-	-
X6CrNiTi18-10	1.4541	X6 CrNiTi 18 10	1.4541	321 S 31	Z 6 10	X6 CrNiTi 18 11	2337	3523	321	S 32100
X5CrNi Mo17-12-2	1.4401	X5CrNiMo 17 12 2	1.4401	316 S 31	Z 6 CND 17-11	X5 CrNiMo 17 12	2347	3534	316	S 31600
X2CrNiMo17-12-2	1.4404	X2CrNiMo 17 13 2	1.4404	316 S 11	Z 2 CND 17-12	X2 CrNiMo 17 12	2348	3533	316L	S 31603
X2CrNiMo17-12-3	1.4432	-	-	-	-	-	-	-	-	-
X2CrNiMo18-14-3	1.4435	X2 CrNiMo 18 14 3	1.4435	316 S 13	Z 2 CND 17-13	X2 CrNiMo 17 13	2353	3533	316 L	S 31603
X1NiCrMoCu25-20-5	1.4539	X1 NiCrMoCuN 25 20 5	1.4539	-	Z 1 CNDU 25-20		2562	-	904 L	N 08904
X6CrNiMoTi17-12-2	1.4571	X6 CrNiMoTi 17 12 2	1.4571	320 S 31	Z 6 CNDT 17-12	X6 CrNiMoTi 17 12	2350	3535	316 Ti	S 31635
X2CrNiN18-10	1.4311	X2 CrNiN 18 10	1.4311	304 S 61	Z 2 CN 18-10 Az	-	2371	-	304 LN	S 30453
X2CrNiMoN17-11-2	1.4406	X2 CrNiMoN 17 12 2	1.4406	316 S 62	Z 2 CND 17-12 Az	-	-	-	316 LN	S 31653
X2CrNiMoN17-13-5	1.4439	X2 CrNiMoN 17 13 5	1.4439	-	-	-	-	-	317	S 31726
X1NiCrMoCuN25-20-7	1.4529	X1 NiCrMoCuN 25 20 6	1.4529	-	-	-	-	-	-	-
X2CrNiN18-7	1.4318	X2 CrNiN 18 7	1.4318	-	-	-	-	-	301 LN	-
X2CrNiMoN22-5-3	1.4462	X2 CrNiMoN 22 5 3	1.4462	Duplex 2205	Z 2 CND 22-5 Az	-	2377	-	-	S 31803